INVESTIGATIONS INTO SOLAR POWERED DIFFUSION-ABSORPTION COOLING MACHINES

ULI JAKOB

PhD

2005

INVESTIGATIONS INTO SOLAR POWERED DIFFUSION-ABSORPTION COOLING MACHINES

Uli Jakob

A thesis submitted in partial fulfilment
of the requirements of De Montfort University
for the degree of Doctor of Philosophy (PhD)

April 2005

Institute of Energy and Sustainable Development
De Montfort University Leicester

Faculty of Civil Engineering, Building Physics and Economics
Stuttgart University of Applied Sciences

ABSTRACT

Solar thermal driven or assisted absorption cooling machines are gaining increasing importance due to the continually growing demand for air-conditioning in domestic housing as well as office and hotel buildings. Presently there are no thermally driven absorption cooling machines available on the market that can provide a smaller cooling capacity than 10kW for cooling buildings.

For this reason, two single-effect solar heated ammonia/water (NH_3/H_2O) Diffusion-Absorption Cooling Machines (DACM) with a design cooling capacity of 2.5kW at evaporator temperatures between -10°C and +5°C were designed, built and operated. The indirectly heated, solar powered generator (bubble pump) is the main new feature of this cooling machine. Data acquisition was conducted under laboratory conditions as well as under simulated field conditions for vacuum-tube collectors. The first pilot plant showed that coefficient of performance values (COP) range from 0.1 to 0.2 and the evaporator cooling capacity of the pilot plant could reach 1.5kW, but that the operation stability was insufficient. The second optimised and compacted pilot plant showed stable and continuous temperature and pressure levels. The reached COPs were between 0.2 and 0.5 and the continuous cooling performance between 1.0kW and 1.6kW. A maximum cooling performance of 2.0kW could be reached if the evaporator temperature was set to the relatively high value of 25°C.

The Diffusion-Absorption Cycle has been modelled using the constant characteristic equation of sorption chillers. An expanded, steady-state model which includes additional specific components of the DACM was developed based on the exact solution of the internal mass and energy balances of each component as well as the heat transfer between external and internal temperature levels. The internal enthalpies are calculated at each time interval using the simulation environment INSEL. The compared experimental and simulated data showed a good accordance.

ACKNOWLEDGEMENTS

This research was carried out at the Institute of Energy and Sustainable Development at De Montfort University Leicester working in collaboration with the Faculty of Civil Engineering, Building Physics and Economics at the Stuttgart University of Applied Sciences.

I would like to thank Prof. Dr. Ursula Eicker, Dr. Ahmad H. Taki and Dr. Malcolm J. Cook for their excellent support, supervision and for their revision of this thesis. Furthermore, I am grateful to my colleagues at the Faculty of Civil Engineering, Building Physics and Economics for their assistance, especially to Andreas Trinkle and Dietrich Schneider.

Finally, I would like to thank my wife Sonja, who has always encouraged and supported me during my work and my parents who financially supported, making my PhD study possible.

I declare that the content of this submission is my own work. The contents of the work have not been submitted for any other academic or professional award. I acknowledge that this thesis is submitted according to the conditions laid down in the regulations. Furthermore, I declare that the work was carried out as part of the course for which I was registered. I draw attention to any relevant considerations of rights of third parties.

CONTENTS

LIST OF FIGURES

LIST OF FIGURES

LIST OF TABLES

NOMENCLATURE

LATIN LETTERS

A	[m²]	area, surface, cross sectional area
A_E	[-]	specific absorber enthalpy coefficient
$A_{E,aux}$	[-]	additional specific absorber enthalpy coefficient
Ar	[-]	Archimedes number
A_1	[m²]	cross section of a small tube
A_2	[m²]	cross section of bigger tube/shell
a	[m²/s]	thermal diffusivity
a	[-]	coefficient of the Clausius-Clapeyron equation
B	[-]	Dühring constant
Bo	[-]	Bond number
$\dot{B}$	[kg/m s]	irrigation density
b	[-]	coefficient of the Clausius-Clapeyron equation
b	[-]	lifting ratio
C	[-]	constant
C_E	[-]	specific condenser enthalpy coefficient
COP	[-]	coefficient of performance for cooling applications, based and defined on the first and second law of thermodynamics as the ratio of cooling output to driving heat input
COP_{heat}	[-]	coefficient of performance for heating applications, ratio of heating output to driving heat input
COP_{meas}	[-]	measured coefficient of performance
COP_{theo}	[-]	theoretical possible coefficient of performance
c	[J/kg K]	specific heat capacity
$c_{L,CE}$	[J/kg K]	specific heat capacity of liquid ammonia
$c_{L,NH3}$	[J/kg K]	specific heat capacity of liquid ammonia
$c_{L,NH3/H2O}$	[J/kg K]	specific heat capacity of liquid ammonia
$c_{L,Sr}$	[J/kg K]	specific heat capacity of rich solution

NOMENCLATURE

$c_{L,Sw}$	[J/kg K]	specific heat capacity of weak solution
$c_{NH3/H2O}$	[J/kg K]	specific heat capacity of ammonia/water solution
c_p	[kJ/kg K]	specific heat capacity at constant pressure
$c_{p,a}$	[kJ/kg K]	specific heat capacity of absorber cooling medium
$c_{p,c}$	[kJ/kg K]	specific heat capacity of condenser cooling medium
$c_{p,d}$	[kJ/kg K]	specific heat capacity of dephlegmator heating medium
$c_{p,e}$	[kJ/kg K]	specific heat capacity of evaporator cooling medium
$c_{p,F20}$	[J/kg K]	specific heat capacity of cooling medium Tyxofit F20
$c_{p,g}$	[kJ/kg K]	specific heat capacity of generator heating medium
$c_{p,He}$	[J/kg K]	specific heat capacity of helium gas
$c_{p,He}$	[kJ/kg K]	specific heat capacity of helium gas
$c_{p,H2O}$	[J/kg K]	specific heat capacity of liquid water
$c_{p,NH3}$	[kJ/kg K]	specific heat capacity of ammonia vapour
$c_{p,RO200}$	[J/kg K]	specific heat capacity of heat transfer medium RO200
$c_{p,S}$	[J/kg K]	specific heat capacity of the mean solution
$c_{p,Vr}$	[kJ/kg K]	specific heat capacity of the rich ammonia/helium gas mixture
$c_{p,Vw}$	[kJ/kg K]	specific heat capacity of the weak ammonia/helium gas mixture
$c_{V,NH3}$	[J/kg K]	specific heat capacity of ammonia vapour
D	[m]	inner tube diameter
D_{BA}	[m²/s]	diffusion coefficient
D_E	[-]	specific dephlegmator enthalpy coefficient
$D_{E,deph}$	[-]	additional specific dephlegmator enthalpy coefficient
D_{NH3-He}	[m²/s]	diffusion coefficient for ammonia into helium
$D_{NH3-NH3/H2O}$	[m²/s]	diffusion coefficient for ammonia into ammonia/water solution
D_S	[m]	inner diameter of the shell
d	[m]	tube diameter
d_b	[m]	Laplace constant
d_e	[m]	real diameter of a bundle of tubes or equivalent diameter of the shell
d_T	[m]	inner diameter of a single tube
d_i	[m]	inner diameter of one tube

d_1	[m]	diameter of a small tube
d_2	[m]	diameter of bigger tube/shell
E	[-]	degassing width
Fr	[-]	Froude number
f	[-]	ammonia mass concentration in the NH_3/He gas mixture
f	[-]	specific solution circulation index which is the ratio of the incoming rich solution to driven out vapour mass flow
f	[-]	ratio
(f-1)	[-]	specific solution circulation index related to lifted weak ammonia/water solution
$f_{s,NH3/He}$	[-]	saturation mass concentration at the interface between the NH_3/He gas mixture and the liquid NH_3 meniscus
f_{Vr}	[-]	NH_3-mass concentration of rich ammonia/helium gas
f_{Vw}	[-]	NH_3-mass concentration of weak ammonia/helium gas
G_E	[-]	specific generator enthalpy coefficient
$G_{E,deph}$	[-]	additional specific dephlegmator enthalpy coefficient
g	[m/s²]	standard acceleration of gravity
H	[m]	tube height/length, propulsion height, reservoir height
H_{AUX}	[kJ/kg]	auxiliary gas circuit enthalpy difference
H_{deph}	[m]	tube height/length of dephlegmator
(H/L)	[-]	submergence ratio which is the ratio of the reservoir height to the bubble pump tube length
h	[kJ/kg]	enthalpy
h_{AUX}	[kJ/kg]	auxiliary gas circulation cooling loss enthalpy
h_B	[W/m² K]	boiling heat transfer coefficient
h_C	[W/m² K]	convective heat transfer coefficient
h_G	[kJ/kg]	specific enthalpy for the ammonia/helium gas mixture
h_L	[kJ/kg]	liquid enthalpy of condensed ammonia/water vapour
h_m	[W/m² K]	mean heat transfer coefficient
h_V	[kJ/kg]	vapour enthalpy of ammonia/water vapour
h_{Vr}	[kJ/kg]	rich ammonia/helium gas mixture enthalpy
Δh	[m]	lifting height, driving head
Δh	[kJ/kg]	enthalpy difference
Δh_E	[kJ/kg]	specific evaporation enthalpy of ammonia

NOMENCLATURE

l	[m]	tube/shell length
l_C	[m]	running length of the falling film
K_1	[m³/kg]	coefficient
K_2	[kJ/kg]	coefficient
L	[m]	tube length
M	[kg/kmol]	relative molecular mass
M	[kg/kmol]	molecular mass of the mean solution
M_A	[kg/kmol]	relative molecular mass of the species A
M_B	[kg/kmol]	relative molecular mass of the species B
M_{He}	[kg/kmol]	relative molecular mass of helium
M_{NH3}	[kg/kmol]	relative molecular mass of ammonia
m	[kg]	mass fraction
$\dot{m}$	[kg/s]	mass flow
$\dot{m}_a$	[kg/s]	mass flow rate of absorption cooling
$\dot{m}_c$	[kg/s]	mass flow rate of condenser cooling
$\dot{m}_d$	[kg/s]	mass flow rate of dephlegmator cooling
$\dot{m}_{diff}$	[kg/s]	mass diffusion of a chemical species in a stationary binary mixture
$\dot{m}_e$	[kg/s]	mass flow rate of evaporator cooling
$\dot{m}_g$	[kg/s]	mass flow rate of generator heating
$\dot{m}_L$	[kg/s]	mass flow of liquid ammonia condensate
$\dot{m}_L$	[kg/h]	mass flow of liquid ammonia/water
$\dot{m}_{L,deph}$	[kg/s]	mass flow rate of condensed water vapour
$\dot{m}_{L,NH3}$	[kg/h]	mass flow of liquid ammonia
$\dot{m}_S$	[kg/h]	mass flow of ammonia/water solution
$\dot{m}_{Sr}$	[kg/s]	mass flow rate of rich ammonia/water solution
$\dot{m}_{Sw}$	[kg/s]	mass flow rate of weak ammonia/water solution
$\dot{m}_V$	[kg/h]	mass flow of ammonia(/water) vapour
$\dot{m}_V$	[kg/s]	mass flow rate of rectified ammonia(/water) vapour
$\dot{m}_{V1}$	[kg/s]	mass flow rate of ammonia/water vapour
$\dot{m}_{Vr}$	[kg/s]	mass flow of the rich ammonia/helium gas mixture

$\dot{m}_{Vw}$	[kg/s]	mass flow of the weak ammonia/helium gas mixture
N_A	[mol^{-1}]	Avogadro number
Nu	[-]	Nußelt value
Nu_c	[-]	Nußelt value for connective heat transfer
Nu_l	[-]	Nußelt value for laminar flow
Nu_t	[-]	Nußelt value for turbulent flow
n	[-]	auxiliary size
n	[-]	number of tubes
Pr	[-]	Prandtl value
p	[Pa]	pressure, total pressure
p*	[-]	reduced pressure which is the ratio of the system to critical pressure of the fluid
p_{ar}	[Pa]	absorber partial pressure of the rich solution
p_{AUX}	[Pa]	auxiliary gas partial pressure
p_{aw}	[Pa]	absorber partial pressure of the weak solution
$p_{A,Sr}$	[Pa]	absorber partial pressure of the rich solution
p_C	[Pa]	condenser pressure
p_{cr}	[Pa]	critical pressure of the fluid
p_D	[Pa]	dephlegmator pressure
p_e	[Pa]	evaporator partial pressure
p_{NH3}	[Pa]	ammonia partial pressure
p_G	[Pa]	generator pressure
p_H	[Pa]	high pressure level
p_{H1}	[Pa]	high pressure level
p_{H2}	[Pa]	high pressure level
p_{Hv}	[Pa]	high vacuum pressure level
p_{Hv1}	[Pa]	medium vacuum pressure level
p_{Hv2}	[Pa]	high vacuum pressure level
p_L	[Pa]	low pressure level
p_{Lv}	[Pa]	low vacuum pressure level
p_{total}	[Pa]	total pressure level
p_{Vr}	[Pa]	partial pressure of the rich gas mixture
p_{Vw}	[Pa]	partial pressure of the weak gas mixture
Δp	[Pa]	driving force

NOMENCLATURE

Δp	[Pa]	pressure drop
Δp_{abs}	[%]	partial pressure difference percentage for the wash out
Δp_{EA}	[Pa]	partial pressure difference evaporator to absorber
Δp_{sat}	[%]	partial pressure difference percentage for the saturation
Q	[kW]	capacity
Q_A	[kW]	absorber cooling capacity
Q_{AUX}	[kW]	auxiliary gas circulation cooling loss capacity
Q_{A0}	[kW]	absorber cooling capacity at low pressure level
Q_{Ax}	[kW]	solution heat loss
Q_{A1}	[kW]	absorber cooling capacity at high pressure level
Q_C	[kW]	condenser cooling capacity
Q_{C1}	[kW]	condenser cooling capacity
Q_{C2}	[kW]	condenser cooling capacity at high-stage pressure level
Q_D	[kW]	dephlegmator cooling capacity
Q_{Deph}	[kW]	dephlegmator cooling capacity
Q_E	[kW]	evaporator cooling capacity
$Q_{E,aux}$	[kW]	evaporator cooling capacity with cooling loss
$Q_{E,\varepsilon}$	[kW]	evaporator cooling capacity with evaporation efficiency
Q_G	[kW]	generator heating capacity
Q_{Gx}	[kW]	solution heat loss
Q_H	[kW]	generator heating capacity
$Q_{H,meas}$	[kW]	measured generator heating capacity
$Q_{H0/1}$	[kW]	generator heating capacity
$Q_{H0/2}$	[kW]	generator heating capacityat high-stage pressure level
Q_{H1}	[kW]	generator heating capacity at high-stage pressure level
Q_{H2}	[kW]	generator heating capacity at high-stage pressure level
Q_O	[kW]	evaporator cooling capacity
$Q_{O,meas}$	[kW]	measured evaporator cooling capacity
$Q_{O,theo}$	[kW]	theoretical possible evaporator cooling capacity
q	[W/m²]	heat flux density
q	[kW/m²]	heat flux density
q_E	[kJ/kg]	specific evaporator enthalpy difference
R	[kJ/kmol K]	universal gas constant
Re	[-]	Reynolds value

Re_{cr}	[-]	critical Reynolds value for the transition from pseudo laminar flow to turbulent flow
Re_W	[-]	limiting Reynolds value for the laminar flow which is related to the forming of waves on the surface of the falling film
r_A	[m]	molecule radius of gas molecule species A
r_B	[m]	molecule radius of gas molecule species B
s_E	[kW/K]	slope of the characteristic equation
T	[°C]	temperature
T	[K]	temperature
-1/T	[°C]	temperature
T_A	[°C]	mean internal absorber temperature
T_A	[K]	absorber temperature
T'_A	[°C]	new mean internal absorber temperature
$T_{A,in}$	[°C]	external absorber inlet temperature
$T_{A,out}$	[°C]	external absorber outlet temperature
T_B	[°C]	boiling temperature
T_b	[K]	mean boiling temperature of the generator
T_C	[°C]	mean internal condenser temperature
T_C	[K]	condenser temperature
T'_C	[°C]	new mean internal condenser temperature
$T_{C,in}$	[°C]	external condenser inlet temperature
$T_{C,out}$	[°C]	external condenser outlet temperature
$T_{C,s}$	[°C]	condensation temperature
T_c	[°C]	cooling water inlet/outlet temperature
TD	[°C]	dew point temperature
T_D	[°C]	mean internal dephlegmator temperature
T'_D	[°C]	new mean internal dephlegmator temperature
$T_{D,in}$	[°C]	external dephlegmator inlet temperature
$T_{D,out}$	[°C]	external dephlegmator outlet temperature
T_E	[°C]	mean internal evaporator temperature
T'_E	[°C]	new mean internal evaporator temperature
$T_{E,e}$	[°C]	evaporation mean temperature
T_G	[°C]	mean internal generator temperature

T'_G	[°C]	new mean internal generator temperature
$T_{H,in}$	[°C]	external generator inlet temperature
$T_{H,out}$	[°C]	external generator outlet temperature
T_h	[°C]	driving heat inlet/outlet temperature
T_{H0}	[K]	generator temperature
T_{H1}	[K]	generator temperature
T_{H2}	[K]	generator temperature
T_{LC}	[°C]	condenser liquid outlet temperature
T_{LE}	[°C]	evaporator liquid inlet temperature
T_O	[°C]	mean internal evaporator temperature
T_O	[K]	evaporator temperature
$T_{O,in}$	[°C]	external evaporator inlet temperature
$T_{O,out}$	[°C]	external evaporator outlet temperature
T_o	[°C]	chilled cooling agent inlet/outlet temperature
$T_{PHL,in}$	[°C]	external preheated line inlet temperature
$T_{PHL,out}$	[°C]	external preheated line outlet temperature
$T_{SG,in}$	[°C]	generator inlet temperature of the solution
$T_{SG,out}$	[°C]	generator outlet temperature of the solution
$T_{SrSHX,in}$	[°C]	SHX inlet temperature of the rich solution
$T_{SrSHX,out}$	[°C]	SHX outlet temperature of the rich solution
T_{SwG}	[°C]	generator outlet temperature of the weak solution
$T_{SwSHX,in}$	[°C]	SHX inlet temperature of the weak solution
$T_{SwSHX,out}$	[°C]	SHX outlet temperature of the weak solution
T_s	[°C]	solidification temperature
T_{VC}	[°C]	condenser vapour inlet temperature
T_{VD}	[°C]	dephlegmator vapour outlet temperature
$T_{VG,out}$	[°C]	generator vapour outlet temperature
T_{VrE}	[°C]	evaporator rich gas mixture outlet temperature
T_{VwA}	[°C]	absorber weak solution inlet temperature
T_{VwE}	[°C]	evaporator weak gas mixture inlet temperature
T_{V1G}	[°C]	generator vapour outlet temperature
ΔT	[K]	temperature difference
ΔT_{bp}	[K]	boiling point temperature distance
t_a	[°C]	mean external absorber temperature

$t_{a,in}$	[°C]	external absorber inlet temperature
$t_{a,out}$	[°C]	external absorber outlet temperature
t_c	[°C]	mean external condenser temperature
$t_{c,in}$	[°C]	external condenser inlet temperature
$t_{c,out}$	[°C]	external condenser outlet temperature
t_d	[°C]	mean external dephlegmator temperature
$t_{d,in}$	[°C]	external dephlegmator inlet temperature
$t_{d,out}$	[°C]	external dephlegmator outlet temperature
t_e	[°C]	mean external evaporator temperature
$t_{e,in}$	[°C]	external evaporator inlet temperature
$t_{e,out}$	[°C]	external evaporator outlet temperature
t_g	[°C]	mean external generator temperature
$t_{g,in}$	[°C]	external generator inlet temperature
$t_{g,out}$	[°C]	external generator outlet temperature
t_0	[s]	delay time
$\Delta\Delta t$	[K]	characteristic double temperature difference
$\Delta\Delta t_{min,E}$	[K]	Intersection of the characteristic equation
U	[m]	irrigation circumference
UA_A	[kW/K]	heat transfer coefficient of the absorber
UA_C	[kW/K]	heat transfer coefficient of the condenser
UA_D	[kW/K]	heat transfer coefficient of the dephlegmator
UA_E	[kW/K]	heat transfer coefficient of the evaporator
UA_G	[kW/K]	heat transfer coefficient of the generator
$\dot{V}$	[m³/s]	volume flow rate
$\dot{V}_{A,ext}$	[m³/s]	volume flow rate of absorber cooling
$\dot{V}_{C,ext}$	[m³/s]	volume flow rate of condenser cooling
$\dot{V}_{D,ext}$	[m³/s]	volume flow rate of dephlegmator cooling
$\dot{V}_{H,ext}$	[m³/s]	volume flow rate of generator heating
$\dot{V}_{O,ext}$	[m³/s]	volume flow rate of evaporator cooling
$\dot{V}_L$	[l/h]	lifted liquid volume flow
$\dot{V}_S$	[m³/s]	liquid volume flow rate

NOMENCLATURE

$\dot{V}_V$	[m³/s]	vapour volume flow rate
$\dot{V}_V$	[l/h]	driven out gas volume flow
$\dot{V}_{Vw}$	[m³/h]	volume flow rate of weak gas mixture
v	[m/s]	vapour flow velocity
w_S	[m/s²]	flow velocity of the mean solution
X	[%]	LiBr-mass concentration
X	[-]	NH_3-mass concentration
X_{He}	[-]	helium concentration in the gas mixture
X_L	[-]	ammonia mass concentration of liquid ammonia
$X_{L,deph}$	[-]	ammonia mass concentration of rectified ammonia/water vapour
X_{NH3}	[-]	ammonia concentration in the gas mixture
X_S	[-]	ammonia mass concentration of ammonia/water solution
X_S	[-]	ammonia initial mass concentration
X_S	[-]	ammonia/water mean solution concentration
X_{Sr}	[-]	ammonia mass concentration of rich ammonia/water solution
X_{Sw}	[-]	ammonia mass concentration of weak ammonia/water solution
X_V	[-]	ammonia vapour mass concentration, vapour purity
X_{V1}	[-]	non-rectified ammonia/water vapour mass concentration
x_{NH3}	[kmol/kmol]	ammonia mol concentration
Y	[m]	minimum height difference between reservoir level and heating zone where the bubbles are formed
y*	[-]	gas circulation loss index
Z_{AUX}	[kJ/kg]	factor for auxiliary gas circuit enthalpy difference
$\frac{c_{p,Vw} \cdot \dot{m}_{Vw}}{\dot{m}_{L,NH3}}$	[kJ/kg K]	auxiliary gas circulation loss

GREEK LETTERS

δ_m	[m]	mean film thickness
ε_W	[-]	surface wetting factor
Φ_{GHX}	[-]	heat recovery rate of the gas heat exchanger
$\Phi_{GHX,Vr}$	[-]	heat recovery rate refereed to rich auxiliary gas side
$\Phi_{GHX,Vw}$	[-]	heat recovery rate refereed to weak auxiliary gas side
Φ_S	[-]	heat recovery factor
Φ_{Sr}	[-]	heat recovery factor refereed to rich solution side
Φ_{Sr}	[%]	heat recovery factor refereed to rich solution side
Φ_{Sw}	[-]	heat recovery factor refereed to weak solution side
Φ_{Sw}	[%]	heat recovery factor refereed to weak solution side
Φ_{SHX}	[-]	heat recovery rate of the solution heat exchanger
Φ_{Vr}	[-]	heat recovery rate refereed to rich auxiliary gas side
Φ_{Vw}	[-]	heat recovery rate refereed to weak auxiliary gas side
η	[Pa s=kg/m s]	dynamic viscosity
$\eta_{G,He}$	[Pa s=kg/m s]	dynamic viscosity of helium gas
$\eta_{L,NH3}$	[Pa s=kg/m s]	dynamic viscosity of liquid ammonia
$\eta_{NH3/He}$	[Pa s=kg/m s]	dynamic viscosity of ammonia/helium gas mixture
$\eta_{NH3/H2O}$	[Pa s=kg/m s]	dynamic viscosity of ammonia/water solution
$\eta_{V,NH3}$	[Pa s=kg/m s]	dynamic viscosity of ammonia vapour
$\eta_{cr,He}$	[Pa s=kg/m s]	critical dynamic viscosity of helium gas
$\eta_{cr,NH3}$	[Pa s=kg/m s]	critical dynamic viscosity of ammonia vapour
$\eta_{cr,NH3/He}$	[Pa s=kg/m s]	critical dynamic viscosity of the gas mixture
η_r	Pa s=kg/m s]	reduced viscosity
η_S	[kg/m s]	dynamic viscosity of the mean solution
λ	[-]	friction coefficient
λ	[W/m K]	thermal conductivity
$\lambda_{G,He}$	[W/m K]	thermal conductivity of helium gas
$\lambda_{L,NH3}$	[W/m K]	thermal conductivity of liquid ammonia
$\lambda_{NH3/He}$	[W/m K]	thermal conductivity of ammonia/helium gas mixture
$\lambda_{NH3/H2=}$	[W/m K]	thermal conductivity of ammonia/water solution

NOMENCLATURE

λ_S	[W/m K]	thermal conductivity of the mean solution
$\lambda_{V,NH3}$	[W/m K]	thermal conductivity of ammonia vapour
ν	[m²/s]	kinematic viscosity
$\nu_{NH3/He}$	[m²/s]	kinematic viscosity of the ammonia/helium gas mixture
ν_S	[m/s]	kinematic viscosity of the mean solution
ρ	[kg/m³]	density
ρ	[kg/m³]	mean density of the gas mixture
ρ_A	[kg/m³]	density of the species A
ρ_{F20}	[kg/m³]	density of cooling medium Tyxofit F20
$\rho_{G,He}$	[kg/m³]	density of helium gas
ρ_{H2O}	[kg/m³]	density of liquid water
$\rho_{L,NH3}$	[kg/m³]	density of liquid ammonia
$\rho_{NH3/He}$	[kg/m³]	density of ammonia/helium gas mixture
$\rho_{NH3/H2O}$	[kg/m³]	density of ammonia/water solution
ρ_{Ro200}	[kg/m³]	density of heat transfer medium RO200
ρ_S	[kg/m³]	density of the mean solution
ρ_S	[kg/m³]	density of liquid
ρ_{Sr}	[kg/m³]	density of rich solution
ρ_{Sw}	[kg/m³]	density of weak solution
ρ_V	[kg/m³]	density of vapour
$\rho_{V,NH3}$	[kg/m³]	density of ammonia vapour
ρ_{Vw}	[kg/m³]	density of weak ammonia/helium gas mixture
$\rho_{Vr} - \rho_{Vw}$	[kg/m³]	density difference of the rich and weak gas mixture
ρ_{V1}	[kg/m³]	density of non-rectified vapour
σ	[N/m = kg/s²]	surface tension
$\sigma_{L,H2O}$	[N/m = kg/s²]	surface tension of liquid water
$\sigma_{L,NH3}$	[N/m = kg/s²]	surface tension of liquid ammonia
$\sigma_{NH3/H2O}$	[N/m = kg/s²]	surface tension of ammonia/water solution
υ_{Vr}	[m³/m³]	volume concentration of the rich gas mixtures
υ_{Vw}	[m³/m³]	volume concentration of the weak gas mixtures
ω	[m/s]	mean flow velocity
ω	[m/s]	flow velocity in the tubes

ω_S	[m/s]	flow velocity in the shell cross sectional area
ω_m	[m/s]	average flow velocity
ξ	[-]	drag coefficient
ξ_E	[-]	drag coefficient of the tube inlet loss by an edged tube reduction

INDICES

F20	cooling medium Tyxofit F20 by Tyforop Chemie GmbH
H2O	cooling water
i, j	index
RO200	heat transfer medium RO200 by aic-regloplas GmbH
1, 2, 7a,...	order, distinction, index, system point
A, C, D	absorber, condenser, dephlegmator
E, G	evaporator, generator

ABBREVIATIONS

ACM	Absorption Cooling Machine
AGHX	auxiliary gas heat exchanger
Ar	argon
CCM	Compression Cooling Machine
CM	Cooling Machine
CPC	compound parabolic concentrator
DACM	Diffusion-Absorption Cooling Machine
DAHP	Diffusion-Absorption Heat Pump
DAR	Diffusion-Absorption Refrigerator
DE	double-effect
DL	double-lift
FPC	flat-plate collector
GHX	gas heat exchanger
GWHX	generator with heat exchanger

NOMENCLATURE

H_2O/LiBr	water/lithium bromide
He	helium
H_2	hydrogen
HX	heat exchanger
ICPC	integrated compound parabolic concentrator
MeOH	methanol
MeOH/H_2O	methanol/water
N_2	nitrogen
NH_3/H_2O	ammonia/water
O_2	oxygen
PTC	parabolic trough collector
SE	single-effect
SE/DL	single-effect/double-lift
SHX	solution heat exchanger
SP	solution pump
T	throttle
TE	triple-effect
VTC	vacuum tube collector

CHAPTER 01

INTRODUCTION

In the last few years, the world-wide selling numbers for air-conditioning show a movement in only one direction – upwards! In 2002 the global market for air-conditioning grew around four percent, meaning nearly 44 million units. For the years 2004/2005, market researchers expected 50 million units. The units that dominate the market are the small split-units (one or two inside units) with a cooling capacity of around 2kW up to 4kW (Der Klimamacher, 2003).

With over forty million cooling units sold per year, room air-conditioning is one of the important application fields of refrigerating technology. Due to the large number of manufactured units, these systems are produced and offered at very low prices. Simultaneously, in many southern countries, these units have been the main reason for the bottleneck in the electric networks in summertime in the last few years. Therefore, it is important to search for alternative air-conditioning units, that are not gas or electrically driven, but with waste or solar thermal heat.

Current thermal driven Diffusion-Absorption Cooling Machines (DACM) with ammonia/water (NH_3/H_2O) and pressure compensated auxiliary gas circuit (helium or hydrogen), are only commercially used in the smallest power range up to 100W. The priority operation criterion is the absolute noiselessness (hotel mini-bars) and the autonomic power supply (camping gas refrigerators).

The well-known Diffusion-Absorption technique which was developed in the 1920s by the Swedish engineers von Platen and Munters (Munters, 1932; Niebergall, 1981; Herold *et al.*, 1996) is based on the principle of pressure equilibration between the high and low pressure side of the unit through an inert auxiliary gas, such as helium or hydrogen. A further peculiarity of this type of absorption cooling machine is the use of a thermally driven gas bubble pump for

the circulation of the solution cycle instead of the mechanical solution pump so that inside the cooling machine no mechanically moving parts are necessary. These cooling machines with the simple mechanical construction have no conventional high-performance pump or valves, but a very low coefficient of performance (COP) and therefore a high energy consumption.

The conventional gas or electrically driven Diffusion-Absorption Refrigerators (DAR) with their directly powered generator / gas bubble pump were theoretically and experimentally investigated in numerous research projects for the operative range of refrigerating as well as in part for air-conditioning (Watts *et al.*, 1958; Stierlin, 1964; Bäckström *et al.*, 1965; Reistad, 1968; Narayankbedkar *et al.*, 1985; Kouremenos *et al.*, 1994; Kim *et al.*, 1995; Chen *et al.*, 1996; Smirnov *et al.*, 1996; Vicatos, 2000; Srikhirin *et al.*, 2002; Al-Shemmeri *et al.*, 2003). These directly driven DARs have been available since 1925 and are manufactured among others by the company Dometic AB, Sweden (formerly Electrolux AB). The cooling power of these DARs is between 40W and 200W.

In the 1990s, these domestic DARs were modified and improved for use as directly heated, gas driven Diffusion-Absorption Heat Pumps (DAHP). Coefficients of performances for heating applications (COP_{heat}, ratio of heating output to driving heat input) between 1.2 and 1.35 were reached for a heating capacity of 80W to 205W and with a cooling capacity between 25W and 51W (Wang and Herold, 1992; Herold and Chen, 1993; Kim *et al.*, 1994; Herold, 1996). Another group of researchers (Stierlin and Ferguson, 1990; Schirp, 1990; Stierlin *et al.*, 1994) developed a directly gas heated DAHP with a heating capacity between 3.0kW and 3.5kW at heating temperatures of 150°C and evaporator temperatures from -15°C up to +5°C. Heating performance numbers between 1.4 and 1.5 were reached. The industrial conversion of this directly heated, gas powered DAHP is carried out by BBT Thermotechnik GmbH, formerly Buderus Heiztechnik GmbH (Buderus, 2003) in combination with a condensing boiler for a near-market unit, but is not yet commercially available.

The output heating capacity of the DAHP is approximately 3.6kW at a COP_{heat} of 1.5 and it requires of 1.2kW power input out of environmental heat through the evaporator by a solar air collector and 2.4kW heating capacity through the gas burner/generator (Schwarz and Lotz, 2001).

Another industrial conversion of the DAHP has been done by Entex Energy Ltd (Entex, 2004a). They realized two DAHPs with 4.0kW and 6.5kW heating capacity with a COP_{heat} of about 1.5. Both heat pumps should be available façade integrated or for indoor installation from 2005 on. They also realized a gas driven DACM with 1.0kW up to 3.5kW cooling capacity (Entex, 2004b).

Up to now, some prototypes of commercial absorption refrigerators with indirectly solar powered generators and hydrogen or helium as inert gas have also been experimentally and theoretically investigated. In these studies, COPs of 0.2 to 0.3 and cooling capacities between 16W and 62W were reached at heating temperatures between 160°C and 230°C and evaporator temperatures of -6°C down to -18°C (Keizer, 1979; Bourseau *et al.*, 1987; Gutiérrez, 1988; Ajib and Schultheis, 1998).

One research group (Braun and Hess, 2002) used the DAHP of the company Buderus and modified it by substituting the direct gas fired generator by an indirectly heated one. The cooling capacity should be approximately 1.2kW and the COP approached 0.5 at a heating temperature of 190°C and an evaporator temperature of -4°C.

A new technology, called 3AC (=Advanced Ammonia Absorption Cooling) was developed and built by the Austrian company Solarfrost International (Kunze, 2000). The normal diffusion absorption refrigeration machine was added with an extra loop, called a bypass, between evaporator, solution cycle and absorber, enabling the achievement of heating temperatures as low as 80°C for use with flat plate collectors. The gas mixture of refrigerant ammonia and auxiliary gas from the evaporator is transferred to the generator outlet and from there into the bypass where the gas mixture is brought into contact with the hot, weak solution coming from the generator and withdraws further refrigerant from the weak solution. Thus, a weak solution with a very low ammonia concentration goes to

the absorber and consequently the auxiliary gas purification in the absorber is very effective. As a result, the refrigerating temperature in the evaporator should be low. The high ammonia content of the auxiliary gas entering the absorber causes a very high ammonia rich solution concentration, allowing for a considerably lower generator boiling point temperature. Different prototypes were built with 400W and 100W cooling capacities and a COP greater than 0.3. They achieved evaporator temperatures for milk refrigeration of +4°C and for refrigeration at -30°C. A new prototype using a "Heronic Pump" as opposed to the classical bubble pump with a 2.0kW cooling capacity was set up in co-operation with the Austrian solar company Solid (SolarFrost, 2002).

To date, there are no suitable indirectly driven absorption cooling machines with small-scale cooling performance (1kW to 10kW) available on the market. Since 1998 the research team at the Department of Building Physics at the Stuttgart University of Applied Sciences has developed two single-stage solar heated ammonia/water DACMs with 2.5kW cooling capacity and helium as the inert gas (Jakob *et al.*, 2001; Jakob, 2001; Jakob and Eicker, 2002; Jakob, 2002; Jakob *et al.*, 2003a; Jakob *et al.*, 2003b; Jakob *et al.*, 2004a; Jakob *et al.*, 2004b).

The main objective of this work is the design, set up and detailed investigation of the performance of solar powered Diffusion-Absorption Cooling Machines, especially of the newly developed indirectly heated generator/bubble pump. For this purpose, two test plants were built: a first prototype and a second improved one, in order to analyse the performance potential, the experimental characterisation and optimisation of the cooling prototypes of especially the bubble pump and the auxiliary gas circuit performance. For the final outcome, a detailed expanded, steady-state component model of the DACM process was developed based on the characteristic equation of sorption chillers in order to evaluate the performance of the DACM with the experimentally measured values of the optimised DACM pilot plant. Moreover a parameter study was carried out to determine the performance potential of the DACM.

CHAPTER 02

STATE-OF-THE-ART ABSORPTION COOLING

2.1 HISTORY ACM - DACM

1859 Ferdinand Carré was the first to develop a continuous, single-stage working Absorption Cooling Machine (ACM). For the closed cycle process of an ACM, a binary working fluid that consists of the refrigerant and the absorbent is necessary. Carré used the working fluid ammonia/water (NH_3/H_2O).

The principal components of an ACM are the generator, condenser, evaporator and absorber (Figure 2.1a). The system consists of two cycles: the refrigerant cycle and the so-called solution cycle between generator and absorber. There is a low and a high pressure level „p_L and p_H“, which are set by throttles between the condenser and the evaporator and in the solution cycle between generator and absorber. A solution pump runs the solution cycle between absorber and generator with a solution heat exchanger for preheating the rich solution flowing to the generator and precooling the weak solution flowing to the absorber in order to bridge the considerable pressure difference between evaporator and condenser (thermal compressor).

For comparison, the Compression Cooling Machine (CCM) in Figure 2.1b, which was introduced in principal in 1834 by Jacob Perkins, has a mechanical compressor instead of the so-called thermal compressor of the ACM described before and with that, the system has only a refrigerant cycle. The purpose of the compressor is to bring the evaporated refrigerant to a high pressure level so

that the refrigerant can be condensed through cooling the condenser by cooling water or air. Consequently, in the cycle process, the condensate is led back to the evaporator.

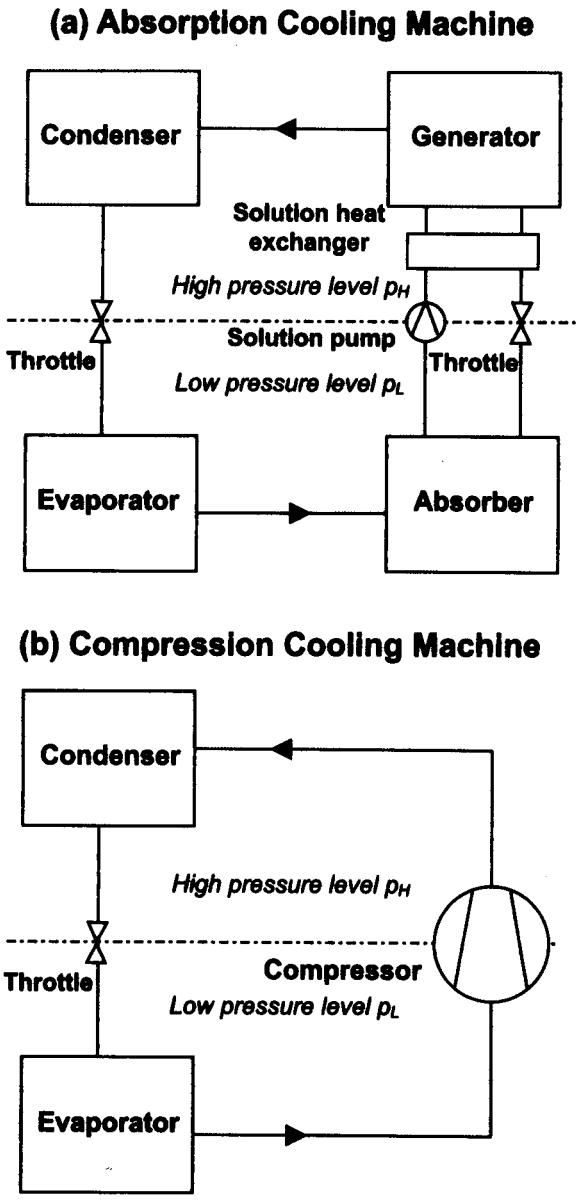

Figure 2.1: Comparison of the principles of an Absorption-Cooling Machine (a) by Carré (1859) and a Compression Cooling Machine (b).

1899 H. Geppert is the first to propose the introduction of an auxiliary inert gas (non condensable gas) into the absorption cooling cycle of Carré and with that, a third cycle, the so-called auxiliary gas cycle. By the heat input to the generator, this kind of gas is first displaced out of the generator and after that out of the condenser. It is assembled inside the evaporator and the absorber, where its partial pressure compensates for the pressure difference between generator and absorber and between condenser and evaporator. This special kind of Absorption Cooling Machine is called a Diffusion-Absorption Cooling Machine (DACM).

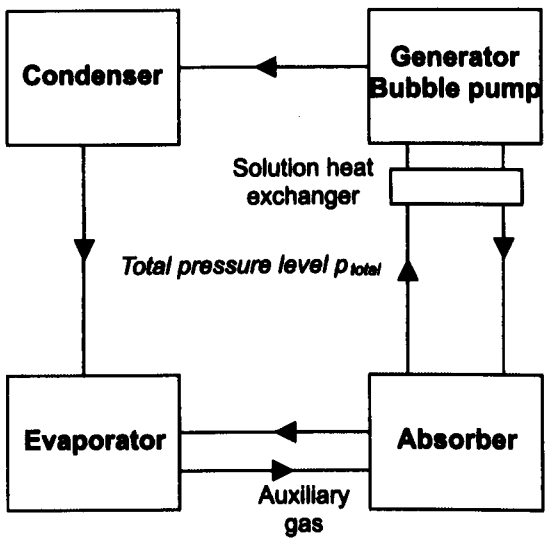

Figure 2.2: Principal of a Diffusion-Absorption Cooling Machine by Geppert (1899).

The throttles for the pressure compensation and the solution pump were removed because the whole unit now had the same total pressure p_{total} (Figure 2.2). Geppert suggested using air as inert gas, but the coefficient of performance (COP) that he reached was too low for commercial use.

This had two reasons; the first one is that the diffusion of ammonia into air is very slow so that only a very small cooling capacity could be achieved. The second and most important reason is that the gas mixture of air and ammonia is less dense than air alone and because of this it was not possible to get an automatic thermosyphon circulation of the gas mixture. For these reasons,

Geppert had to use a mechanical device e.g. auxiliary propeller or ventilator for the circulation of the gas cycle (Niebergall, 1981; Herold *et al.*, 1996).

1922 The two Swedish engineers Baltzar von Platen and Carl G. Munters picked up on the idea of a DACM with pressure compensated auxiliary gas and no mechanically moving parts without knowledge of Geppert's proposal. They suggested hydrogen (H_2) as auxiliary gas and at first they also reached low COP's. Hydrogen alone is lighter than the gas mixture of ammonia and hydrogen, and with this mixture an automatic thermosyphon circulation is possible.

With the use of a gas heat exchanger between evaporator and absorber (Figure 2.3), von Platen and Munters could clearly reduce the cooling losses in the auxiliary gas cycle and with that they reached higher COP values. Consequently, the Diffusion Absorption Cooling technology was interesting for commercial use e.g. for absorption refrigerators. Later, Helium (He) was also used as auxiliary gas.

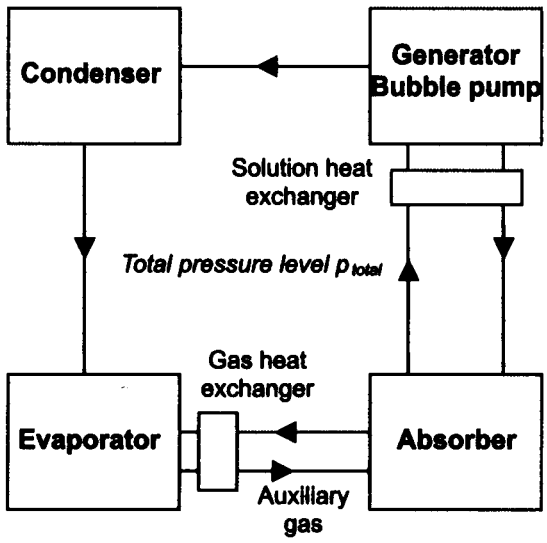

Figure 2.3: Principal of a Diffusion-Absorption Cooling Machine by Platen-Munters (1922).

The company Electrolux AB, Sweden (today Dometic AB) brought out the first refrigerator in 1925 (Niebergall, 1981). Another company Servel Inc. in Evansville, USA (today Robur SpA, Italy) produced the Refrigerators with small capacity under license starting in the 1930s and later, according to their own design. Servel developed and produced a gas driven heat pump in 1937. This DAHP was water-cooled and the auxiliary gas used was hydrogen. The unit had a COP of 0.192 with a cooling capacity of 1.75kW and a heating capacity of 9.12kW (Plank *et al.*, 1960; Creatherm, 1987).

1945 The company Carrier Corp, USA developed and introduced the first large commercial single-effect ACM with the working fluid water/lithium bromide (H_2O/LiBr), in which the water was the refrigerant and the lithium bromide was the absorbent. In contrast to the ammonia/water ACM with its pressure levels above the ambient pressure, the water/lithium bromide ACM works in vacuum pressure levels because of the refrigerant water. The principal components of the water/ lithium bromide ACM (Figure 2.4) are the same as of the ammonia/water ACM (Figure 2.1a).

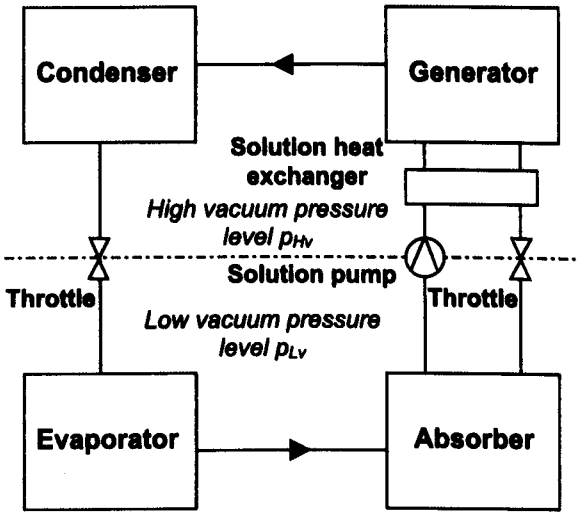

Figure 2.4: Principal of a Absorption Cooling Machine by Carrier (1945).

The first Carrier machine had a cooling capacity of 523kW and was installed by the company Sealright Corporation, Fulton, N.Y. (Hartmann, 1992).

1964 The company Kawasaki Heavy Industry Co., Japan introduced the first double effect ACM (Figure 2.5) with the working fluid water/lithium bromide (H_2O/LiBr) to the public (Hartmann, 1992). The double-effect ACM had two stages of generation: high-stage generator 1 and low-stage generator 2, to separate the refrigerant from the absorbent. The temperature of the heat source required to drive the high-stage generator must be higher than that used for a single-effect ACM.

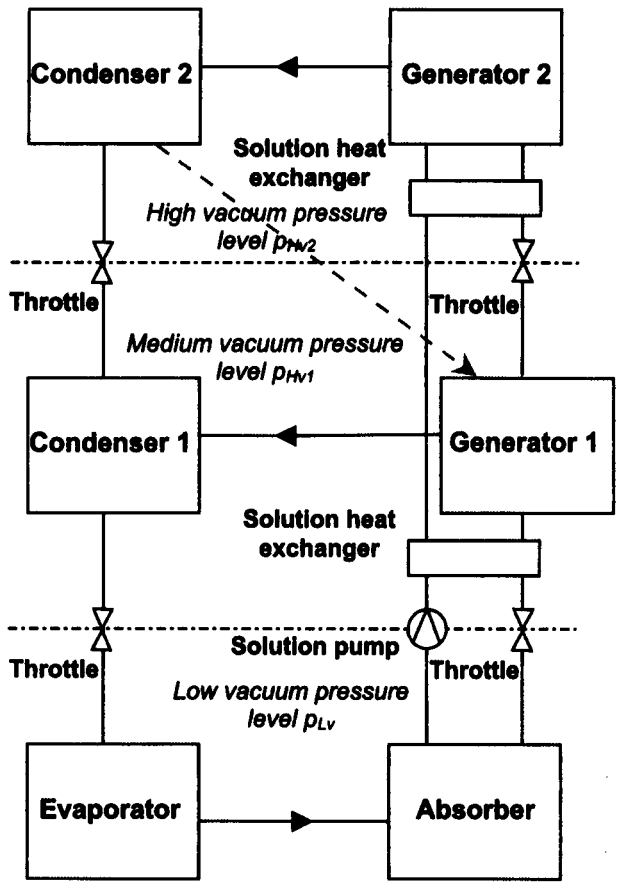

Figure 2.5: Principal of a double-effect Absorption Cooling Machine (1964).

2.2 WORKING PAIRS

This chapter describes the common working pairs of closed, continuous absorption cycles and with that the advantages or disadvantages of them. The open absorption cycles and the closed, periodical absorption cycles are not subject matter of this work.

For the cold production through ACMs, a two-component mixture is used which consists of a refrigerant and an absorbent. Principally, the absorbent should have a high affinity for the refrigerant and, in comparison to the refrigerant, a higher boiling point. With these characteristics the refrigerant can be well absorbed and simply desorbed. The current commonly used working pairs are water/lithium bromide (H_2O/LiBr) for air-conditioning and ammonia/water (NH_3/H_2O) for refrigeration. Water and ammonia respectively are used as refrigerant and the salt lithium bromide and water respectively as absorbent. Both refrigerants are environmental friendly and due to the greenhouse effect, they are classified as neutral.

2.2.1 WATER/LITHIUM BROMIDE

The advantages of water/lithium bromide are that water as refrigerant has a very high specific evaporation enthalpy of 2256kJ/kg and that the lithium bromide solution is not volatile. The working pair itself is odourless and neither toxic nor flammable. The disadvantages are that the freezing point of water is fixed and lithium bromide is not unlimitedly dissolvable in water because of the crystallisation line (Figure 2.6). Moreover, the vacuum for the machines requires a very high tightness. Due to the high specific volume of water vapour as refrigerant, the compactness of the machines is limited.

For the operation of a water/lithium bromide ACM, the thermodynamic characteristics of the refrigerant water set the possible temperature range. The freezing point of water is at 0.0°C, the boiling point temperature is 100°C at

1x10^{5}Pa pressure and the critical temperature of the water vapour is 375.3°C. For preliminary investigations and comparisons the pressure-temperature diagram with isosteres (lines of constant mass fraction) in the log p, -1/T-diagram (Figure 2.6) is very helpful. Herewith it is possible to determine the specific solution circulation and consequently the respective solution concentrations by defining e.g. the condenser and evaporator temperatures and pressures respectively.

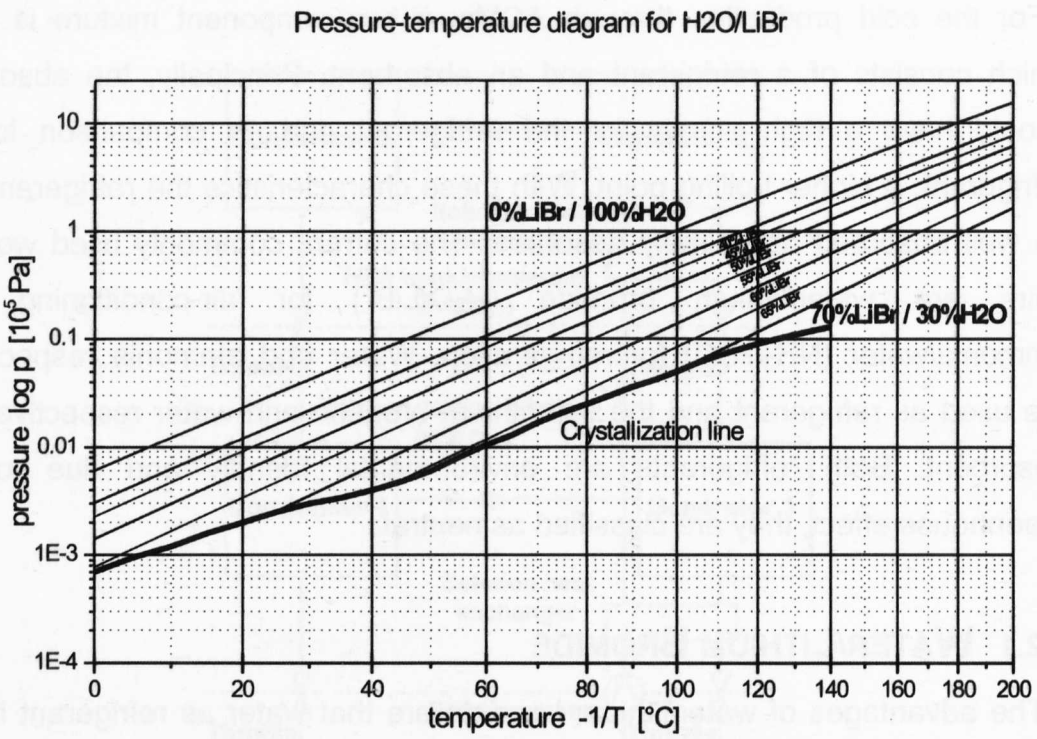

Figure 2.6: Pressure-temperature diagram for water/lithium bromide due to the absorbent mass concentration (Dühring plot).

For pure water (X = 0%) the vapour pressure is calculated with the equation (2.1) from Lansing (Lansing, 1976), which depends only on the temperature T [°C] and is converted by the author into pressure p [Pa].

$$\log_{10} p = \left(9.980203 - \frac{1555}{(T + 273.15)} - \frac{112414}{(T + 273.15)^2} \right) \qquad (2.1)$$

The further calculation of the pressure for different LiBr mass concentrations is done with the equation (2.2), which is also converted by the author into p [Pa], and the dew point temperature TD [°C] (2.3) for H_2O/LiBr solutions according to Kaita (Kaita, 2001) for temperatures T [°C] ranges between 0°C and 210°C and solution mass concentrations X [%] due to the absorbent lithium bromide of 40% up to 70%.

$$\log_{10} p = \left(10.05 - \frac{1603.54}{(TD + 273.15)} - \frac{104095.5}{(TD + 273.15)^2} \right) \tag{2.2}$$

$$TD = \sum_{i=0}^{2} \left[\sum_{j=0}^{3} A_{ij} \cdot (X - 40)^j \right] \cdot T^i \tag{2.3}$$

Table 2.1: Coefficients for the dew point temperature TD (Kaita, 2001).

j	A_{0j}	A_{1j}	A_{2j}
0	-9.133128 E 0	9.439697 E-1	-7.324352 E-5
1	-4.759724 E-1	-2.882015 E-3	-1.556533 E-5
2	-5.638171 E-2	-1.345453 E-4	1.992657 E-6
3	1.108418 E-3	5.852133 E-7	-3.924205 E-8

The water/lithium bromide ACM's are usually water-cooled by wet cooling towers to avoid the possibility of a crystallisation of the solvent lithium bromide (Chinnappa, 1992). When water is used as refrigerant, the evaporator temperature is restricted to temperatures above the freezing point of at least +5°C. Therefore the possible temperature range of such machines is limited to pure air-conditioning and therefore they are exclusively used for cold water generation.

Further equations for the calculation of the properties of H_2O/LiBr solutions e.g. as solution or vapour enthalpies can be found in (Lansing, 1976; Hellmann *et al.*, 1996; Kaita, 2001).

2.2.2 AMMONIA/WATER

The advantages of ammonia/water as a working pair are the high affinity, the high stability and an environment-friendly refrigerant. There is no vacuum required for evaporator temperatures above -30°C. Moreover, the refrigerant ammonia has a high specific evaporation enthalpy of 1370kJ/kg, it is lighter than air and a compact construction is possible i.e. through plate heat exchangers.

The disadvantages are the high refrigerant operating pressure (up to $25x10^5$Pa) due to the condensation temperature, causing the production costs of the machines to be higher than those of the water/lithium bromide units. Because of the volatility of the absorbent by the desorption a rectification through a dephlegmator/rectification column is necessary due to the small boiling point distance between ammonia and water of 133K at $1x10^5$Pa pressure (Fig. 2.7). The refrigerant ammonia is corrosive i.e. in connection with copper and copper based alloy, has a very unpleasant odour and is toxic.

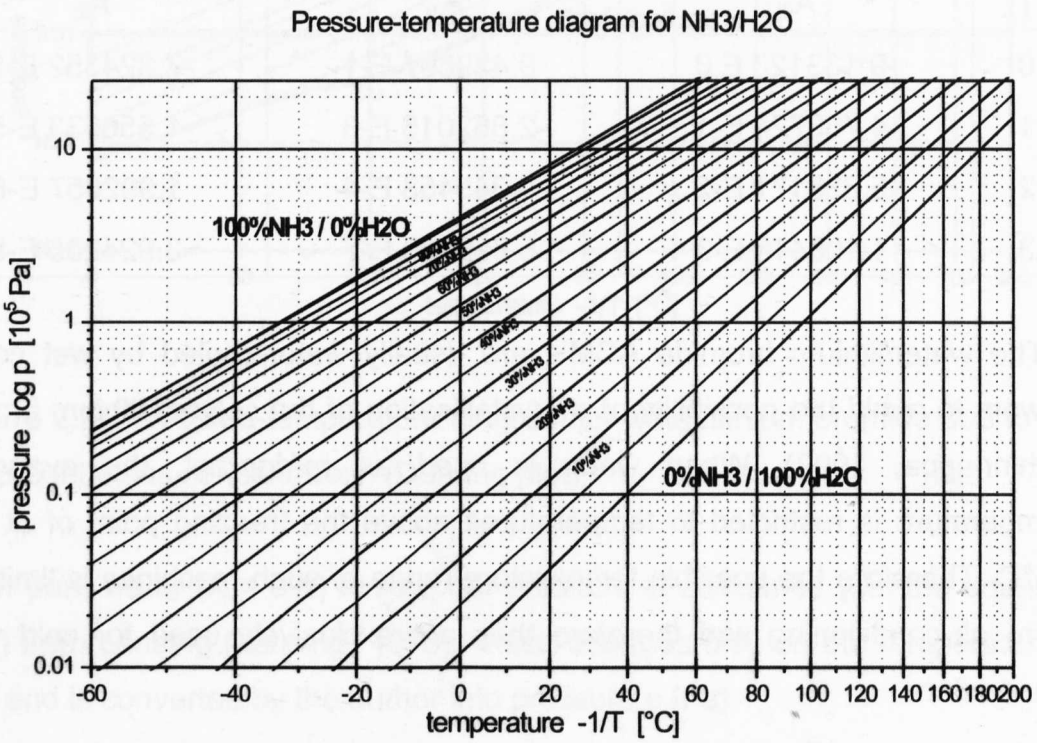

Figure 2.7: Pressure-temperature diagram for ammonia/water as function of refrigerant mass concentration (Dühring plot).

The thermodynamic properties of the refrigerant ammonia also determine the operation temperature range of the ammonia/water ACM. The critical temperature of the refrigerant ammonia is 132.4°C. Ammonia has a low freezing point at -77.7°C and the boiling point temperature is -33.3°C at $1x10^5$Pa pressure.

The plotted pressure-temperature log p -1/T-diagram (Figure 2.7) is calculated with the equation (2.4) which is based on the Clausius-Clapeyron equation. With this equation the pressure p [Pa] is calculated for NH_3/H_2O solutions according to Bourseau (Bourseau et al., 1986) for temperatures T [°C] between -60°C and 200°C and solution mass concentrations X [-] referred to the refrigerant ammonia from 0% up to 100%.

$$\log_{10} p = \left(\frac{(10.44 - 1.767\,X + 0.9823\,X^2 + 0.3627\,X^3)}{-\dfrac{(2013.8 - 2155.7\,X + 1540.9\,X^2 - 194.7\,X^3)}{(T + 273.15)}} \right) \qquad (2.4)$$

The ammonia/water ACMs are able to be air-cooled for air-conditioning applications but usually they are also water-cooled (Chinnappa, 1992). By using ammonia as a refrigerant, the evaporator temperature could be lower, even down to -60°C. With that, the temperature range of the machines is suitable for air-conditioning and for industrial refrigerant processes i.e. for the chemical industry.

The further equations for the thermodynamic properties of NH_3/H_2O e.g. vapour concentration or enthalpy are given in (Jain *et al.*, 1971; Kaushik, 1983; Pátek *et al.*, 1995; Hellmann *et al.*, 1996). The equations of Kaushik, Jain and Gable respectively are described in chapter 3.3 and used in this work.

2.3 MULTISTAGE CYCLES

Absorption cooling machines are categorised either by the number of effects or by the number of lifts:

"Effects" refers to the number of times the input heat is used by the absorption machine, either directly or indirectly. In general, the effect stage is used to increase the COP which means to raising the driving heat temperature.

"Lifts" refers to the number of evaporator/absorber pairs at different temperatures in an absorption machine and with that the frequency of the heat input supply for one refrigerating use. The lift stage is used for the reduction of the heat input temperature level.

The most important restrictions of single-effect absorption cooling machines are the limitation of the temperature lifting through the solution field, the fixed coupling of the driving temperature with the temperature of heat source and heat sink and the COP not being larger than 1.0 which is independent from the temperature lifting (Ziegler, 1998c). The aim of multistage processes is to overcome these restrictions.

For several years, two fundamental types of absorption cooling machines have been available on the market: single-effect (SE) and double-effect (DE) ACMs with the working pair water/lithium bromide as well as single-effect (SE) and double-lift (DL) ACMs with the working pair ammonia/water. In the first case, (DE) through the two stages, the COP of the unit is increased, whereas in the second case (DL), the temperature lifting is increased due to the ratio of the driving temperature. The single-effect/double-lift (SE/DL) cycle with the working pair water/lithium bromide which is a superposition of the double-lift cycle with a single-effect cycle is a novel technique.

Further cycle designs such as triple-effect (TE) ACM and other multistage cycles as well as additional descriptions for the use of the described cycles for solar cooling are given in (Kimura, 1992; Lamp *et al.*, 1997; Höper, 1999; Ziegler, 1999; Srikhirin *et al.*, 2001; Schweigler, 2004).

2.3.1 SINGLE-EFFECT CYCLE

The four main components of a single-effect (SE) ACM are the generator, to which the driving heat is transferred and used only once, the evaporator, where cooling or refrigerating is provided and the absorber and condenser, from which the cooling heat is disposed of (Figure 2.8).

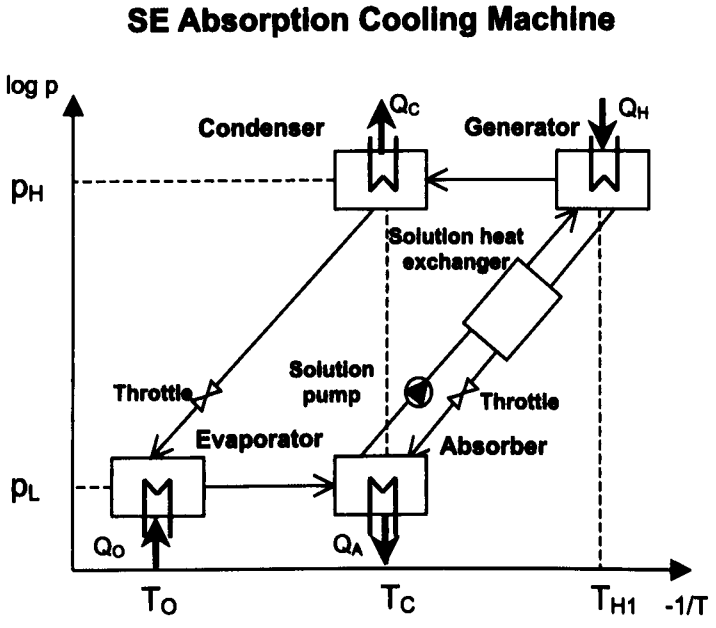

Figure 2.8: Single-effect (SE) ACM cycle in the log p -1/T diagram.

In the generator, vapour is desorbed from the ammonia/water or water/lithium bromide solution due to the heat input. The refrigerant vapour is condensed in the condenser, throttled and evaporated. After evaporation, the vapour is absorbed in the solution which is cooled in the absorber. The solution is pumped to the generator by a solution pump where it is regenerated and throttled back to the absorber. A solution heat exchanger (SHX) is inserted into the solution cycle to improve the COP.

2.3.2 DOUBLE-EFFECT CYCLE

The double-effect (DE) ACM is equipped with a second generator and condenser to increase the overall COP by indirectly using the input heat a second time for generator 1 (Figure 2.9).

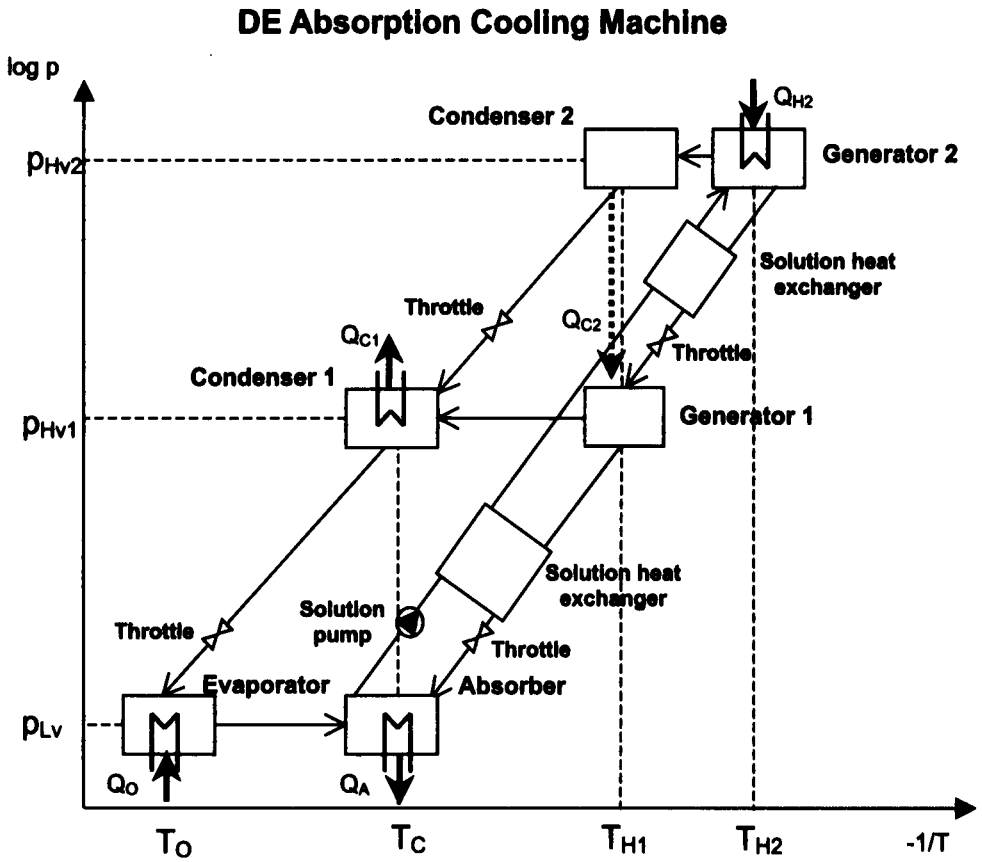

Figure 2.9: Double-effect (DE) ACM cycle in the log p -1/T diagram.

The high-stage generator 2 uses heat supplied by an outside process at the appropriate pressure of the condenser 2 p_{Hv2}. The heat from the refrigerant vapour off the high-stage generator 2 is then used internally to evaporate the refrigerant out of the solution in the low-stage generator 1 a second time at middle pressure level p_{Hv1}. This heat transfer is accomplished by passing the high-stage refrigerant vapour through a tube bundle in the low-stage generator 1. The heat transfer from the high-stage refrigerant vapour to the low-stage solution causes condensation of the high-stage vapour refrigerant.

Cooling water requirements for a double-effect ACM are less than those for a single-effect ACM because the heat of condensation for the refrigerant vapour from the high-stage generator 2 is used to desorb the refrigerant from the solution in the low-stage generator 1 (Dorgan *et al.*, 1995).

2.3.3 DOUBLE-LIFT CYCLE

The basic idea of a double-lift (DL) ACM is to repeat the evaporation-absorption process at different temperatures, which is a different idea as compared to the single-effect cycle (Figure 2.10).

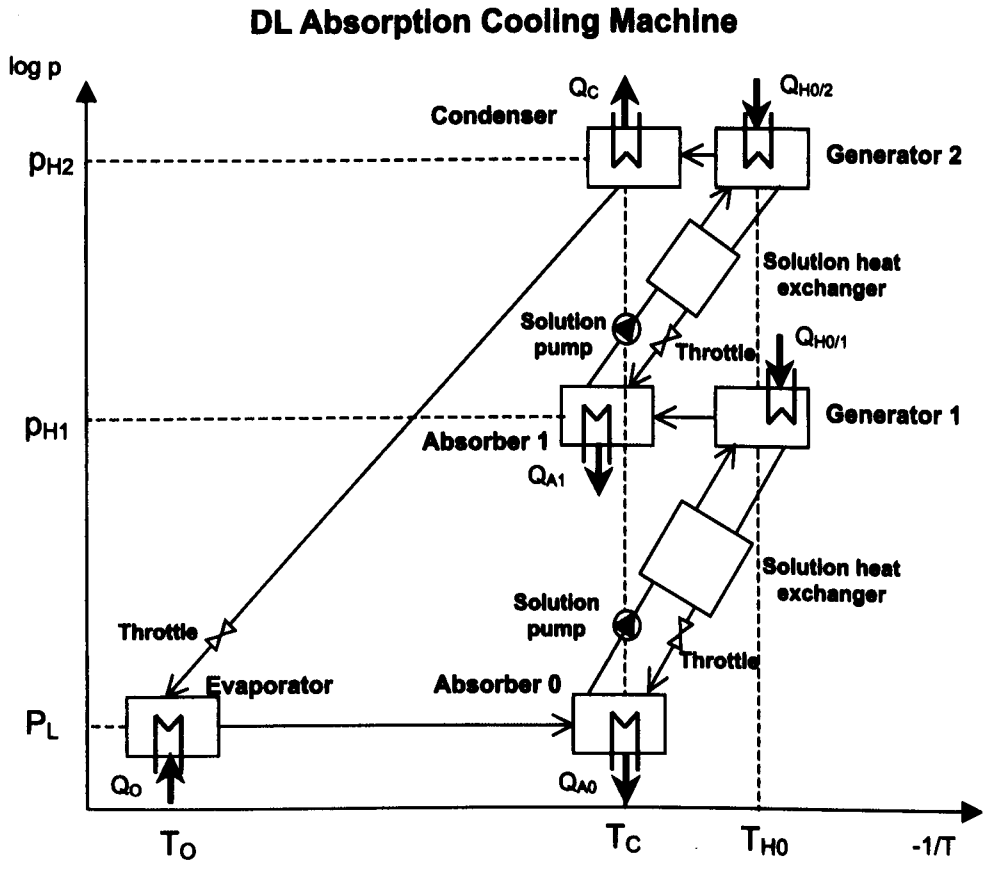

Figure 2.10: Double-lift (DL) ACM cycle in the log p -1/T diagram.

For this, a second absorber and generator is introduced into the system. The refrigerant vapour is produced first in generator 1 at an intermediate pressure level p_{Hv1} and resorbed once more by absorber 1 in a second solution circuit.

The second regeneration is done at the appropriate pressure of the condenser p_{H2}. The effect is that both regeneration steps in the generator 1 and generator 2 take place at a reduced driving heat temperature compared to a single-effect ACM. For this reason, the COP is lower than of a single-effect ACM.

2.3.4 SINGLE-EFFECT / DOUBLE-LIFT CYCLE

The single-effect/double-lift (SE/DL) ACM has been designed for producing chilled water in district heating networks. Based on the double-lift cycle a third generator and solution heat exchanger was introduced that formed an integrated single-effect cycle (Figure 2.11). Herewith it is possible to couple the heat input at three different temperature levels, guaranteeing a large cool-down of the heat input.

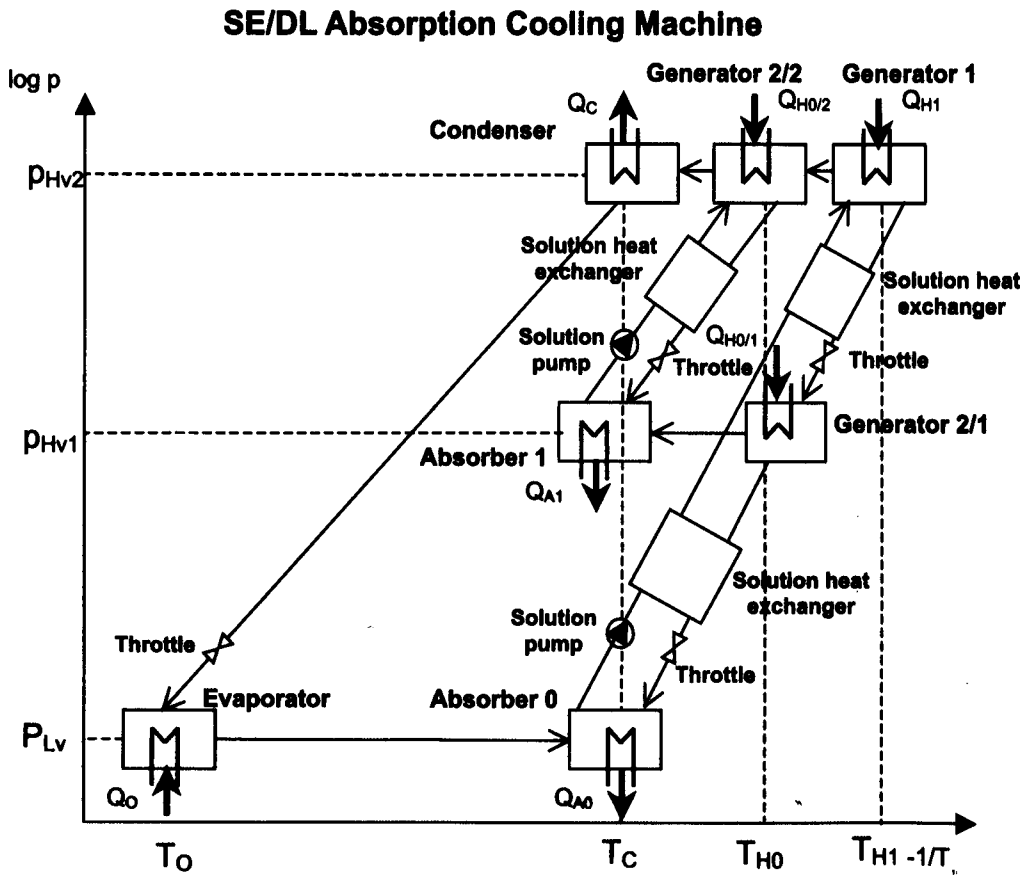

Figure 2.11: Single-Effect/Double-lift (SE/DL) ACM cycle in the log p -1/T diagram.

The district heating water releases heat first in generator 1 of the single-effect stage and then in the two generators, generator 2/1 and generator 2/2, of the double-lift stage, leading to the high temperature spread. The boundary conditions are, in general, low heat input temperatures of the district heating water supply and a high temperature spread between supply and return of about 20K to 30K (Schweigler *et al.*, 1997; Schweigler, 1999).

2.4 PERFORMANCE

The performance characteristics for the closed ACM cycles described above and the DAR/DACM cycle are stated in the table (2.2) for water/lithium bromide and in the table (2.3) for ammonia/water.

Table 2.2: Performance of H_2O/LiBr Absorption Cooling Machines.

	ACM H_2O/LiBr	**ACM H_2O/LiBr**	**ACM H_2O/LiBr**
multistage cycle	SE	DE	SE/DL
refrigerant	water	water	water
absorbent	lithium bromide	lithium bromide	lithium bromide
cooling agent	water	water	water
refrigerant output temp.	6°C – 20°C	6°C – 20°C	6°C – 20°C
heat input temperature	80°C – 110°C	130°C – 160°C	80°C – 100°C
cooling input temperature	30°C – 35°C	30°C – 35°C	30°C – 35°C
COP	0.5 – 0.7	1.1 – 1.3	0.4 – 0.7

Table 2.3: Performance of NH_3/H_2O Absorption and Diffusion-Absorption CMs.

	ACM NH_3/H_2O	**ACM NH_3/H_2O**	**DAR / DACM $NH_3/H_2O/H_2$ or He**
multistage cycle	SE	DL	SE
refrigerant	ammonia	ammonia	ammonia
absorbent	water	water	water
auxiliary gas	-	-	hydrogen/helium
cooling agent	water-glycol	water-glycol	water-glycol
refrigerant output temp.	-30°C – 20°C	-50°C – 20°C	-20°C – 20°C
heat input temperature	100°C – 160°C	55°C – 65°C	100°C – 140°C
cooling input temperature	30°C – 50°C	30°C – 35°C	30°C – 50°C
COP	0.4 – 0.6	0.4	0.1 – 0.2 / 0.5

By using the condensation heat, the performance figure can be clearly improved for water/lithium bromide absorption chillers from approximately 0.7 for single-effect (SE) processes to 1.3 for double-effect (DE) absorption chillers and 1.7 for triple effect (TE) as shown in Figure 2.12.

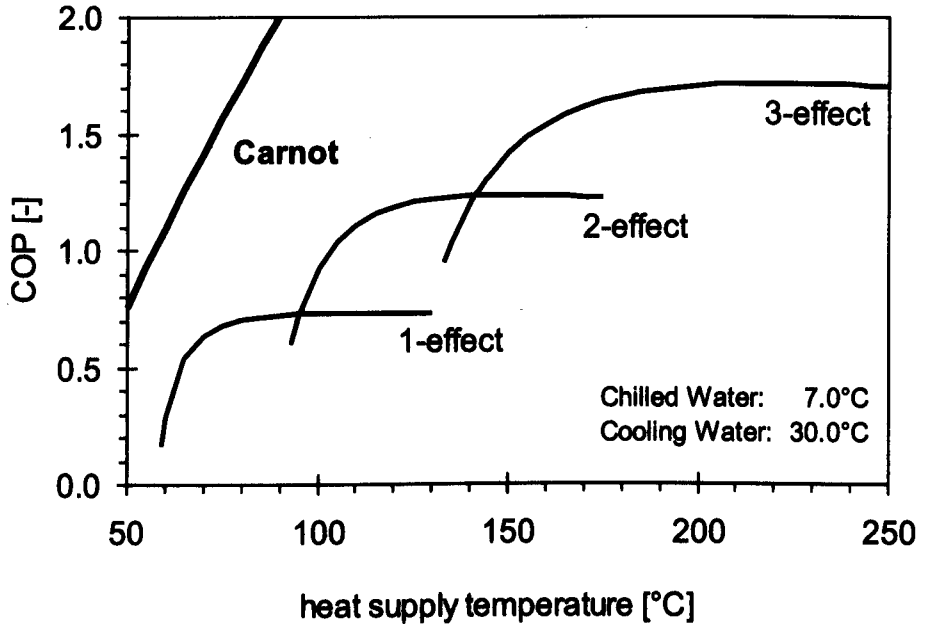

Figure 2.12: Comparison of coefficients of performance (COP) for multi-effect water/lithium bromide absorption chillers (Grossmann, 2002).

With the ammonia/water absorption chillers, the COP is approximately 0.6 for single-effect (SE) cycles and reduces to 0.4 for double-lift (DE) because of the reduced driving heat temperatures. The COP of the DAR with the auxiliary gas however, is much lower: between 0.1 and 0.2 maximum. In comparison, the COP of the DACM is approximately 0.5.

2.5 SOLAR COOLING

2.5.1 HISTORY

In the seventies of the 20th century, the company Arkla Industries Inc. in Evansville, USA (now owned by Robur SpA, Italy) developed the first commercial, indirectly driven, single-effect H_2O/LiBr ACM for solar cooling with two different nominal cooling capacities. The first one was the "3-TR Solaire" or "Solaire 36" unit with 10kW and the other was the "Solaire" unit and had a 75kW cooling capacity. The driving heat temperatures were in the range of 90°C and the cooling water temperature was 29°C for 7°C cold water temperature. The machine was installed in demonstration projects more than 100 times in the USA (Loewer, 1978; Lamp *et al.*, 1997; Grossmann, 2002).

At the End of the seventies, Arkla and also Carrier Corp., USA developed a small size single-effect H_2O/LiBr ACM that could work with air cooling. There was no market success mainly due to the high investment costs for solar cooling. Carrier Corp. further decreased the driving temperature of a water-cooled single-effect H_2O/LiBr ACM by using a falling film generator with a large surface area. The driving heat temperature was 82°C and the cooling water temperature was 28°C for 7°C cold water temperature (Lamp *et al.*, 1997). The production of these ACMs was stopped and the technology's licence was given to the Japanese company Yazaki. Up to the beginning of the nineties of the 20th century, the company Yazaki offered H_2O/LiBr ACMs with 5kW to 10kW cooling capacities, e.g. the WFC-600 with 7kW, which were used for solar cooling projects. Due to the missing demand, the production was also stopped.

At the beginning of the eighties of the 20th century, Arkla developed a double-effect H_2O/LiBr ACM in which the lower generator was supplied with solar energy and thus as the temperature of the single-effect cycle, while in fossil mode the double-effect generator was fired using the higher COP. Due to the lack of demand on the market for solar cooling, the production of this cooling

machine was stopped and the technology was also licensed to the Japanese company Yazaki. They sold the machines for several years, but they are no longer available today (Lamp *et al.*, 1997).

2.5.2 PROJECTS H2O/LIBR SE ACM

The following is a presentation of selected past and current international projects which consist of partly solar assisted or complete solar powered water- or air-cooled single-effect water/lithium bromide Absorption Cooling Machines. A general view of some old H_2O/LiBr ACM projects before 1979 are extensively presented in (Loewer, 1978).

2.5.2.1 WATER-COOLED MEDIUM-SIZED SE ACMs

In the medium-sized performance range, the most project experiences for solar cooling over several years exist up to now for the single-effect water/lithium bromide ACM WFC-10 from the company Yazaki, Japan with a cooling capacity range of 35kW to 46kW. In spite of the experiences gained in operation over the last ten years, there are hardly published, measured COPs, but the operation is generally rated as dependable and unproblematic.

An early solar cooling project involved the cooling of a **winery** of the Groupement Interproducteurs du Cru **Banyuls** in southern France, started in August 1991. The wine cellar is operated by a Yazaki WFC-15 with 52kW cooling capacity and 130m² vacuum tube collectors (VTC) with an only 1.0m³ hot-water storage tank. The operating heating input temperature T_h is 80°C and the reached COPs are about 0.57 and 0.58 (Eicker, 2002; Quinette *et al.*, 2002).

The **Hotel Belroy** in Benidorm, Spain is also an early project where a 125kW, H_2O/LiBr single-effect ACM has been used since 1992. 344.5m² vacuum tube collectors and three hot-water storage tanks with each 12m³ were installed for the required heat input. The ACM reached COPs between 0.5 and 0.6 at temperatures of T_h 96/86°C, T_c 29/36°C and T_o 14/9°C (Hansen, 1993a; Hansen, 1993b).

One other project is the air-conditioning of the **office building** of the company J. **Wollferts** GmbH in Cologne-Porz, Germany which has been in operation since August 1995. Two solar driven 46kW WFC-10 ACMs are installed for an air-conditioned surface over four floors of 1628m² and are powered by 176m² VTCs at driving heat temperature T_h 95/88°C, cooling water temperature T_c 29/35°C and chilled cooling agent temperature T_o 22/16°C. A 5.0m³ cold water storage tank as buffer was also installed (Ohn, 1995; Karbach *et al.*, 1997; Karbach 1998).

A further project is the **office building** of the company **Ott & Spieß** in Langenau, Germany (started in 1998) with a 35kW ACM (probably a Yazaki WFC-10 as well) which is driven by 30m² vacuum tube collectors. A 2.0m² hot-water storage tank and a 1.0m³ cold-water buffer tank are also installed. The operation parameters are T_h 76/71°C, T_c 24/29°C and T_o 17/13°C at a COP of 0.73 (Mößle, 2000; Henning, 2001).

Two further projects are located in Berlin, Germany, each with two solar assisted ACMs which have been in operation since the year 2000. In the **administrative building** of the German Federal Information Ministry (**BPA**) there are two 44kW WFC-10 ACMs installed with a COP of 0.73, assisted by 230m² vacuum tube collectors and 1.6m³ hot-water storage tanks with the operation parameters T_h 88/82°C, T_c 26/32°C and T_o 16/10°C.

The second **administrative building** is the German Federal Ministry of Traffic, Building and Housing (**BMVBW**). Here there are also two solar assisted, single-effect WFC-10 ACMs installed, each with a 42kW cooling capacity and a COP of 0.73. The solar heat is produced by 210m² high-performance flat plate collectors (FPC) and stored by 6.0m³ hot-water storage tanks. There is also a 0.5m³ cold-water storage tank for the chilled water. The operation parameters are T_h 88/82°C, T_c 27/35°C and T_o 18/12°C (Albers, 2002).

The **M+W Zander** Holding AG built an **office and production building** in Weilimdorf, Germany and installed a single-effect ACM with a nominal 650kW cooling capacity and 360m² vacuum tube collectors for a solar assisted cooling system which has been in operation since 2000. The operation temperature ranges are T_h 65°C to 95°C, T_c 22/27C to 27/32°C and T_o 12/8°C to 21/15°C (Wolkenhauer *et al.*, 2001)

Further commercial applications since 2001 include the **Hotel Rethymno Village** in Greece where a 105kW H_2O/LiBR ACM is installed. 500m² flat plate solar collectors and also seven hot-water storage tanks with total 10.0m³ are used for the heat source.

An additional hotel project is the **Hotel Olympic II** in Greece where also a 105kW ACM has been running since 2001. There are 450m² FPCs and five hot-water storage tanks with total 5.0m³ installed. (Balaras, 2003).

Another project is the **office building** of the company **Viessmann** in Madrid, Spain where a single-effect Yazaki WFC-30 ACM with a 105kW cooling capacity and 105m² FPCs is installed (Schibel, 2002). Operation start and current operating results are not known.

A new project is the reconstructed **office building** - the **EAR Tower** in Pristina, Kosovo where two WFC-10 ACMs each producing 45kW of cooling capacity which have been in operation since 2003. They are solar driven by 227m² FPCs at operation temperatures of T_h 87/77°C, T_c 25/31°C and T_o 13.5/8.5°C and a COP of 0.7. A 4.0m³ hot-water and a 1.0m³ cold-water storage tank are used (Holter *et al.*, 2003; Meißner *et al.*, 2004a).

The project of an **office building** at **Basse Terre**, Guadeloupe with a 30kW ACM (probably a Yazaki WFC-10 as well) and 61.2m² VTCs has also been in operation since 2003. The heating input temperature T_h is 85°C-95°C at a cooling input temperature T_c of 24°C and T_o 12/7°C at a COP of 0.7. 570m² floor area are cooled by a solar powered system which also consists of a small

hot-water buffer tank (less than 0.1m³) and a normal cold-water storage tank (Henning, 2004).

Further projects are a 35kW SE ACM with 70m² VTC's in **Perpignan**, France (Eicker, 2002) and an SE ACM with 35kW cooling capacity and 60m² collectors at the **CSTB** in Valbonne, France (Eicker, 2002). Both ACMs are probably Yazaki WFC-10 units. More details about these projects are not yet known.

2.5.2.2 WATER-COOLED SMALL-SIZED SE ACMs

After the experiences made in the seventies of the 20th century with the small-scaled performance range systems from Arkla (see chapter 2.5.1), there were once again some projects carried out with in principal, newly developed small-scale ACMs.

Since 1999/2000 there has been a 7kW H_2O/LiBr ACM Yazaki WFC-600 installed for **laboratory and office** cooling at **ZAE Bayern** in Garching, Germany. The driving heat is produced by 19.6m² VTC's and stored in two 0.6m³ hot-water storage tanks. The operation characteristics of the ACM are T_h 88°C and T_o 16/14°C with a COP of 0.6 (Egger, 2000).

A newly developed, single-effect H_2O/LiBr ACM from PHÖNIX with a 10kW cooling capacity was installed for a first field test at an **office building** in **Berlin Treptow**, Germany on August 2003, providing 152m² of cooled office space. The ACM is driven alternately with 42m² FPC or 25m² VTC and a 0.75m³ hot-water buffer tank is also installed. The nominal operation temperatures are T_h 72/62°C, T_c 27/35°C and T_o 18/15°C and the COP ranges between 0.76 and 0.82 (Storkenmaier *et al.*, 2003; Kohlenbach *et al.*, 2004a; Kohlenbach *et al.*, 2004b).

Further field tests, each based on the EAW 15 kW H_2O/LiBr ACM Wegracal SE 15, have been carried out since the summer of 2003. The first field test is at a **sales store** in **Neumarkt**, Italy were 55m² flat plate collectors and a 0.75m³

hot-water storage tank are used as heat sources for the ACM which was reduced to a 10kW cooling capacity to limit the required collector surface. Operation data is not yet available.

The second field test is being performed at the **technology centre TZ Köthen**, Germany in **office cooling** with 77m² vacuum tube collectors. The determined operation parameters are T_h 90/80°C, T_c 32/38°C, T_o 21/15°C and an average COP of 0.5. Within the system, there is also a paraffin latent heat storage with a melting temperature of 90°C, a 0.5m² conventional hot-water storage tank and a 0.2m³ cold-water buffer tank (Safarik *et al.*, 2004).

A further EAW H_2O/LiBr ACM has been used since 2003/2004 for a **laboratory test stand** at the Technical University of Ilmenau, **TU Ilmenau**, Germany. This test cooling machine however, has a reduced cooling capacity of 10kW. The ACM is driven by 10m² flat plate collectors and a 2m³ hot-water buffer tank. The nominal data of operating temperatures are T_h 85/75°C, T_c 30/35°C and T_o 14/8°C. The reached COPs are about of 0.4 (Ajib *et al.*, 2004).

2.5.2.3 AIR-COOLED SE ACMs

There are only a few laboratory prototypes of air-cooled, SE water/lithium bromide ACMs. One of which is described below.

A **prototype** of an air-cooled H_2O/LiBr absorption chiller can be found at the **University Polytechnic of Catalonian**, Terrassa, Spain. The unit has measured cooling capacities of 1.2kW to 1.8kW and COPs from 0.3 to 0.5 for input temperature T_h 75-95°C, input cooling air T_c 32°C and input chilled water T_o 20°C (IEA, 2002a; Castro, 2003).

2.5.3 PROJECTS H2O/LIBR DE ACM

The following described projects are a selection of old and current partly solar-assisted or complete solar-powered, water-cooled, double-effect water/lithium bromide Absorption Cooling Machines. Some of the older projects are no longer in operation.

2.5.3.1 WATER-COOLED MEDIUM-SIZED DE ACMs

Tanaka introduced a single-double-effect H_2O/LiBr ACM that works in double-effect by using fuel at a higher COP and in single-effect using solar energy. Two ACMs with 20kW (DE) / 30kW (SE) cooling capacity and COPs of 1.1(DE) / 0.6(SE) are installed in the **office building** Energy Engineering Department of **Oita University** in Kyushu, Japan and at the **Kabe Office Building** of the Chugoku Electric Company in Hiroshima, Japan. (Kimura, 1992).

The American company Solargenix Energy, LCC (formerly Duke Solar Energy, LCC) has had a **commercial building** project in **Sacramento**, California, USA since 1997, where a double-effect McQuay ACM with a 70kW cooling capacity and a COP of 1.1 to 1.2 is used, which is driven by 200m² of Integrated Compound Parabolic Concentrator (ICPC) vacuum tube collectors at 165°C heating temperature. These special VTCs are internal mirror coated (Duff *et al.*, 2003; Eicker 2004).

Solargenix Energy also developed a roof integrated system with a fixed parabolic reflector and tracking evacuated tube receiver and has been running a modified hot-water driven Yazaki 176kW double-effect ACM (probably replaced by Broad 174kW DE ACM) with a 930m² Power Roof tied by a 7.5m³ storage tank at a large commercial **office building** in **Raleigh**, North Carolina, USA since July 2002. The chiller has a COP of 1.23 (Gee *et al.*, 2003; Guiney *et al.*, 2003). Operation results for the ACM are not yet available.

Another current project of Solargenix Energy (since 2003), is the **municipal utility's building** at Sand Hill Power Plant control center in **Austin**, Texas,

USA. The solar system has a 360m² aperture area of non-evacuated CPC solar thermal collectors tied to a 9.5m³ pressurised thermal storage tank which drives a 95kW Yazaki hot-water, single-effect ACM. Further detailed operation data for the ACM are not available (Sklar, 2004).

A further current solar cooling project of the company, Solitem GmbH, Germany is the **Hotel Iberotel Sarigermepark** in Dalamen, southern Turkey. A steam fired, double-effect Broad ACM with a 140kW cooling capacity has been running since April 2004 by superheated steam which is produced by 180m² of newly developed parabolic trough collectors (PTC). The operation conditions are: for the saturated steam, $4x10^5$Pa at a temperature of T_h 144°C and a cooling water inlet temperature of 27°C. A COP of 1.3 could be reached (Lokurlu *et al.*, 2002; Krüger *et al.*, 2002).

Further projects are under construction or planned e.g. at the **Hotel Grand Kaptan** in Alanya, Turkey and at the **Hotel Iberotel** in **Ortaca**, Turkey (Solitem, 2004).

2.5.4 PROJECTS NH_3/H_2O SE ACM

The here represented old and present projects of solar powered water- or air-cooled single-effect ammonia/water Absorption Cooling Machines are mainly situated in Europe. Further NH_3/H_2O ACM projects before 1979 are comprehensively described in (Loewer, 1978).

2.5.4.1 WATER-COOLED SMALL-SIZED SE ACMs

One already terminated project, was the 12kW NH_3/H_2O SE ACM with flat plate collectors for a **laboratory test stand** at the Gradevinski Institute of the **University of Split**, Croatia which was installed in 1979. The unit was in operation for 200 hours and ran from July to September of 1979. The installed ACM reached a COP of 0.55 at temperatures T_h 80/76°C, T_c 25/33°C and T_o 12/6°C (Podesser, 1982).

At the **technology centre TZ Köthen**, Germany, a single-effect ammonia-water (NH_3/H_2O) ACM from ABB in the small-scale performance range with 15kW cooling capacity has been operated since 1998 to air-condition a 260m² **office space**. The ACM is driven by 77.3m² of vacuum tube collectors at working conditions of T_h 95/88°C, T_c 27/31°C, T_o 14/8°C and a COP's between 0.4 and 0.5. Moreover, the system consists of a 1.0m³ paraffin latent heat storage (melting temperature about 90°C), a 0.5m² conventional hot-water storage tank and a 0.2m³ cold-water buffer tank (Safarik *et al.*, 2002; Safarik *et al.*, 2003).

A further small-scale ACM project is the 20 kW NH_3/H_2O ABB ACM, which was installed in 2001 and began operating in September of 2002 at the Innovation Centre Wiesenbusch **IWG Gladbeck** in Gladbeck, Germany. The produced refrigeration is used to demonstrate comfort cooling, refrigeration for food preservation and also for a 1.0m³ ice storage. The driving heat T_h of 100/90°C is produced by 72m² of VTCs and thereby evaporator temperatures T_o down to -6°C are reached at a COP of 0.63 (Albring, 2001; Braun *et al.*, 2002).

A field test has been being carried out on a 10-17kW ammonia-water ACM developed by the Joanneum Research – Institut für Energieforschung and the company S.O.L.I.D. GmbH (both from Austria) which is installed at the **winery** Ing. J. **Peitler** in Schloßberg, Austria since the summer of 2003. The cooling system is used to refrigerate the winery. 100,8m² of flat plate collectors, 4,0m³ hot-water storage tanks and a 0.5m³ sole storage tank are parts of the solar cooling system which operates at T_h 100/85°C, T_c 25/35°C and T_o 8/3°C and at higher heating temperatures at T_o -10°C down to -15°C (Meißner *et al.*, 2004b).

2.5.4.2 AIR-COOLED SE ACMs

Only a few laboratory prototypes of air-cooled SE ammonia/water ACMs and components have been developed and set up until now. Some of these units are described below.

The **prototype** of the air-cooled, single-effect, NH_3/H_2O ACM from **AoSol**, Portugal and **INETI/IST**, Portugal is driven by 14.3m² of CPC vacuum tube collectors or gas. The ACM has a cooling capacity of 5-6kW at COPs between 0.54 and 0.62. The heating temperature is T_h 105-110°C and the evaporator temperature is T_o of 10°C (IEA, 2002b; Afonso, 2003).

The Technical University **TU Delft**, Netherlands developed a **prototype** of an air-cooled solar driven absorption NH_3/H_2O ACM with a cooling capacity of 10kW. The required heating temperature is expected to be around T_h 92°C and the cooling water temperature is T_c 30°C (Kim *et al.*, 2003).

An air-cooled Solar-GAX absorption **prototype** (GAX - heat exchange between absorber-generator) with the working pair NH_3/H_2O and 10.6kW cooling capacity was developed at the **University Autónoma de Baja California**, Mexico and the **University Autónoma de Méxica**, Mexico. The unit is powered in a hybrid manner by natural gas and a solar energy source. The determined COP of the ACM is 0.86 (Velázquez *et al.*, 2003).

The institute **ITW Stuttgart** of the University of Stuttgart, Germany set up a test and demonstration **prototype** of a solar driven absorption NH_3/H_2O ACM with a cooling capacity of 10kW which is mainly based on plate heat exchangers. The cooling machine has been in operation since September of 2004 and is exclusively cooled by a closed water cycle with ambient air. The heating temperatures vary for different operation parameters between T_h 70/65°C and 127/117°C and with that, the cooling water temperatures for the condenser are T_c 22.5/24.5°C or 38/41°C and for the absorber, T_a 24/27°C or 38.5/43.5°C. The reached evaporator temperatures are between T_o 13°C and 5°C at COPs of 0.6 and 0.77 (Brendel *et al.*, 2004).

CHAPTER 03

THEORY DACM PROCESS

3.1 SIMILAR DACM CYCLES

The following chapter describes the theory behind the von Platen and Munters-cycle for domestic refrigerators as well as of the up-scaled DACM in general.

Another Diffusion-Absorption cycle, is the Maiuri-cycle which was developed in the 1930s by G. Maiuri for large-sized absorption cooling machines and low evaporator temperature ranges down to -100°C basing on the von Platen and Munters-cycle. The machine is used for cooling liquids and gases. The used working pair is ammonia/water and hydrogen or nitrogen as auxiliary gas. Through the inert auxiliary gas, the changing evaporator partial pressure allows a large temperature range for the evaporation. An example of one of the units built, was a DACM with 9.3kW cooling capacity for an evaporation temperature range from -30°C down to -75°C (Niebergall, 1981). Further descriptions and performance information's are described in (Vaziri-Elahi, 1944; Bäckström *et al.*, 1965; Niebergall, 1981).

A further absorption cycle for refrigerators with bubble pumps is the Einstein-cycle which was patented by Albert Einstein and Leo Szilard in November of 1930. Unlike the Platen-Munters cycle, the Einstein cycle uses a pressure-equalizing absorbate fluid rather than an inert gas. In the Einstein cycle, butane is the refrigerant, water remains the absorbent, and ammonia becomes the pressure-equalizing fluid. The generator, bubble pump, and evaporator are the same as the Platen-Munters cycle, but the condenser and absorber are combined into a single unit. Further information about the Einstein-cycle, its components and performance can be found in (Delano, 1998; Schaefer, 2000).

3.2 CYCLE DESCRIPTION

The core components of a DACM are the generator, condenser, evaporator and absorber as shown in Figure 3.1. A solution heat exchanger (SHX) in the solution circuit and a gas heat exchanger (GHX) in the auxiliary gas circuit are also components of the DACM as well as a dephlegmator for the condensation of the evaporated solvent. The used working pair for the solution circulation is an ammonia/water mixture, whereby the ammonia is the refrigerant and the water is the solvent. The inert auxiliary gas used for the pressure compensation between the high and low ammonia partial pressure level and for the gas circulation is helium.

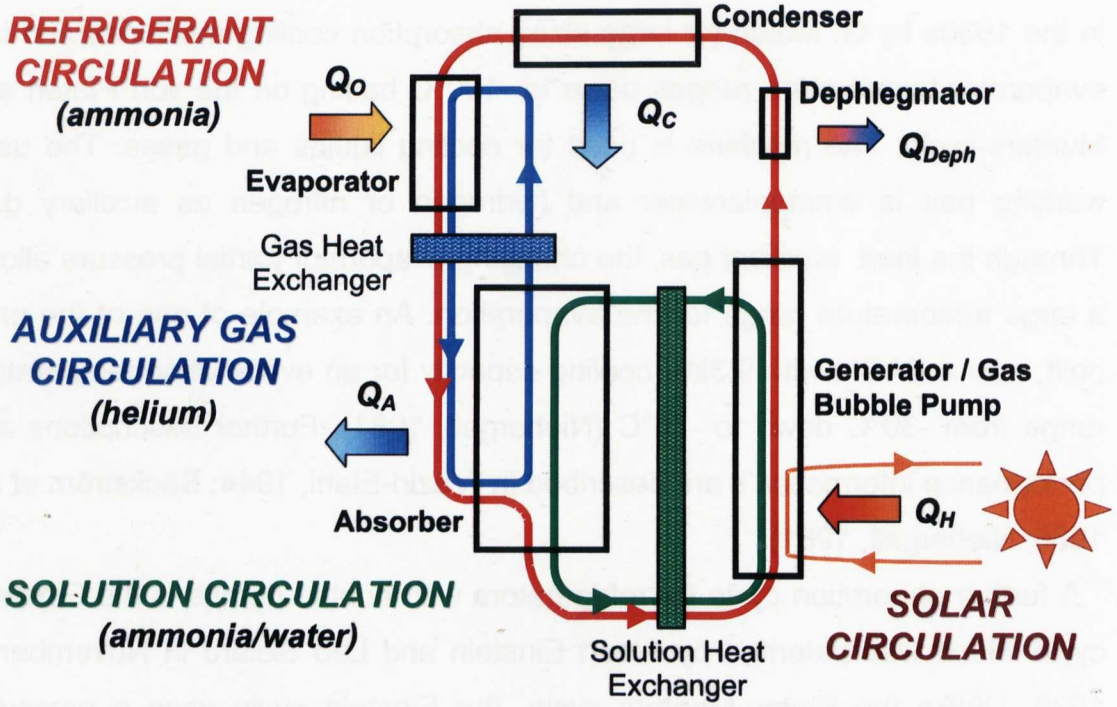

Figure 3.1: Principle of the DACM process.

In the indirectly solar powered **generator**, the refrigerant ammonia is expelled of the rich ammonia/water solution by the heating capacity Q_H with high heating temperatures and thereby a high refrigerant vapour pressure is generated which suffices for the condensation of the refrigerant in the condenser. Hereby, the

pressure compensated, inert auxiliary gas helium flows at the beginning of the operation to the evaporator and the absorber. Furthermore, the usual mechanical solution pump of normal absorption cooling machines is replaced in a DACM by a thermal gas bubble pump. The circulation of the solution between the generator and absorber is maintained by vapour bubbles which are generated in nucleation cells at the lower part of the lifting pipes and forms in the best case a slug flow regime to raise a liquid column. In this way, the processes of desorption of the refrigerant and of lifting the solution are combined in one component.

During the operation there is a simultaneous appearance of water vapour within the rising ammonia vapour meaning that the water vapour has to be condensed by a **dephlegmator** with the cooling capacity Q_{Deph} before reaching the condenser. This can be done e.g. by using a simple counter flow water cooled double-pipe heat exchanger. The ammonia vapour which flows to the **condenser** liquefies at a condenser temperature of 45°C and with that at a given total pressure (high pressure level) of 17.1×10^5Pa (Figure 3.2). The condenser has to either be water-cooled or air-cooled in order to reach and to keep this temperature by dissipating the heat Q_C.

After being in the condenser, the condensed ammonia enters the **evaporator**. Through the heat supply Q_O from the cooling cycle, the refrigerant ammonia evaporates at an evaporator temperature e.g. of five degree Celsius and a low partial pressure of 4.9×10^5Pa (Figure 3.2). The pressure compensation between high and low (partial) pressure is realised by the inert auxiliary gases, helium or hydrogen. In contrast to a normal ACM with its evaporator increases the partial pressure of the ammonia inside the DACM evaporation evaporator with the progress of the evaporation, so that in the upper part of the evaporator the partial pressure is lower than at the end of the evaporator, where the partial pressure rises up to the given maximum evaporator temperature. Corresponding to the increasing of the pressure, an increasing of the

temperature also takes place. Consequently, the coldest part of the evaporator is situated in the upper part of the unit.

The circulation of the ammonia/helium gas mixture of the auxiliary gas circulation between the evaporator and the absorber is caused by the effect of the difference in density. This comes from the diffusion of the specifically heavier and colder ammonia gas into the light and weak ammonia/helium gas from the absorber. Thereby with that the gas mixture becomes heavier than the pure helium gas. The cold gas mixture falls down through the **GHX** in counter flow to the rising weak and warm ammonia/helium gas mixture flowing into the absorber.

Inside the **absorber**, the ammonia vapour is absorbed out of the entered ammonia/helium gas mixture by the weak ammonia/water solution from the generator, again causing the gas mixture to be lighter. The warmed weak ammonia/helium gas mixture connects in the upper part of the absorber and rises then through the GHX to the evaporator. The warm and weak auxiliary gas is cooled in the GHX by the falling cold and rich ammonia/helium gas mixture so that the cooling effect of the evaporator is not substantially reduced. A cooling water circuit dissipates the heat Q_A constantly from the absorber and thereby the auxiliary gas circuit and the absorption are maintained. The cooling water for the absorber is connected in series with the condenser.

The rich and cold ammonia/water solution that is produced inside of the absorber is then preheated with the **SHX** in counter flow by the weak and hot solution from the generator. Therefore, the weak solution cools down and flows automatically to the absorber due to the height difference between generator outlet and absorber inlet.

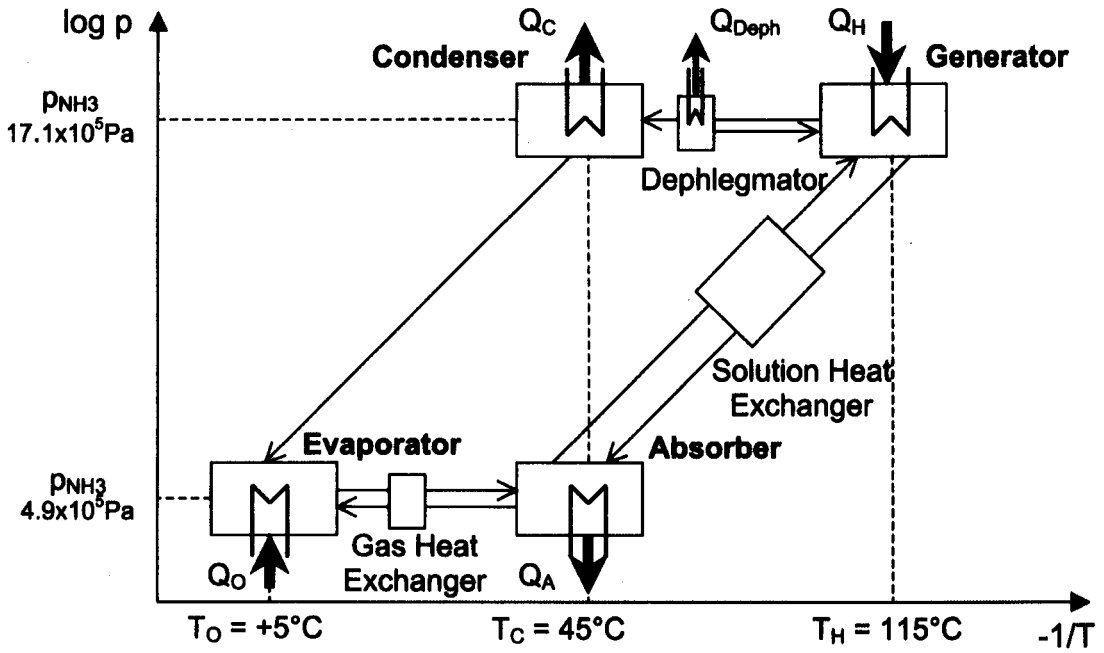

Figure 3.2: Principle of the DACM process in the Dühring plot depending on the partial pressure of refrigerant ammonia.

The whole absorption cooling process of a single-stage DACM can be represented in a Dühring plot depending on the ammonia partial pressure, the different temperature conditions and the ammonia concentrations (Figure 3.2). Because in the complete cooling unit there are no mechanically moving components, it is nearly free of maintenance, silent, and every point in the cooling unit has the same total pressure. Further descriptions about the Diffusion-Absorption process can be found in (Plank *et al.*, 1960; Bäckström, 1965; Niebergall, 1981).

3.3 THERMODYNAMIC PROPERTIES

For the design or simulation of the DACM process based on the mass and energy balance, calculation equations of the thermodynamic properties are necessary. For this reason, equations for the liquid or vapour enthalpies, mass concentrations and temperatures, specific heat capacity, density, thermal conductivity, dynamic viscosity and surface tension of the substances ammonia, ammonia/water, helium and ammonia/helium are presented in this chapter.

3.3.1 LIQUID AMMONIA

The equations for the **specific heat capacity** $c_{L,NH3}$ [J/kg K], **density** $\rho_{L,NH3}$ [kg/m³], **thermal conductivity** $\lambda_{L,NH3}$ [W/m K], **dynamic viscosity** $\eta_{L,NH3}$ [Pa s = kg/m s] and **surface tension** $\sigma_{L,NH3}$ [N/m = kg/s²] of liquid ammonia are given by (Hirschberg, 1988) for the temperature range of -50°C to 50°C as follows:

$$c_{L,NH3} = 4597 + 5.9 \cdot T + 0.0432 \cdot T^2 \tag{3.1}$$

$$\rho_{L,NH3} = 638.6 - 1.393 \cdot T - 2.42 \cdot 10^{-3} \cdot T^2 \tag{3.2}$$

$$\lambda_{L,NH3} = 0.5372 - 2.226 \cdot 10^{-3} \cdot T + 5.76 \cdot 10^{-7} \cdot T^2 \tag{3.3}$$

$$\eta_{L,NH3} = 10^{\left(\frac{876.4}{273.15+T} - 3.9628 + 7.08 \cdot 10^{-3} \cdot T - 3.612 \cdot 10^{-5} \cdot T^2\right)} \cdot 10^{-3} \tag{3.4}$$

$$\sigma_{L,NH3} = 9.276 \cdot 10^{-5} \cdot (132.35 - T)^{1.1548} \tag{3.5}$$

T [°C] stands for the temperature in all of these equations.

3.3.2 AMMONIA VAPOUR

The approximate equations for the **specific heat capacity** at saturation pressure $c_{V,NH3}$ [J/kg K], the **density** $\rho_{V,NH3}$ [kg/m³], the **thermal conductivity** $\lambda_{V,NH3}$ [W/m K] and the **dynamic viscosity** $\eta_{V,NH3}$ [Pa s = kg/m s] of pure ammonia vapour for the temperature range of -50°C to 50°C are given by (Hirschberg, 1988) as follows:

$$c_{V,NH3} = 2700 + 17.47 \cdot T + 0.1094 \cdot T^2 \tag{3.6}$$

$$\rho_{V,NH3} = 10^{5.541 - \frac{1194.5}{(273.15+T)} - 0.2586 \cdot \log(273.15+T)} \tag{3.7}$$

$$\lambda_{V,NH3} = 2.22 \cdot 10^{-2} + 1.13 \cdot 10^{-4} \cdot T + 9.29 \cdot 10^{-8} \cdot T^2 - 3.63 \cdot 10^{-11} \cdot T^3 \tag{3.8}$$

$$\eta_{V,NH3} = \left(9.384 + 0.03658 \cdot T - 4.405 \cdot 10^{-6} \cdot T^2\right) \cdot 10^{-6} \tag{3.9}$$

T [°C] stands for the temperature in all of these equations.

The **vapour pressure** of pure ammonia is given by the Clausius-Clapeyron equation (Bourseau and Bugarel, 1986). Using the equation (2.4) and substituting the ammonia mass concentration X [-] with 1.00, the resulting equation (3.10) is:

$$\log_{10} p = \left(10.018 - \frac{1204.3}{(T + 273.15)}\right) \tag{3.10}$$

where p [Pa] is the pressure and T [°C] is the temperature. The equation is valid for the temperature range between -60°C and 132.35°C.

3.3.3 AMMONIA/WATER SOLUTIONS

For the binary ammonia/water solution, the **specific heat capacity** $c_{NH3/H2O}$ [J/kg K], the **density** $\rho_{NH3/H2O}$ [kg/m³], the **thermal conductivity** $\lambda_{NH3/H2O}$ [W/m K] (dependent on the ammonia mass concentration X_S [-]) and the **dynamic viscosity** $\eta_{NH3/H2O}$ [Pa s = kg/m s] are consequently presented according to (Hirschberg, 1988) for a temperature range of -50°C to 100°C, where T [°C] is the temperature and X_S [-] is the ammonia mass concentration.

$$c_{NH3/H2O} = \begin{pmatrix} 4178.5 + 0.0314 \cdot (T-35)^2 \cdot (1-X_S) \\ +X_S \cdot \left(4200 + \left(410 + 6.2 \cdot T + 0.044 \cdot T^2\right) \cdot X_S\right) \end{pmatrix} \quad (3.11)$$

$$\rho_{NH3/H2O} = \begin{pmatrix} 1000 - 369 \cdot X_S + 219 \cdot X_S{}^2 \cdot (1-X_S) \\ -(0.0075 + 1.98 \cdot X_S - 0.54 \cdot X_S{}^2) \cdot T \\ -(0.0016 + 0.001 \cdot X_S{}^3) \cdot T^2 \end{pmatrix} \quad (3.12)$$

Thermal conductivity for $0.00 < X_S \leq 0.30$:

$$\lambda_{NH3/H2O} = 5.685 \cdot 10^{-1} - 7.70 \cdot 10^{-1} \cdot X_S + 8.67 \cdot 10^{-1} \cdot X_S{}^2 + 1.73 \cdot 10^{-3} \cdot T \quad (3.13)$$

Thermal conductivity for $0.30 < X_S \leq 1.00$:

$$\lambda_{NH3/H2O} = \begin{pmatrix} 4.51 \cdot 10^{-1} + 5.9 \cdot 10^{-4} \cdot T \\ -\left(2.07 \cdot 10^{-1} - 6.65 \cdot 10^{-3} \cdot T\right) \cdot X_S \\ +\left(2.96 \cdot 10^{-1} - 9.5 \cdot 10^{-3} \cdot T\right) \cdot X_S{}^2 \end{pmatrix} \quad (3.14)$$

$$\eta_{NH3/H2O} = 10^{\left(10^{\left(\frac{2000}{500+T} - 4.41 + 0.925 \cdot X_S - 1.743 \cdot X_S{}^2 + 0.0215 \cdot X_S{}^3\right)}\right)} \cdot 10^{-3} - 1 \cdot 10^{-3} \quad (3.15)$$

The equation (3.18) for the **surface tension** $\sigma_{NH3/H2O}$ [N/m = kg/s²] for ammonia/water solutions is prepared by the author with the use of equation (3.5) for liquid ammonia, equation (3.16) for liquid water $\sigma_{L,H2O}$ [N/m] according

to (Hirschberg, 1988) and equation (3.17) for the relation of both surface tensions and the ammonia mass concentration as follows:

$$\sigma_{L,H2O} = \left(6.61 \cdot 10^{-4} + 2.29 \cdot 10^{-7} \cdot T - 2.48 \cdot 10^{-9} \cdot T^2\right) \cdot \left(374.15 - T\right)^{0.8} \quad (3.16)$$

$$\sigma_{NH3/H2O} = \sigma_{L,NH3} \cdot X_S + \sigma_{L,H2O} \cdot \left(1 - X_S\right) \quad (3.17)$$

$$\sigma_{NH3/H2O} = \begin{pmatrix} 9.276 \cdot 10^{-5} \cdot \left(132.35 - T\right)^{\frac{2887}{2500}} \cdot X_S \\ + \left(6.61 \cdot 10^{-4} + 2.29 \cdot 10^{-7} \cdot T - 2.48 \cdot 10^{-9} \cdot T^2\right) \cdot \left(374.15 - T\right)^{\frac{4}{5}} \cdot \left(1 - X_S\right) \end{pmatrix} \quad (3.18)$$

where T [°C] is the temperature and X_S [-] is the ammonia mass concentration.

A further approximation equation (3.19) for the **solidification temperature** T_s [°C] is given by (Hirschberg, 1988) and is applicable for ammonia mass concentrations X_S [-] between $0.00 \leq X_S \leq 0.3333$ till T_s is -100.3°C.

$$T_s = 77.1 - \frac{24}{0.3113 + \log\left(1 - X_S\right)} \quad (3.19)$$

The Figure 3.3 shows the solidification temperature curve for ammonia/water solutions. For ammonia mass concentrations above 0.30 the solidification temperature is at least -80°C and below 0.30 it decreases to 0°C. Therefore, for a weak ammonia concentration of 0.20, the solidification temperature is -34.8°C.

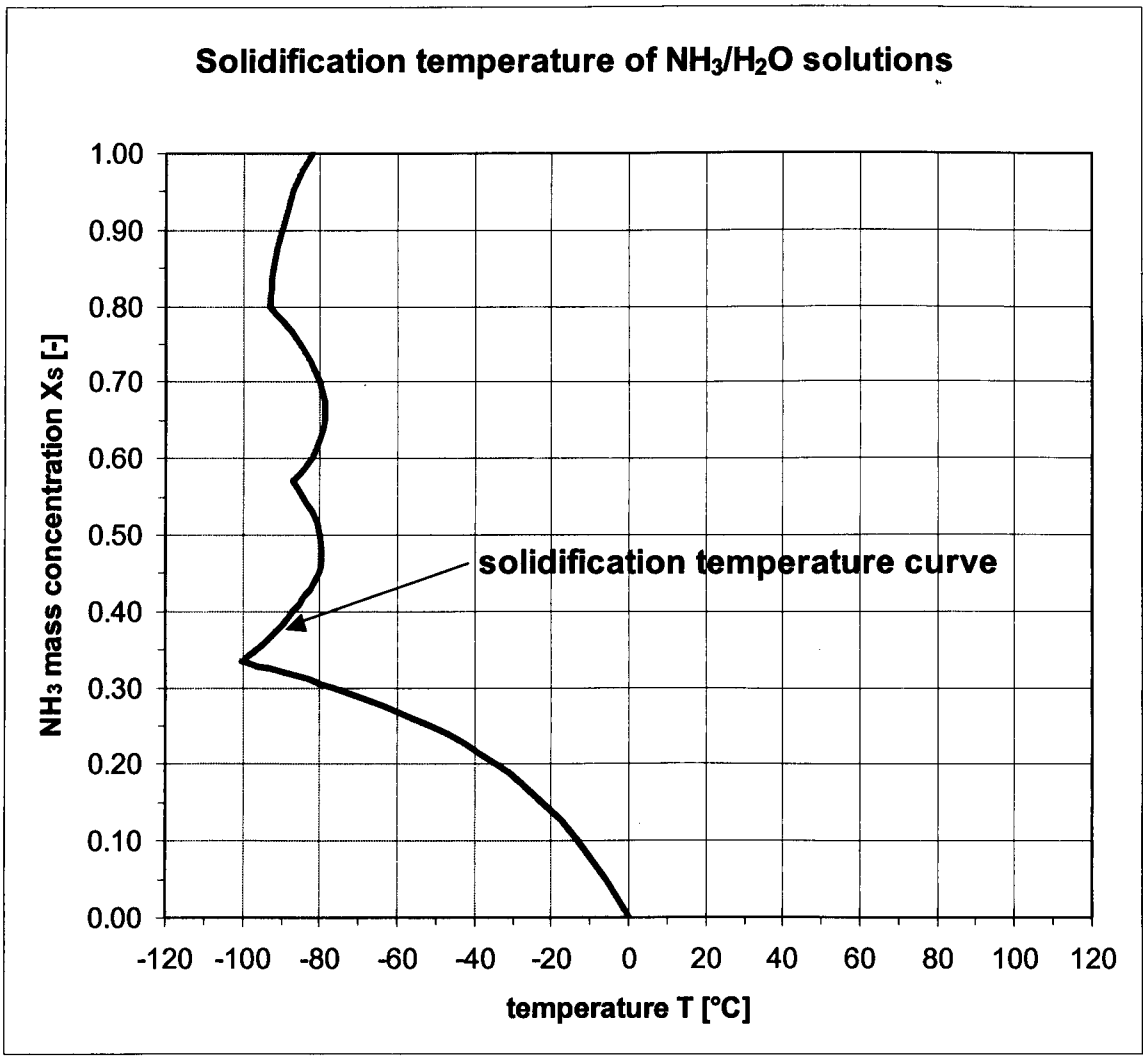

Figure 3.3: Solidification temperature of ammonia/water solutions depending on ammonia mass concentration (Hirschberg, 1988).

For a liquid mixture, a saturation **vapour pressure** p [Pa] is adjusted that is in thermal equilibrium according to the temperature and the refrigerant concentration. This connection is defined by equation (2.4) which is the approach of the Clausius-Clapeyron equation where the coefficients a and b were stated for ammonia/water by (Bourseau et al., 1986) depending on the ammonia mass concentration X [-].

The vapour pressure is plotted as pressure-temperature log p -1/T-diagram in Figure 2.7 for temperatures between -60°C and 200°C and solution mass concentrations referred to the refrigerant ammonia from 0.00 to 1.00. The

ammonia/water mass concentration can be iteratively calculated by the equations (2.4).

The **temperature** T [°C] is defined by three different equations. The first equation (3.20) is the converted equation (2.4) by (Bourseau et al., 1986)

$$T = \frac{\left(2013.8 - 2155.7\,X + 1540.9\,X^2 - 194.7\,X^3\right)}{\left(10.44 - 1.767\,X + 0.9823\,X^2 + 0.3627\,X^3\right) - \log_{10} p} - 273.15 \quad (3.20)$$

where X [-] is the ammonia mass concentration and p [Pa] is the pressure.

The Figure 3.4 shows three different temperature curves that are calculated by the equation (3.20) for the pressures $5x10^5$Pa, $11x10^5$Pa and $17x10^5$Pa depending on the ammonia mass concentrations of 0.00 to 1.00. This means, the temperature decreases with an increase in the ammonia mass concentration.

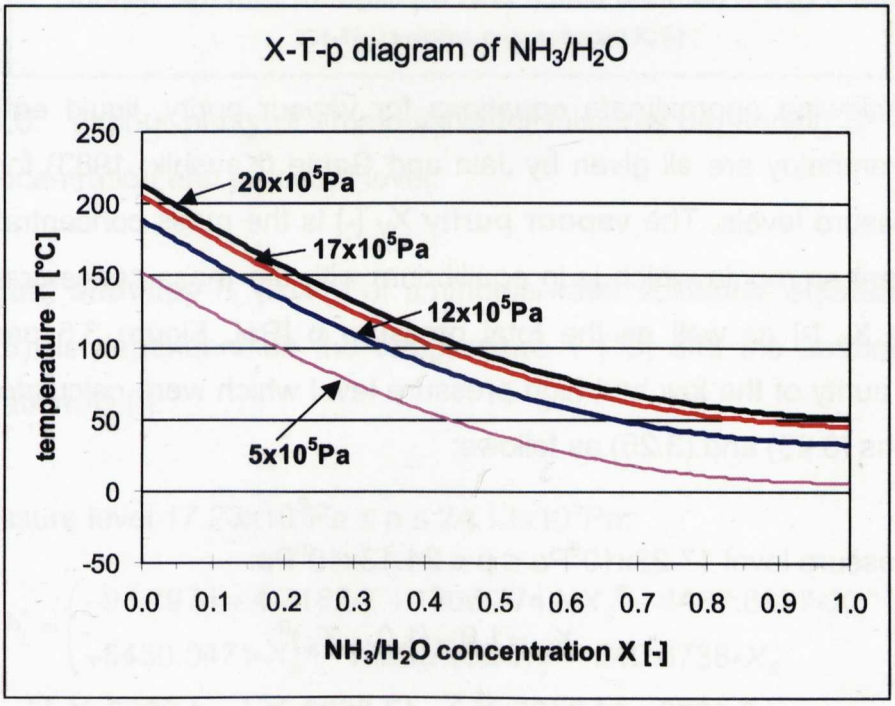

Figure 3.4: Temperature of ammonia/water mixtures depending on ammonia mass concentration and pressure.

The two other equations (3.21) and (3.22) for the temperature and the boiling temperature of the solution respectively are given by Jain and Gable (Kaushik, 1983) for two different pressure levels.

high pressure level 17.23×10^5Pa ≤ p ≤ 24.13×10^5Pa:

$$T = \begin{pmatrix} 151.6889 - 133.4051 \cdot X_S^5 + 192.4098 \cdot X_S^4 - 15.0679 \cdot X_S^3 + 92.7520 \cdot X_S^2 \\ -297.6683 \cdot X_S + 3.1 \cdot p \cdot X_S - 2.1089 \cdot p^2 \cdot X_S + 36.0 \cdot p - 2.8 \cdot p^2 \end{pmatrix} \quad (3.21)$$

low pressure level 3.45×10^5Pa ≤ p ≤ 5.52×10^5Pa:

$$T = \begin{pmatrix} 95.444 - 384.931 \cdot X_S^5 + 929.686 \cdot X_S^4 - 791.719 \cdot X_S^3 + 437.696 \cdot X_S^2 \\ -324.904 \cdot X_S - 27.7 \cdot p \cdot X_S + 1.32 \cdot p^2 \cdot X_S + 147.9 \cdot p - 70.22 \cdot p^2 \end{pmatrix} \quad (3.22)$$

where X_S [-] is the ammonia mass concentration and p [Pa] is the pressure.

The condensation temperature of the vapour can be calculated with the boiling temperature of the solution which is in equilibrium with the vapour.

The following approximate equations for vapour purity, liquid enthalpy and vapour enthalpy are all given by Jain and Gable (Kaushik, 1983) for high and low pressure levels. The **vapour purity** X_V [-] is the mass concentration of the refrigerant ammonia which is in equilibrium with the mass concentration of the solution X_S [-] as well as the total pressure p [Pa]. Figure 3.5 presents the vapour purity of the low and high pressure level which were calculated with the equations (3.23) and (3.25) as follows:

High pressure level 17.23×10^5Pa ≤ p ≤ 24.13×10^5Pa:

$$X_V = 1.0 - (1.0 - X_S)^R \quad (3.23)$$

where

$$R = \begin{pmatrix} 7.1588 + 10.7490 \cdot X_S^5 - 17.8690 \cdot X_S^4 + 4.0297 \cdot X_S^3 \\ -1.3086 \cdot X_S^2 + 0.3715 \cdot 10^{-6} \cdot p \cdot X_S - 0.6171 \cdot 10^{-6} \cdot p \end{pmatrix} \quad (3.24)$$

Low pressure level 3.45×10^5Pa ≤ p ≤ 5.52×10^5Pa:

$$X_V = 1.0 - (1.0 - X_S)^R \tag{3.25}$$

where
$$R = \begin{pmatrix} 11.2925 + 108.485 \cdot X_S^{\,5} - 229.009 \cdot X_S^{\,4} + 155.247 \cdot X_S^{\,3} \\ -41.0442 \cdot X_S^{\,2} + 3.0934 \cdot 10^{-6} \cdot p \cdot X_S^{\,2} - 4.532 \cdot 10^{-6} \cdot p \end{pmatrix} \tag{3.26}$$

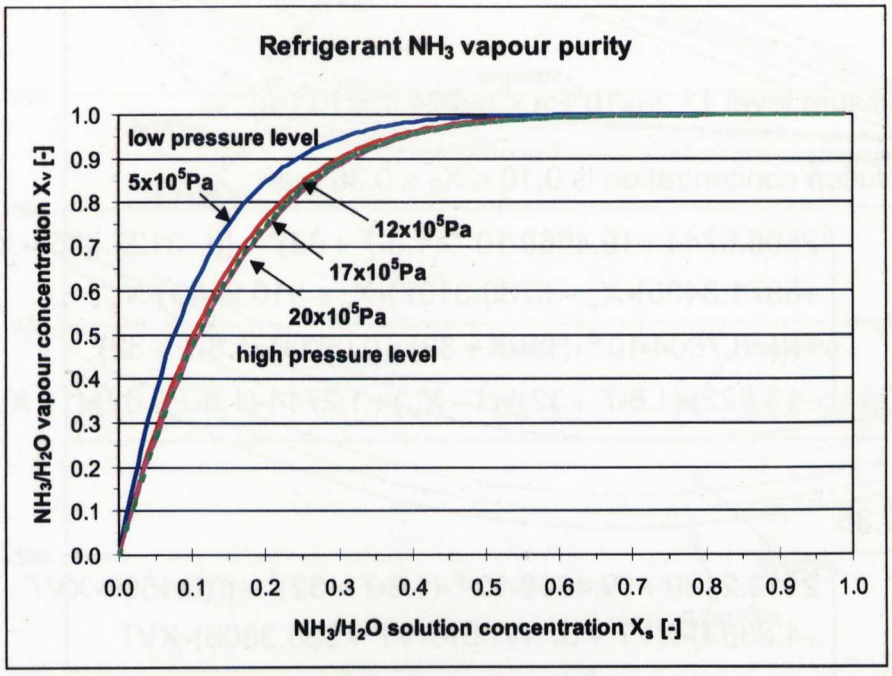

Figure 3.5: Vapour purity of ammonia/water mixtures depending on ammonia mass concentration and pressure level.

The **liquid enthalpy** h_L [kJ/kg] of ammonia/water solutions, equations (3.27) and (3.28), is dependant on the temperature T [°C] and the ammonia mass concentration X_S [-].

High pressure level 17.23×10^5Pa ≤ p ≤ 24.13×10^5Pa:

$$h_L = \begin{pmatrix} -94.7974 + 4.7182 \cdot T + 1306.7740 \cdot X_S^{\,5} - 4487.8637 \cdot X_S^{\,4} \\ +5450.0471 \cdot X_S^{\,3} - 1926.7160 \cdot X_S^{\,2} - 240.6738 \cdot X_S \end{pmatrix} \tag{3.27}$$

Low pressure level 3.45×10^5Pa ≤ p ≤ 5.52×10^5Pa:

$$h_L = \begin{pmatrix} -51.7296 + 4.5705 \cdot T - 1526.79 \cdot X_S^{\,4} + 3160.60 \cdot X_S^{\,3} \\ -1158.988 \cdot X_S^{\,2} - 424.528 \cdot X_S \end{pmatrix} \tag{3.28}$$

The **vapour enthalpy** h_V [kJ/kg] equations (3.29), (3.30) and (3.32) of ammonia/water vapour are dependant on the temperature T [°C], the ammonia vapour mass concentration X_V [-] and the ammonia mass concentration X_S [-] respectively.

high pressure level $17.23 \times 10^5 Pa \le p \le 24.13 \times 10^5 Pa$:

if the solution concentration is $0.10 \le X_S \le 0.36$ than:

$$h_V = \begin{pmatrix} 2506.6744 + 19.4669 \cdot 10^{-9} \cdot (1.8 \cdot T + 32)^4 + (((-3122.7354 \cdot X_V \\ +6871.3435) \cdot X_V - 5780.3107) \cdot X_V + 910.2483) \cdot X_V \\ +(((-8.7804 \cdot 10^{-5} \cdot (1.8 \cdot T + 32) + 0.0634) \cdot (1.8 \cdot T + 32) \\ -13.822) \cdot (1.8 \cdot T + 32)) \cdot (1 - X_V) + 1.2714 \cdot (1.8 \cdot T + 32) \cdot (1 - X_V)^2 \end{pmatrix} \tag{3.29}$$

if $X_S > 0.36$:

$$h_V = \begin{pmatrix} 2113.2189 + 19.4669 \cdot 10^{-9} \cdot (1.8 \cdot T + 32)^4 + (((0.1599 \cdot XVT \\ +4.8363) \cdot XVT + 57.7705) \cdot XVT + 336.3805) \cdot XVT \\ +(((-8.7804 \cdot 10^{-5} \cdot (1.8 \cdot T + 32) + 0.0634) \cdot (1.8 \cdot T + 32) \\ -13.822) \cdot (1.8 \cdot T + 32)) \cdot (1 - X_V) + 1.2714 \cdot (1.8 \cdot T + 32) \cdot (1 - X_V)^2 \end{pmatrix} \tag{3.30}$$

where

$$\begin{aligned} XVT &= \log_e(1 - X_V) \quad for\ X_V < 0.99996 \\ XVT &= \log_e(0.00004) \quad for\ X_V \ge 0.99996 \end{aligned} \tag{3.31}$$

low pressure level $3.45 \times 10^5 Pa \le p \le 5.52 \times 10^5 Pa$:

$$h_V = \begin{pmatrix} 1234.944 + ((-11.5081 \cdot 10^{-6} \cdot (1.8 \cdot T + 32) \\ +3.4775 \cdot 10^{-3}) \cdot (1.8 \cdot T + 32) + 0.9672) \cdot (1.8 \cdot T + 32) \\ +(((9.4324 \cdot 10^{-5} \cdot (1.8 \cdot T + 32) - 0.0675) \cdot (1.8 \cdot T + 32) \\ +15.7951) \cdot (1.8 \cdot T + 32)) \cdot (1 - X_V) \end{pmatrix} \tag{3.32}$$

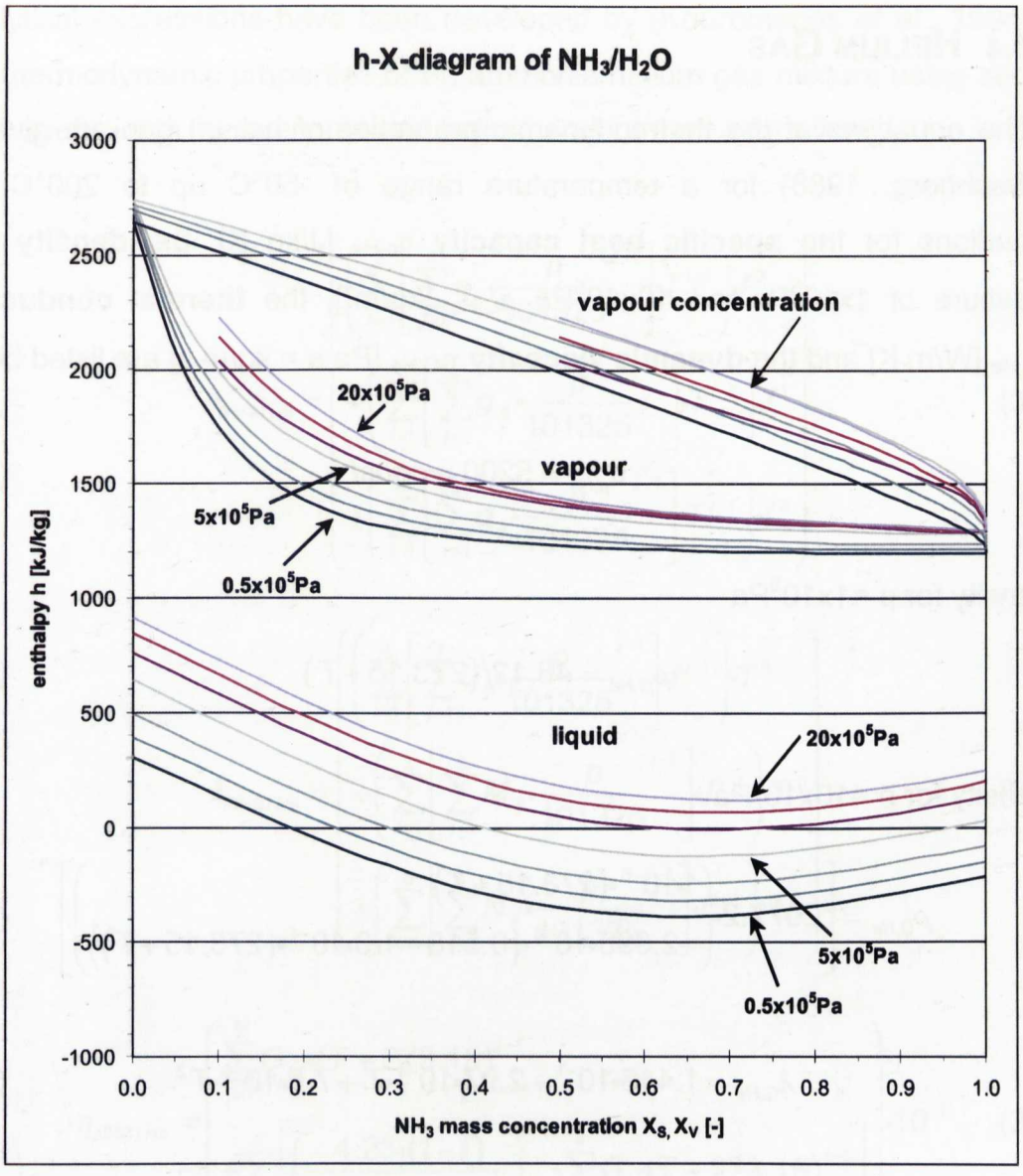

Figure 3.6: Enthalpy-concentration diagram for ammonia/water mixtures for pressure curves of 20, 15, 10, 5, 2, 1 and $0.5x10^5$Pa.

Figure 3.6 shows that the equations by Jain and Gable for the high pressure level could be used with adequate accuracy up to the upper boundary condition of the low pressure level of $5.52x10^5$Pa.

3.3.4 HELIUM GAS

The equations of the thermodynamic properties of helium gas are given by (Hirschberg, 1988) for a temperature range of -50°C up to 200°C. The equations for the **specific heat capacity** $c_{p,He}$ [J/kg K], the **density** for a pressure of $1x10^5$Pa and $10x10^5$Pa $\rho_{G,He}$ [kg/m³], the **thermal conductivity** $\lambda_{G,He}$ [W/m K] and the **dynamic viscosity** $\eta_{G,He}$ [Pa s = kg/m s] are listed below.

$$c_{p,He} = 5200 = const \tag{3.33}$$

Density for p =$1x10^5$Pa

$$\rho_{G,He} = 48.12/(273.15+T) \tag{3.34}$$

Density for p =$10x10^5$Pa

$$\rho_{G,He} = \left[2077.2 \bullet \begin{pmatrix} 1 \bullet 10^{-6} \bullet (273.15+T) \\ +2.696 \bullet 10^{-6} \bullet (0.518 - 1.3 \bullet 10^{-4} \bullet (273.15+T)) \end{pmatrix}\right]^{-1} \tag{3.35}$$

$$\lambda_{G,He} = 1.445 \bullet 10^{-1} + 2.97 \bullet 10^{-4} \bullet T + 7.6 \bullet 10^{-8} \bullet T^2 \tag{3.36}$$

$$\eta_{G,He} = \left(18.69 + 0.0469 \bullet T - 1.87 \bullet 10^{-5} \bullet T^2\right) \bullet 10^{-6} \tag{3.37}$$

where T [°C] is the temperature for all equations.

3.3.5 AMMONIA/HELIUM GAS MIXTURE

For the ammonia/helium gas mixture the **density** $\rho_{NH3/He}$ [kg/m³], the **thermal conductivity** $\lambda_{NH3/He}$ [W/m K], the **dynamic viscosity** $\eta_{NH3/He}$ [N s/m² = kg/m s] and the **saturation mass concentration** $f_{s,NH3/He}$ [-] are presented. Hereby p [Pa] is the total pressure of the gas mixture, T [°C] is the temperature and f [-] is the ammonia mass concentration in the ammonia/helium gas mixture. The

analytical expressions have been developed by (Kouremenos *et al.*, 1994) for the thermodynamic properties of an ammonia/helium gas mixture using second virial coefficients for ammonia and helium and for their interaction.

$$\rho_{NH3/He} = \left(\begin{array}{l} \left(\sum_{i=1}^{3} \left[\sum_{j=1}^{3} e_{ij} \bullet \left(\frac{p}{101325} \right)^{j-1} \right] \bullet T^{i-1} \right) \bullet f^{0} \\ + \left(\sum_{i=1}^{3} \left[\sum_{j=1}^{3} g_{ij} \bullet \left(\frac{p}{101325} \right)^{j-1} \right] \bullet T^{i-1} \right) \bullet f^{1} \\ + \left(\sum_{i=1}^{4} \left[\sum_{j=1}^{3} q_{ij} \bullet \left(\frac{p}{101325} \right)^{j-1} \right] \bullet T^{i-1} \right) \bullet f^{2} \end{array} \right)^{-1} \tag{3.38}$$

$$\lambda_{NH3/He} = \left(\begin{array}{l} \left(\sum_{i=1}^{3} \left[\sum_{j=1}^{3} L_{ij} \bullet \left(\frac{p}{101325} \right)^{j-1} \right] \bullet f^{i-1} \right) \bullet T^{0} \\ + \left(\sum_{i=1}^{3} \left[\sum_{j=1}^{3} M_{ij} \bullet \left(\frac{p}{101325} \right)^{j-1} \right] \bullet f^{i-1} \right) \bullet T^{1} \\ + \left(\sum_{i=1}^{3} \left[\sum_{j=1}^{4} N_{ij} \bullet \left(\frac{p}{101325} \right)^{j-1} \right] \bullet f^{i-1} \right) \bullet T^{2} \end{array} \right) \tag{3.39}$$

$$\eta_{NH3/He} = \left(\begin{array}{l} \sum_{j=1}^{3} G_{1j} \bullet (T + 273.15)^{j-1} \\ + \sum_{i=2}^{5} \left[\left(\frac{4.25 \bullet (1-f)}{4.25 \bullet (1-f) + f} \right)^{i-1} \bullet \sum_{j=1}^{4} G_{ij} \bullet (T + 273.15)^{j-1} \right] \end{array} \right) \bullet 10^{-7} \tag{3.40}$$

$$f_{s,NH3/He} = \sum_{i=1}^{6} \left[\sum_{j=1}^{3} t_{ij} \bullet \left(\frac{p}{101325} \right)^{j-1} \right] \bullet T^{i-1} \tag{3.41}$$

The coefficients e_{ij}, g_{ij}, and q_{ij} are the density coefficients for the equation (3.38). L_{ij}, M_{ij}, and N_{ij} are the thermal conductivity values of coefficients for the equation (3.39). G_{1j}, and G_{ij} are the viscosity coefficients for the equation (3.40). t_{ij} is the value of coefficients for the saturation mass concentration equation (3.41). These coefficients are all stated in Appendix A.

The specific **enthalpy** h_G [kJ/kg] for the ammonia/helium gas mixture is given by (Kouremenos *et al.*, 1994) using second virial coefficients as can be seen in equation (3.42)

$$h_G = \left(\left(\sum_{i=1}^{3} \left[\sum_{j=1}^{4} a_{ij} \bullet \frac{p}{101325}^{j-1} \right] \bullet T^{i-1} \right) \bullet f^0 + \left(\sum_{i=1}^{3} \left[\sum_{j=1}^{4} b_{ij} \bullet \frac{p}{101325}^{j-1} \right] \bullet T^{i-1} \right) \bullet f^1 + \left(\sum_{i=1}^{4} \left[\sum_{j=1}^{4} c_{ij} \bullet \frac{p}{101325}^{j-1} \right] \bullet T^{i-1} \right) \bullet f^2 + \left(\sum_{i=1}^{4} \left[\sum_{j=1}^{4} d_{ij} \bullet \frac{p}{101325}^{j-1} \right] \bullet T^{i-1} \right) \bullet f^3 \right) \quad (3.42)$$

where p [Pa] is the total pressure of the gas mixture, T [°C] is the temperature, f [-] is the ammonia mass concentration in the NH_3/He mixture and a_{ij}, b_{ij}, c_{ij} and d_{ij} are the enthalpy coefficients for the equation (3.42). These are also stated in Appendix A. The enthalpies for ammonia/helium at different total pressures and temperatures versus the ammonia mass concentration in the ammonia/helium gas mixture are shown in Figure 3.7.

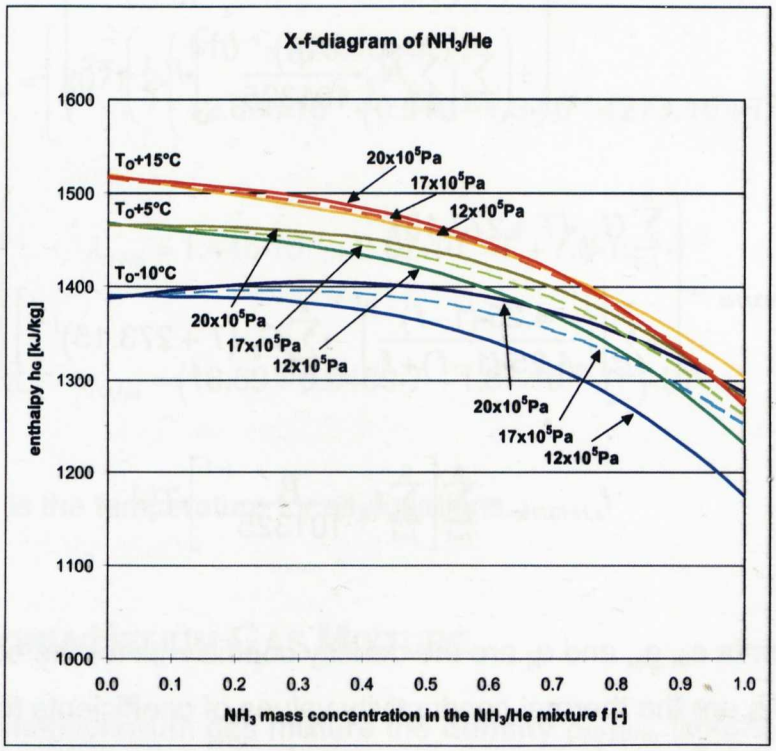

Figure 3.7: Enthalpy-concentration diagram for ammonia/helium gas mixtures for pressure curves of 20, 17 and 12x10^{5}Pa and temperatures of +15°C, +5°C and -10°C respectively ammonia partial pressures of 6.90, 4.88 and 2.76x10^{5}Pa.

3.4 GENERATOR / BUBBLE PUMP

The bubble pump, also called generator is used instead of the usual mechanical solution pump of an absorption cooling machine for circulating the ammonia/water solution between the generator and the absorber of the DACM (Figure 3.8). There are two kinds of bubble pumps: the direct gas or electrically driven ones, which are commonly used in DARs and the indirect thermally driven bubble pumps used for DACMs.

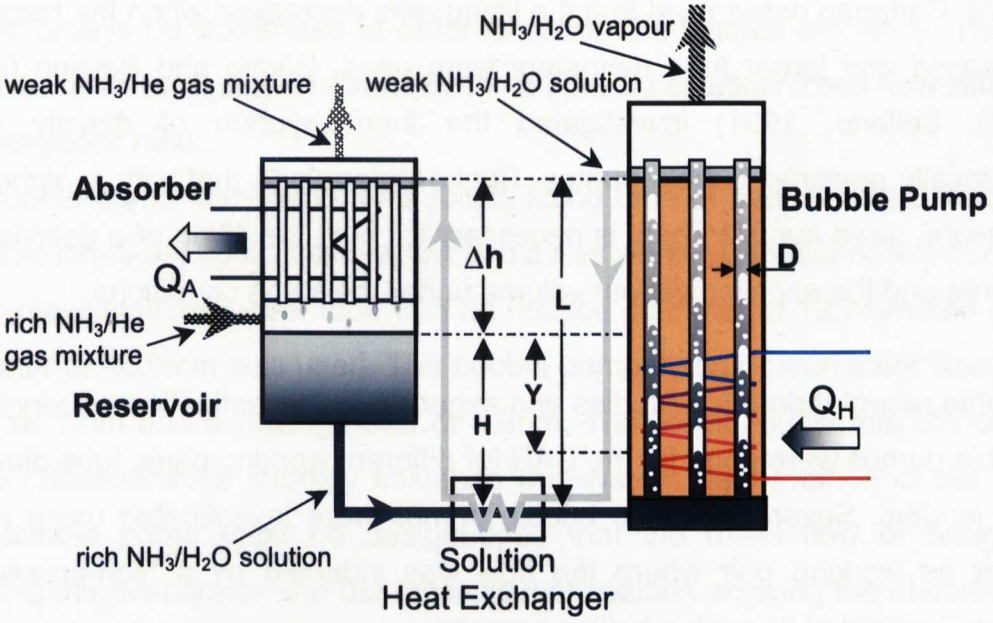

Figure 3.8: Bubble pump configuration.

The solution in the reservoir initially fills the tubes in the bubble pump to the same level H (Figure 3.8) that height difference also determines the lowest point on the bubble pump. At the bottom of the bubble pump, heat input Q_H is applied to generate at best a slug-flow for expelling vapour and lifting the solution to the top of the bubble pump to compensate the pressure losses due to friction in the tubing and the altitude difference between the generator solution outlet and the reservoir level which is called the lifting height or the driving head Δh. The inner pump tube diameter D and tube length L are parameters for the flow regime and the submergence ratio which is the ratio of the reservoir height H to the tube length. The main characteristic values needed to judge the performance of the bubble pump are the lifting ratio, solution flow rate and specific solution circulation index which are described in chapter 3.4.4 and 3.4.5.

3.4.1 LITERATURE REVIEW

The bubble pump operates on the same principle as that of the mammoth pump or the airlift pump principle. In this case, ammonia/water liquid is raised by its own vapour bubbles according to the thermosyphon principle. The theoretical basics for this, according to the mammoth pumping principle, were investigated in the 1930s by (Behringer, 1930; Pickert, 1931). Later thermosyphon pumping was investigated and described in detail by (Cattaneo, 1935). Cattaneo determined that the lifting ratio decreased when the height was increased and larger tube diameters were used. Büche and Sellerio (Büche, 1935; Sellerio, 1951) investigated the thermosyphon of directly driven, electrically powered bubble pumps. Büche determined that with a higher total pressure, more supplied heat is necessary for both the lifting of a definite liquid volume and the expelled vapour volume under the same conditions.

Some recent theoretical studies and experimental investigations of single tube bubble pumps were done for the DAR for different working pairs, tube diameters and lengths. Several of these bubble pumps were investigated using air and water as working pair where the flow was inducted by a high-pressure air source instead of through a boiling process.

For the Einstein Refrigeration Cycle, a bubble pump made of stainless steel with a 7.62mm inner diameter and a length of 0.736 meters was investigated with water by (Delano, 1998). Delano mathematically modelled the bubble pump based on conservation equations of mass and momentum for the design analysis and showed that an increase in the tube diameter decreases the friction factor and thereby increases the flow rate through the bubble pump. With increasing submergence ratio (H/L), the relative height to which the bubble pump must lift the liquid decreases, so that the liquid flow rate increases. For a fixed submergence ratio, the liquid mass flow rate increases with increasing heat input, reaches a maximum, and then decreases with further heat input increase.

Further experimental studies on an air lift pump using water and air as working pair were carried out by (White, 2001; Shelton *et al.*, 2002). Two

experimental set-ups were built, one with a lift tube length of 0.9144m and the other 1.8288m, in order to establish length effect. The lift tubes used were transparent and made of Pyrex with inner diameters of 6mm, 8mm, and 10mm. Measurements were made for each of the three different lift tube diameters at each of the three submergence ratios for varying injected airflow rates. White presented a different analytical approach based on air-lift pump theory related to the drift flux method for modelling the bubble pump. The results showed, that the most important parameter is the submergence ratio, and that this parameter should always be maximised in order to obtain the highest efficiency. There is however, also an optimum diameter for a specific solution mass flow rate and submergence ratio.

A bubble pump correlation for a single lifting tube of a DAR was determined by (Srikhirin *et al.*, 2002) using water and air as working fluids. For this purpose, a seamless stainless steel tube with an outside diameter of 12.7mm and inside diameter of 10.9mm was used. The bubble pump design parameters were a lift head of 1.0m and a driving head of 0.65m. The results show that the bubble pump characteristics strongly influence the system performance of the DAR. The bubble pump must be designed so that the mass flow of refrigerant entering the evaporator and the mass flow of solution entering the absorber are matched.

Further results have been presented for practical working fluids which are lifted by boiling different binary mixtures. Pfaff (Pfaff *et al.*, 1998) investigated glass tubes for use as bubble pumps using the working fluid water/lithium bromide and modelled the bubble pump using the manometer principle. The bubble pump was tested experimentally in a test rig that did not operate continuously for tube diameters of 10mm, 14mm and 18mm and different lifting heights. It was found that the lifting ratio is not dependent on the heat input. The frequency of the pumping action increases when the heat input to the bubble pump is increased, however the lifting ratio increases with a decrease in pump tube diameter, a decrease in pump lift and an increase in driving head.

Experimental continuous studies of a bubble pump using the working fluid methanol were done by (Sathe, 2001). In these studies, the bubble pump tube was made of copper and was tested for three different pump tube diameters (6mm, 8mm and 10mm) and three different levels of liquid in the liquid reservoir (0.45m, 0.50m and 0.55m). Hence, the height of the bubble pump tube was set at 1.6m. The results showed that the frequency of pumping action increases with an increase in pump heat input. The mass flow rate of vapour increases linearly with the heat input whereas the mass flow rate of the pumped liquid first increases, reaches a maximum value and then decreases with the increase in the heat input. Furthermore, Sathe used the bubble pump model from (Delano, 1998) to confirm the experimental data.

A further continuous investigation of a bubble pump with two working fluids, first methanol and second methanol/water, was carried out by (Jakob, 2001). The tested bubble pump consisted of a tubular heat exchanger with a length of 1.6m and inside, was equipped with 12 tubes made of steel. The same quantity of maximum lifting ratios were determined for the different fluids.

An extensive investigation of the performance and the different flow regimes of a bubble pump using an organic solvent and hydrochlorofluorocarbon refrigerant as working fluid was carried out by (Koyfman *et al.*, 2001; Koyfman, 2002; Koyfman *et al.*, 2003a; Koyfman *et al.*, 2003b). For these investigations, a glass tube with 9mm inner diameter was used in a continuous experimental system. Three different levels of liquid in the liquid reservoir were studied: 0.486m, 0.536m and 0.586m. It was determined that the performance of the bubble pump depends mainly on the driving head and on the heat input to the bubble pump. It was concluded that a low driving head is recommendable for the achievement of higher refrigerant flow rates and thus higher cooling capacities. Furthermore, a change in the system initial pressure changes the volumetric flow through the system while the solution mass flow remains almost constant. In addition it was found that the higher the initial pressure, the higher is the heat input required by the system to start-up the bubble pump.

Maiya (Maiya, 1988) analysed the performance of the bubble pump for parameters such as system pressure, pump lift and modelled the solution circuit of the DAR system using a mathematical model. An improved solution circuit was also suggested and the performance of the bubble pump for simple and improved solution circuits was compared. The bubble pump was made of a single glass tube with a inner tube diameter of 4mm and a tube length of 0.6m. The used working pairs were ammonia/water with hydrogen or helium as auxiliary gas. It was determined that the mass flow of the solution circuit depends mainly on the two parameters of the bubble pump, namely on the driving head and the pump diameter.

An investigated bubble pump using the working pair ammonia/water was set up in a pilot plant of a DACM (Biesinger, 2002). Biesinger made measurements of the weak solution volume flow and temperature profiles of the generator. The bubble pump consisted of a tubular heat exchanger with 19 tubes made of steel, each with a length of 1.6m and an inner diameter of 5mm. A continuous solution lifting could be confirmed for the indirectly driven generator. The characteristic bubble pump curve was determined with its characteristic continual increase up to a maximum and the following decrease. Occasional breaks of the solution lifting were compensated by the quantity of lifting tubes in the tubular heat exchanger.

3.4.2 BUBBLE PUMP DESIGN

A detailed general view of different designed bubble pumps (Figure 3.9) is given by (Niebergall, 1956). A special directly driven, electrically powered bubble pump capable of working efficiently both with high and low heating capacities was investigated by (Lucas, 1967). Another advanced, directly driven bubble pump (Figure 3.9) with electrical heating cartridge was developed by (Stierlin, 1980) and resulted in a heat consumption reduction of one third because the total recycling of the rectification lost energy. Chen designed and tested a new directly driven bubble pump otherwise known as generator with heat exchanger (GWHX) powered by an electrical heater for the purpose of

reusing the waste heat from the rectifier to heat the rich solution from the absorber (Chen, 1995; Chen *et al.*, 1996). The newly improved generator showed a significantly increased COP of 50% compared to a standard DAR which used hydrogen as inert gas.

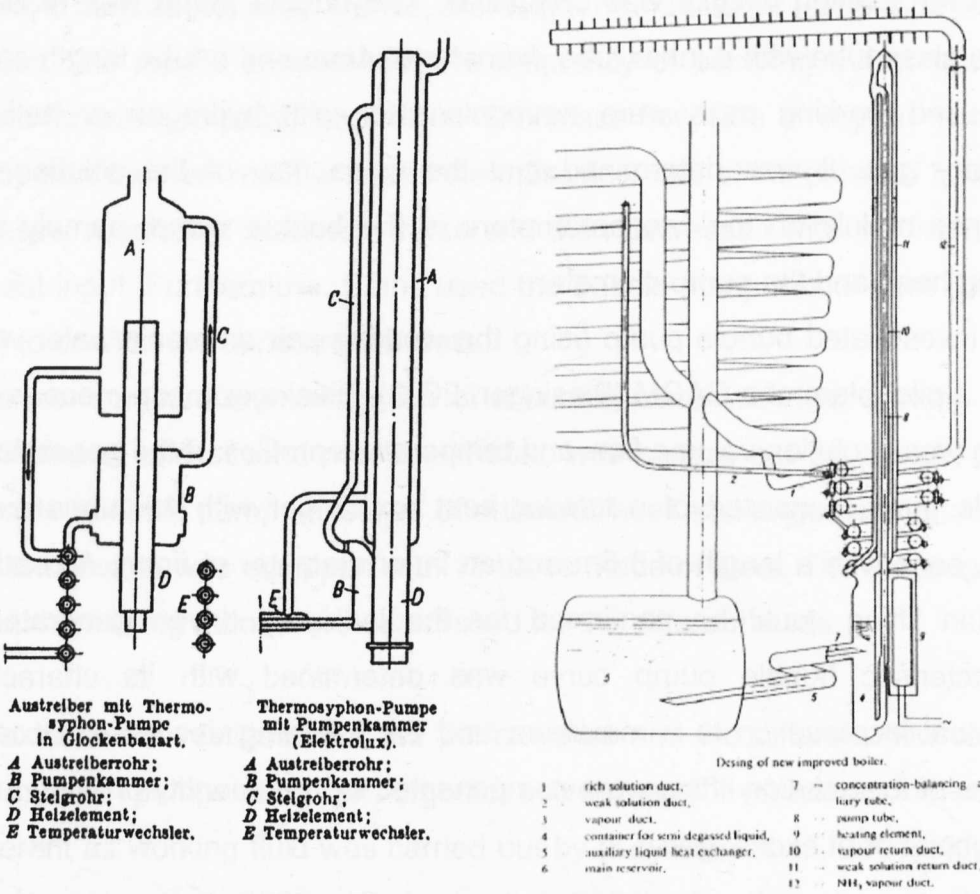

Austreiber mit Thermosyphon-Pumpe in Glockenbauart.
A Austreiberrohr;
B Pumpenkammer;
C Steigrohr;
D Heizelement;
E Temperaturwechsler.

Thermosyphon-Pumpe mit Pumpenkammer (Elektrolux).
A Austreiberrohr;
B Pumpenkammer;
C Steigrohr;
D Heizelement;
E Temperaturwechsler.

Dessing of new improved boiler.

1 — rich solution duct,
2 — weak solution duct,
3 — vapour duct,
4 — container for semi-degassed liquid,
5 — auxiliary liquid heat exchanger,
6 — main reservoir,
7 — concentration-balancing auxiliary tube,
8 — pump tube,
9 — heating element,
10 — vapour return duct,
11 — weak solution return duct,
12 — NH_3 vapour duct.

Figure 3.9: Directly driven bubble pumps used in Diffusion Absorption Refrigerators, on the left in bell style and with pumping chamber (Niebergall, 1959) and on the right with integrated rectification (Stierlin 1980).

A simple expression given by (Narayankhedkar *et al.*, 1985) relates the required **minimum height difference** Y [m] (Figure 3.8) to the rich solution level in the reservoir and the level of the heating zone at which the bubbles are formed in the bubble pump for the circulation. The derivation of the minimum height difference equation (3.43) with the substituted coefficients K_1 [m³/kg] and K_2 [kJ/kg] (equation (3.44) and (3.45)) is described in (Chen, 1995). The analysis is based on the assumptions that all bubbles are formed at the bottom of the minimum height difference Y, there is no relative velocity between the

weak solution and the refrigerant vapour bubbles in the tube and the friction loss and vapour pressure of the absorbent water are negligible.

$$Y = \frac{p \bullet \Delta h}{\rho_{Sr} \bullet \left(K_1 \bullet p + K_2 \bullet 10^3\right) - p} \tag{3.43}$$

$$K_1 = \frac{1 - X_{Sr}}{(1 - X_{Sw}) \bullet \rho_{Sw}} \tag{3.44}$$

$$K_2 = \frac{(X_{Sr} - X_{Sw}) \bullet R \bullet T_b}{(1 - X_{Sw}) \bullet M_{NH3}} \tag{3.45}$$

Here p [Pa] is the total pressure, Δh [m] is the lifting height of the bubble pump, ρ_{Sr} and ρ_{Sw} are the rich and weak solution densities [kg/m³], X_{Sr} [-] and X_{Sw} [-] are the rich and weak solution concentrations. R is the universal gas constant (8.31451kJ/kmol K), T_b [K] is the mean boiling temperature of the generator and M_{NH3} [kg/kmol] is the relative molecular mass of the refrigerant ammonia.

The directly driven bubble pump of DARs consist usually of a single lifting tube where the heat input is restricted to a small heating zone by a heating cartridge or the flame of a gas burner with a high heat flux density. The indirectly driven DACM consists on the other hand, of a bundle of tubes as bubble pump where the heating zone is spread and lower heat flux densities are reached. The developed bubble pumps of the two DACM pilot plants are basically vertical shell-and-tube heat exchangers where the solution flows inside the tubes of small circular cross-section forming slug-flow at best and the heating medium flows through baffled tube bundles on the shell side (Figure 3.10).

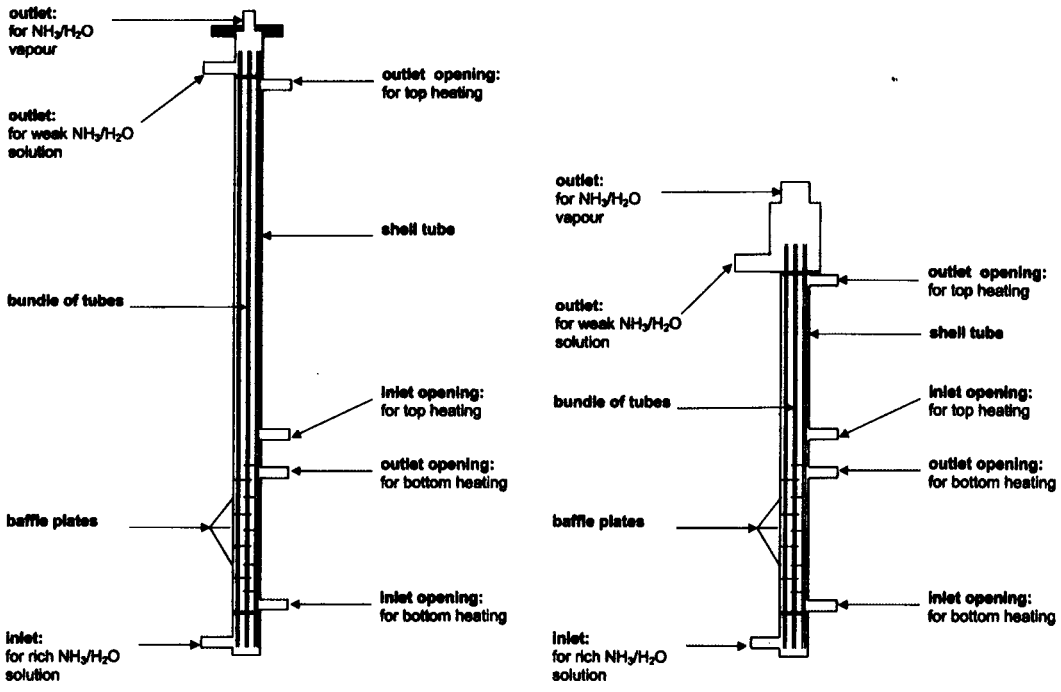

Figure 3.10: Indirectly driven bubble pump/generator No.3 (left side) and No.5 (right side) of the of the first and second pilot plant.

The analysis of the minimum height difference Y of the used bubble pumps for the DACMs No.1 and No.2 is applied to a mid heating zone. For a relative molecular mass of the refrigerant ammonia of 17kg/kmol and the given data in table 3.1 of mean boiling temperatures, rich and weak solution concentrations and densities, the total pressures and the two different lifting heights, the minimum height difference of 0.12m for DACM No.1 and 0.03m for DACM No.2 is reached. In both cases the minimum height difference is observed.

Table 3.1: Investigated minimum height difference between the top level of the reservoir and the heating zone of the bubble pump.

	DACM No.1	DACM No.2
generator mean boiling temperature T_b [°C]	130	110
NH3 rich/weak mass concentration X_{Sr} / X_{Sw} [-]	0.42 / 0.34	0.37 / 0.27
rich/weak solution density ρ_{Sr} / ρ_{Sw} [kg/m³]	742 / 783	789 / 837
total pressure p [Pa]	$20x10^5$	$12x10^5$
lifting height Δh [m]	1.00	0.50
minimum height difference Y [m]	0.12	0.03

3.4.3 FLOW REGIMES

The operation of the gas bubble pump is based on internal forced convection boiling, commonly referred to as two-phase flow, and is characterised by rapid changes from liquid to vapour in the flow direction. By external heating of the vertical pipes of the bubble pump, the pipes are surrounded by a heat transfer medium e.g. a water-glycol mixture or thermooil. The ammonia/water solution rests in the bundle of pipes in such a way that when the tube walls are overheated ammonia is expelled from the solution. Thereby, bubbles are formed at the inner surface of the tube walls under constant heat supply. In this case, the procedure is called flow boiling. The internal flow boiling has to be distinguished into five two-phase flow regimes (bubbly flow, slug flow, annular flow, transition flow and mist flow) as shown in Figure 3.11.

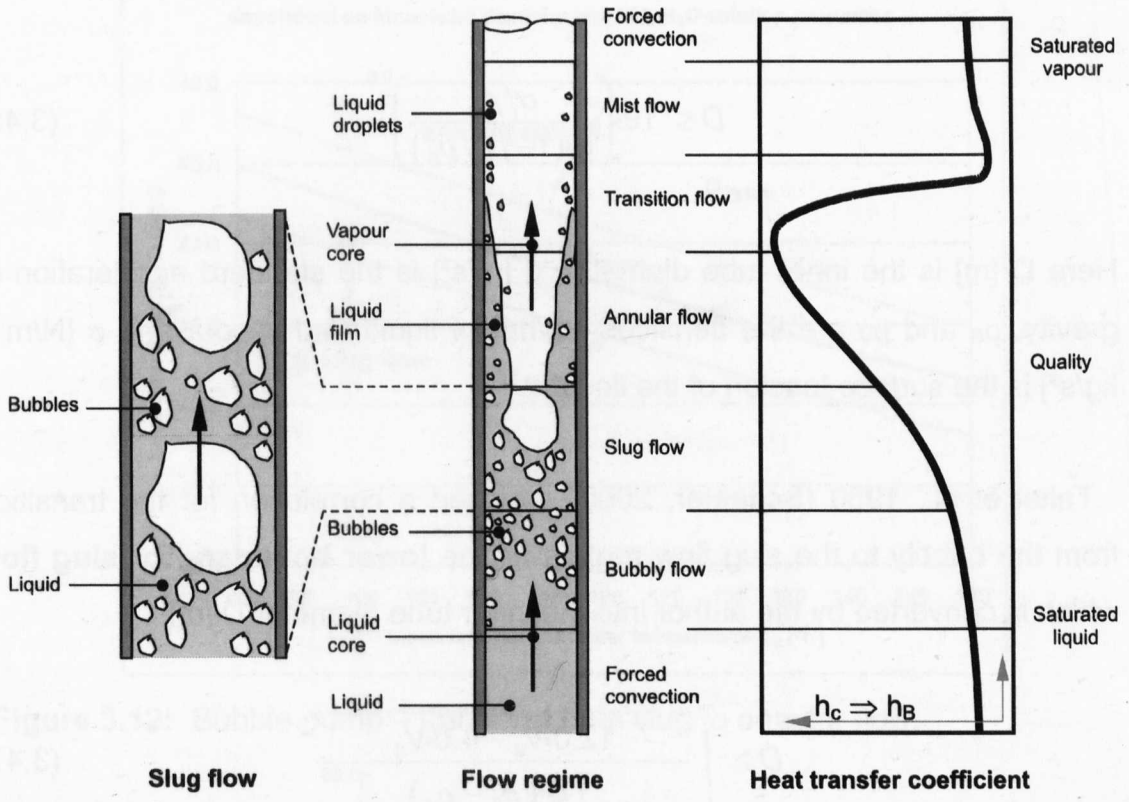

Figure 3.11: Flow regimes of two-phase vertical flows.

At very low heat flux densities, little bubbles are formed on the heating walls that then separate from the inner tube wall and flow upward. This flow regime is

called bubbly flow. Increasing the heat flux density, slug flow is formed by more and more germ cells. The bubbles form plugs which engage the whole circular tube section. This flow regime must be reached in order for the operation of the DACM to be able to guarantee the solution lifting and with that the solution circulation. Heating up the tube wall still more, causes the shared vapour to increase, changing the slug flow regime into annular flow. If the tube wall is then overheated, then vapour is mainly produced with some liquid droplets. This is the flow regime change describing the transition to mist flow. The vapour is then superheated by forced convection on the surface (Çengel, 1998; Incropera *et al.*, 1996). For the generators investigated only the slug flow regime is relevant.

An **upper boundary for slug flow** is provided by Chisholm, 1983 (Delano, 1998; Schaefer, 2000), which predicts a transition from slug to annular flow as is described below:

$$D \leq 19 \cdot \left(\frac{\sigma / \rho_S}{g \cdot (1 - \rho_V / \rho_S)} \right)^{0.5} \tag{3.46}$$

Here D [m] is the inner tube diameter, g [m/s²] is the standard acceleration of gravity, ρ_S and ρ_V are the densities [kg/m³] of liquid and vapour and σ [N/m = kg/s²] is the surface tension of the liquid.

Taitel et al., 1980 (Schaefer, 2000) provided a correlation for the transition from the bubbly to the slug flow regime as the **lower boundary for slug flow** which is converted by the author into the inner tube diameter D [m]:

$$D \geq \sqrt{\frac{12.0 \cdot \dot{V}_V - 4.0 \cdot \dot{V}_S}{\pi \cdot 1.15 \cdot \left[\frac{g \cdot (\rho_S - \rho_V)}{\rho_S^{\,2}} \cdot \sigma \right]^{0.25}}} \tag{3.47}$$

where $\dot{V}_S$ and $\dot{V}_V$ are the liquid and vapour volume flow rates [m³/s], g

[m/s²] is gravity, ρ_S and ρ_V are the densities [kg/m³] of liquid and vapour, . [kg/s²] is the surface tension of the liquid.

For the indirectly driven generator of the DACM, the limit values for the inner tube diameter are presented in Figure 3.12 for the transition from slug to churn flow and Figure 3.13 for the transition from bubbly to slug flow. The calculated values are dependant on the ammonia/water properties as liquid and vapour densities (equation (3.12) and (3.7)) and liquid surface tension (3.18) as well as the internal mean generator temperature T_G [°C], different ammonia/water mean solution concentrations X_S [-] or ammonia vapour m_V [kg/h] and ammonia/water solution m_S [kg/h] mass flows. Slug flow usually occurs within tubes that have an inner diameter ranging from 5mm and 41mm.

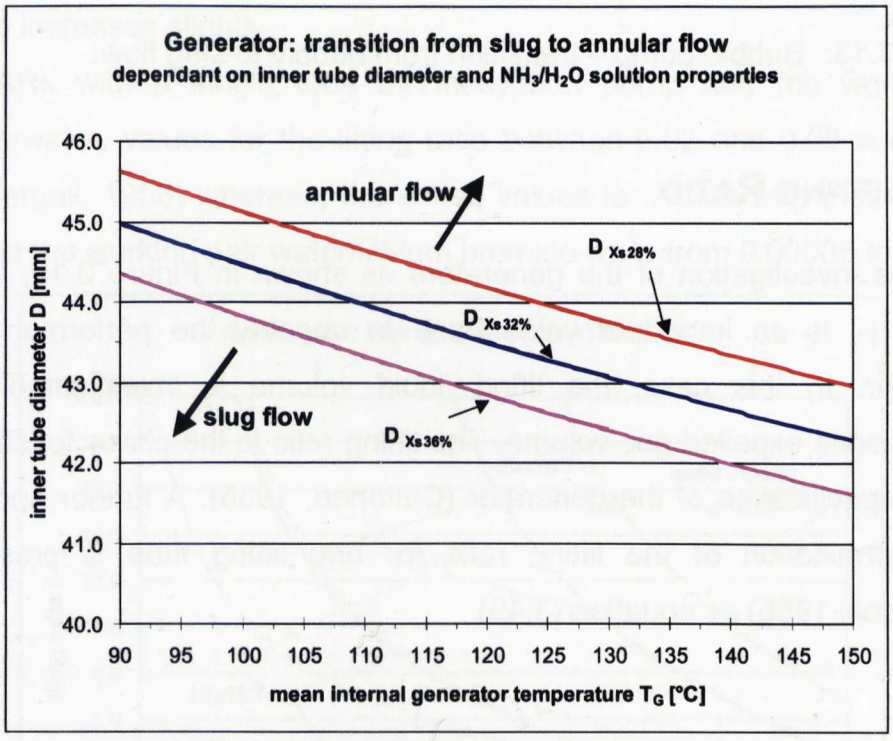

Figure 3.12: Bubble pump – transition from slug to annular flow.

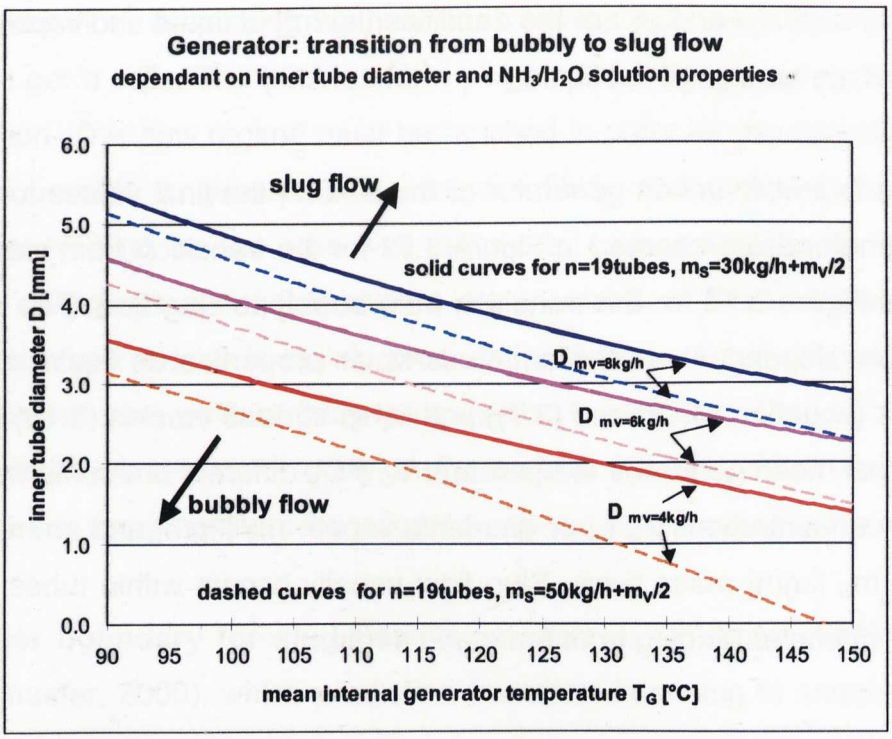

Figure 3.13: Bubble pump – transition from bubbly to slug flow.

3.4.4 LIFTING RATIO

For the investigation of the generators as shown in Figure 3.10, the **lifting ratio** b [-] is an important value used to quantify the performance of the generator. In this case, the lifted liquid volume is investigated with the simultaneous expelled gas volume. The lifting ratio is the characteristic number for the specification of the generator (Cattaneo, 1935). A further approach for the determination of the lifting ratio for one lifting tube is presented by (Niebergall, 1956) as equation (3.49).

$$b = \frac{\dot{V}_L}{\dot{V}_V} \tag{3.48}$$

$$b = \frac{X_{V1} - X_{Sr}}{X_{Sr} - X_{Sw}} \cdot \frac{\rho_{V1}}{\rho_{Sw}} \tag{3.49}$$

Here V_L [l/h] is the lifted liquid volume and V_V [l/h] is the simultaneously expelled gas volume. X_{V1} [-] is the vapour concentration, X_{Sr} [-] and X_{Sw} [-] are the rich

and weak solution concentrations, ρ_{V1} [kg/m³] and ρ_{Sw} [kg/m³] are the vapour and lifted weak solution densities calculated by equation (3.7) and (3.12). If more than one lifting tube is used as bubble pump, the equation (3.49) has then to be multiplied by the total number n [-] of lifting tubes.

Figure 3.14 shows the theoretical lifting ratios depending on the total pressure for the used and investigated generator No.3 and No.5, each with nineteen lifting tubes. For an internal generator outlet as well as weak solution temperature of 150°C lifting ratios for rich solution concentrations X_{Sr} of 0.30 and 0.40 occurs to 4.3, 10.0 and 15.9 as well as 1.8, 4.0 and 5.5 for the constant total pressures of $12x10^5$Pa, $17x10^5$Pa and $20x10^5$Pa respectively. In reality, the total pressure increases slightly with the increased generator heating as well as internal weak solution outlet temperature, meaning that the lifting ratio also increases slightly.

For DARs with a single tube thermosyphon pump and the working pair ammonia/water, values for the lifting ratio between 0.02 and 0.08 were stated by (Niebergall, 1956) whereas, the stated values for ACMs with thermosyphon pump and the working pair water/lithium bromide were from 0.00005 to 0.0005.

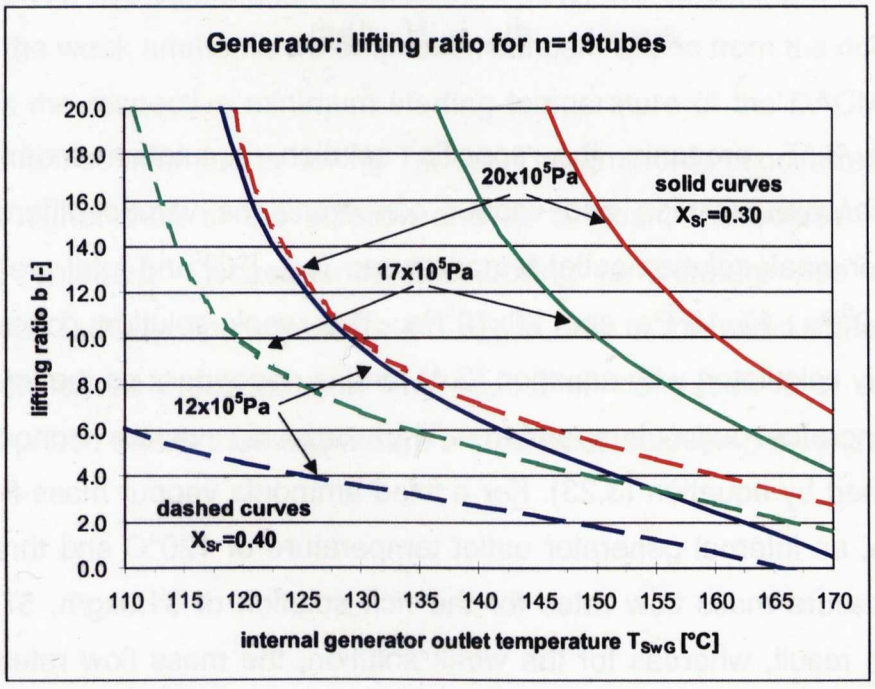

Figure 3.14: Lifting ratio versus internal generator outlet temperature for constant total pressure levels of $12x10^5$Pa, $17x10^5$Pa and $20x10^5$Pa .

3.4.5 SPECIFIC SOLUTION CIRCULATION INDEX AND MASS FLOW

Another important characteristic value of the generator is the **specific solution circulation index** f [-] (equation (3.50)), which is defined as the ratio of the mass flow rates of the rich solution m_{Sr} [kg/s] to the ammonia vapour m_V [kg/s] as well as the ratio between the vapour X_{V1} [-] and weak solution X_{Sw} [-] concentration to the degassing width E [-] which is the difference between the weak and the rich solution concentration X_{Sr} [-].

$$f = \frac{\dot{m}_{Sr}}{\dot{m}_V} = \frac{X_{V1} - X_{Sw}}{X_{Sr} - X_{Sw}} \tag{3.50}$$

Depending on the specific solution circulation index, the **mass flow rate** of the rich m_{Sr} [kg/s] or weak m_{Sw} [kg/s] ammonia/water solution can be calculated by equations (3.51) and (3.52) as follows:

$$\dot{m}_{Sr} = f \bullet \dot{m}_V \tag{3.51}$$

$$\dot{m}_{Sw} = (f-1) \bullet \dot{m}_V \tag{3.52}$$

Figure 3.15 presents the specific solution circulation index with the ammonia/water solution and vapour concentrations versus different internal generator weak solution outlet temperatures T_{SwG} [°C] and total pressures p_{total} of $12x10^5$Pa, $17x10^5$Pa and $20x10^5$Pa. The weak solution concentration is iteratively calculated with equation (2.4), and is dependant on the total pressure and generator outlet temperature. The ammonia vapour concentration is determined by equation (3.23). For a fixed ammonia vapour mass flow rate m_V of 8kg/h, an internal generator outlet temperature of 120°C and three different total pressure mass flow rates for the rich solution of 31.9kg/h, 57.4kg/h and 97.2kg/h result, whereas for the weak solution, the mass flow rates are 8kg/h lower.

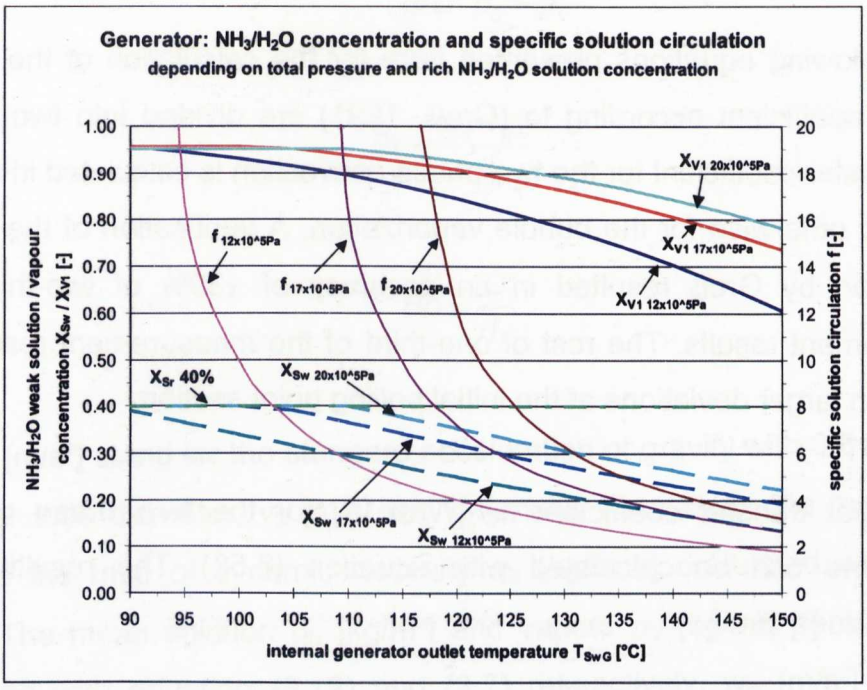

Figure 3.15: NH_3/H_2O weak solution and vapour concentration and specific solution concentration versus the internal generator outlet temperature for a rich NH_3/H_2O solution concentration of 40%.

For the given rich solution concentration of 40%, the beginning of the dashed curves of the weak ammonia/water solution concentrations from the rich solution line shows the respective minimum starting temperature of the DACM process where the rich solution starts boiling $T_B(X_{Sr})$. The ammonia concentration in the vapour is higher than in the solution and as a result, the solution becomes noticeably depleted. Consequently, the boiling temperature rise up to its maximum at $T_B(X_{Sw})$. The concentration X_{Sw} is now in the exact state in which the solution leaves the generator. The vapour concentration is in equilibrium with liquid phase and is thus dependant on the weak solution concentration.

3.4.6 HEAT TRANSFER COEFFICIENT

The following equations presented here for the calculation of the inner heat transfer coefficient according to (Groß, 1991) are divided into two parts. The heat transfer coefficient for the two-phase convection is calculated in the vertical tube and otherwise for the bubble vaporization. A verification of the suggested calculation by Groß resulted in an accuracy of ±30% of two-thirds of the measurement results. The rest of one-third of the measurement results occurs mainly on larger deviations at the initial boiling point section.

The heat transfer coefficient h_C [W/m² K] for the **two-phase convection conditions** can be calculated with equation (3.53). The resulting Nusselt number Nu [-] is

$$h_C = \frac{Nu \bullet \lambda_S}{d_b} \tag{3.53}$$

$$Nu = 4 \bullet \left(Ar \bullet Fr^{0.5}\right)^{1/3} \bullet \mathrm{Pr}^{0.5} \bullet \left(\frac{Bo}{10}\right)^{n} \tag{3.54}$$

where λ_S [W/m K] is the thermal conductivity of the mean solution calculated by equation (3.13) or (3.14), d_b [m] is the Laplace constant given by equation (3.60) and n [-] is an auxiliary size given by equation (3.61).

For the determination of the Nusselt number, the following characteristic numbers are necessary: the Archimedes Ar [-], Froude Fr [-], Prandtl Pr [-] and the Bond number Bo [-] which are calculated with the following equations (3.55), (3.56), (3.57) and (3.58) respectively.

$$Ar = \frac{g \bullet D^3}{\nu_S^{\,2}} \bullet \frac{\rho_S - \rho_V}{\rho_S} \tag{3.55}$$

$$Fr = \frac{w_S^2}{g \cdot D} \cdot \frac{\rho_S}{\rho_S - \rho_V} \tag{3.56}$$

$$Pr = \frac{\eta_S \cdot c_{p,S}}{\lambda_S} \tag{3.57}$$

$$Bo = \frac{D}{d_b} \tag{3.58}$$

Here, g [m/s²] stand for the standard acceleration of gravity with 9.81m/s², D [m] the inner tube diameter, ν_S [m/s] the kinematic viscosity of the mean solution which is the ratio of dynamic viscosity η_S [kg/m s] calculated with equation (3.15). The mean solution ρ_S [kg/m³] and vapour ρ_V [kg/m³] densities can be calculated with equation (3.12) and (3.7) respectively. w_S [m/s²] is the flow velocity of the mean solution given with equation (3.59) and $c_{p,S}$ [J/kg K] is the specific heat capacity of the mean solution calculated with equation (3.11).

For the calculation of the Froude number, the flow velocity of the mean solution w_S [m/s²] is required as given by equation (3.59). The Bond number normally requires the bubble diameter, however, as this value is variable and normally unknown, the Laplace constant is used instead which an be calculated with equation (3.60).

$$w_S = \frac{q}{\rho_S \cdot \Delta h_E} \tag{3.59}$$

$$d_b = \left(\frac{\sigma}{(\rho_S - \rho_V) \cdot g} \right)^{0.5} \tag{3.60}$$

Here, q [kW/m²] is the heat flux density, Δh_E [kJ/kg] is the specific evaporation enthalpy of ammonia calculated with equation (4.25) and σ [N/m = kg/s²] is the surface tension of the bubble surface calculated with equation (3.18).

The auxiliary size n [-] for the Nusselt number is stated in equation (3.61) as follows:

$$n = \frac{1}{2} \quad for \quad Bo \leq 10 \quad \text{as well as} \quad n = \frac{1}{6} \quad for \quad Bo > 10 \tag{3.61}$$

For the **bubble vaporization conditions**, a separate heat transfer coefficient h_B [W/m² K] equation is given by (Groß, 1991) as follows:

$$h_B = 55 \cdot (q)^{0.7} \cdot M^{-0.5} \cdot \frac{(p^*)^{0.12}}{(-\log p^*)^{0.55}} \tag{3.62}$$

$$p^* = \frac{p}{p_{cr}} \tag{3.63}$$

where q [W/m²] is the heat flux density, M [kg/kmol] is the molecular mass of the mean solution and p* [-] is the reduced pressure which is the ratio of the system p [Pa] to critical pressure of the fluid p_{cr} [Pa].

For the calculation the following data of the pure substance ammonia and water are given in table 3.2 as taken from the (VDI Wärmeatlas, 1988). The ammonia/water mixture values are determined by a mass concentration weighting, which is given by the arithmetical mean solution concentration X_S [-] of the rich and weak solutions.

Table 3.2: Properties for the calculation of the inner heat transfer coefficient (VDI Wärmeatlas, 1988).

substance	ammonia NH_3	water H_2O	NH_3/H_2O	
			X_S=0.25	X_S=0.35
critical pressure p_{cr} [Pa]	113.00x10^5	220.64 x10^5	193.73x10^5	182.97x10^5
molecular mass M [kg/kmol]	17	18	17.75	17.65

For the determination of the final mean heat transfer coefficient h_m, the largest calculated value from the convective or boiling field must be used (Groß, 1991).

An example of kind of heat transfer coefficients is presented in Figure 3.16. The convective heat transfer coefficient is independent of the pressure level, whereas the boiling heat transfer coefficient is calculated for the total pressure levels of $12x10^5$Pa, $17x10^5$Pa and $20x10^5$Pa. The calculated results of the inner heat transfer coefficient show a reached 0.6kW to 7.2kW heating capacity with applied heat flux densities of the heating cycle of 5kW/m² to 60kW/m² for a 0.12m² generator heat transfer surface. The inner tube diameter is 0.005m and the properties for the convective heat transfer coefficient are calculated for a mean solution temperature of 100°C. For the design heating capacity of 5.2kW as well as approximately 43.3kW/m² heat flux density, the calculated boiling heat transfer coefficients result in a range of 15,000W/m²K to 18,000W/m²K depending on the total pressure and the mean solution concentration.

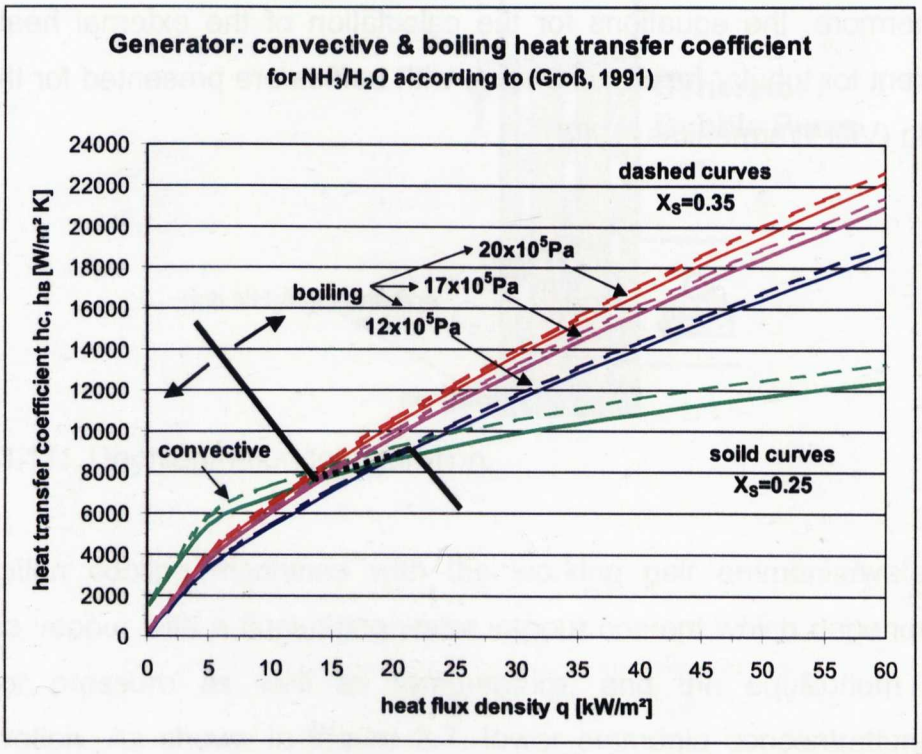

Figure 3.16: Inner convective heat transfer coefficient independent of pressure and boiling heat transfer coefficient for total pressure levels of $12x10^5$Pa, $17x10^5$Pa and $20x10^5$Pa versus heat flux densities.

If the heat transfer coefficient collapses at one single heating tube wall due to superheating, the slug-flow then breaks down. However, this does not occur simultaneously in all of the tubes in the bundle used by the generator. The fact that the change of state does not take place at the same time in every tube, causes a gradual increase of the volume flow curve because the solution lifting in the single tubes starts gradually. A gradual decrease occurs as well due to the fact that no abrupt standstill of the lifting takes place simultaneously in all of the tubes at once.

Further equations for the calculation of the inner heat transfer coefficient for vertical tubes are given in (VDI Wärmeatlas, 1988). Using the heat transfer coefficient equations for the boiling process, the resulted values by the author and from (Biesinger 2002) showed a 1.2 times lower value than those determined by the used equations from (Groß, 1991).

Furthermore, the equations for the calculation of the external heat transfer coefficient for tubular heat exchangers with baffles are presented for the bubble pump in (VDI Wärmeatlas, 1988).

3.5 DEPHLEGMATOR

As described before in chapter 3.2, the dephlegmator, which can also be called a rectifier or knock-out pod, is situated between the generator and the condenser (as shown in Figure 3.17) and is used to condense a part of the water vapour out of the ammonia/water vapour.

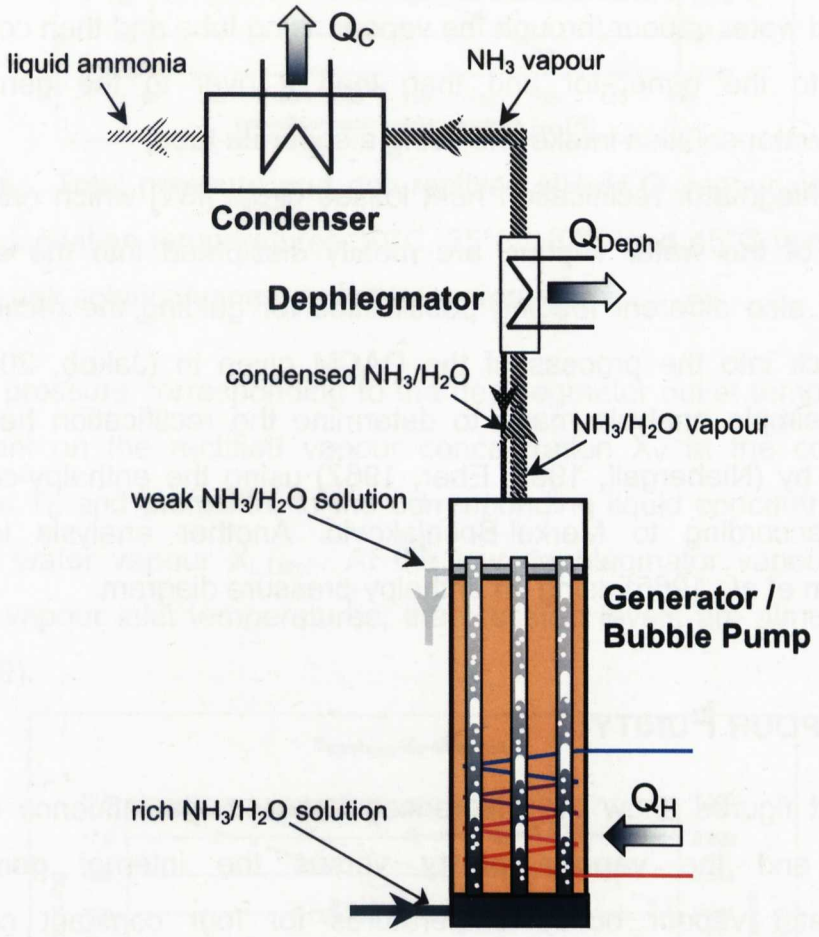

Figure 3.17: Dephlegmator configuration.

Absorption cooling machines with the working pair ammonia/water expel ammonia vapour with a fluctuating water vapour content which depends on the generator pressure as well as temperature, and the equilibrium solution concentration. As shown in Figure 2.7, lower ammonia concentrations of the solution lead to higher generator temperatures and thereby more water vapour is evaporated due to the low boiling point temperature distance ΔT_{bp} between

the refrigerant ammonia and the solvent water with 133K. Therefore, the dephlegmator increases the vapour purity of the ammonia/water vapour which enters the condenser.

The condensed water vapour containing a large amount of ammonia could be led, in the simplest case, through the vapour rising tube directly to the weak ammonia/water solution in the upper part of the generator (Figure 3.17) as was the case in the two pilot plants. The better alternative however, is to lead the condensed water vapour through the vapour rising tube and then collect it at the entrance to the generator and then lead it over to the generators rich ammonia/water solution intake line using a separate tube.

The dephlegmator rectification heat losses Q_{Deph} [kW] which result from the liquefying of the water vapour, are mostly dissipated into the environment. There are also different feeding possibilities for guiding the rectification heat losses back into the process of the DACM given in (Jakob, 2000; Teußer, 2004). A simple analysis made to determine the rectification heat losses is described by (Niebergall, 1959; Eber, 1967) using the enthalpy-concentration diagram according to Merkel-Bosnjakovic. Another analysis is given by (Bäckström *et al.*, 1965) using an enthalpy-pressure diagram.

3.5.1 VAPOUR PURITY

The next figures show the differences between the influence on the total pressure and the **vapour purity** versus the internal generator and dephlegmator vapour outlet temperatures for four constant condensation temperatures depending on the external cooling water temperatures.

The total pressure corresponding to the generator outlet temperature T_{V1G} is dependant on the non-rectified vapour concentration X_{V1} at the condensation temperature T_C and with that, to the corresponding solution concentration of the lifted weak solution X_{Sw}. The determined vapour concentrations are much lower this way than if the vapour is cooled down by a dephlegmator before entering the condenser. Hereby, the pressure levels decreases with an increase in the internal generator weak solution/vapour outlet temperatures (Figure 3.18).

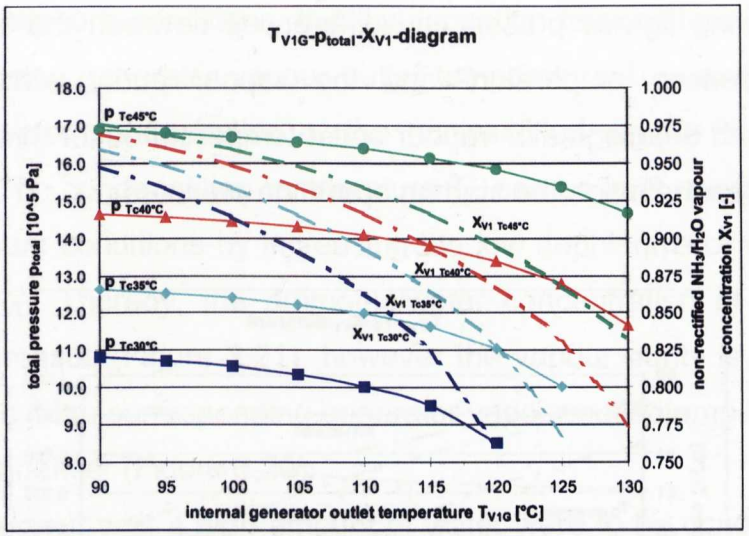

Figure 3.18: Total pressure and non-rectified NH_3/H_2O vapour concentration for the condensation temperatures 30°C, 35°C, 40°C and 45°C versus internal generator weak solution/vapour outlet temperatures.

The total pressure corresponding to the dephlegmator outlet temperature T_{VD} is dependant on the rectified vapour concentration X_V at the condensation temperature T_C and therewith, to the corresponding liquid concentration of the condensed water vapour $X_{L,Deph}$. At the low dephlegmator vapour outlet, or condenser vapour inlet temperatures, the pressure levels are almost constant (Figure 3.19).

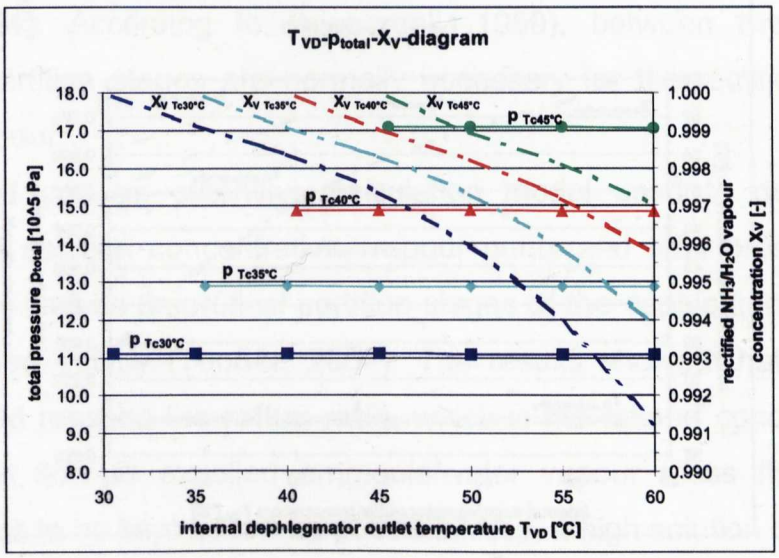

Figure 3.19: Total pressure and rectified NH_3/H_2O vapour concentration for the condensation temperatures 30°C, 35°C, 40°C and 45°C versus internal dephlegmator vapour outlet temperatures.

The following figures present the differences between the influence on the mean condenser temperature and the vapour purity versus the internal generator and dephlegmator vapour outlet temperatures for three constant total pressures depending on the starting operation pressure.

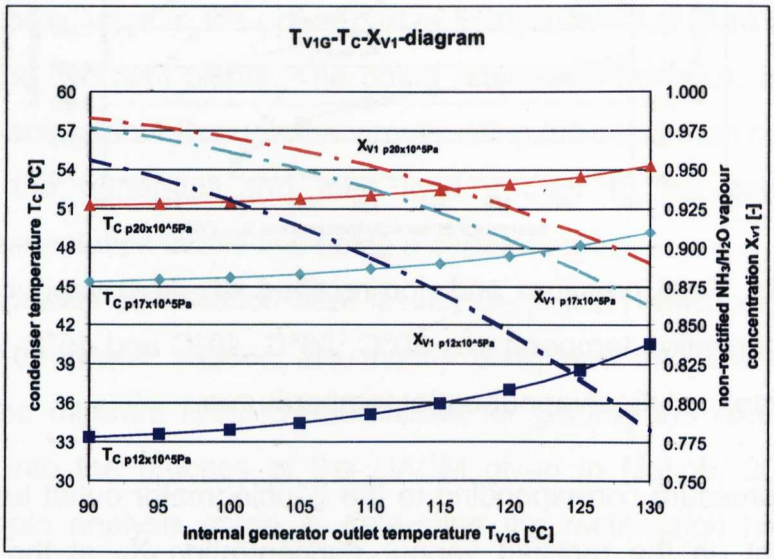

Figure 3.20: Condenser temperature and non-rectified NH_3/H_2O vapour concentration for constant total pressure levels of $12x10^5$Pa, $17x10^5$Pa and $20x10^5$Pa versus internal generator vapour outlet temperatures.

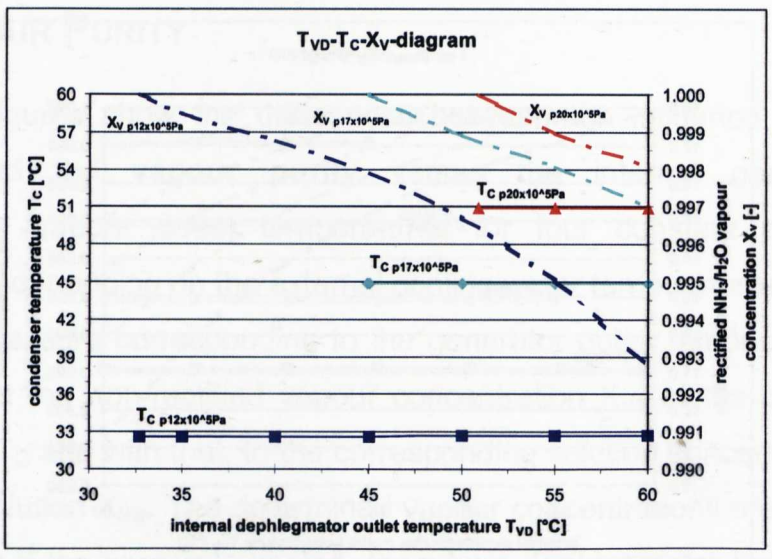

Figure 3.21: Condenser temperature and rectified NH_3/H_2O vapour concentration for constant total pressure levels of $12x10^5$Pa, $17x10^5$Pa and $20x10^5$Pa versus internal dephlegmator vapour outlet temperatures.

At constant pressure conditions, the condensation temperature T_C increases with the increasing generator vapour outlet temperature T_{V1G} and as a result, the ammonia/water concentration of the non-rectified vapour X_{V1} decreases (Figure 3.20). The condensation temperature T_C can be kept nearly constant at constant pressure conditions by increasing the low dephlegmator vapour outlet temperature T_{VD}. Thereby, the ammonia/water concentration of the rectified vapour X_V decreases (Figure 3.21), however the vapour purity is much higher than it would be if the corresponding generator vapour outlet temperatures were to enter the condenser (Figure 3.20).

If ammonia vapour with a high amount of water were to be condensed inside of the condenser and were to enter the evaporator, large cooling capacity losses would occur because the ammonia would not be able to evaporate completely, but would leave the evaporator in a partly liquid state dissolved in the water. Normally the rectified ammonia vapour that leaves the dephlegmator consists approximately of 99.8% ammonia and 0.2% rest water vapour.

3.5.2 PARTITION STAGES AND REFLUX RATIO

Further descriptions and interpretations of the dephlegmator, especially of the principle of theoretical **partition stages**, are described in (Niebergall, 1959; Teußer, 2004). According to (Niebergall, 1959), between two and three theoretical partition stages are normally necessary for the rectification of the ammonia vapour.

A simplified and an extensive calculation model used to determine the influences of solution concentration, vapour purity and total pressure on the reflux ratio as well as theoretical partition stages of the dephlegmator, were set up and carried out by (Teußer, 2004). The results showed that because of energy-related reasons the **reflux ratio**, which is the ratio of condensed water vapour mass flow to expelled ammonia/water vapour mass flow from the generator, has to be kept as low as possible. Also, a high solution concentration reduces the reflux ratio. If the DACM process is driven with the least possible pressure, then the reflux ratio and the required generator heating temperatures are minimal. Compared to the solution circulation, the reflux ratio is usually low.

3.6 AUXILIARY GAS CIRCUIT

In the following chapters, the theories and calculation equations of partial pressure, auxiliary gas cooling losses, pressure drop, diffusion, film thickness and heat transfer coefficients for the auxiliary gas circuit as well as falling film evaporator, gas heat exchanger and falling film absorber are described and investigated in detail. Figure 3.22 shows the auxiliary gas circuit with the investigated fields.

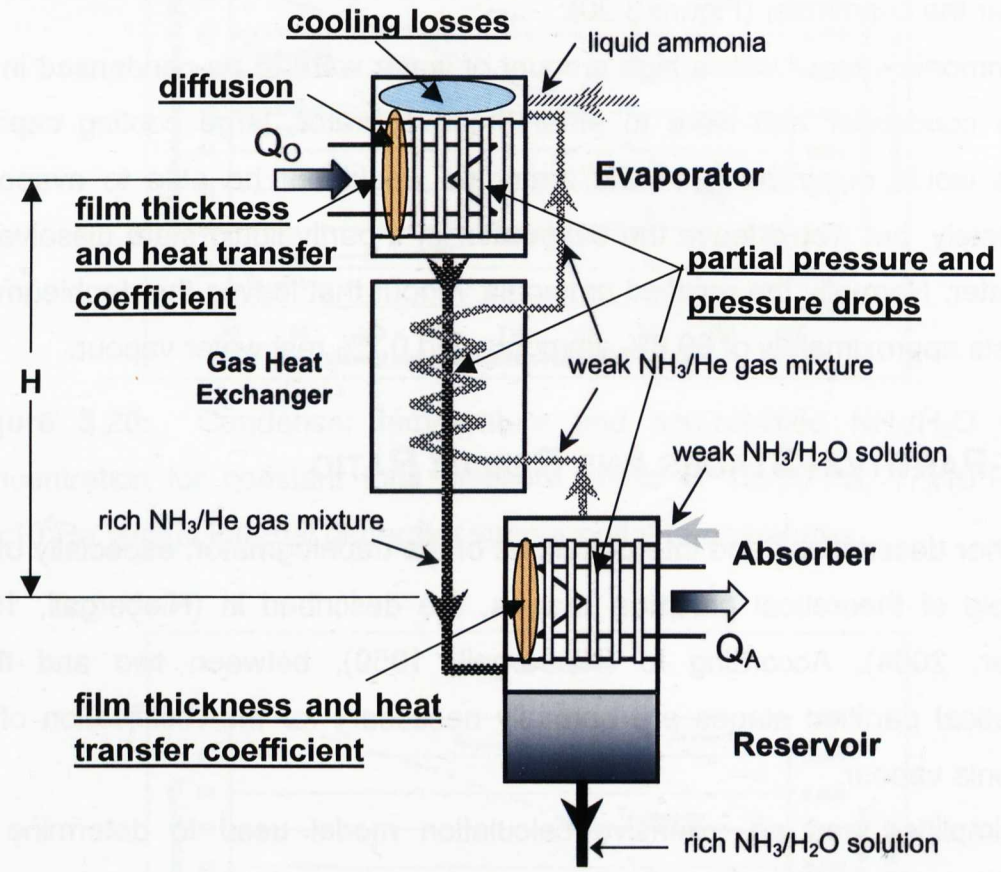

Figure 3.22: Auxiliary gas circuit configuration.

In evaporators of CCMs or ACMs, the refrigerant simply boils into its own vapour, whereas in an evaporator of a DACM, the refrigerant is evaporated into an inert auxiliary gas atmosphere by diffusion. Hydrogen or helium are used as inert gases. In order to maintain the mentioned evaporation process, the progressive saturation of the inert gas through the refrigerant has to be prevented by the absorber which absorbs the refrigerant vapour out of the inert gas mixture before it flows back into the evaporator.

3.6.1 LITERATURE REVIEW

Several theoretical and experimental investigations of the auxiliary gas circuit were done for the DAR. The most extensive investigations and posing of theories regarding the auxiliary gas circuit, especially the gas circulation with the cooling loss and the optimal distribution of the driving force, were done by (Bäckström, 1954; Bäckström, 1956; Bäckström *et al.*, 1965). The existence of an optimum flow rate of hydrogen through the gas circuit was determined by (Watts *et al.*, 1958). Different types of counter-flow gas heat exchangers using hydrogen as inert gas were experimentally investigated by (Stierlin, 1971) in order to reach the best propulsion height H [m] for deep-freezers. Further experimental investigations of gas circuits, especially the gas mixture velocities and the optimum driving head, were done by (Narayankhedkar *et al.*, 1985). It was found by (Narayankhedkar *et al.*, 1985; Kouremenos *et al.*, 1994) that the optimum driving height is greater when using helium as inert gas, despite it has higher density and viscosity in comparison to hydrogen. Furthermore, the lower specific heat and thermal conductivity of helium reduces the internal heat load (gas circulation loss) and a slightly higher cooling capacity is observed with an ammonia/helium mixture.

Many measurements and simulations on the irreversible evaporation of ammonia into ammonia/hydrogen or ammonia/helium gas atmospheres for horizontal annular tubes were performed by (Kouremenos *et al.*, 1987; Kouremenos *et al.*, 1988a; Kouremenos *et al.*, 1988b; Kouremenos *et al.*, 1994) in order to determine the inlet concentration of the gas mixtures and the gas mass flow rate entering the evaporator. A vertical annular tube was also modelled using helium as inert gas (Kouremenos *et al.*, 1990). In addition, the main thermodynamic and transport properties of ammonia/hydrogen or ammonia/helium binary gas mixtures were presented in (Kouremenos *et al.*, 1988a; Kouremenos *et al.*, 1994).

A further absorber counterflow model and a combined evaporator and AGHX parallel flow model each for a horizontal pipe was developed by (Shi, 1994) based on heat and mass transfer. The latest presented theoretical study on the

gas circuit of a DAR was done by (Maiya, 2003). The influences of total pressure and flow rate of inert gas on refrigerator performance were studied and compared for hydrogen and helium as the inert gas. Results showed that an excessive charging of inert gas is undesirable, and that the propulsion height always decreases with increased total pressure.

Investigations of a falling film evaporator of a DACM were done by (Päßler, 2002), specifically temperature measurement profiles along the evaporator surface and thermography photos of the running auxiliary gas circuit.

3.6.2 PARTIAL PRESSURE

Mixtures of ideal gases, which do not react chemically with each other, behave as ideal gases. This means, that the total pressure of an ideal gas mixture is equal to the sum of the **partial pressures** of the single gases. Each gas component behaves as if it could fill-out the entire given volume alone by itself and as if the other gas components are not present. Therefore, the total pressure p_{total} [Pa] in the evaporator and absorber is composed of the sum of the partial pressures of the refrigerant vapour p_{NH3} [Pa] and the auxiliary gas p_{AUX} [Pa]. This idea is described by Dalton's law (Bäckström *et al.*, 1965) as is given by the following equation (3.64):

$$p_{total} = p_{NH_3} + p_{AUX} \tag{3.64}$$

In the falling film evaporator, the driving force for evaporation through diffusion is the partial pressure of the refrigerant in the inert gas mixture which is lower than the refrigerant's vapour pressure. The evaporation process itself of a liquid within the evaporator is based on the effect of the elimination of fast molecules from the liquid. The evaporation in a DACM however, can be distinguished from the conventional vaporization performed in ACMs because with this method, the particles are removed with high kinetic energy. For the removal of the fast molecules, an inert gas is introduced over the liquid surface, causing the liquid

to evaporate into the inert gas. Thus, the driving force for this effect is the difference between the unsaturated gas and the liquid surface. Evaporation is an endothermic process which is combined with heat absorption. The cooling effect by the evaporation is reduced if the inert gas is nearly saturated.

In the falling film absorber, the refrigerant is absorbed into the weak solution to reach the weak solution's vapour pressure which must be lower than the partial pressure of the refrigerant in the gas mixture. The corresponding vapour pressure of the solutions are a function of the temperature and the mass concentration. The minimum partial pressure of refrigerant in the weak gas mixture leaving the absorber is thus determined by the vapour pressure of the weak solution entering the absorber. On the other hand, the rich solution leaving the absorber is determined by the partial pressure of the refrigerant in the rich gas mixture entering the absorber.

3.6.3 DRIVING PRESSURE DIFFERENCE

The absorption of the refrigerant vapour in the absorber is afflicted by a resistance which is formed by the **driving pressure difference between the evaporator and the absorber**. With DACMs, the partial pressure difference between evaporator pressure and saturated vapour pressure above the rich solution in the absorber has to be essentially higher then of common ACMs. The partial pressure difference Δp_{EA} [Pa] is sufficient with 0.5×10^5Pa for ACMs but for the DACM it has to be between approximately 1.0×10^5Pa and 1.5×10^5Pa (Bäckström *et al.*, 1965) because of the diffusion resistance. The relationship between the partial pressure of the evaporator and the absorber is given in equation (3.65) as follows:

$$p_e = p_{ar} + \Delta p_{EA} \tag{3.65}$$

Here, p_{ar} [Pa] is the absorber partial pressure of the rich solution and p_e [Pa] is the evaporator partial pressure. An example for the partition of the partial pressures in a DAR can be found in (Bäckström *et al.*, 1965).

3.6.4 COOLING LOSSES

A further characteristic of the DACM is the **cooling loss** which is caused by the temperature rise of the circulated auxiliary gas from the absorber. If the warm, weak ammonia/helium auxiliary gas mixture enters the upper part of the evaporator (Figure 3.22), a part of the useable cooling capacity has to be used to cool down the auxiliary gas to a temperature near that of the evaporator. Therefore, it is necessary to cool the warm and weak auxiliary gas from the absorber with a gas heat exchanger in counterflow to the cold and rich ammonia/helium gas mixture from the evaporator in order to reduce cooling losses.

The evaporator cooling capacity Q_O [kW] for the DACM differs from the usual calculation of the evaporator cooling capacity of ACMs where only the first term is used. In equation (3.66) the second term represents the influence of the gas circulation on the resulting cooling capacity as follows:

$$Q_O = \left(\dot{m}_{L,NH3} \bullet \Delta h\right) - Q_{AUX} = \dot{m}_{L,NH3} \bullet \left[\left(h_{Vr} - h_L\right) - h_{AUX}\right] \tag{3.66}$$

where $m_{L,NH3}$ [kg/s] is the mass flow of the liquid ammonia, Δh [kJ/kg] is the enthalpy difference of the outlet rich ammonia/helium gas mixture enthalpy h_{Vr} [kJ/kg] and the inlet ammonia liquid enthalpy h_L [kJ/kg]. Q_{AUX} [kW] and h_{AUX} [kJ/kg] are the auxiliary gas circulation cooling loss capacity and enthalpy respectively.

The gas circulation cooling loss Q_{AUX} [kW] or h_{AUX} [kJ/kg] are fundamentally defined by equation (3.67) and (3.68) as follows:

$$Q_{AUX} = c_{p,Vw} \bullet \dot{m}_{Vw} \bullet \Delta T \tag{3.67}$$

$$h_{AUX} = \frac{c_{p,Vw} \bullet \dot{m}_{Vw}}{\dot{m}_{L,NH3}} \bullet (T_{VwE} - T_{VrE}) \tag{3.68}$$

where $c_{p,Vw}$ [kJ/kg K] is the specific heat capacity of the weak ammonia/helium gas mixture, m_{Vw} [kg/s] is the mass flow of the weak ammonia/helium gas mixture and ΔT [K] is the temperature difference of the evaporator weak gas mixture inlet temperature T_{VwE} [°C] which depends on the heat recovery factor of the GHX and the evaporator rich gas mixture outlet temperature T_{VrE} [°C].

The auxiliary gas circulation loss $\frac{c_{p,Vw} \bullet \dot{m}_{Vw}}{\dot{m}_{L,NH3}}$ [kJ/kg K] is defined by (Bäckström et al., 1965) in equation (3.69). The derivation of the equation can be found in (Bäckström et al., 1965; Päßler, 2002).

$$\frac{c_{p,Vw} \bullet \dot{m}_{Vw}}{\dot{m}_{L,NH3}} = \frac{(1-\upsilon_{Vr}) \bullet \left[M_{He} \bullet c_{p,He} + \upsilon_{Vw} \bullet \left(M_{NH3} \bullet c_{p,NH3} - M_{He} \bullet c_{p,He} \right) \right]}{M_{NH3} \bullet (\upsilon_{Vr} - \upsilon_{Vw})} \tag{3.69}$$

Here, M_{He} is the molecular mass of helium with 4kg/kmol, M_{NH3} is the molecular mass of ammonia with 17kg/kmol, υ_{Vr} [m³/m³] and υ_{Vw} [m³/m³] are the volume concentration of the rich and weak gas mixtures calculated using equation (3.71) and (3.70), $c_{p,He}$ [kJ/kg K] is the specific heat capacity of helium gas calculated with equation (3.33) and $c_{p,NH3}$ [kJ/kg K] is the specific heat capacity of ammonia vapour calculated with equation (3.6).

The volume concentration of the weak and rich gas mixture are resulted from the respective relationships of the refrigerant partial pressures of the weak p_{Vw} [Pa] and rich p_{Vr} [Pa] gas mixtures to the total pressure p_{total} [Pa] and condenser pressure as described in equations (3.70) and (3.71):

$$\upsilon_{Vw} = \frac{p_{Vw}}{p_{total}} \tag{3.70}$$

$$\upsilon_{Vr} = \frac{p_{Vr}}{p_{total}} \tag{3.71}$$

The total pressure is calculated with equation (2.4) using the mean internal condenser temperature and the ammonia liquid concentration. Furthermore, the partial pressures of the weak and rich gas mixtures are defined under the assumption that the gas mixture is not completely saturated in the evaporator or washed out of, or absorbed by the absorber (Bäckström *et al.*, 1965). Therefore, a partial pressure difference percentage is assumed for the saturation Δp_{sat} for up to 95% of the partial pressure and for the wash out Δp_{abs} of 90% of the partial pressure. The resulting equations (3.72) and (3.73) are:

$$p_{Vr} = p_e \bullet \Delta p_{sat} \tag{3.72}$$

$$p_{Vw} = p_{aw} / \Delta p_{abs} \tag{3.73}$$

where p_e [Pa] and p_{aw} [Pa] are the evaporator and absorber weak solution partial pressures which are calculated with equation (2.4) with the mean internal evaporator temperature and the ammonia liquid concentration as well as the absorber weak solution inlet temperature and weak solution concentration.

Data taken from literature for the partial pressure difference percentage is available, for example, from (Bäckström *et al.*, 1965) who determined 94.4% for the saturation and 85.7% for the wash out. Another example is given by (Päßler, 2002) where for the saturation 96.0% and for the wash out 92.9% are assumed.

Figure 3.23 shows the auxiliary gas circulation cooling loss capacities for different total pressures of $12x10^5$Pa, $17x10^5$Pa and $20x10^5$Pa and two heat recovery factors of the GHX $\Phi_{GHX,Vr}$ [-] refereed to the rich gas side. For the design liquid ammonia mass flow for the DACM with 8kg/h, cooling loss capacities of 0.21kW, 0.35kW and 0.43kW for $\Phi_{GHX,Vr}$ of 0.30, and values of 0.01kW, 0.05kW and 0.08kW for a $\Phi_{GHX,Vr}$ of 0.80 are reached. This shows that the influence of the heat recovery factor of the GHX is not to be underestimated. The evaporator weak gas mixture inlet temperatures T_{VwE} [°C] reach high

values of 30.31°C to 31.75 °C for a low $\Phi_{GHX,Vr}$ of 0.30 and low temperature values of 5.82°C to 9.65°C for a high $\Phi_{GHX,Vr}$ of 0.80.

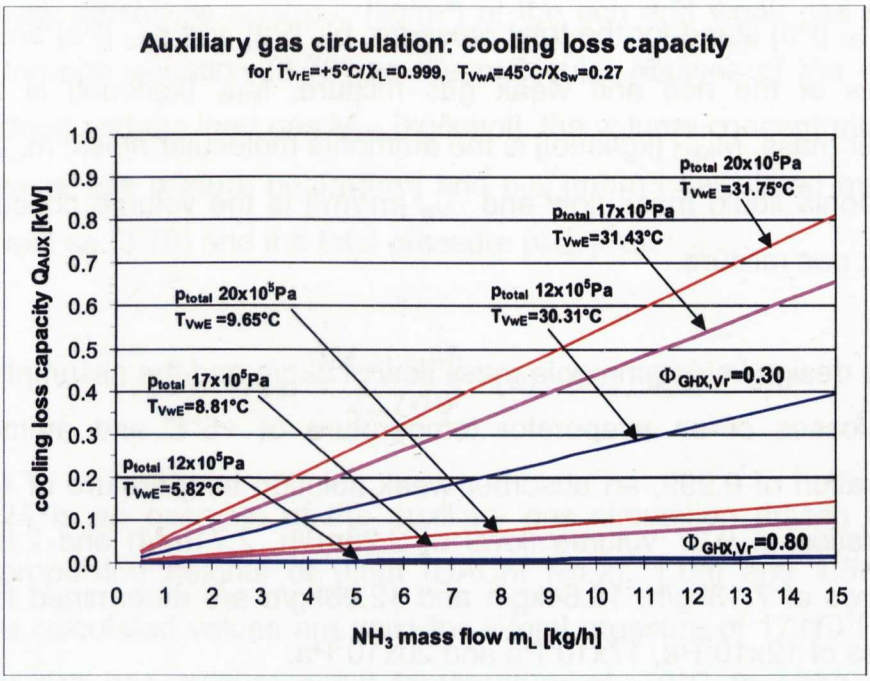

Figure 3.23: Auxiliary gas circulation cooling loss capacities versus ammonia liquid mass flows for three different total pressures and two GHX heat recovery factors.

3.6.5 MASS FLOW WEAK GAS MIXTURE

The required **volume flow** of the circulated **weak gas mixture** V_{Vw} [m³/h] is determined by equation (3.74). The density ρ_{Vw} [kg/m³] and consequently the **mass flow** m_{Vw} of the weak ammonia/helium gas mixture are calculated with equation (3.75) and (3.76) as follows:

$$\dot{V}_{Vw} = \left(\frac{(p_{total} - p_{Vr})}{M_{NH3} \cdot (p_{Vr} - p_{Vw})} \cdot \frac{22.7 \cdot 10^5}{p_{total}} \right) \cdot \dot{m}_{L,NH3} \tag{3.74}$$

$$\rho_{Vw} = \frac{M_{He} + (M_{NH3} - M_{He}) \cdot \upsilon_{Vw}}{22.7 \cdot 10^5} \cdot p_{total} \tag{3.75}$$

$$\dot{m}_{Vw} = \dot{V}_{Vw} \bullet \rho_{Vw} \tag{3.76}$$

Here, p_{total} [Pa] stand for the total pressure, p_{Vr} [Pa] and p_{Vw} [Pa] are the partial pressures of the rich and weak gas mixture, M_{He} [kg/kmol] is the helium molecular mass, M_{NH3} [kg/kmol] is the ammonia molecular mass, $m_{L,NH3}$ [kg/h] is the ammonia liquid mass flow and υ_{Vw} [m^3/m^3] is the volume concentration of the weak gas mixture.

For the design liquid ammonia mass flow of 8kg/h and the assumptions for the cooling losses of an evaporator temperature of +5°C and ammonia liquid concentration of 0.999, an absorber weak solution temperature of 45°C and a concentration of 0.27 volume flows of 2.28m^3/h, 2.71m^3/h and 2.86m^3/h and mass flows of 7.13kg/h, 10.84kg/h and 12.96kg/h are determined for the total pressures of 12x10^5Pa, 17x10^5Pa and 20x10^5Pa.

3.6.6 PRESSURE DROP

The circulation of the auxiliary gas depends on the opposing of the driving force by the propulsion height and the pressure drops of the configuration of the auxiliary gas circuit. The driving force is determined with equations from (Bäckström *et al.*, 1965) and the pressure drop is calculated with equations found in the (VDI-Wärmeatlas, 1988).

3.6.6.1 DRIVING FORCE

The **driving force** Δp [Pa] is dependant on the inert gas used, the predominating temperatures and the total pressure. The total driving force is defind by equation (3.77) as: the density difference of the rich and weak gas mixture and the propulsion height H [m] (the mean height difference between the evaporator and absorber (Figure 3.22) of the gas circuit).

$$\Delta p = g \bullet (\rho_{Vr} - \rho_{Vw}) \bullet H \tag{3.77}$$

Here, g [m/s²] is the standard acceleration of gravity with 9.81m/s².

The density difference ρ_{Vr} - ρ_{Vw} [kg/m³] of the rich and weak gas mixture is obtained through equation (3.78) as the molecular masses of the refrigerant M_{NH3} [kg/kmol] and the inert gas M_{He} [kg/kmol], the volume concentrations of the rich and weak gas mixture υ_{Vr} [m³/m³] and υ_{Vw} [m³/m³] calculated by equation (3.71) as well as (3.70) and the total pressure p_{total} [Pa].

$$\rho_{Vr} - \rho_{Vw} = \frac{M_{NH3} - M_{He}}{22.7 \cdot 10^5} \cdot (\upsilon_{Vr} - \upsilon_{Vw}) \cdot p_{total} \qquad (3.78)$$

Figure 3.24 is an example of the auxiliary gas circulation driving forces for different propulsion heights of 0.5m (DACM No.2), 1.0m and 1.5m (DACM No.1). The calculated values are valid for a total pressure of 17x10^{5}Pa and an evaporator rich gas mixture outlet temperature of -10°C to +20°C. With an evaporator temperature of +5°C, driving forces of 8.1Pa, 16.1Pa and 24.2Pa are reached.

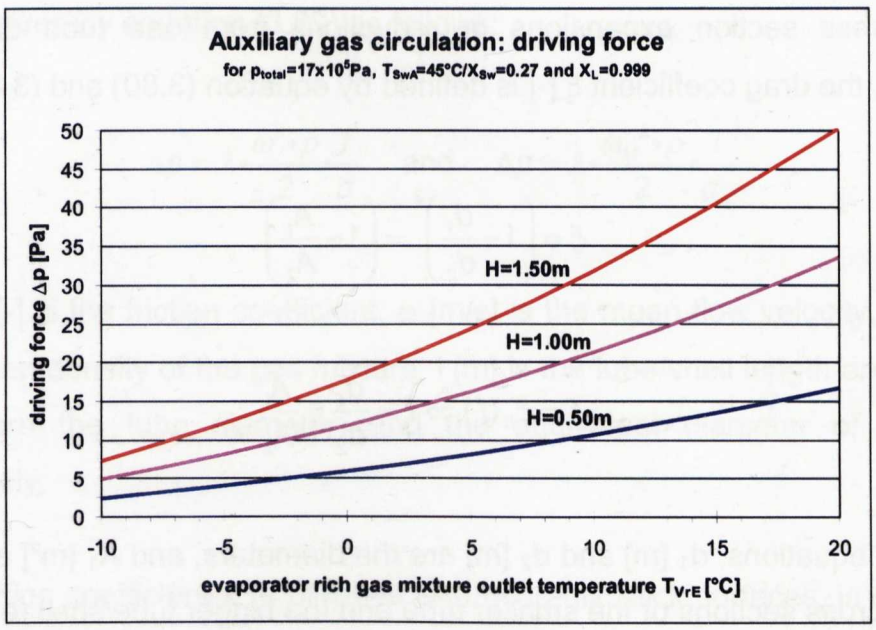

Figure 3.24: Auxiliary gas circulation driving forces versus evaporator rich gas mixture outlet temperatures for three different propulsion heights.

Maiya (Maiya, 2003) determined that the density differences for hydrogen and helium differ only marginally. Helium however, requires about 1.8 to 2.0 times the propulsion height H than that required for hydrogen. This is because the total pressure drop in the gas circuit for helium is about two times of that with hydrogen.

3.6.6.2 PRESSURE DROP

The following fundamental equations for the calculation of the **pressure drop** of the auxiliary gas circuit are given in the (VDI-Wärmeatlas, 1988). For the oppose of the driving force to the total pressure drop of the auxiliary gas circuit, the partial pressure drop Δp [Pa] for a change in the cross section is given with equation (3.79) as follows:

$$\Delta p = \xi \bullet \frac{\omega^2 \bullet \rho}{2} \tag{3.79}$$

Here, ξ [-] is the drag coefficient, ω [m/s] is the mean flow velocity and ρ [kg/m³] is the mean density of the gas mixture.

For cross section expansions or reductions from one tube diameter to another, the drag coefficient ξ [-] is defined by equation (3.80) and (3.81).

$$\xi = \left(1 - \frac{d_1}{d_2}\right)^2 = \left(1 - \frac{A_1}{A_2}\right)^2 \tag{3.80}$$

$$\xi = \xi_E(f) \Rightarrow f = \frac{d_1}{d_2} = \frac{A_1}{A_2} \tag{3.81}$$

In these equations, d_1 [m] and d_2 [m] are the diameters, and A_1 [m²] and A_2 [m²] are the cross sections of the smaller tube and the bigger tube/shell respectively. f [-] is the ratio for determining the drag coefficient for the tube inlet loss from

Figure 3.25. Further drag coefficients for different conditions can be found in the (VDI-Wärmeatlas, 1988).

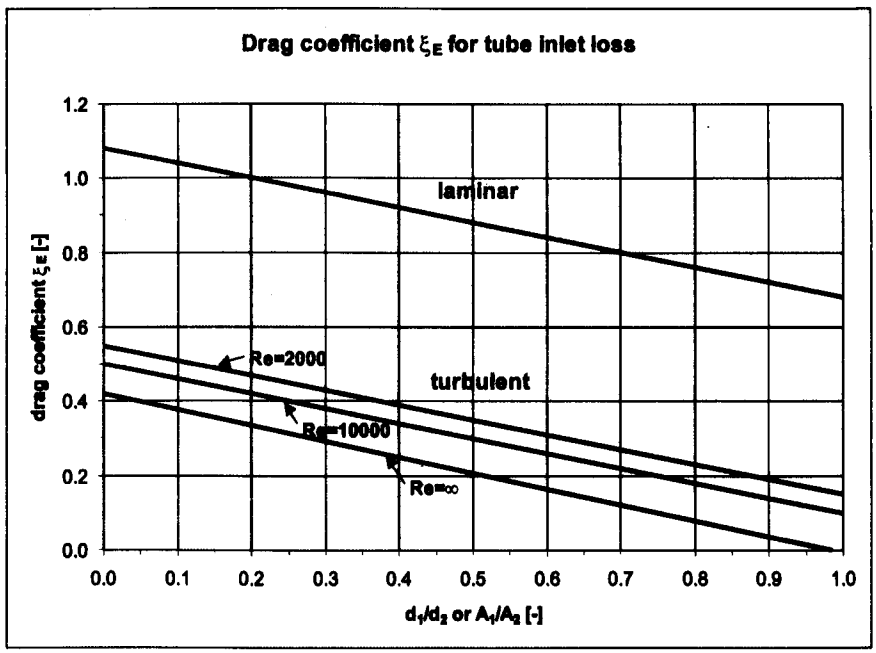

Figure 3.25: Drag coefficient ξ_E of the tube inlet loss by an edged tube reduction for laminar and turbulent flow (VDI-Wärmeatlas, 1988).

The further partial pressure drop Δp [Pa] for the flow through single tubes and shells is given by equation (3.82) as follows:

$$\Delta p = \lambda \bullet \frac{\omega^2 \bullet \rho}{2} \bullet \frac{l}{d} \quad \text{and} \quad \Delta p = \lambda \bullet \frac{\omega_M{}^2 \bullet \rho}{2} \bullet \frac{l}{d_e} \tag{3.82}$$

where λ [-] is the friction coefficient, ω [m/s] is the mean flow velocity, ρ [kg/m³] is the mean density of the gas mixture, l [m] is the tube/shell length and d [m] or d_e [m] are the tube diameter, and the equivalent diameter of the shell respectively.

The friction coefficient λ [-] of tubes with hydraulic slick surfaces, is calculated for laminar flow (Re < 2,300) with equation (3.84), and for turbulent flow (Re > 2,300 up to 100,000) with equation (3.84) as follows:

$$\lambda = \frac{64}{\mathrm{Re}} \tag{3.83}$$

$$\lambda = \frac{0.3164}{\mathrm{Re}^{0.25}} \tag{3.84}$$

The Reynolds value Re [-] for either single, or bundle of tubes is dependent on the tube inside flow and is defined by equation (3.85) as follows:

$$\mathrm{Re} = \frac{\omega \bullet d}{\nu} \quad \text{and} \quad \mathrm{Re} = \frac{\omega \bullet d_e}{\nu} \tag{3.85}$$

where d [m] is the diameter of a single tube, d_e [m] is the real diameter of a bundle of tubes or the equivalent diameter of the shell, ω [m/s] is the mean flow velocity and ν [m²/s] is the kinematic viscosity. The real diameter of a bundle of tubes and the equivalent diameter of the shell are calculated with equations (3.86) and (3.87).

$$d_e = \sqrt{n} \cdot d_T \tag{3.86}$$

$$d_e = \frac{D_S^{\,2} - n \cdot d_T^{\,2}}{D_S + n \cdot d_T} \tag{3.87}$$

n [-] is the amount of tubes in the bundle of tubes, d_T [m] is the diameter of a single tube and D_S [m] is the diameter of the shell.

The thermodynamic property for the caluclation of the Reynolds value is the kinematic viscosity $\nu_{NH3/He}$ [m²/s] of the ammonia/helium gas mixture, which is defined by equation (3.88).

$$\upsilon_{NH3/He} = \frac{\eta_{NH3/He}}{\rho_{NH3/He}} \tag{3.88}$$

$\eta_{NH3/He}$ [Pa s] is the dynamic viscosity of the gas mixture and $\rho_{NH3/He}$ [kg/m³] is the density of the ammonia/helium gas mixture calculated with equation (3.38). The dynamic viscosity of the gas mixture is stated in equation (3.89) as follows:

$$\eta_{NH3/He} = \eta_r \bullet \eta_{cr,NH3/He} = \eta_r \bullet \left(X_{NH3} \bullet \eta_{cr,NH3} + X_{He} \bullet \eta_{cr,He} \right) \tag{3.89}$$

where η_r [Pa s] is the reduced viscosity of 0.47, $\eta_{cr,NH3/He}$ [Pa s] is the critical dynamic viscosity of the gas mixture resulting from the ammonia X_{NH3} [-] and helium X_{He} [-] concentrations in the gas mixture as well as the critical dynamic viscosities $\eta_{cr,NH3}$ of 3.09×10^{-5}Pa s and $\eta_{cr,He}$ of 2.54×10^{-6}Pa s (VDI-Wärmeatlas, 1988).

Finally, the flow velocity ω [m/s] in the tubes and the flow velocity ω_S [m/s] in the shell cross sectional area can be calculated with equation (3.90) and (3.91) respectively.

$$\omega = \frac{\dot{V}}{A} = \frac{4 \bullet \dot{V}}{\pi \bullet d_T^{\,2}} \tag{3.90}$$

$$\omega_S = \frac{4 \bullet \dot{V}}{\pi \bullet \left(D_S^{\,2} - n \bullet d_T^{\,2} \right)} \tag{3.91}$$

Here, $\dot{V}$ [m³/s] is the volume flow, A [m²] is the cross sectional area, d_T [m] is the inner diameter of a single tube, n [-] is the amount of tubes in the tubular heat exchanger and D_S [m] is the inner diameter of the shell.

Due to the thermosyphon principle of the gas circulation, usually a vertical falling film evaporator and absorber are used due to the low pressure drops in the gas mixture flow. To examine the auxiliary gas circuit, the pressure drops within the thermosyphon cyclic process were calculated for both pilot plants. The results are presented in chapter 4.8.

3.6.7 DIFFUSION

The spreading of one gas within another gas is called diffusion. The diffusion within a gas phase is the exchange of gas without a volume exchange. The simplest case is called binary diffusion. Under constant conditions, lighter gases diffuse faster than heavier ones. The diffusion of one gas in other gases at atmospheric pressure or at higher pressures is normally a very slow process. Consequently, ammonia (NH_3) diffuses slowly into a helium atmosphere because its molecules are heavier than those of helium (He).

The general rate of the mass diffusion $\dot{m}_{diff}$ [kg/s] of a chemical species A in a stationary binary mixture of species A and B in a specified direction x [m] is expressed by Fick's law of diffusion (Çengel, 1998) in the equation (3.92).

$$\dot{m}_{diff} = -\rho \bullet D_{AB} \bullet A \bullet \frac{d(\rho_A/\rho)}{dx} \tag{3.92}$$

where D_{BA} is the transport property called the diffusion coefficient [m^2/s] of the species in the mixture, A is the area [m^2] normal to the direction, and ρ and ρ_A are the densities [kg/m^3] of the binary mixture and the species A at that location. The density of the binary mixture is given in equation (3.93).

$$\rho = \rho_A + \rho_B \tag{3.93}$$

Due to the complex nature of mass diffusion, the diffusion coefficients are usually determined experimentally. The kinetic theory of gases indicates that the diffusion coefficient for dilute gases at ordinary pressures is essentially independent of the mixture composition and tends to increase with raising temperature and decrease with raising pressure as is shown in equation (3.94) by (Çengel, 1998).

$$D_{AB} \propto \frac{T^{1.5}}{p} \quad or \quad \frac{D_{AB,1}}{D_{AB,2}} = \frac{p_2}{p_1} \bullet \left(\frac{T_1}{T_2}\right)^{1.5} \tag{3.94}$$

This relation is useful for determining the diffusion coefficient for gases at different temperatures and pressures when the diffusion coefficient at a specified temperature and pressure is known. At pressure levels above approximately 1Pa, gas molecules behave similarly to liquids; the molecules are so close together so that they bump into each other. If they are pumped or if there is a differential pressure, the molecules flows together. In a laminar flow, the molecules of a binary gas mixture flow in the direction of the partial pressure difference.

In literature, some diffusion coefficients for binary gas mixtures and liquid solutions are given which are presented in table 3.3. The diffusion coefficients of gases are several orders of magnitude greater than those of liquids.

Table 3.3: Binary diffusion coefficients and relative molecular masses of different gas and liquid solution mixtures at 1.01325×10^5Pa (Incropera *et al.*, 1996; Çengel, 1998).

substance A	relative molecular mass M [kg/kmol]	substance B	relative molecular mass M [kg/kmol]	tem-perature T [K]	diffusion coefficient D_{AB} [m²/s]
helium (He)	4	air (71.8% N_2 20.9% O_2 1.0% Ar)	29	298	72.0×10^{-6}
helium (He)	4	water vapour (H_2O)	18	298	92.0×10^{-6}
ammonia (NH_3)	17	air (71.8% N_2 20.9% O_2 1.0% Ar)	29	298	26.0×10^{-6} 28.0×10^{-6}
ammonia (NH_3)	17	water (H_2O)	18	285	1.6×10^{-9}

An expression for the binary diffusion coefficient D_{AB} [m²/s] for ammonia into a helium atmosphere is given by (Kouremenos *et al.*, 1994). For a wide range of pressures, the mass diffusion coefficient D_{AB} is expressed by the equation (3.95), where T is the temperature in [°C].

$$D_{AB} = D_{NH3-He} = 8.57 \cdot 10^{-10} \cdot (273.15 + T)^{1.435} \quad (3.95)$$

The calculated values for the binary diffusion coefficient of ammonia into a helium atmosphere D_{NH3-He} are presented in the Figure 3.26 for mean internal evaporator temperature from -10°C to +20°C. The calculated diffusion coefficients varied from 2.55×10^{-6}m²/s for -10°C to 2.97×10^{-6}m²/s for +20°C.

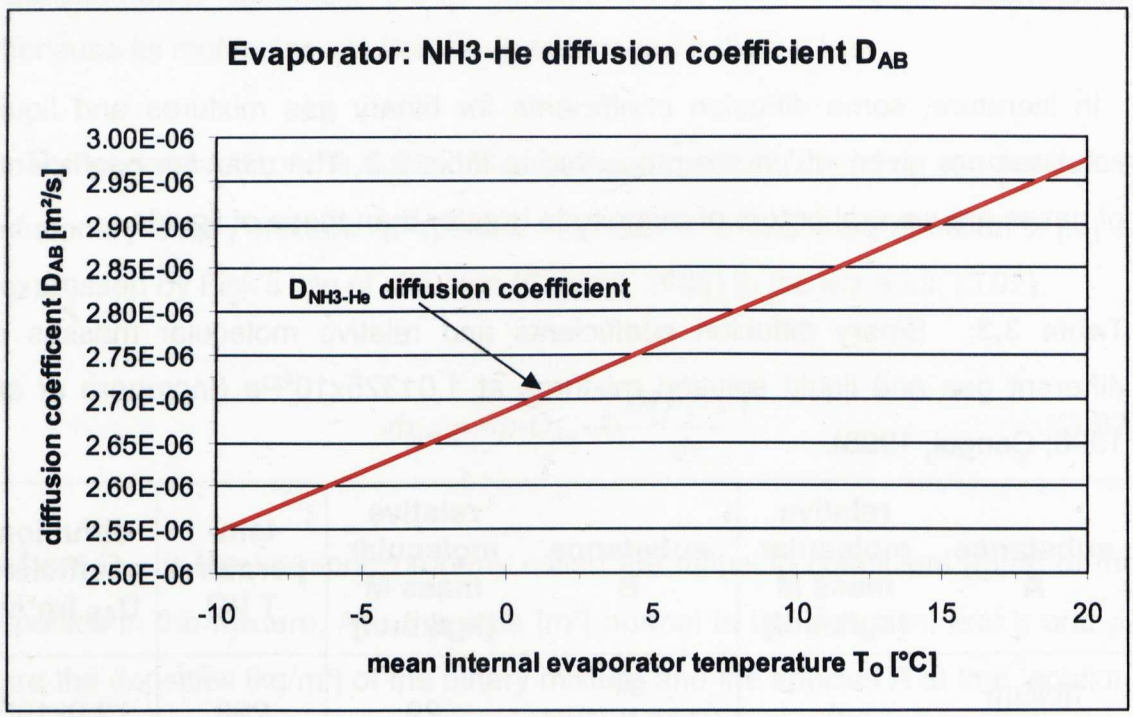

Figure 3.26: Binary diffusion coefficient for ammonia into helium at different internal mean evaporator temperatures.

The binary diffusion coefficient D_{AB} [m²/s] for ammonia into an ammonia/water solution dependant on the ammonia solution concentration is given by (Amous, 1998) in equation (3.96)

$$D_{AB} = D_{NH3-NH3/H2O} = (1.65 + 2.47 \cdot x_{NH3}) \cdot 10^{-6} \cdot e^{\left(-\frac{16600}{R \cdot (273.15+T)}\right)} \quad (3.96)$$

Here, T is the temperature in [°C], x_{NH3} is the ammonia mol concentration in the solution [kmol/kmol] and R is the universal gas constant (8.31451kJ/kmol K).

The conversion of the normally used ammonia mass concentration X [-] into the ammonia mol concentration x_{NH3} [kmol/kmol] is given in equation (3.97) as follows:

$$x_{NH3} = -\frac{X \cdot M_{H2O}}{X \cdot M_{NH3} - X \cdot M_{H2O} - M_{NH3}} = -\frac{X \cdot 16}{X \cdot 17 - X \cdot 16 - 17} \qquad (3.97)$$

The resulting diffusion coefficients for mean internal absorber temperatures from 30°C to 60°C and a mean ammonia mass concentration of 0.320, are shown in Figure 3.27. As an example, the calculated binary diffusion coefficient of ammonia in ammonia/water is 2.194.10x10^{-9}m²/s for a 40°C internal absorber temperature.

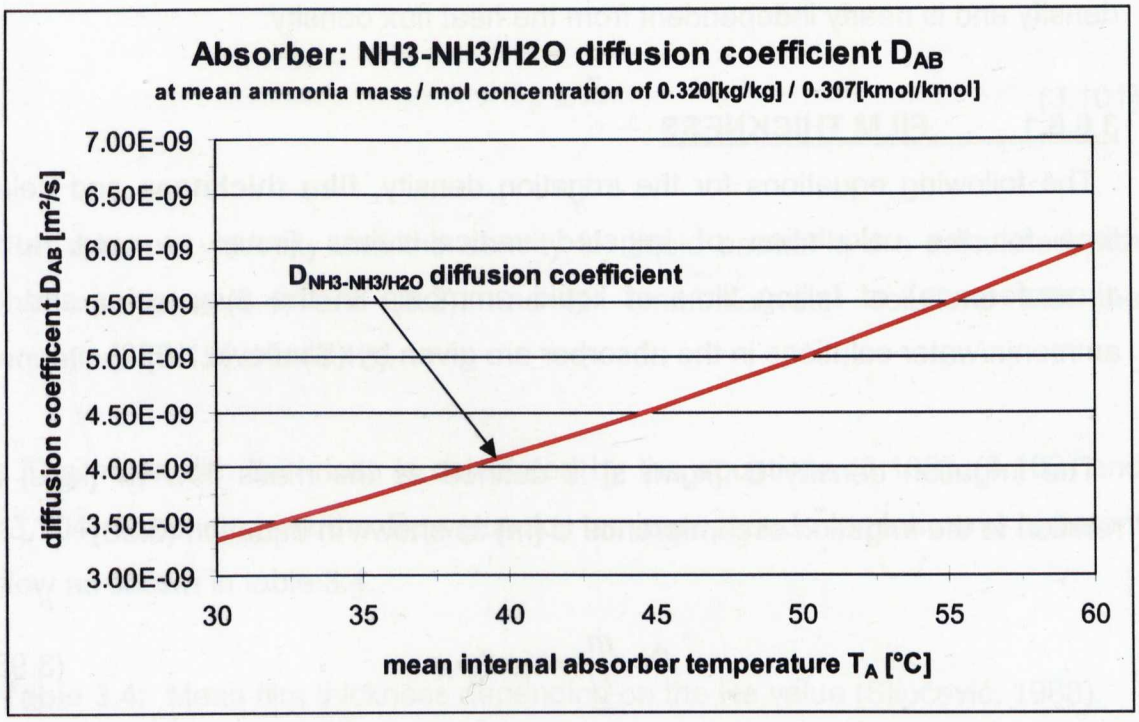

Figure 3.27: Binary diffusion coefficient for ammonia into ammonia/water solution at different internal mean absorber temperatures.

The previous information about to mass diffusion is valid only for a stationary medium. A more complex kind of mass diffusion is the diffusion in a moving medium, which is in general, difficult to analyse. Further descriptions of this kind of diffusion can be found in (Incropera *et al.*, 1996; Çengel, 1998).

3.6.8 FILM THICKNESS AND HEAT TRANSFER COEFFICIENT

The used construction of the DACM falling film evaporator consists of vertical tubes, in which the falling film of the liquid refrigerant ammonia evaporates into the helium gas atmosphere as described in the chapter 3.6.7. The flow characteristics of the falling film are defined by the irrigation density and the film thickness which are necessary for the calculation of the inner convective heat transfer coefficient h_c [W/m² K]. Very important for a satisfactory operation is the equal spreading of the refrigerant in all of the evaporation tubes and thereby as well, a wetted surface. At low heat flux densities q [W/m²], convection boiling, meaning surface boiling or boiling on the phase change surface occurs. The heat transfer coefficient in this range principally depends on the irrigation density and is nearly independent from the heat flux density.

3.6.8.1 FILM THICKNESS

The following equations for the irrigation density, **film thickness** and delay time for the calculation of irrigated vertical tubes (inner or outer tube circumference) of falling films of liquid ammonia in the evaporator and of ammonia/water solutions in the absorber are given by (Slipčević, 1988).

The irrigation density $\dot{B}$ [kg/m s] is defined as the mass flow $\dot{m}$ [kg/s] in relation to the irrigation circumference U [m] as shown in equation (3.98)

$$\dot{B} = \frac{\dot{m}}{U} = \omega_m \bullet \delta_m \bullet \rho \tag{3.98}$$

The irrigation density can also be calculated with the average flow velocity ω_m [m/s], the mean film thickness δ_m [m] and the density of the fluid ρ [kg/m³]. The irrigation circumference U for several tubes is calculated with equation (3.99) as follows:

$$U = n \bullet (\Pi \bullet d_i) \tag{3.99}$$

where n [-] is the number of tubes and d_i [m] is the inner diameter of one tube.

The Re value [-] is defined and calculated using the average flow velocity and the mean film thickness in equation (3.100) as follows:

$$\mathrm{Re} = \frac{\omega_m \bullet \delta_m}{\nu} = \frac{\dot{B}}{\eta} \tag{3.100}$$

where ν [m²/s] is the kinematic viscosity and η [Pa s = kg/m s] is the dynamic viscosity. The kinematic viscosity is calculated as follows with equation (3.101) as the ratio of the dynamic viscosity to the density.

$$\nu = \frac{\eta}{\rho} \tag{3.101}$$

The dynamic viscosity and the density for liquid ammonia are calculated with the equations (3.4) and (3.2), and for ammonia/water solutions with the equations (3.15) and (3.12).

The mean film thickness is calculated by the equations (3.102), (3.103) and (3.104) depending on the Re value for laminar, pseudo laminar and turbulent flow as shown in table 3.4.

Table 3.4: Mean film thickness depending on the Re value (Slipčević, 1988).

laminar flow	**pseudo laminar flow**	**turbulent flow**
$0 \le \mathrm{Re} \le \mathrm{Re_W}$	$\mathrm{Re_W} \le \mathrm{Re} \le \mathrm{Re_{cr}}$	$\mathrm{Re_{cr}} \le \mathrm{Re}$
$\delta_m = \left(\frac{3 \bullet \nu^2}{g}\right)^{1/3} \bullet \mathrm{Re}^{1/3}$	$\delta_m = \left(\frac{2.4 \bullet \nu^2}{g}\right)^{1/3} \bullet \mathrm{Re}^{1/3}$	$\delta_m = 0.369 \bullet \left(\frac{3 \bullet \nu^2}{g}\right)^{1/3} \bullet \mathrm{Re}^{1/2}$
(3.102)	(3.103)	(3.104)

The limiting Re_W value for laminar flow with the index w which has to do with the forming of waves on the surface of the falling film is calculated with equation (3.105) as follows:

$$Re_W = C \bullet \left(\frac{\rho \bullet \sigma^3}{g \bullet \eta^4} \right)^{1/8} \tag{3.105}$$

where the constant C [-] is given as 0.217 and the standard acceleration of gravity g is 9.81m/s². The density and the surface tension σ [N/m = kg/s²] are calculated for liquid ammonia with equations (3.2) and (3.5), and for ammonia/water solutions, with the equations (3.12) and (3.18). The critical Re value for the transition to turbulent flow is Re_{cr} = 400 (Slipčević, 1988).

3.6.8.2 DELAY TIME

The delay time t_0 [s] is the available time in that the complete liquid ammonia is given to be evaporated along a fixed falling film tube length for the purpose of taking up still energy from the external evaporator cycle. The ammonia that is not completely changed in this time into the gas phase inside the evaporator, remains as liquid and runs towards the absorber. Therefore, the inert gas mass flow must be high enough to take up the mass flow of the ammonia during the delay time, which is calculated with equation (3.106)

$$t_0 = \frac{H}{\omega_m} \tag{3.106}$$

Here, H [m] is the tube height/length and ω_m [m/s] the average flow velocity.

3.6.8.3 HEAT TRANSFER COEFFICIENT

According to Schnabel and Schlünder (Slipčević, 1988), the Nu values [-] for vertical tubes in the range of convective boiling are calculated for the inner convective **heat transfer coefficient** with the equations (3.107), (3.108) and (3.109):

$$Nu = \sqrt{Nu_l^2 + Nu_t^2} \tag{3.107}$$

where the laminar Nu_l value [-] and the turbulent Nu_t value [-] are:

$$Nu_l = 0.9 \cdot Re^{-1/3} \tag{3.108}$$

$$Nu_t = 0.0062 \cdot Re^{0.4} \cdot Pr^{0.65} \tag{3.109}$$

The Re values are calculated with equation (3.100) and the Pr value [-] with equation (3.110) as follows:

$$Pr = \frac{\eta \cdot c}{\lambda} = \frac{\nu}{a} \tag{3.110}$$

where η [kg/m s] is the dynamic viscosity, c [J/kg K] is the specific heat capacity and λ [W/m K] is the thermal conductivity. The dynamic viscosity, the specific heat capacity and the thermal conductivity for liquid ammonia are calculated with equation (3.4), (3.1) and equation (3.3) and for ammonia/water solutions with the equations (3.15), (3.11) and equations (3.13) or (3.14). The Pr value can also be expressed by the kinematic viscosity ν [m²/s] and the thermal diffusivity a [m²/s].

The inner convective heat transfer coefficient h_C [W/m² K] and the running length of the falling film l_C [m] are then defined by equation (3.111) and equation (3.112) as follows:

$$h_C = \frac{Nu_c \cdot \lambda}{l_C} \tag{3.111}$$

$$l_C = \left(\nu^2/g\right)^{1/3} \tag{3.112}$$

where Nu_c is the Nu value of equation (3.107) and λ [W/m K] is the thermal conductivity. The thermal conductivity for liquid ammonia is calculated by equation (3.3) and for ammonia/water solutions by the equations (3.13) or (3.14). ν [m²/s] is the kinematic viscosity which is given in equation (3.101) and g [m/s²], the standard acceleration of gravity which is 9.81m/s².

Furthermore, the equations for the calculation of the external heat transfer coefficient for tubular heat exchangers with baffles are presented for the evaporator and the absorber in (VDI Wärmeatlas, 1988).

3.6.8.4 FALLING FILM EVAPORATOR

For the used falling film evaporator of the second DACM pilot plant, the film thickness, the delay times, the irrigation densities and the heat transfer coefficients were calculated for three different mean internal evaporator temperatures T_O -10°C, +5°C and +15°C using the following assumptions. Regarding the design values, the inner tube diameter d_i is 0.01m, the number of tubes n is 143 and the length/height H of the tubes is 0.23m.

Figure 3.28 shows the film thickness δ_m and the delay time t_0 in comparison to the liquid ammonia mass flow for the temperature range of the mean internal evaporator temperature from -10°C for refrigeration to +15°C for air-conditioning with cooling surfaces.

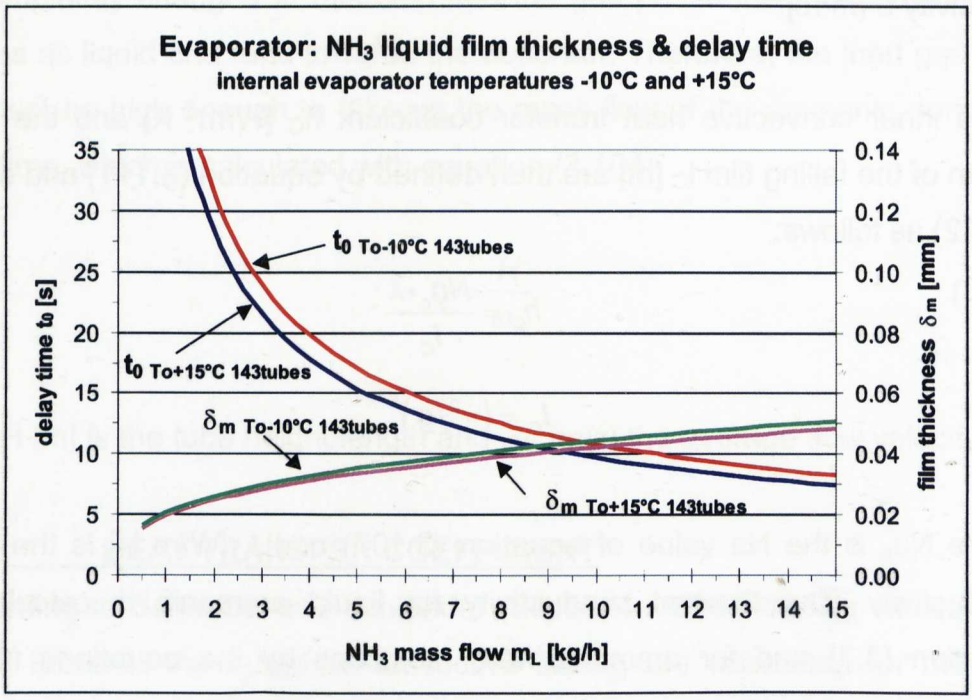

Figure 3.28: Comparison of film thickness and delay times for the falling film evaporator at two internal mean evaporator temperatures for refrigeration and air-conditioning.

The differences between the film thickness and the delay time are insignificant for the presented liquid ammonia mass flow of 0.5kg/h to 15kg/h for the film thickness. For a delay time above 8 kg/h the difference is one second and below 8kg/h, the delay time increases to 3 seconds with the decreasing ammonia mass flow. The film thickness for the design liquid ammonia mass flow of the 8kg/h amounts to 0.04mm with delay times of 11 seconds to 12.5 seconds.

Next, the influences and the effects of the distribution of the liquid ammonia on the falling film evaporator as well as the film thickness and the delay times were investigated. The question posed here is what happens if only half or a quarter of the tubes are irrigated and if the falling film is formed as a complete wetted circumference.

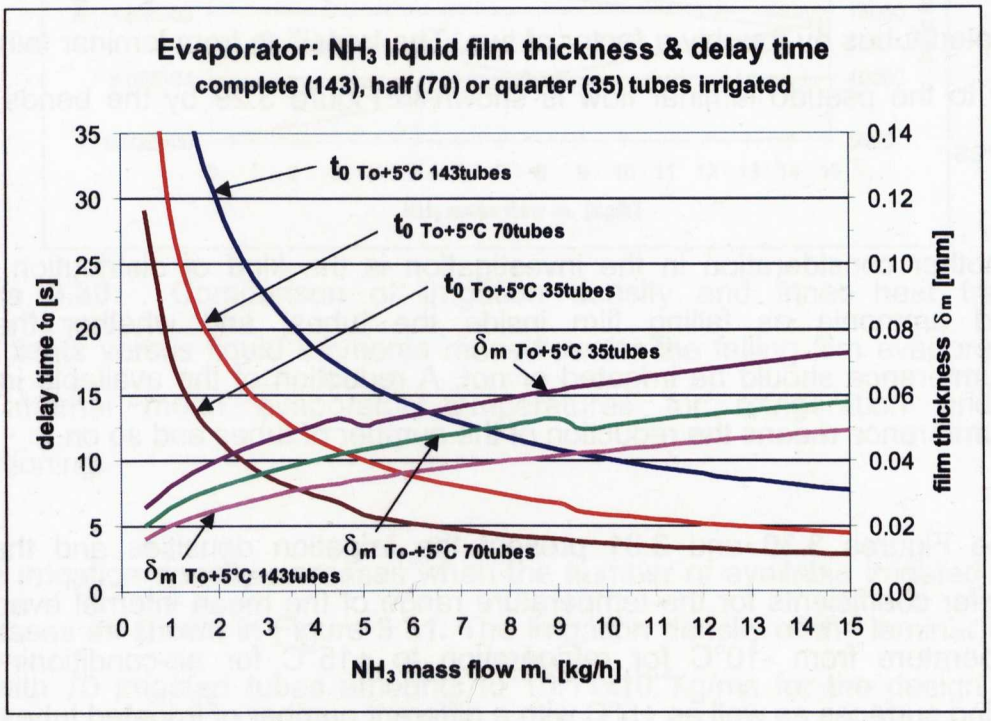

Figure 3.29: Film thickness and delay time versus ammonia mass flow for three different number of irrigated tubes of the falling film evaporator for a internal mean evaporator temperature of +5°C.

As shown in Figure 3.29 for the application field of air-conditioning with a mean internal evaporator temperature of +5°C and the design liquid ammonia

mass flow for the DACM of 8kg/h, the delay time for the falling film amounts to 12 seconds if all of the tubes are irrigated.

The delay time decreases with the number of irrigated tubes to 7 seconds or to 4 seconds respectively when only half or a quarter of the tubes are irrigated. The tube lengths are not long enough to evaporate the liquid ammonia into the He atmosphere, consequently the tube lengths should be approximately doubled or tripled. The non-evaporated liquid ammonia then flows down through the GHX towards the absorber. The resulted irrigation densities are $4.95x10^{-4}$kg/ms for complete tubes, $10.11x10^{-4}$kg/ms for half and $20.21x10^{-4}$kg/ms for quarter tubes.

If a 4kg/h liquid ammonia mass flow is available for the evaporation process, the resulting delay times are 18.5 seconds for complete tubes, 11.5 seconds for half and up to 7 seconds for quarter tubes. In both cases, increases in the film thickness by about 0.01mm can be reached by decreasing the number of irrigated tubes by roughly a factor of two. The transition from laminar falling film flow to the pseudo laminar flow is shown in Figure 3.29 by the bends in the curves.

Another consideration in the investigation is the kind of distribution of the liquid ammonia as falling film inside the tubes, and whether the total circumference should be irrigated or not. A reduction of the available irrigated circumference means the reduction of the number of tubes and so on.

The Figures 3.30 and 3.31 present the irrigation densities and the heat transfer coefficients for the temperature range of the mean internal evaporator temperature from -10°C for refrigeration to +15°C for air-conditioning with cooling surfaces as well as +5°C with a different number of irrigated tubes.

The comparison in Figure 3.30 shows that the inner heat transfer coefficients for the falling film evaporator vary within a range of approximately 45,000W/m²K to 13,500W/m²K depending on the liquid ammonia mass flow of 0.5kg/h to 15kg/h. The differences between the two mean internal evaporator

temperatures are insignificant, meaning that the heat transfer coefficient for the design liquid ammonia mass flow for the DACM of 8kg/h roughly amounts to 17,500W/m²K. The corresponding irrigation density of the laminar falling film is $4.95x10^{-4}$kg/ms.

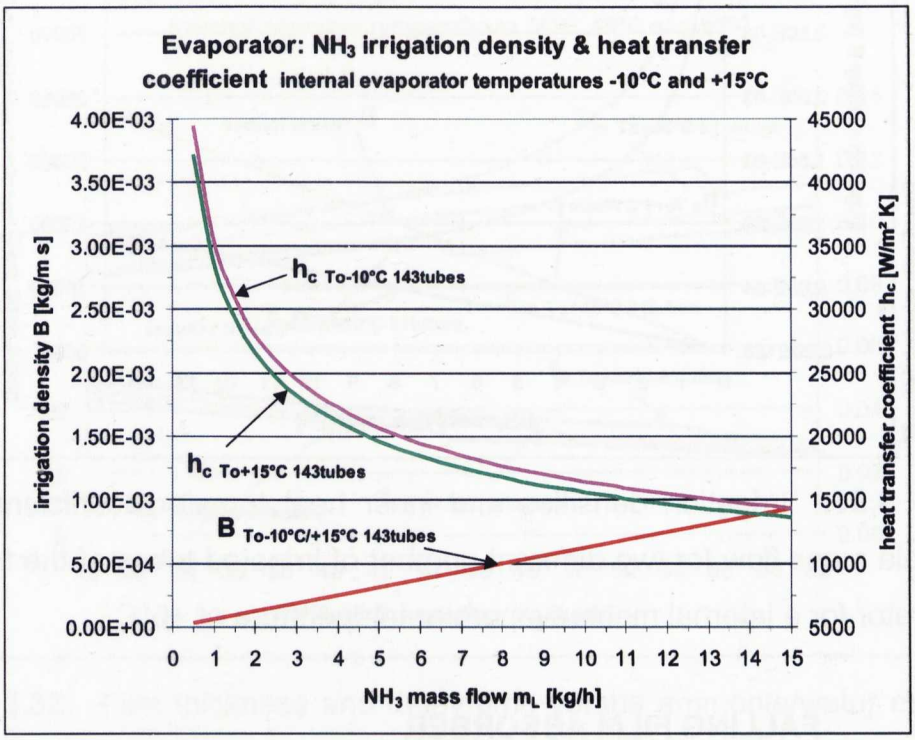

Figure 3.30: Comparison of irrigation density and inner heat transfer coefficients versus liquid ammonia mass flow for the falling film evaporator at two internal mean evaporator temperatures for refrigeration and air-conditioning.

The irrigation density increases when the number of available irrigated tubes decreases as shown in Figure 3.31. The irrigation density of the laminar falling film with 70 irrigated tubes amounts to $10.11x10^{-4}$kg/ms for the design liquid ammonia mass flow for the DACM of 8kg/h. The corresponding heat transfer coefficients decrease from 17,000W/m²K for complete tubes to 13,500W/m²K for half irrigated tubes.

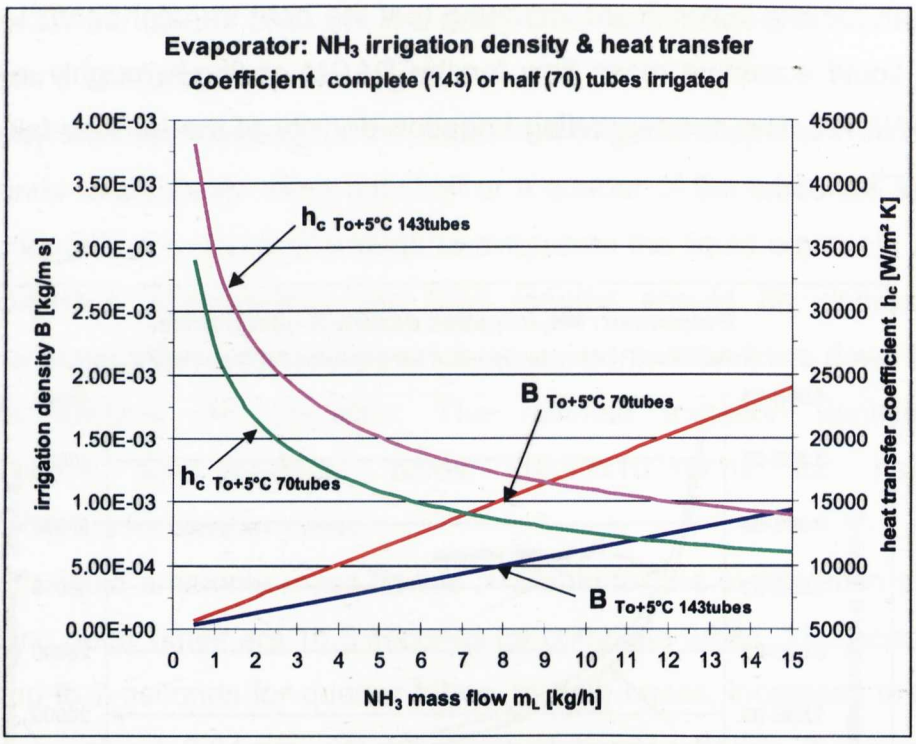

Figure 3.31: Irrigation densities and inner heat transfer coefficients versus ammonia mass flow for two different number of irrigated tubes of the falling film evaporator for a internal mean evaporator temperature of +5°C.

3.6.8.5 FALLING FILM ABSORBER

The film thickness, the delay times, the irrigation densities and the heat transfer coefficients for the used falling film absorber of the second DACM pilot plant were calculated for three different mean internal absorber temperatures: T_A 30°C, 40°C and 50°C using the following assumptions. Regarding the design values, the inner tube diameter d_i is 0.015m, the number of tubes n is 81, the mean ammonia mass concentration X_s of the ammonia/water solution is 0.32 and the length/height H of the tubes is 0.326m.

The conditions of the falling film absorber are different than those of the evaporator. For the DACM, the ammonia/water mass flow is about 5 to 15 times larger than the liquid ammonia mass flow, depending on the specific solution circulation.

The differences between the absorber temperatures for the film thickness and the delay times are minimal. More dramatic differences appear only if the flow

regime changes from laminar to pseudo laminar flow as shown in Figure 3.32. This occurs for example, with the film thickness curve for the internal absorber temperature of 50°C at an ammonia/water mass flow of 44kg/h.

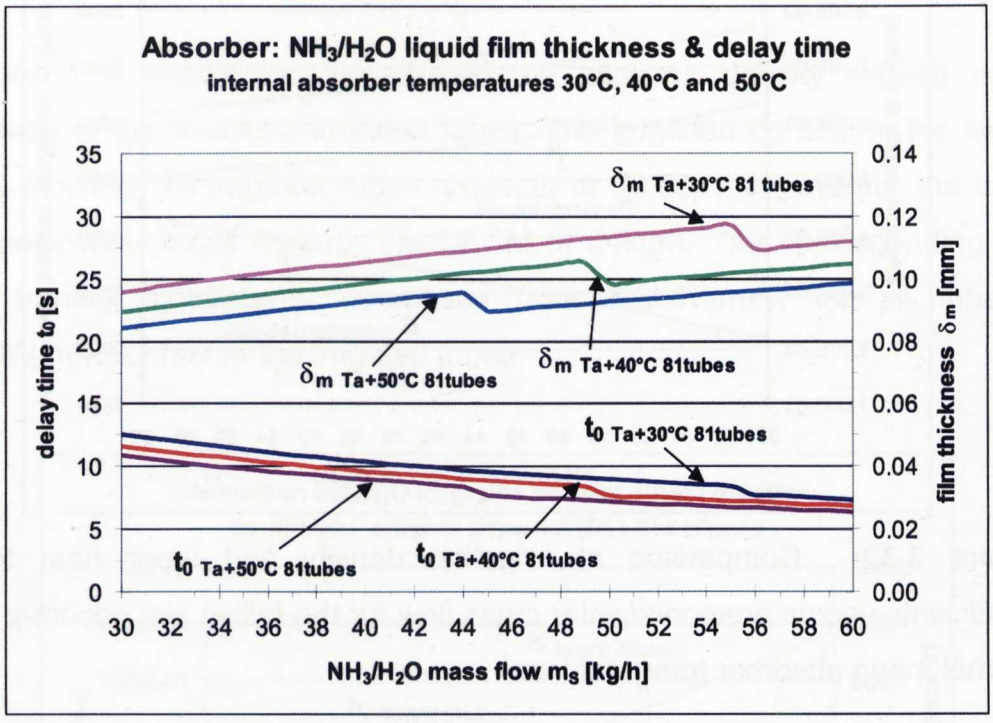

Figure 3.32: Film thickness and delay time versus ammonia/water mass flow for the falling film absorber at different internal mean absorber temperatures.

The design ammonia/water mass flow for the DACM is 54kg/h which is based on 50kg/h of weak ammonia/water solution and half of 8kg/h of ammonia vapour/liquid mass flow. The film thickness is about 0.095mm to 0.116mm depending on the mean internal absorber temperature between 50°C to 30°C. The delay times decrease from 8.5 seconds to 7.3 seconds and 6.8 seconds, and are therefore all in the same range level.

The Figures 3.33 and 3.34 shows the irrigation densities and the inner heat transfer coefficients for the temperature range of the mean internal absorber temperatures ranging from 30°C and 50°C as well as 40°C with a different number of irrigated tubes.

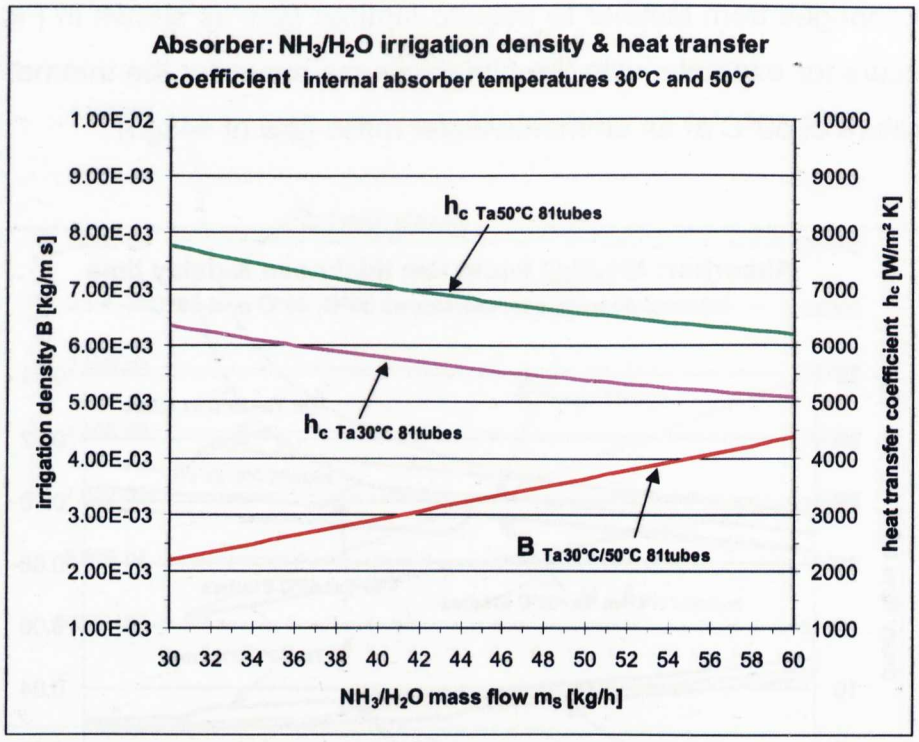

Figure 3.33: Comparison of irrigation density and inner heat transfer coefficients versus ammonia/water mass flow for the falling film absorber at two internal mean absorber temperatures.

The comparison in Figure 3.33 shows that the inner heat transfer coefficients for the falling film absorber varies in a range of approximately 6,600W/m²K to 5,100W/m²K versus to the ammonia/water mass flow of 30kg/h to 60kg/h. The differences between the two mean internal absorber temperatures are minimal, meaning the heat transfer coefficient for the design ammonia/water mass flow for the DACM of 54kg/h amounts to 5,350W/m²K. The corresponding irrigation density of the falling film is 39.30×10^{-4}kg/ms. The heat transfer coefficients for the evaporator are about 2.5 to 6.5 times higher than those of the absorber because of the irrigation density which is increases with the mass flow, causing the Re value to increase as well. The Nu value however is decreased and thereby the heat transfer coefficient as well.

In the work of (Amous, 1998) for comparison, investigations were made about the heat and mass transfer of a falling film absorber. At an irrigation density of 20×10^{-4}kg/ms, an absorber wall temperature of 47°C and an inlet ammonia mass concentration of 18%, an inner heat transfer coefficient for laminar film

absorption was determined of approximately 6,500W/m²K, which is in the range of the own investigated values. For the turbulent film absorption with an irrigation density of 2,700x10^{-4}kg/ms, a turbulent heat transfer coefficient of about 3,000W/m²K was determined.

Figure 3.34 shows the increase in the irrigation density caused by the decrease of the available irrigated tubes. The irrigation density of the laminar falling film with 40 irrigated tubes amounts to 79.58x10^{-4}kg/ms for the design ammonia/water mass flow for the DACM of 54kg/h. The corresponding inner heat transfer coefficients decreases from 5,800W/m²K for all tubes to 4,600W/m²K for half of the irrigated tubes.

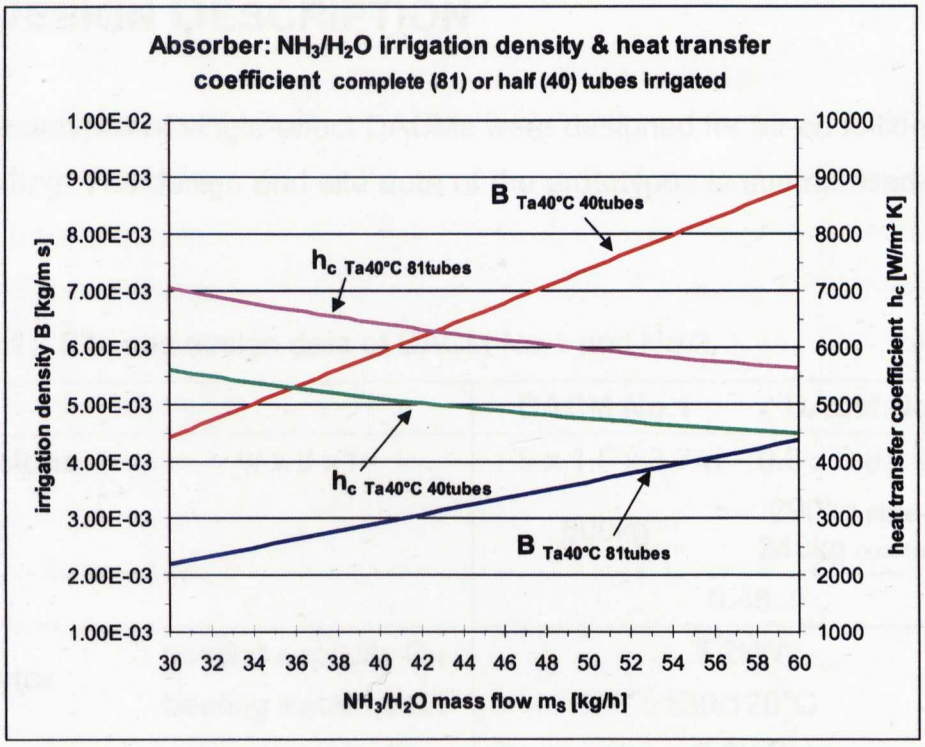

Figure 3.34: Irrigation densities and inner heat transfer coefficients versus ammonia/water mass flow for two different number of irrigated tubes of the falling film absorber for a internal mean absorber temperature of 40°C.

Further detailed descriptions of vertical falling films especially on film boiling, film thickness and heat transfer coefficients for evaporators and absorbers can be found in (Carey, 1992; Amous, 1998; Höhne, 1998).

CHAPTER 04

MEASUREMENTS, ANALYSIS AND OPTIMISATION OF THE DACM PILOT PLANTS

4.1 DESIGN DESCRIPTION

Two prototypes of single-effect DACMs were designed for air-conditioning and refrigerating. The design and site data of the prototypes is summarised in table 4.1.

Table 4.1: Site and design data of DACM No.1 and No.2.

		DACM No.1	DACM No.2
dimensions	w x d x h	1.5 x 1.5 x 3.7m	0.8 x 0.8 x 2.4m
weight		800kg	290kg plate-SHX 240kg coaxial-SHX
COP		0.48	
Generator	heating capacity Q_H	5.2kW	
	heating water in/out	130/120°C	
Dephlegmator	cooling capacity Q_{Deph}	0.9kW	
	cooling water in/out	42/47°C	
Condenser	cooling capacity Q_C	2.8kW	
	cooling water in/out	35/37°C	
Evaporator	cooling capacity Q_O	2.5kW	
	chilled water in/out	13/10°C	
Absorber	cooling capacity Q_A	4.0kW	
	cooling water in/out	30/35°C	

4.2 DEVELOPMENT AND OPTIMISATION

4.2.1 DACM NO. 1

The development of the first prototype of the solar driven DACM was carried out in October of 2000 at the Stuttgart University of Applied Sciences. The designed performance range of the cooling machine of 2.5kW led to the development of a newly constructed generator with indirect heating, an efficient bubble pump, as well as a change in the geometry of the heat exchanger. The first pilot plant was put into operation in November of 2000 and after two years of detailed investigations, it was dismounted in March of 2002. The pilot plant had a total height of 3.70m and weighed approximately 800kg.

4.2.1.1 STANDARD COMPONENTS

The standard components, dephlegmator, condenser, falling film evaporator, gas heat exchanger, falling film absorber and solution heat exchanger were constructed in the form of vertical or horizontal tubular heat exchangers (Figure 4.1). The dephlegmator, the condenser and the absorber were water-cooled, whereas water-glycol was used for the refrigeration cycle of the evaporator.

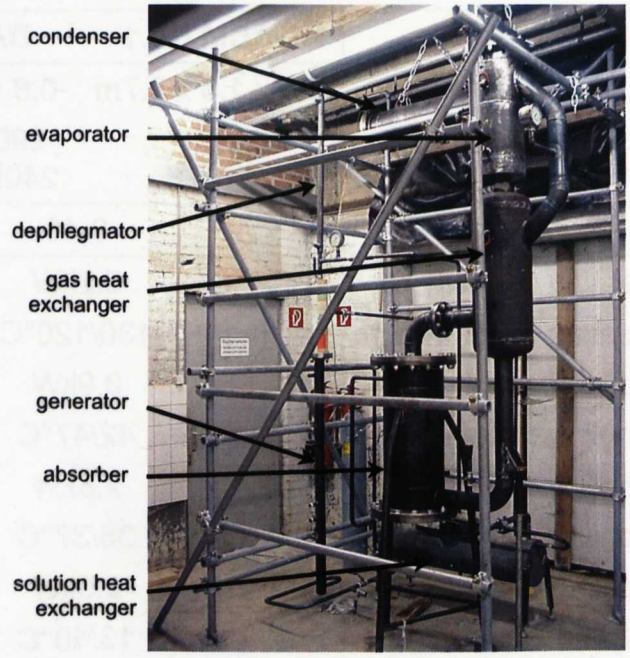

Figure 4.1: First pilot plant of the DACM at the laboratory of the Stuttgart University of Applied Sciences.

4.2.1.2 NEWLY DEVELOPED COMPONENTS

The normal mechanical solution pump of absorption cooling machines is replaced in a DACM by a thermal gas bubble pump. With indirect heat input, vapour bubbles are generated which, at best, produce a two-phase slug flow in several lifting tubes pushing liquid upwards through columns in order to circulate the solution between the generator and absorber. Because of the low heat flux densities in the solar heating section of the generator, it is necessary to achieve good heat transfer.

In total, three generator prototypes, each with different designs were newly developed and built. Prototype No.1 led the ammonia vapour through a central tube running from the top towards the bottom of it. Due to the difficulty of the welding tasks, further development was stopped. The next prototype (No.2) was constructed with smaller dimensions and with a direct ammonia outlet on the top of the generator head. Here, a simpler construction was selected to avoid the problems experienced with the previous generator. This second generator was separately investigated with methanol and a methanol/water solution (Jakob, 2001). An additional third generator was developed and built in order to achieve an improved heat transmission in the solar heating section. Prototype No.3 (Figure 3.10), with a height of 1.6m and equipped with 19 tubes (∅ 8mm x 1.5mm), was installed in the first DACM pilot plant (Figure 4.1).

The solutions for the construction problems of the generator were difficult because of the required high pressure level of 18bar. The tube design and fixation led to leakage's in the first prototype construction. In the end, two prototypes of the indirectly heated generator were manufactured for the first prototype of the DACM.

4.2.2 DACM No. 2

A second, further optimised pilot plant based on the experiences and results of the first pilot plant was finished in July 2003 at the Stuttgart University of Applied Sciences. At the same time, the existing 19.3m² CPC vacuum tube collector plant on the roof or the Stuttgart University of Applied Sciences was coupled with the pilot plant so that instead of the previous indirect liquid heating

system, a direct operation of the pilot plant by the collector plant would be possible.

For the designed and realized cooling capacity range of the second cooling machine of 2.5kW, a further constructed and improved indirectly heated bubble pump was developed. The auxiliary gas circuit was also constructively reworked. These changes resulted in weight reduction down to 290kg and height reduction down to 2.40m which are important factors for a future, more marketable unit.

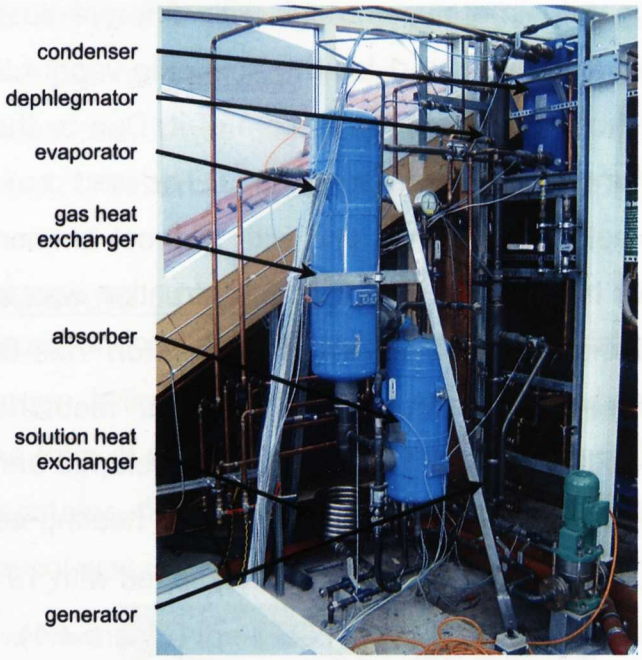

Figure 4.2: Second pilot plant of the DACM in the laboratory of the Stuttgart University of Applied Sciences.

4.2.2.1 STANDARD COMPONENTS

Figure 4.2 shows the second prototype of the DACM with standard commercial condenser and solution heat exchanger (nickel soldered plate heat exchanger). The heat transfer in the previously used horizontal tubular heat exchangers between the rich and weak ammonia/water solution in the solution heat exchanger and between the condensed refrigerant and the external cooling liquid in the condenser was insufficient.

During the cooling machines starting phase, helium, which is normally subsumed into the evaporator by ammonia vapour coming from the generator, is always in the condenser. In the first prototype, helium remained partly in the

condenser, so that the maximum heat transfer surface was not achieved and as a result, the condenser capacity was reduced. Due to this reduction, higher generator temperatures and thus higher condenser pressures were necessary to condense the ammonia vapour.

The dephlegmator is a simple double-pipe heat exchanger that is cooled with water and serves to reduce the temperature and to increase the ammonia concentration of the ammonia vapour coming from the generator.

The solution heat exchanger for this part had an included reservoir for the ammonia/water solution with an approximate capacity of 60l, which led to a very long preheating phase of the whole solution heat exchanger and therefore to a sluggish heat exchange between the cold and rich solution from the absorber and the hot and weak solution from the generator. In the second prototype, the reservoir was removed from the solution heat exchanger and re-installed below the absorber. With the use of plate heat exchangers, the pressure drop of both components was slightly increased.

The SHX plate heat exchanger achieved only poor heat recovery factors, and therefore the SHX was replaced in March of 2004 by a stainless steel coaxial heat exchanger. This replacement led to an additional weight reduction of 50kg and with that the total weight of the second pilot plant was lowered to 240kg.

In the second pilot plant, the components of the auxiliary gas circuit falling film evaporator, gas heat exchanger and falling film absorber were constructed as vertical tubular heat exchangers, but in a more compact size (Figure 4.2). The condenser and the absorber are water-cooled. Water-glycol mixture is used for the refrigeration circulation in the evaporator.

4.2.2.2 NEWLY DEVELOPED COMPONENTS

As a new development, a further generator prototype was developed, constructed and built. Due to the smaller overall height of the second prototype, the lifting height of the bubble pump could be reduced from 1.03m to 0.54m. This led to a higher efficiency of the bubble pump and a noticeable reduction of the generator heating temperatures. Generator No.5, with a height of 1.1m and 19 tubes (∅ 8mm x 1.5mm) was installed in the second pilot plant (Figure 4.2).

4.3 MEASUREMENT RESULTS AND PERFORMANCE

4.3.1 MEASURING METHODS PILOT PLANTS

One of the main problems of measuring mass flow rates of the ammonia vapour, the liquid ammonia, the weak and rich ammonia/water solution and the helium gas inside of the pilot plants of the DACM, was their very low volume flow inside the pipes and the high pressure losses of the commercially available measurement equipment. The operation temperatures inside of the cooling machine could not be directly measured because of the additional pressure losses through the measuring head (Jakob, 2001).

The used measuring data acquisition for both pilot plants was a type 349070A data acquisition system from Agilent, where the signals of the sensors were logged and converted in the respective measured variables.

4.3.1.1 DACM NO.1

The following measuring set-up (Figure 4.3) was used for the first pilot plant and for the secondary system (heating and cooling cycles): the relevant temperatures of the generator, dephlegmator, condenser, evaporator, gas heat exchanger, absorber, solution heat exchanger and also the secondary fluid cycles were measured by externally applied, type T thermoelements.

The pressure inside of the cooling machine was measured by an ammonia resistant chemistry manometer with an integrated pressure transformer. The measuring range was between zero and $25x10^5$Pa.

The flow rate of the secondary fluid cycles (absorber, evaporator, condenser) was measured by miniature turbine flowmeters with measuring ranges of between 2l/min and 40l/min. In the heating cycle, the flow rate was measured by a suspended flowmeter with a measuring range of 7 to 70l/min. The flow rate of the dephlegmator cooling circulation was measured by a manual flowmeter with a bypass. The measuring range of the flowmeter can be adjusted from zero to 8l/min.

The heating and cooling cycle of the generator and evaporator were operated with indirect liquid heating systems. The condenser, absorber and dephlegmator were directly cooled with water from the city water supply. Further information about the used measuring devices can be found in (Blessing, 2001; Sattler, 2002).

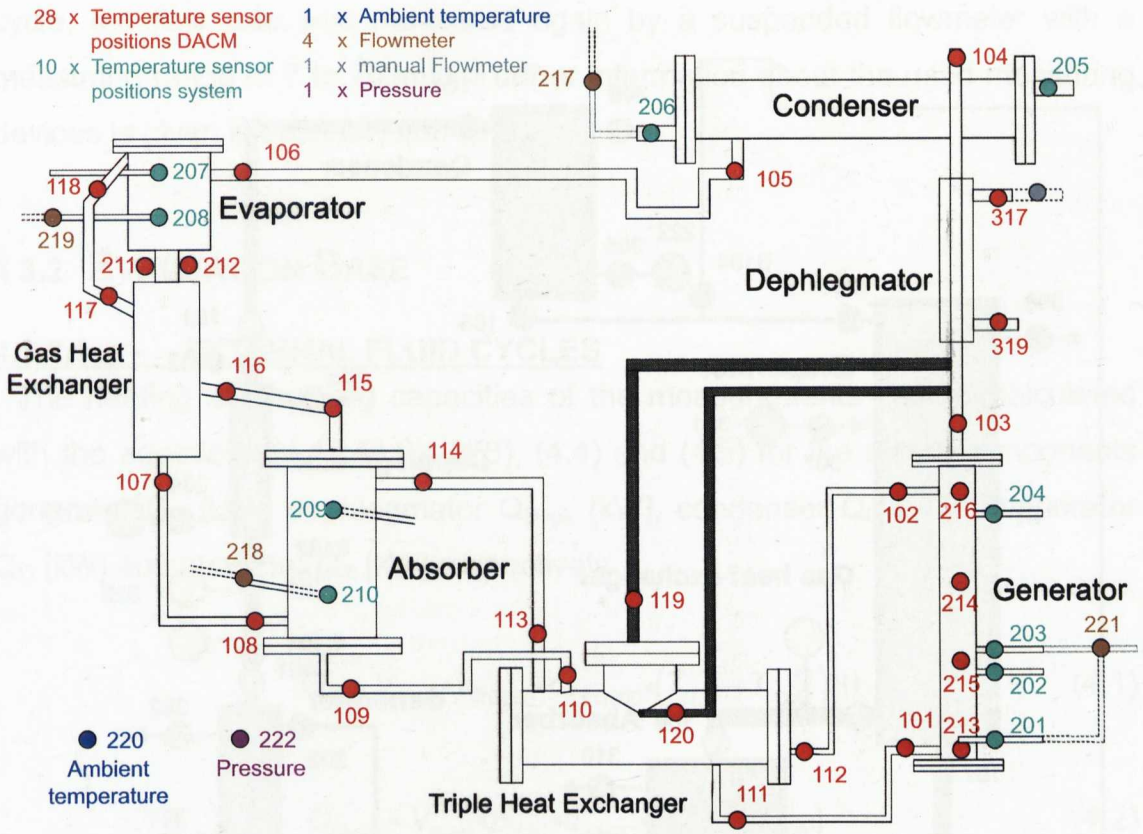

Figure 4.3: Schema of the first pilot plant of the DACM with temperature, pressure and mass flow measuring points.

4.3.1.2 DACM NO.2

The measuring sensors for the temperature, mass flow rate and pressure measurements were affixed to the second pilot plant as Figure 4.4 shows. The external heating and cooling cycles were all separately run by indirect liquid heating or cooling systems. Each cycle could be run with its own flow temperature as well as mass flow rate.

The measurements of the inlet and outlet temperatures of the cooling machine components as well as the secondary systems were taken by Pt100 foil

resistance temperature sensors which were mostly attached to the surface of the tubing. Some Pt100 platinum glass temperature sensors were also installed in dip tubes in the gas cycles of the ammonia vapour between generator and condenser and in the auxiliary gas circuit. The influence of the ambient temperature on the temperature measurements was minimised by enclosing the sensors with heat insulation.

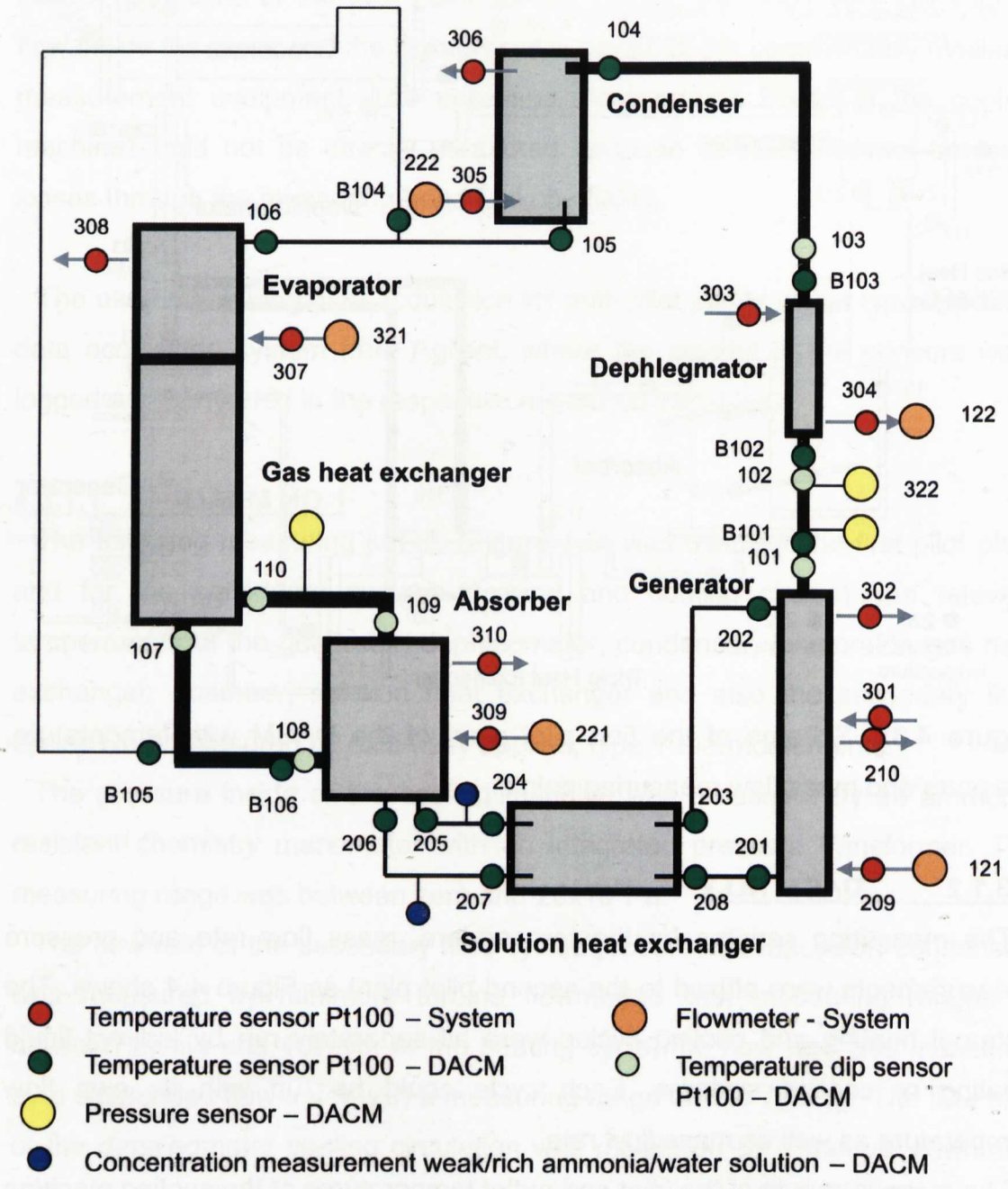

Figure 4.4: Schema of the second pilot plant of the DACM with temperature, pressure and mass flow measuring points.

The pressure inside of the DACM was measured again by an ammonia resistant chemistry manometer with an integrated pressure transformer. The measuring range of the manometer is between zero and $25x10^5$Pa.

The volume flow rates of the secondary cooling cycles were measured by turbine flowmeters with a measuring range of zero and 60l/min. In the heating cycle, the flow rate was measured again by a suspended flowmeter with a measuring range of 7 to 70l/min. Further information about the used measuring devices is given in (Teußer, 2004).

4.3.2 EVALUATION BASE

4.3.2.1 EXTERNAL FLUID CYCLES

The heating and cooling capacities of the measurements can be calculated with the equations (4.1), (4.2), (4.3), (4.4) and (4.5) for the single components generator Q_H [kW], dephlegmator Q_{Deph} [kW], condenser Q_C [kW], evaporator Q_O [kW] and absorber Q_A [kW] respectively.

$$Q_H = \dot{V}_{H,ext} \cdot \rho_{RO200} \cdot c_{p,RO200} \cdot \left(T_{H,in} - T_{H,out}\right) \tag{4.1}$$

$$Q_{Deph} = \dot{V}_{D,ext} \cdot \rho_{H2O} \cdot c_{p,H2O} \cdot \left(T_{D,out} - T_{D,in}\right) \tag{4.2}$$

$$Q_C = \dot{V}_{C,ext} \cdot \rho_{H2O} \cdot c_{p,H2O} \cdot \left(T_{C,out} - T_{C,in}\right) \tag{4.3}$$

$$Q_O = \dot{V}_{O,ext} \cdot \rho_{F20} \cdot c_{p,F20} \cdot \left(T_{O,in} - T_{O,out}\right) \tag{4.4}$$

$$Q_A = \dot{V}_{A,ext} \cdot \rho_{H2O} \cdot c_{p,H2O} \cdot \left(T_{A,out} - T_{A,in}\right) \tag{4.5}$$

Here, $\dot{V}_{i,ext}$ are the measured volume flows [l/h = m³/h], ρ_i are the densities [kg/m³], $c_{p,i}$ [J/kg K] are the specific heat capacities and $T_{i,in}$ [°C] and $T_{i,out}$ [°C] are the external inlet and outlet temperatures of the single components.

The coefficient of performance (COP) [-] is calculated with equation (4.6) and is the ratio of the evaluated evaporator cooling capacity to the heating capacity.

$$COP = \frac{Q_O}{Q_H} \tag{4.6}$$

The thermodynamic properties of the heating, cooling and refrigerating fluid of the external cycles are presented in the Figure 4.5 for thermo oil (Regloplas, 1999), Figure 4.6 for water (Hirschberg, 1988) and Figure 4.7 for water/glycol (Tyforop, 1999). These diagrams are used to evaluate the external capacities using the measured temperatures and volume flow rates.

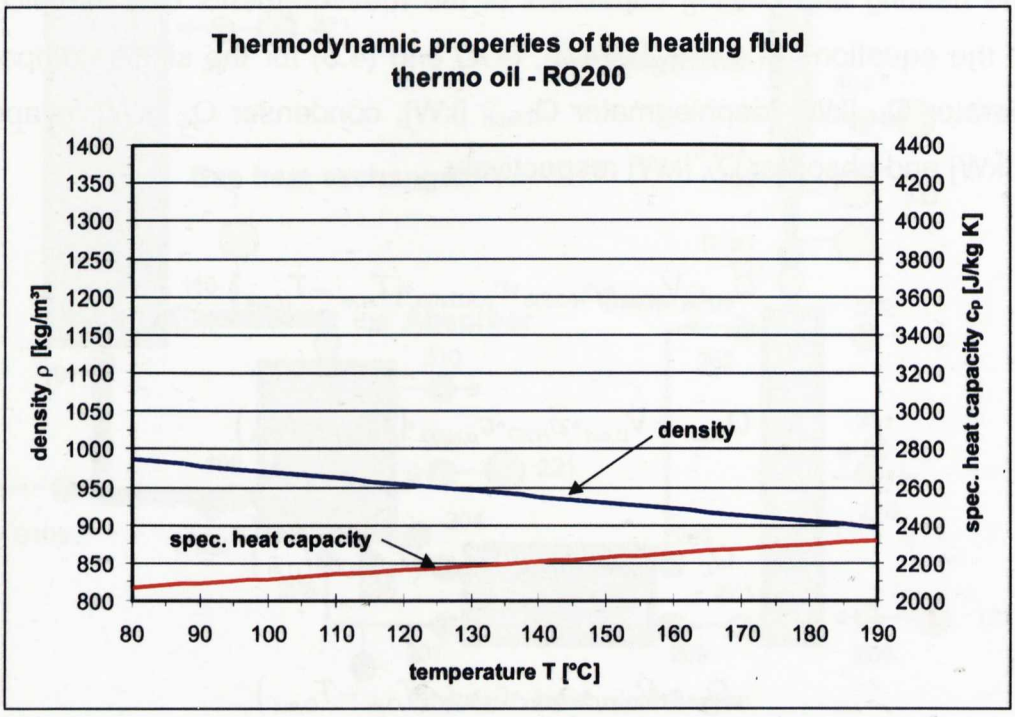

Figure 4.5: Thermodynamic properties of the heating fluid (thermo oil) from aic-regloplas (Regloplas, 1999).

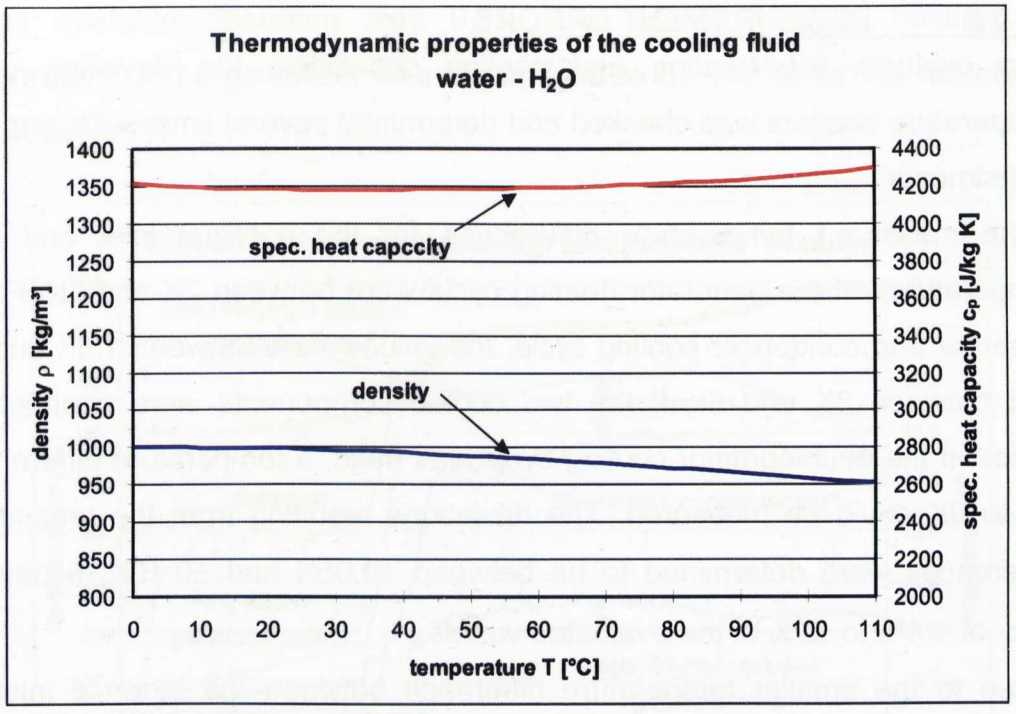

Figure 4.6: Thermodynamic properties of the cooling fluid (water) by (Hirschberg, 1988).

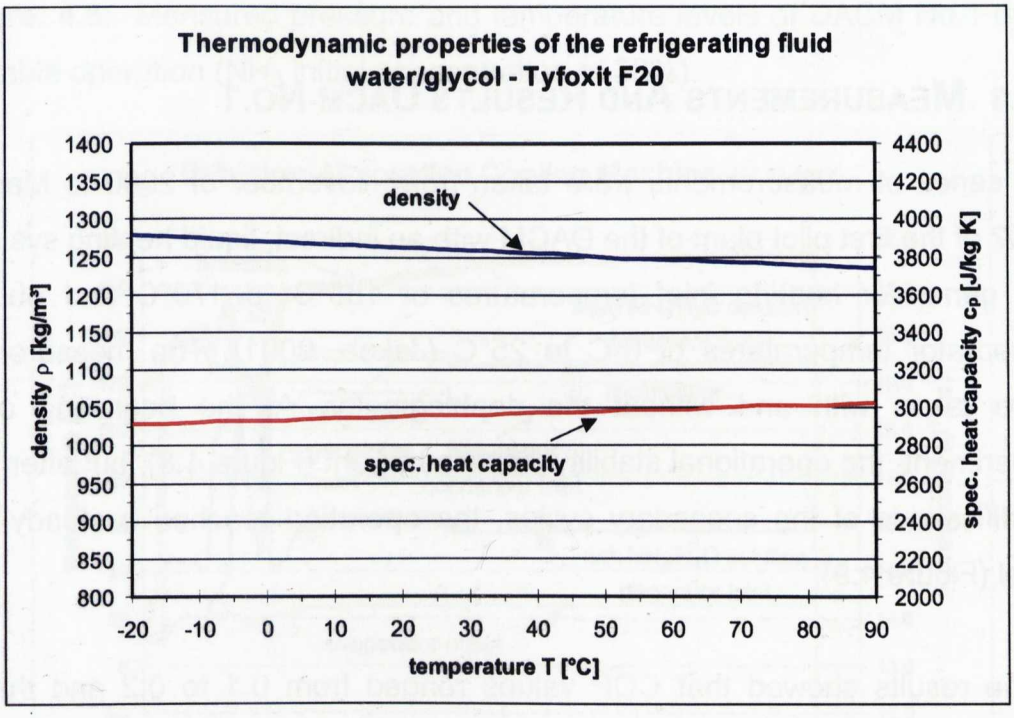

Figure 4.7: Thermodynamic properties of the refrigerating fluid (water/glycol) from Tyforop (Tyforop, 1999).

4.3.2.2 MEASUREMENT ERRORS

To evaluate the heating and cooling capacities, the deviation of the temperature sensors was checked and determined several times with zero point adjustments.

The measured temperature differences for the external inlet and outlet temperatures of the generator heating cycle were between 2K and 7K. For the absorber and condenser cooling cycle, the values were between 1.5K and 3K , and between 3K and 6K if the two cooled components were connected in series. If the dephlegmator cooling cycle was used, a temperature difference of 5K to 9K could be measured. The deviations resulting from the temperature differences were determined to be between ±0.05K and ±0.10K, a deviation error of ± 1% to ±5% of the evaluated values.

Due to the smaller temperature difference between the external inlet and outlet temperatures of the evaporator cooling cycle of 1.0K to 1.5K, the resulting deviation error was higher than that of the other cycles. In part the deviation was ±0.10K to ±0.15K, resulting in a deviation error of ± 5% to ±13%.

4.3.3 MEASUREMENTS AND RESULTS DACM NO.1

A series of measurements were taken from November of 2000 to March of 2002 of the first pilot plant of the DACM with an indirect, liquid heating system at the generator heating inlet temperatures of 150°C to 170°C and obtained evaporator temperatures of 0°C to 25°C (Jakob, 2001). The measurements were taken with and without the dephlegmator. At the beginning of the experiment, the operational stability was insufficient (Figure 4.8), but after some modifications of the secondary cycles, the operation reached a steady-stage level (Figure 4.9).

The results showed that COP values ranged from 0.1 to 0.2 and that the evaporator cooling capacity of the pilot plant was able to reach 0.5kW to 1.5kW. The measured heating capacities range from 4.0kW to 13.5 kW, depending on the mass flow rate and the heating temperature. The maximum measured COP

during unstable operation was 0.30. The lowest reached heating inlet temperature of the generator was determined to be 147°C for the retention of the process.

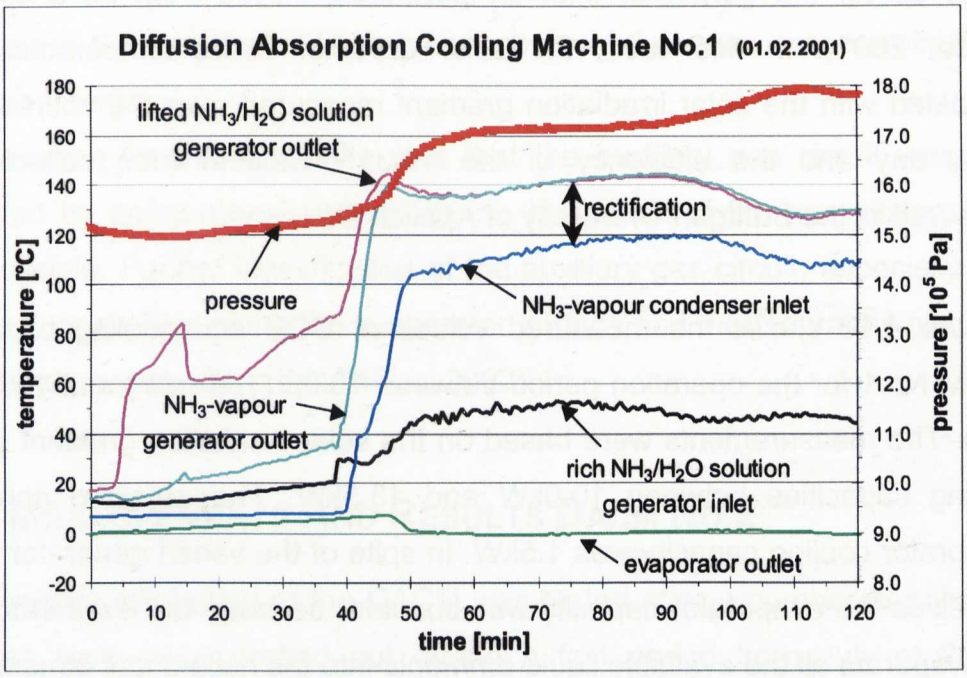

Figure. 4.8: Measured pressure and temperature levels of DACM No.1 during unstable operation (NH_3 initial concentration of 38%).

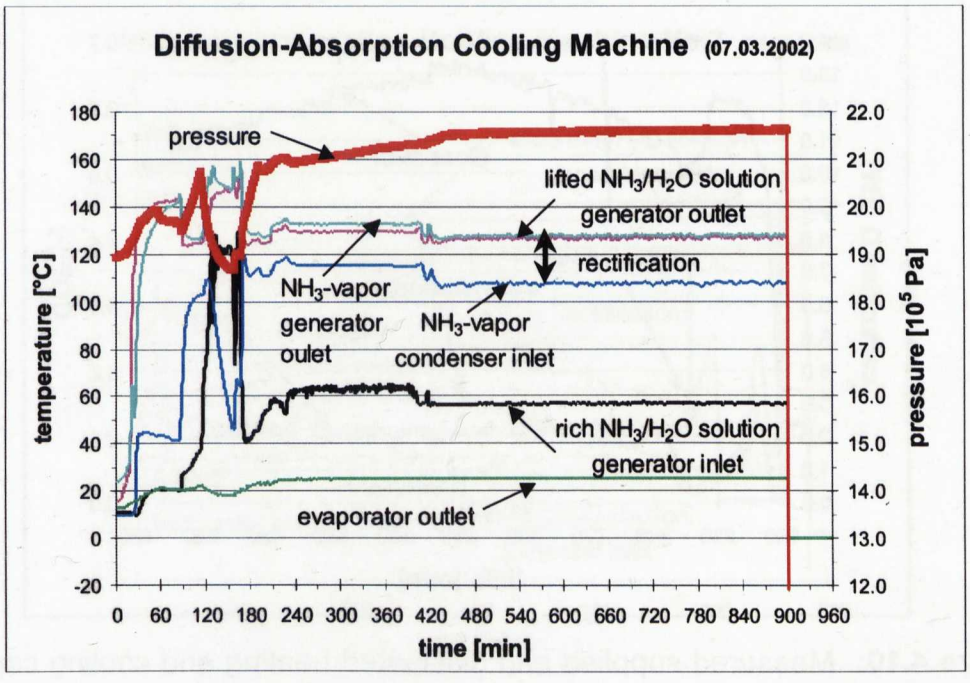

Figure. 4.9: Measured pressure and temperature levels of DACM No.1 at steady-stage operation level (NH_3 initial concentration of 38%).

More experiments were also carried out with the indirect liquid heating system based on a simulated solar irradiation gradient for a vacuum tube collector field with a maximum irradiation of 900 W/m² and solar collector outlet temperatures (same as for the generator inlet temperatures) varied from 80°C to 170°C (Jakob, 2001). In this case, the solar collector outlet temperatures were calculated with the solar irradiation gradient measured over the course of one sunny day and the efficiency of the 19.3m² vacuum tube collector field measured at the Stuttgart University of Applied Sciences.

Figure 4.10 shows the measured values of COP and cooling capacity of DACM No.1 for the operation period between 10:00 (180 min.) and 15:00 (480 min.). The measurements were based on the solar irradiation gradient given to heating capacities between 10.0kW and 13.5kW. The obtained continuous evaporator cooling capacity was 1.5kW. In spite of the varied generator heating capacities the evaporator capacity was constant because the evaporator could not evaporate all the available liquid ammonia into the helium gas atmosphere.

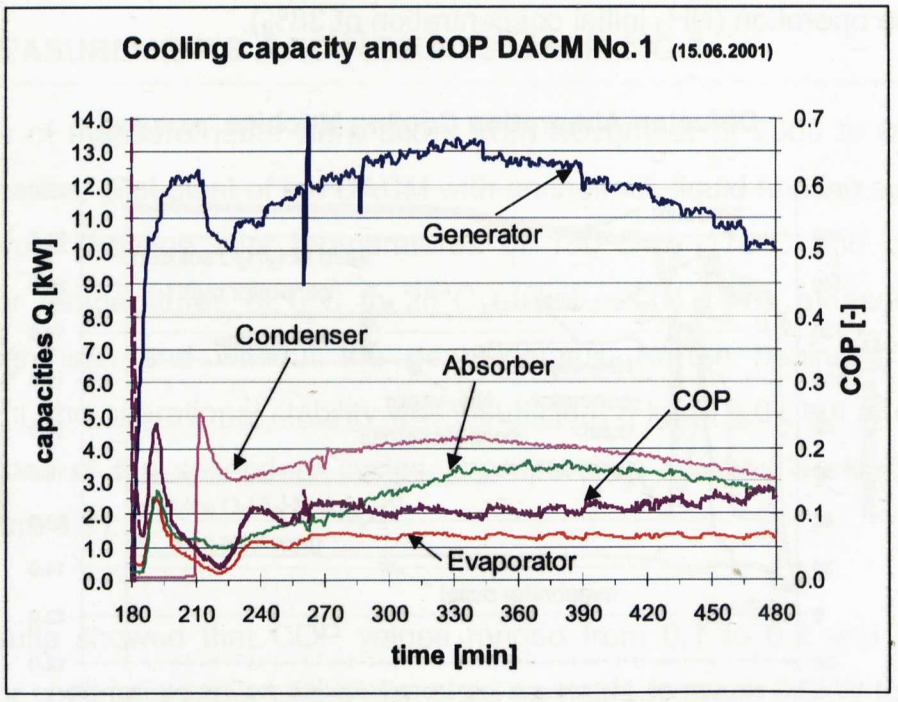

Figure 4.10: Measured supplied and dissipated heating and cooling capacities and COP of DACM No.1 based on a simulated irradiation gradient (NH_3 initial concentration of 38%).

During operation of the first pilot plant, instabilities occurred within the pure thermosyphon cyclic process of the pressure compensated, auxiliary gas circuit, which led to fluctuation of the generated evaporator cooling capacity. A decrease in the evaporator cooling capacity over time was observed in most of the experiments.

The reason for this decrease was that the auxiliary gas circuit was totally saturated by ammonia and therefore, no circulation of the gas mixture inside was possible. Further investigation of the auxiliary gas circuit, especially of the temperature profiles along the evaporator surface and thermography pictures of the saturation were done by (Päßler, 2002).

4.3.4 MEASUREMENTS AND RESULTS DACM NO.2

The second pilot plant of the DACM was tested after a number of safety and pressure tests were carried out during a first period from July of 2003 to November of 2003 with stable and continuous temperature and pressure levels (Figure 4.11).

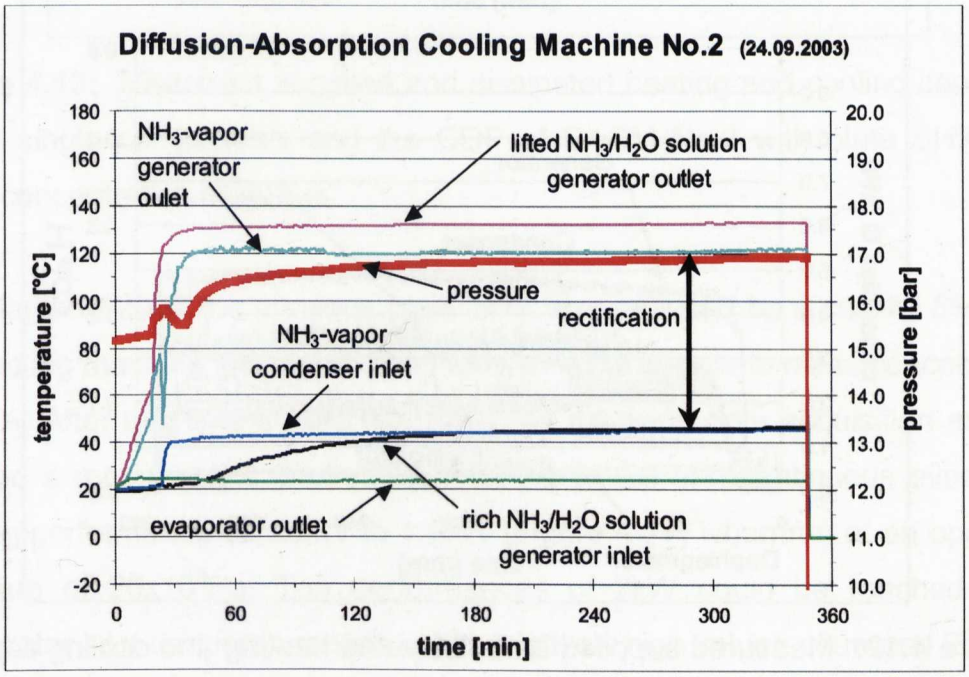

Figure 4.11: Measured pressure and internal temperature levels of DACM No.2 with plate SHX (NH_3 initial concentration of 30%).

Tests with running times of 24 hours and more were also carried out. The tests of the second pilot plant were concentrated on the newly developed generator and the reworked auxiliary gas circuit.

The determined heating temperature range of the generator was reduced from 150°C to 170°C of the first pilot plant, first to 130°C to 160°C and finally to 110°C to 140°C for the second pilot plant. Due to the lower total height of the second pilot plant the lifting height of the bubble pump could be reduced. With a commensurate heat transfer surface the efficiency of the bubble pump increased. This effect is indicated by a reduction of the heating temperatures as described previously.

The continuous evaporator cooling capacities of the first measurements evaluated at an operation pressure of $18x10^5$Pa were around 0.5kW (Figure 4.12) with COPs between 0.1 and 0.2. The maximum cooling capacity reached at an initial ammonia mass concentration of 30% was 0.8kW.

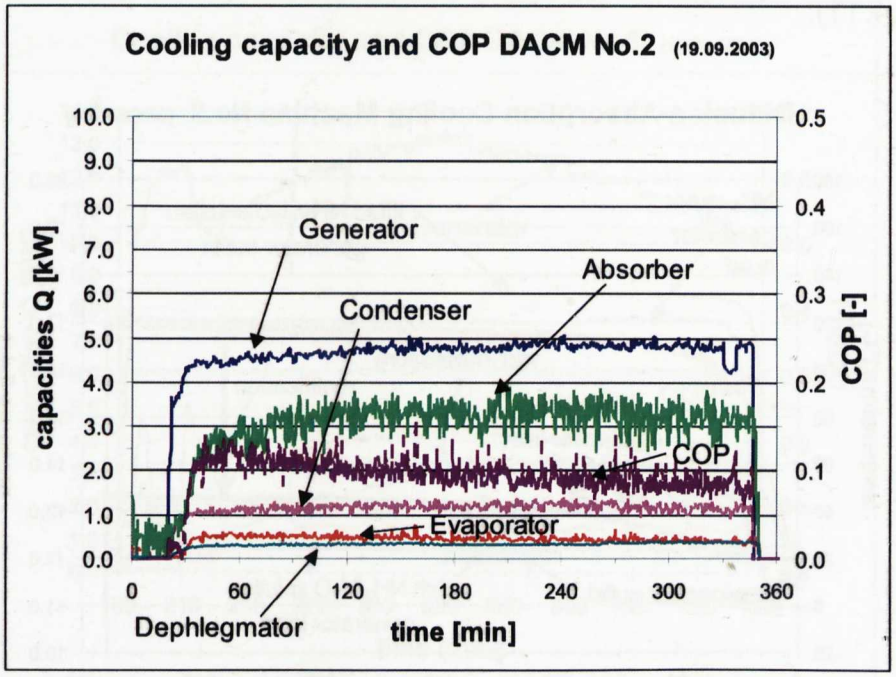

Figure 4.12: Measured supplied and dissipated heating and cooling capacities of the single components and the COP of DACM No.2 with plate SHX (NH_3 initial concentration of 30%).

In October of 2003, after the first tests including problem and error analysis had been carried out, the system was refilled with a new initial ammonia mass concentration of 40%. Measurements were taken until the end of November 2003 and again the new result was an evaporator cooling capacity of around 0.5kW (Figure 4.13).

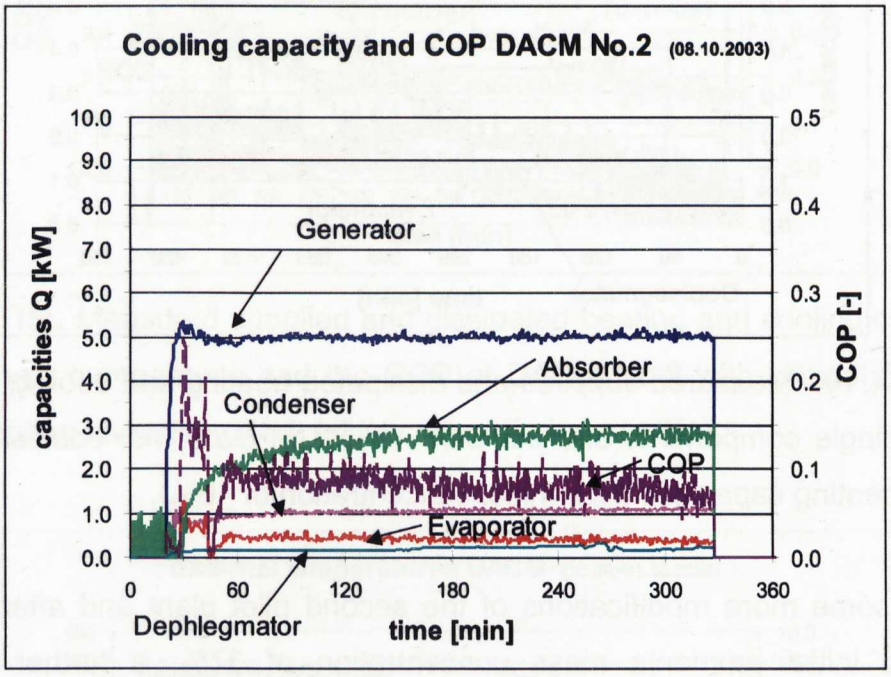

Figure 4.13: Measured supplied and dissipated heating and cooling capacities of the single components and the COP of DACM No.2 with plate SHX (NH_3 initial concentration of 40%).

In March of 2004 the previous plate SHX was replaced by a coaxial SHX and the cooling machine was again filled with an initial ammonia mass concentration of 40%. After this change the test runs and following data acquisition analysis showed a remarkably improved COP of 0.2 to 0.3 and continuous evaporator cooling performance of 0.5kW to 1.5kW (Figure 4.14) when run at an operation pressure of $20x10^5$Pa. Top performances of 2kW could be reached if the evaporator inlet temperature was set to relatively high values of around 25°C.

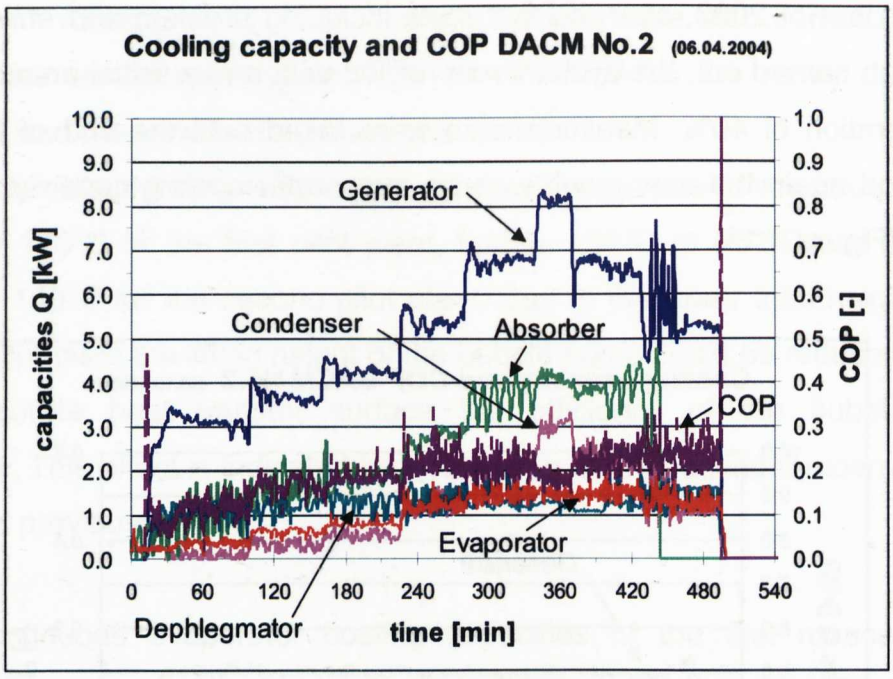

Figure 4.14: Measured supplied and dissipated heating and cooling capacities of the single components and the COP of DACM No.2 with coaxial SHX with varied heating capacities (NH_3 initial concentration of 40%).

After some more modifications of the second pilot plant and after refilling it with an initial ammonia mass concentration of 37%, a further period of measurements was begun in September of 2004 and was run until November of 2004 at a lower operating pressure of $12x10^5$Pa. Many long term measurements of up to 11 days were carried out with out shutting down the machine.

The new results showed a further improved COP of 0.3 to 0.5 (Figure 4.15) and a continuous evaporator cooling performance up 1.6kW at evaporator outlet temperatures for air-conditioning between 22°C and 15°C. Figure 4.16 shows the external inlet and outlet temperature curves of the heating, cooling and chilled water e.g. for varied heating temperatures, a constant cooling water inlet temperature of 27°C and a corresponding adjusted evaporator temperature.

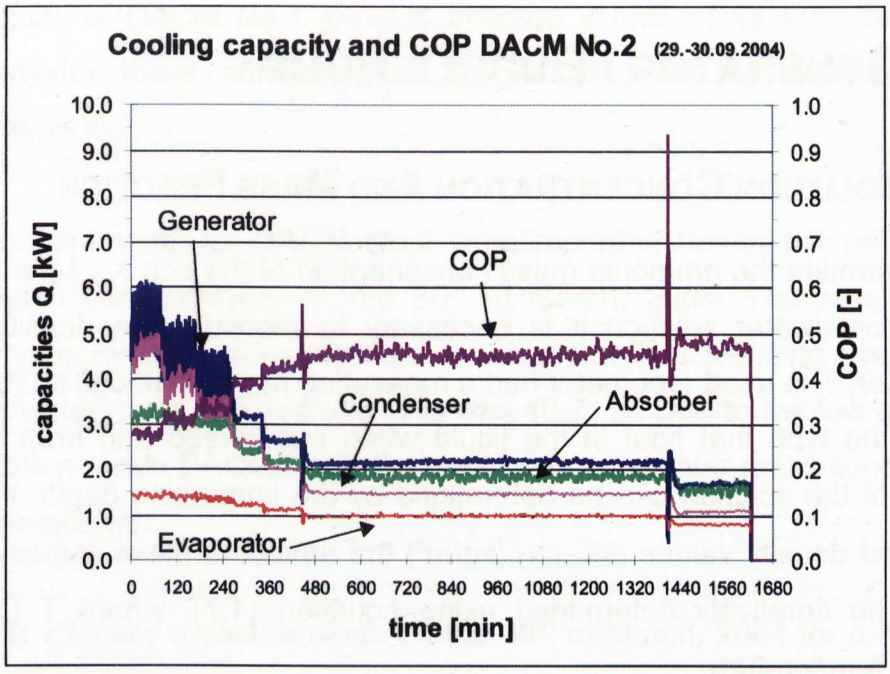

Figure 4.15: Measured supplied and dissipated heating and cooling capacities of the single components and the COP of DACM No.2 with coaxial SHX with varied heating capacities (NH_3 initial concentration of 37%).

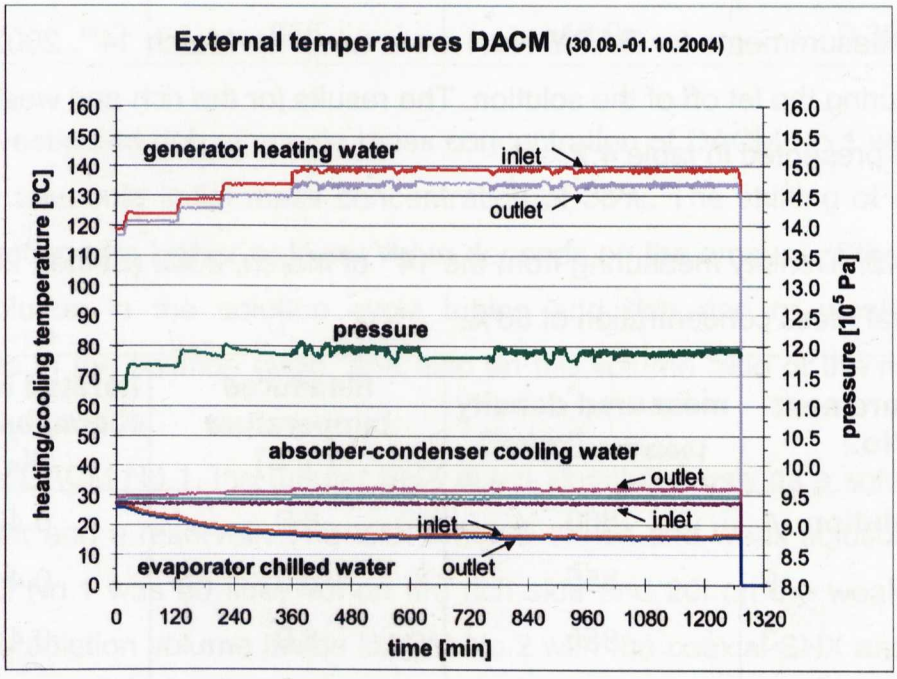

Figure 4.16: Measured external temperatures of the heating, cooling and chilled circuits of DACM No.2 with coaxial SHX with varied heating temperatures (NH_3 initial concentration of 37%).

4.4 GENERATOR / BUBBLE PUMP

4.4.1 SOLUTION CONCENTRATION AND MASS FRACTION

To determine the ammonia mass concentration of the rich X_{Sr} [-] or weak X_{Sw} [-] ammonia/water solution it is necessary to measure the density with an areometer. The used areometer had a measuring range of 650g/l to 1000g/l and was of the type that float in the liquid when submersed and from which the density of the solution can be determined by the immersion depth. With these measured density values $\rho_{NH3/H2O}$ [kg/m³] the ammonia mass concentration X_S [-] can be iteratively determined using equation (4.7), where T [°C] is the solution temperature.

$$\rho_{NH3/H2O} = \begin{pmatrix} 1000 - 369 \cdot X_S + 219 \cdot X_S^2 \cdot (1 - X_S) \\ -(0.0075 + 1.98 \cdot X_S - 0.54 \cdot X_S^2) \cdot T \\ -(0.0016 + 0.001 \cdot X_S^3) \cdot T^2 \end{pmatrix} \tag{4.7}$$

The measurements for **DACM No.1** were taken on March 14th, 2002 (Sattler, 2002) during the let off of the solution. The results for the rich and weak solution side are presented in table 4.2.

Table 4.2: Density measuring from the 14th of March, 2002 (Sattler, 2002) for a NH_3 initial mass concentration of 38%.

measurement No.		measured density $\rho_{NH3/H2O}$ [kg/m³]	measured temperature T [°C]	iterated NH_3 mass concentration X_S [-]
rich solution	1	860	8.0	0.4243
	2	855	8.0	0.4402
	3	855	8.0	0.4402
	4	845	8.0	0.4717
weak solution	1	895	8.0	0.3115
	2	895	8.0	0.3115

The results of DACM No.1 showed average values of 44.41% for the rich ammonia/water mass concentration X_{Sr} and 31.15% for the weak mass concentration X_{Sw}.

The measurements for **DACM No.2** were recorded before the refilling of a new solution concentration on the 30th of March, 2004. The results of the density measurements are presented in table 4.3. The resulting average rich ammonia/water mass concentration X_{Sr} was 40.21%. Due to the low amount of weak solution inside DACM No.2, the weak ammonia/water mass concentration was not measured.

Table 4.3: Density measurements on the 30th of March, 2004 for a NH_3 initial mass concentration of 40%.

measurement No.		measured density $\rho_{NH3/H2O}$ [kg/m³]	measured temperature T [°C]	iterated NH_3 mass concentration X_S [-]
rich solution	1	860	13.9	0.4099
	2	855	13.9	0.3943

The investigated rich ammonia mass concentration of DACM No.1 was higher than the ammonia initial mass concentration of 38%. The shifting of the mass concentration to a higher or lower value depends on the amount of the rich and weak solution in the solution cycle tubing and rich and or weak solution reservoirs in the solution cycle, and also on the volume ratio of the rich to the weak solution side.

For the DACM No.1, the tubular SHX acted simultaneously as a solution heat exchanger and a reservoir. The total amount of rich and weak solution volume in DACM No.1 was 60 litre; 40l on the rich side and 20l on the weak solution side. The solution volume inside DACM No.2 with the coaxial SHX and the rich solution reservoir below the absorber, totalled 11.5 litres (9.7 litre rich solution and 1.8 litre weak solution). The resulted mass fractions of the solution which were used in DACM No.1 and No.2 are stated in table 4.4 for the different ammonia initial mass concentrations.

Table 4.4: Mass fractions of the solution cycles of DACM No.1 and No.2 for different NH_3 initial mass concentrations.

pilot plant DACM	ammonia initial mass concentration X_S [-]	mass fraction m [kg]	
		ammonia (NH_3)	water (H_2O)
No. 1	38%	19.72kg	32.18kg
No. 2	30%	3.08kg	7.18kg
No. 2	40%	3.95kg	5.92kg
No. 2	37%	3.69kg	6.29kg

The ratio between the mass fractions of DACM No.1 and No.2 for an ammonia initial mass concentration of 38% and 40% respectively is approximately the factor five. The preheating phase of the solution cycle for DACM No.2 was only 30 minutes in comparison to the two or three hour-long phase of DACM No.1.

4.4.2 SPECIFIC SOLUTION CIRCULATION INDEX

The ammonia/water solution mass concentration X_S which is generated by the generator can be calculated iteratively with the modified Clausius-Clapeyron equation (4.8). The calculation of the weak solution concentration X_{Sw} [-] is done assuming stable operating conditions with the measured total pressure p [Pa] which is equal to the condenser pressure and the measured generator outlet temperature of the weak solution T_{SwG} [°C].

$$\log_{10} p = \left(\frac{10.44 - 1.767 \cdot X_{Sw} + 0.9823 \cdot X_{Sw}^{2} + 0.3627 \cdot X_{Sw}^{3}}{2013.8 - 2155.7 \cdot X_{Sw} + 1540.9 \cdot X_{Sw}^{2} - 194.7 \cdot X_{Sw}^{3}} \right) \qquad (4.8)$$

Another characteristic value of the gas bubble pump is the degassing width E [-] which is the difference between the rich X_{Sr} and weak X_{Sw} solution as shown in equation (4.9).

$$E = X_{Sr} - X_{Sw} \qquad (4.9)$$

Using equations (3.23) and (3.24), both for high pressure levels of $5.52x10^5$Pa $\leq p \leq 24.13x10^5$Pa, the ammonia vapour concentration X_{V1} [-] was calculated using the weak solution concentration X_{Sw} [-] and the measured total pressure p [Pa]. With these three different mass concentrations, the specific solution circulation index f [-] (for receiving 1kg ammonia vapour m_V [kg/s] simultaneously expelled of the incoming rich ammonia/water solution m_{Sr} [kg/s] within the generator) can then be calculated using equation (4.10). The specific solution circulation index (f-1) [-], relative to the lifted weak ammonia-water solution m_{Sw} [kg/s], was calculated using equation (4.11).

$$f = \frac{\dot{m}_{Sr}}{\dot{m}_V} = \frac{X_{V1} - X_{Sw}}{X_{Sr} - X_{Sw}} \tag{4.10}$$

$$f - 1 = \frac{\dot{m}_{Sw}}{\dot{m}_V} = \frac{X_{V1} - X_{Sr}}{X_{Sr} - X_{Sw}} \tag{4.11}$$

For the characterisation of the gas bubble pump, generator No.3 from **DACM No.1** and generator No.5 from **DACM No.2**, the characteristic values of both generators were determined and compared. The values of the investigated range of generator heating temperatures and mass flows are presented in table 4.5. The specific solution circulation is especially important for the investigation of the gas bubble pump.

Table 4.5: Determined characteristic values of generator No.3 and No.5 for different initial ammonia concentrations of DACM pilot plants No.1 and No.2.

characteristic values	generator No.3	generator No.5		
average total pressure p [Pa]	**$20x10^5$Pa**	**$18x10^5$Pa**	**$20x10^5$Pa**	**$12x10^5$Pa**
NH_3-initial concentration	38%	30%	40%	37%
rich NH_3-solution conc. X_{Sr} [-]	45–42%	30%	40%	37%
weak NH_3-solution conc. X_{Sw} [-]	31–34 %	24–26%	31–33%	24–29%
degassing width E [-]	14 – 8%	6 – 4%	9 – 7%	13 – 8%
vapour concentration X_{V1} [-]	88–91 %	82–85%	89–91%	84–89%
specific solution circulation f [-]	4–7	11–15	6.5–8.5	4.5–7.5

For a comparison, the measured solution concentrations of the first pilot plant were 31% for X_{Sw} and 44% for X_{Sr} with an analysed degassing width of 13%. The determined characteristic values of the generator show that the specific solution circulation index of generator No.5 is about 1.5 to 3 times higher than that of the old generator No.3 of DACM No.1. The following figures show the different mass concentrations, the degassing width and the specific solution circulation index for generator No.3 (Figure 4.17) and generator No.5 (Figure 4.18) respectively.

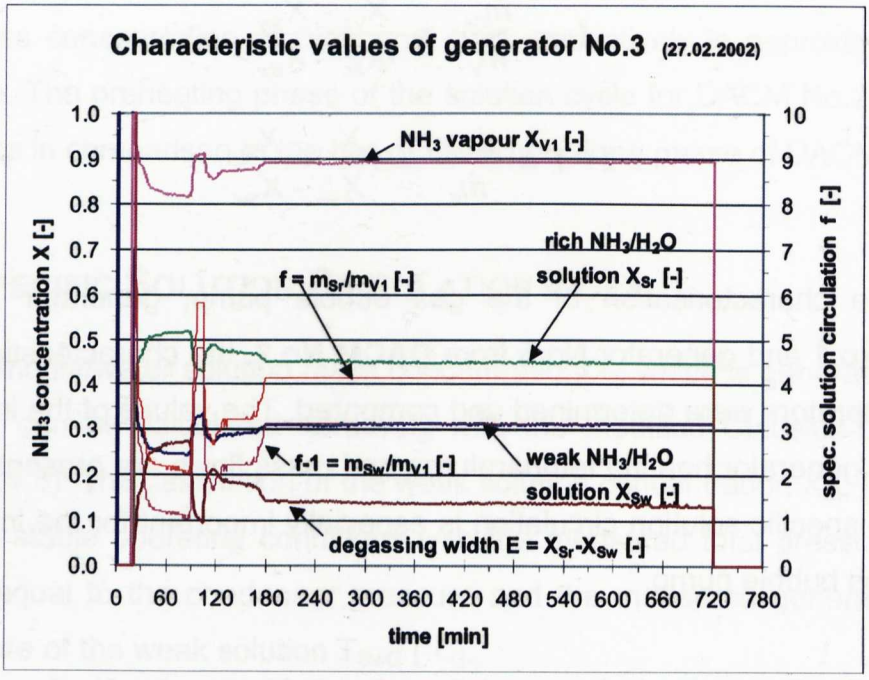

Figure 4.17: Calculated characteristic values of generator No.3 and ammonia concentrations of DACM No.1.

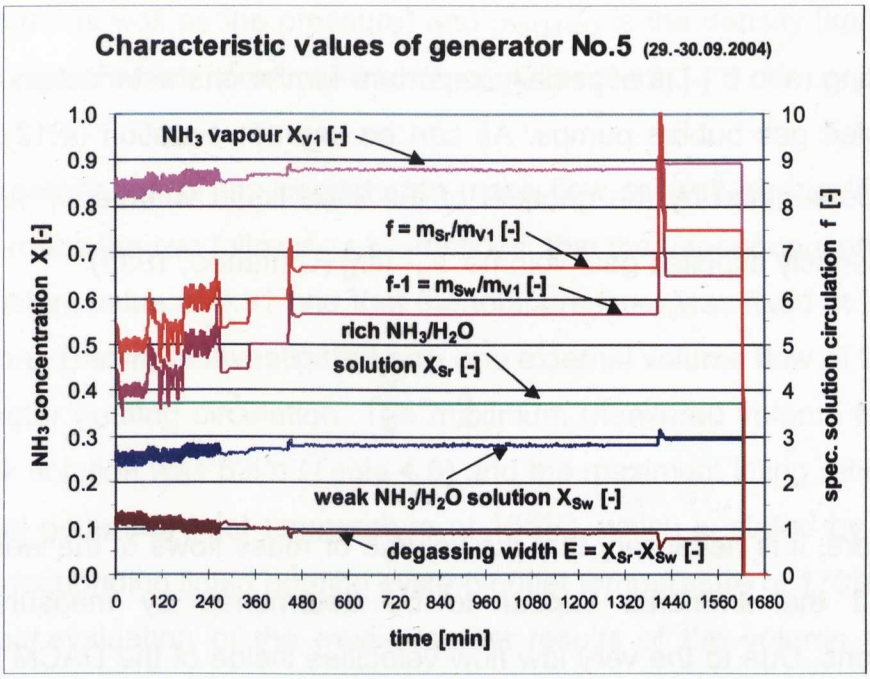

Figure 4.18: Calculated characteristic values of generator No.5 and ammonia concentrations of DACM No.2 with coaxial SHX.

4.4.3 LIFTING RATIO

The designed gas bubble pumps introduced previously (chapter 4.2) and therewith the thermosyphon cycle process of the solution circulation had a state-of-the-art performance. Figure 4.19 shows the three generators of the test rig, the first and second pilot plant, generator No.2, No.3 and No.5.

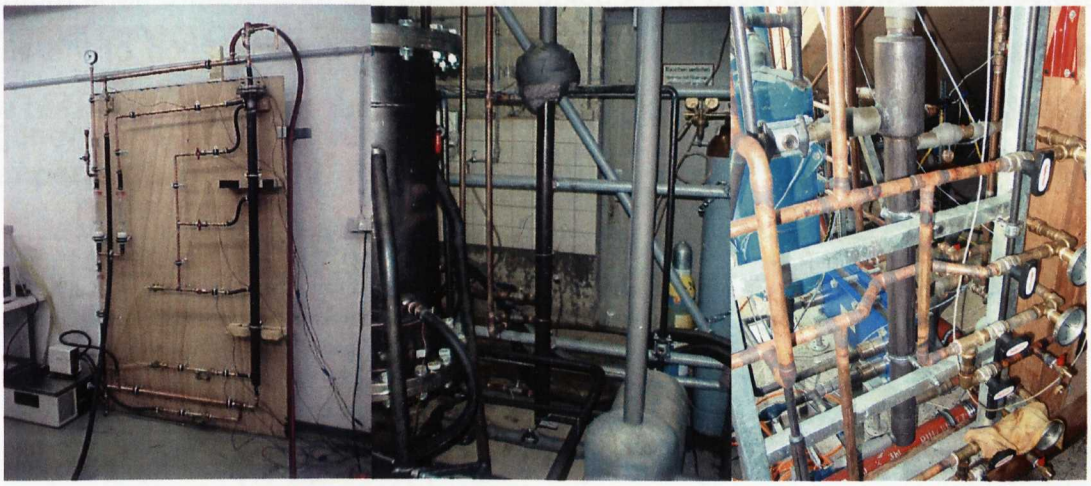

Figure 4.19: Pictures of generator No.2 of the test rig, generator No.3 of DACM No.1 and generator No.5 of DACM No.2 (from left to right respectively).

The lifting ratio b [-] is especially important for the characterisation of different constructed gas bubble pumps. As can be seen in equation (4.12), the lifting ratio is determined by the quotient of the lifted liquid volume $\dot{V}_L$ [l/h] and the simultaneously expelled gas volume $\dot{V}_V$ [l/h] (Cattaneo, 1935).

$$b = \frac{\dot{V}_L}{\dot{V}_V} \tag{4.12}$$

Therefore, it is necessary that the volume or mass flows of the weak solution side and the ammonia vapour to be determined by measurements or calculations. Due to the very low flow velocities inside of the DACM tubing, the measurements could not be taken with any of the commercially available measurement systems. The best working point for the generator is determined by the lifting ratio. Should the performance of a generator be determined according to varied construction features such as length, inner tube diameter or amount of tubes, the characteristic value b should be selected.

During the measurements of **DACM No.1**, the volume flow for generator No.3 was determined by (Biesinger, 2002) for different heating inlet temperatures as well as transferred heat capacities. The measuring method for the acquisition of the volume flow of the lifted weak solution, called the temperature flank method, is described in detail in (Biesinger, 2002). For the determination of the lifting ratio, the volume flow $\dot{V}_V$ [l/h] of the desorbed vapour has to be calculated with equation (4.13) as follows:

$$\dot{V}_V = \frac{\dot{m}_V \cdot 3600\left[\frac{s}{h}\right]}{\rho_{NH3/H2O} \cdot 1000\left[\frac{l}{m^3}\right]} \tag{4.13}$$

Here, m_V is the mass flow [kg/s] of the condensate (calculated with equation (4.14) using the measured condenser internal and external inlet and outlet

temperatures as well as the pressure) and $\rho_{NH3/H2O}$ is the density [kg/m³] of the ammonia vapour which is calculated with equation (3.12).

For the calculation of the condensate mass flow as well as the lifting ratio, Biesinger made the two following assumptions: that the vapour concentration X_V had a constant value of 0.91 and that the total pressure was fixed at $20x10^5$Pa. Furthermore, Biesinger investigated only one external volume flow of 21l/min for the generator heating circulation. The maximum measured volume flow of the lifted weak solution was 53l/h (Table 4.6) and the maximum lifting ratio of 3.8 at an external generator inlet temperature of 165°C, which is stated by Biesinger for the corresponding liquid heating system outlet temperature of 170°C.

A revised evaluation of the measurement results of the volume flows was done by the author with the corresponding measured pressures and vapour concentrations. Herewith, lower values of the calculated vapour volume flow as well as higher lifting ratios were determined (Table 4.6). The author used an extensive calculation method for the condensed ammonia vapour mass flow with superheated vapour and sub-cooled liquid.

For the maximum measured volume flow of the lifted weak solution of 53l/h, the revised evaluated vapour volume flow is 12.2l/h and thereby the maximum lifting ratio is 4.3 when the external generator inlet temperature is 165°C.

Table 4.6: Lifting ratio b of generator No.3 of DACM No.1 dependant on external generator inlet temperatures.

external generator inlet temperature $T_{H,in}$ [°C]	pressure p [10^5 Pa]	measured $\dot{V}_L$ [l/h] (Biesinger, 2002)	calculated $\dot{V}_V$ [l/h]	lifting ratio b [-]
146.5	17.99	19.90	6.84	2.91
151.5	18.40	30.40	9.18	3.31
156.0	18.84	38.90	10.93	3.56
160.0	19.46	42.30	11.02	3.84
165.0	19.75	53.00	12.22	4.34
170.0	20.09	52.80	13.61	3.88
175.0	20.25	51.30	16.56	3.10

The Figure 4.20 shows the three curves of the measured liquid volume flow, the calculated vapour volume flow and the lifting ratio of DACM No.1. The volume flow of the vapour was continually increased because of the changing flow regime. The slug flow collapsed and converted to annular flow, and thereby the nucleate boiling changed to film boiling. Therefore, at heating temperatures above 165°C, more vapour is generated but the solution lifting decreases.

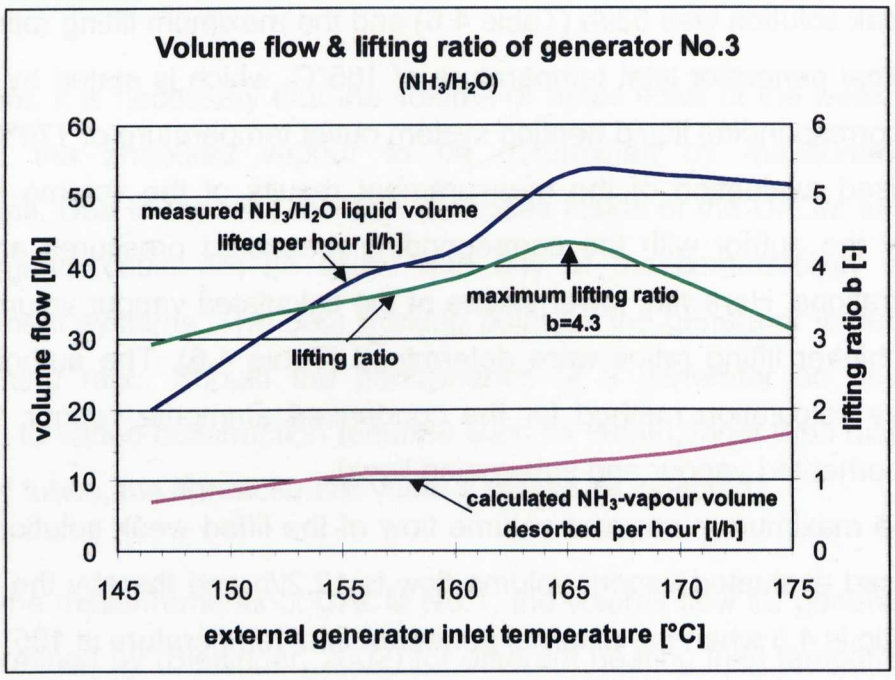

Figure 4.20: Volume flow and lifting ratio of generator No.3 of DACM No.1 for the investigated working pair ammonia/water.

In order to obtain a comparison of the lifting ratios of the previously investigated generator No.2 (Jakob, 2001), further investigations of the volume flow were done by the author. The generator No.2 with a height of 1.6m and 12 tubes (∅ 6mm x 1mm) was investigated at a separate **test rig** (Figure 4.19) using the two working fluids methanol (MeOH) and methanol/water (40% methanol). The lifting height in the experiments was set to 1.03m. The boiling point temperature for methanol is about 64.5°C at $1x10^5$Pa with a specific evaporation enthalpy of 1100kJ/kg, which is similar to this of ammonia.

The relevant temperatures of the preheated line, the generator inlets and outlets and the condenser were measured by thermoelements. The lifted methanol or methanol/water as well as the condensed methanol were measured by two drip funnels each with a bypass (Figure 4.21).

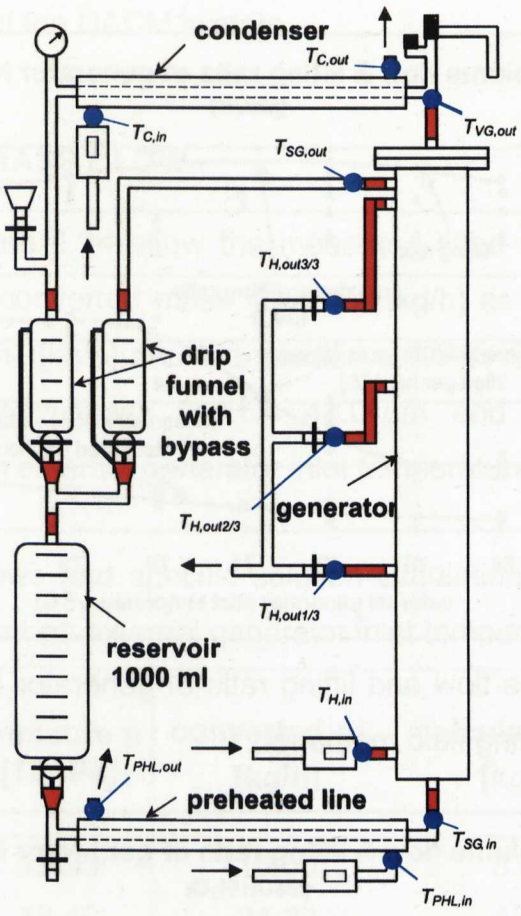

Figure 4.21: Scheme of the test rig of generator No.2.

The generator was coupled to three outlet valves to investigate the effect of the different heating possibilities (Figure 4.21). Decreasing the heating length of the generator increases the amount of condensate, this is due to the possible collapsing of the slug flow by overheating in the upper part of the generator. The operation of the bubble pump is therefore more efficient, if only the lower part of the generator is heated. The generator heating inlet temperatures for the start up were 70°C to 72°C for MeOH and 84°C for methanol/water and the minimal generator heating inlet/outlet temperatures in nominal operation were 66.7°C/65.5°C for methanol as well as 83.8°C/82.4°C for MeOH/H_2O.

The main outcomes of the investigation were that the preheating of the complete generator shell and good thermal insulation of the whole component is absolutely necessary for a quick start up, as the generated vapour condenses otherwise. The preheating of the solution in the preheated line is also necessary which is taken over later by the SHX.

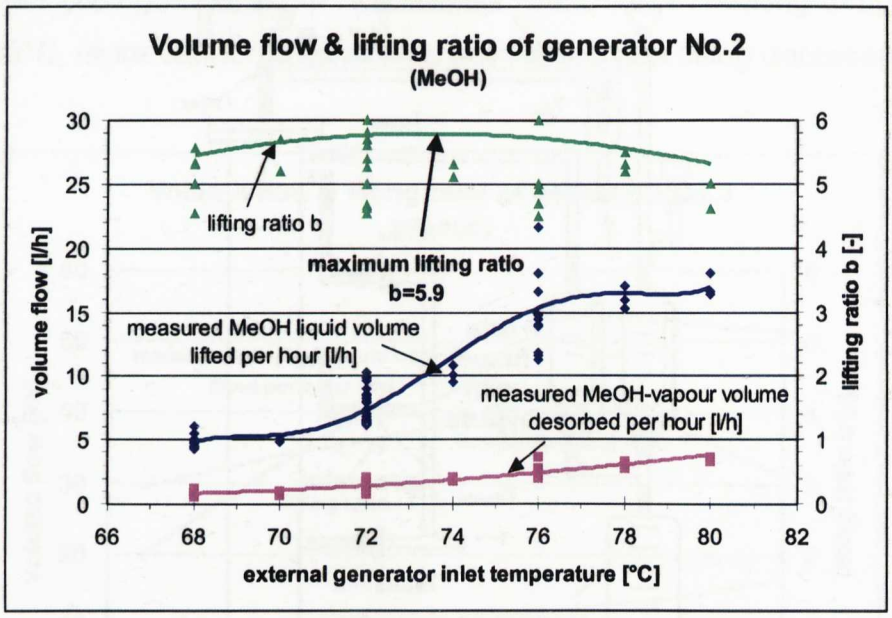

Figure 4.22: Volume flow and lifting ratio of generator No.2 of the test rig for the investigated working fluid methanol.

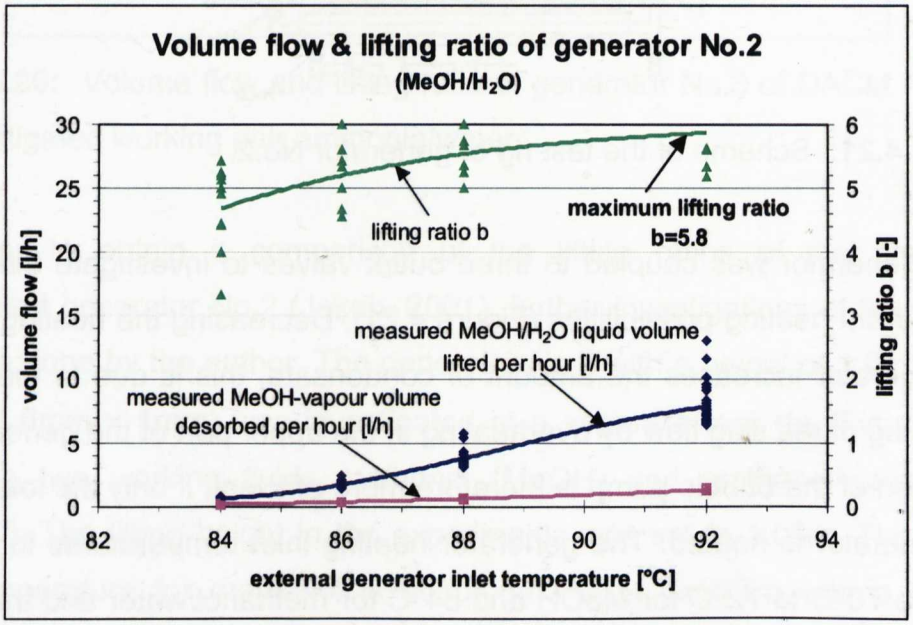

Figure 4.23: Volume flow and lifting ratio of generator No.2 of the test rig for the investigated working pair methanol/water.

The resulting measurements at different external generator inlet temperatures showed a maximum lifting ratio in both cases about 5.8 to 5.9. The general behaviour of the measured volume flows, presented in the Figures 4.22 and 4.23, is similar to those of generator No.3, but the results are not usable for a further investigation of the DACM system.

4.4.4 SOLUTION MASS FLOW

Table 4.7 and Figure 4.24 show the measured lifted weak solution volume flows in the form of converted mass flows m_S [kg/h] as well as the evaluated vapour mass flows m_V [kg/h] and the specific solution circulation indexes f [-]. The maximum solution mass flow is 42.0kg/h and the specific solution circulation is 8.0 at an external generator inlet temperature of 165°C.

Table 4.7: Mass flows and specific solution circulation of generator No.3 of DACM No.1 dependant on external generator inlet temperatures.

external generator inlet temperature $T_{H,in}$ [°C]	pressure p [10^5 Pa]	converted $\dot{m}_S$ [kg/h]	calculated $\dot{m}_V$ [kg/h]	specific solution circulation f [-]
146.5	17.99	16.00	3.56	5.50
151.5	18.40	24.32	4.68	6.20
156.0	18.84	30.99	5.52	6.62
160.0	19.46	33.56	5.42	7.19
165.0	19.75	42.03	5.97	8.04
170.0	20.09	41.82	6.79	7.16
175.0	20.25	40.65	8.20	5.96

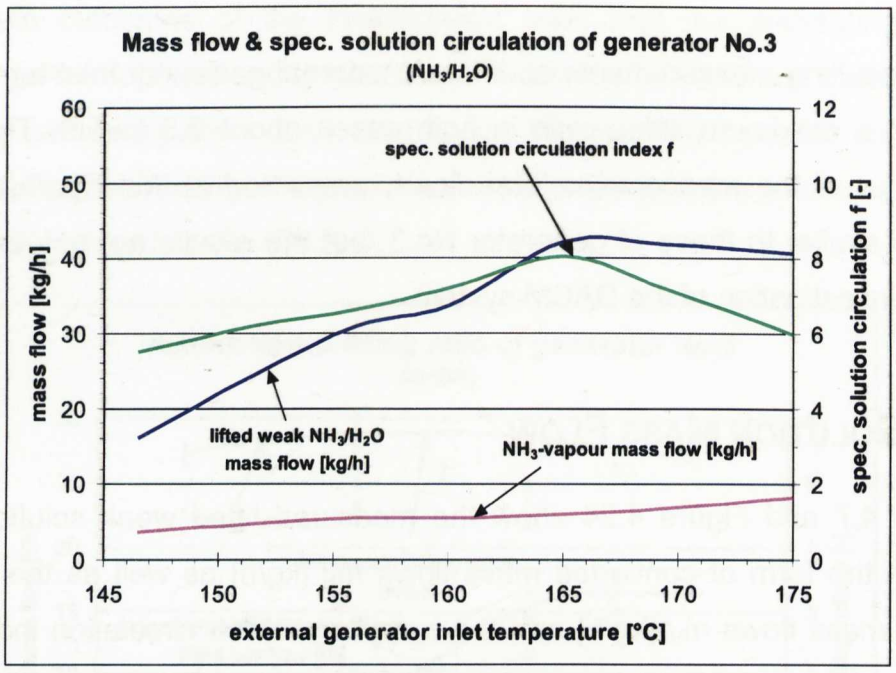

Figure 4.24: Mass flow and specific solution circulation of generator No.3 of DACM No.1 for the investigated working pair ammonia/water.

For the calculation of the solution mass flows, first the ammonia vapour mass flow m_V [kg/s] has to be calculated. The vapour mass flow is defined by the equation (4.14) or (4.20) as follows:

$$\dot{m}_V = \frac{Q_C}{c_{V,NH3} \bullet \left(T_{VC} - T_{C,s}\right) + h_V - h_L + c_{L,NH3/H2O} \bullet \left(T_{C,s} - T_{LC}\right)} \tag{4.14}$$

Here, Q_C [kW] is the condenser capacity, $c_{V,NH3}$ [kJ/kg K] is the specific heat capacity of ammonia vapour, T_{VC} [°C] and T_{LC} [°C] are the measured condenser vapour inlet and condensate outlet temperatures, $T_{C,s}$ [°C] is the condensation temperature, $c_{L,NH3/H2O}$ [kJ/kg K] is the specific heat capacity of liquid ammonia and h_V [kJ/kg] and h_L [kJ/kg] are the vapour and liquid enthalpies. The equations that are required for the calculation of the named variables are presented in chapter 4.6.

Next, the weak m_{Sw} [kg/s] and rich m_{Sr} [kg/s] solution mass flows are calculated with equations (4.15) and (4.16) as follows:

$$\dot{m}_{Sw} = \left(\frac{X_V - X_{Sr}}{X_{Sr} - X_{Sw}} \right) \bullet \dot{m}_V \tag{4.15}$$

$$\dot{m}_{Sr} = \left(\frac{X_V - X_{Sw}}{X_{Sr} - X_{Sw}} \right) \bullet \dot{m}_V \tag{4.16}$$

where X_{Sr} [-] is the rich solution mass concentration given in DACM No.2 by the initial mass concentration, X_{Sw} [-] is the weak solution mass concentration calculated with equation (2.4), which is dependant on the pressure and the generator weak solution outlet temperature. X_V [-] is the vapour concentration calculated with equation (3.23), which is dependant on the pressure and the weak solution or the rectified liquid concentration.

Therefore, for **DACM No.1**, the calculated solution mass flows for external generator inlet temperatures of 147°C to 172°C resulted in values of 20kg/h to 40kg/h with the weak solution and 25kg/h up to 46kg/h with the rich solution (Figure 4.25). The resulted values were valid for an external generator volume flow of 21l/min and an average total pressure of $20x10^5$Pa.

The comparison of the measured and the calculated mass flows of generator No.3 of DACM No.1 (Figure 4.20 and Figure 4.25 respectively) show that the calculated values correspond to those obtained from the measurements. Therefore, the calculation method is sufficient for accurately determining the mass flow rates. For example, the calculated lifted weak solution mass flow of approximately 37kg/h at an 165°C external generator inlet temperature, differs only about 4kg/h to 5kg/h from the measured value of 42.0kg/h. The measuring temperature flank method however, has not yet been perfected.

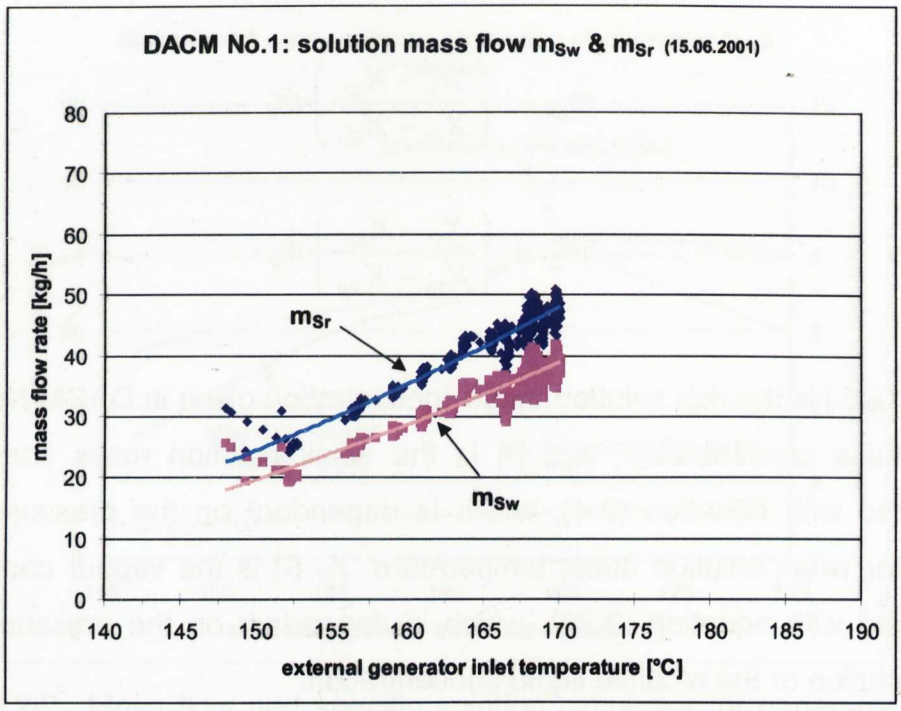

Figure 4.25: Evaluated weak and rich solution mass flow versus external generator inlet temperatures of DACM No.1 at an external generator volume flow of 21l/min.

For the operation of **DACM No.2**, lower external generator inlet temperatures of 115°C to 150°C were sufficient (Figure 4.26). For comparison, the external generator inlet temperatures of DACM No.1 ranged between 147°C and 172°C. Due to the measured temperature fluctuations, the evaluated mass flow values varied within a large range starting at heating inlet temperatures of 135°C. The calculated average mass flows were between 14kg/h and 38kg/h with the weak solution and between 17kg/h and 46kg/h with the rich solution (Figure 4.26).

In table 4.8, the average mass flows of DACM No.2 for the weak and rich solutions are presented for the used plate SHX and coaxial SHX, as well as the different ammonia initial concentrations.

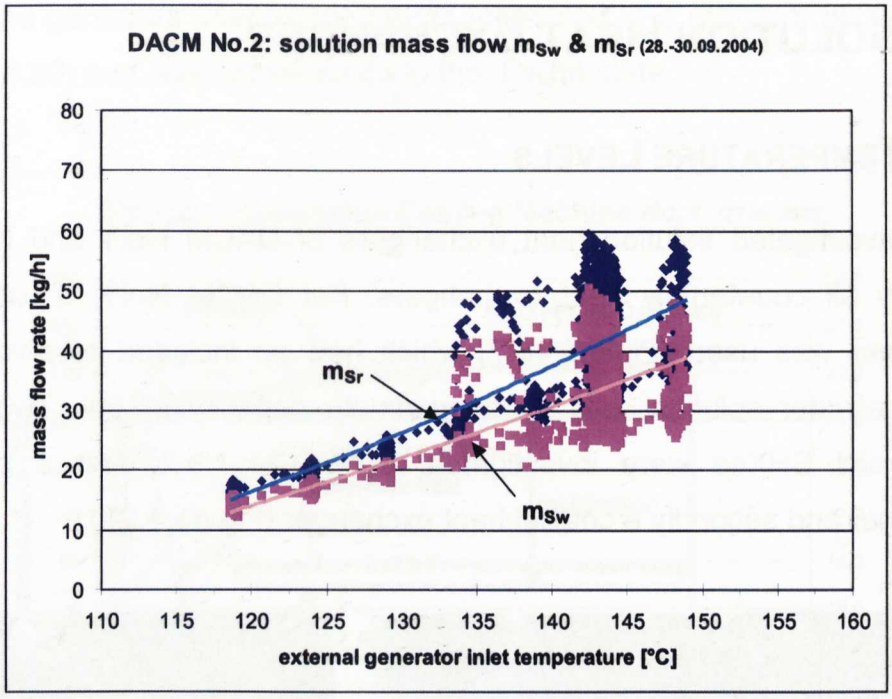

Figure 4.26: Evaluated weak and rich solution mass flow versus external generator inlet temperatures of DACM No.2 with an external generator volume flow of 25l/min.

Table 4.8: Evaluated average weak and rich mass flows of DACM No.2 at different external generator inlet temperatures and volume flows from 15l/min to 34l/min.

DACM No.2	plate SHX		coaxial SHX	
NH_3 initial concentration [-]	30%	40%	40%	37%
ext. generator temp $T_{H,in}$ [°C]	142-164	142-145	136-183	115-154
weak mass flow m_{Sw} [kg/h]	25-35	22-26	7-16	14-38
rich mass flow m_{Sr} [kg/h]	27-39	24-28	12-22	17-46

The design mass flow of the weak solution for a 2.5kW evaporator cooling capacity is 50kg/h, and the ammonia vapour mass flow is 8kg/h. The final set-up with the coaxial SHX and 37% ammonia initial concentration reached the optimal value of approximately 40kg/h, meaning that for the bubble pump, more lifting tubes and additional baffle plates were necessary. The mass flow curves could be approximately linearly interpolated within the measured temperature range.

4.5 SOLUTION HEAT EXCHANGER

4.5.1 TEMPERATURE LEVELS

The investigated solution heat exchangers of DACM No.1 and No.2 were basically all counterflow heat exchangers. For DACM No.1, a tubular heat exchanger was used (Figure 4.27) which had an included reservoir for the ammonia/water solution with an approximate capacity of 60l. Two different commercial SHXes were investigated for DACM No.2; first a plate heat exchanger and secondly a coaxial heat exchanger (Figure 4.27).

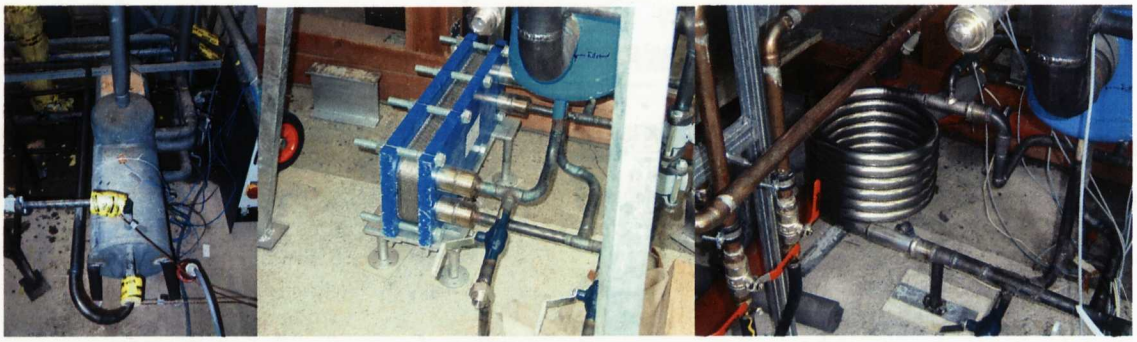

Figure 4.27: Pictures of the tubular SHX of DACM No.1, the plate and the coaxial SHX of DACM No.2 (from left to right).

The high volumetric capacity of the tubular SHX of **DACM No.1** led to a very long preheating phase of the whole heat exchanger and therefore to a sluggish heat exchange between the cold and rich solution from the absorber and the hot and weak solution from the generator. The preheating of the rich solution was insufficient, and therefore instead of a generator inlet temperature of 100°C, the maximum reached temperature was only 50°C to 60°C after two to three hours of operation (Figure 4.28).

Using the plate heat exchanger for **DACM No.2**, the measured generator inlet temperatures were only about 50°C and on the other hand, the entering weak ammonia/water solution temperature from the SHX into the absorber was too high. The weak solution inlet temperatures were about 70°C to 90°C instead of 40°C to 50°C. After replacing the SHX with a coaxial heat exchanger, the

measured generator inlet temperatures increased to a range of 80°C to 100°C (Figure 4.29) and now corresponds to the design state.

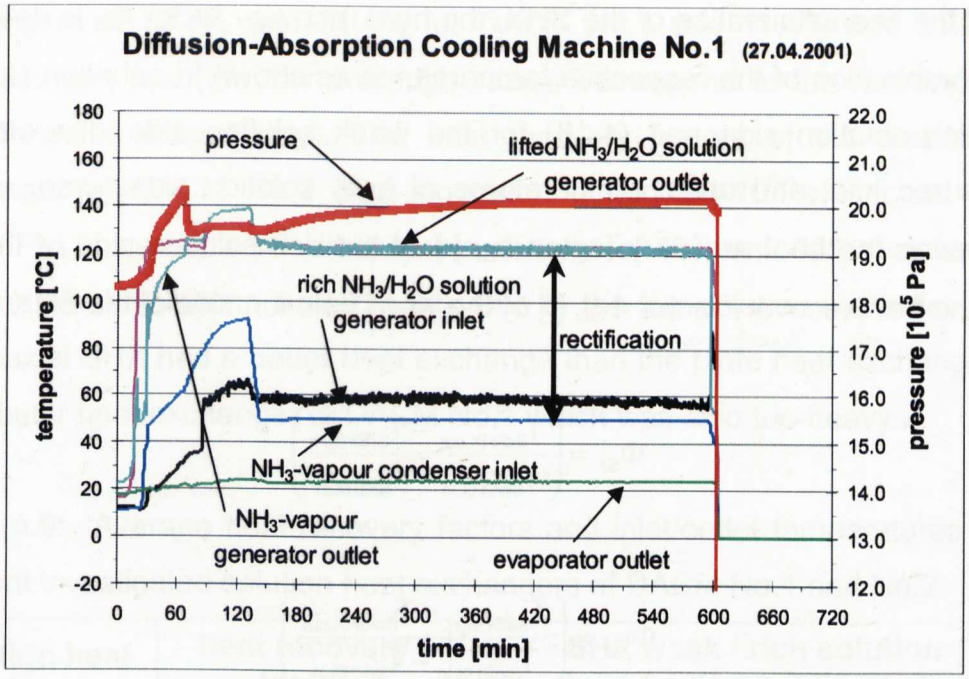

Figure 4.28: Measured pressure and internal temperature levels of DACM No.1 with tubular SHX (NH_3 initial concentration of 38%).

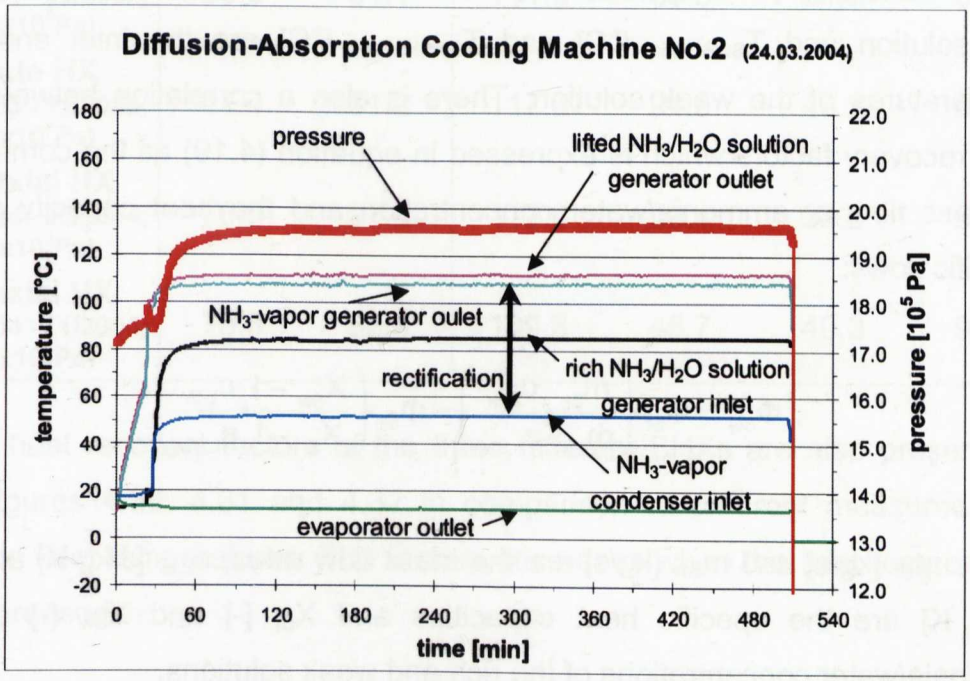

Figure 4.29: Measured pressure and internal temperature levels of DACM No.2 with coaxial SHX (NH_3 initial concentration of 40%).

4.5.2 HEAT RECOVERY FACTOR

For the characterisation of the SHX, the heat recovery factor Φ_S is defined by the combination of the respective temperatures as shown in equation (4.17) for the rich solution side and (4.18) for the weak solution side. Therefore the measured inlet and outlet temperatures of both solution sides were used to determine the heat recovery factor Φ_{Sr} [-] of the rich solution side of the SHX and the heat recovery factor Φ_{Sw} [-] of the weak solution side of the SHX.

$$\Phi_{Sr} = \left(\frac{T_{SrSHX,out} - T_{SrSHX,in}}{T_{SwSHX,in} - T_{SrSHX,in}} \right) \tag{4.17}$$

$$\Phi_{Sw} = \left(\frac{T_{SwSHX,in} - T_{SwSHX,out}}{T_{SwSHX,in} - T_{SrSHX,in}} \right) \tag{4.18}$$

where $T_{SrSHX,in}$ [°C] and $T_{SrSHX,out}$ [°C] are the inlet and outlet temperatures of the rich solution and $T_{SwSHX,in}$ [°C] and $T_{SwSHX,out}$ [°C] are the inlet and outlet temperatures of the weak solution. There is also a correlation between both heat recovery factors which is expressed in equation (4.19) as the combination of mass flow or ammonia/water concentration and the heat capacity of both specific flows:

$$\Phi_{Sw} = \Phi_{Sr} \bullet \left(\frac{\dot{m}_{Sr}}{\dot{m}_{Sw}} \bullet \frac{c_{L,Sr}}{c_{L,Sw}} \right) = \Phi_{Sr} \bullet \left(\frac{X_{Sw} - 1}{X_{Sr} - 1} \bullet \frac{c_{L,Sr}}{c_{L,Sw}} \right) \tag{4.19}$$

where m_{Sr} [kg/s] and m_{Sw} [kg/s] are the mass flow rates, $c_{L,Sr}$ [J/kg K] and $c_{L,Sw}$ [J/kg K] are the specific heat capacities and X_{Sr} [-] and X_{Sw} [-] are the ammonia/water concentrations of the rich and weak solutions.

For comparison, the heat recovery factors Φ_{Sr} and Φ_{Sw} and the weak/rich solution inlet/outlet temperatures of the three different investigated SHXs are presented in table 4.9. The heat recovery factors of the tubular and plate heat exchangers of 39.6% and 51.1% for DACM No.1 and 11.4% and 31.2% for No.2 are very low (the low and high values correspond to the rich and weak solution sides respectively). The heat recovery factors of the coaxial heat exchanger of DACM No.2 (first operation period $20x10^5$Pa, second period $12x10^5$Pa) however, were within a normal range of 76% and 92% (values of the rich and weak solutions respectively). Due to the low solution mass flow rates, the coaxial SHX had a better heat exchange than the plate heat exchanger and the tubular heat exchanger of DACM No.1 which was also too heavy.

Table 4.9: Average heat recovery factors and inlet/outlet temperatures of the different investigated solution heat exchangers of DACM No.1 and No.2.

solution heat exchanger (operation period; total pressure)	heat recovery factor		SHX weak / rich solution inlet / outlet temperature			
	Φ_{Sr} [%]	Φ_{Sw} [%]	$T_{SwSHX,In}$ [°C]	$T_{SwSHX,out}$ [°C]	$T_{SrSHX,In}$ [°C]	$T_{SrSHX,out}$ [°C]
tubular HX (02/2001 - 03/2002; $20x10^5$Pa)	39.6	51.1	111.2	65.8	21.2	57.3
plate HX (09/2003 - 11/2003; $18x10^5$Pa)	11.4	31.2	117.6	94.3	43.2	51.7
coaxial HX (03/2004 - 06/2004; $20x10^5$Pa)	76.9	91.5	112.6	39.4	33.0	94.0
coaxial HX (09/2004 - 11/2004; $12x10^5$Pa)	75.8	92.3	109.8	45.7	40.3	93.0

The heat recovery factors of the three different SHXs are also presented in the Figures 4.30, 4.31 and 4.32 in comparison to different measured weak solution inlet temperatures. The factors decreases when the inlet temperatures are increased.

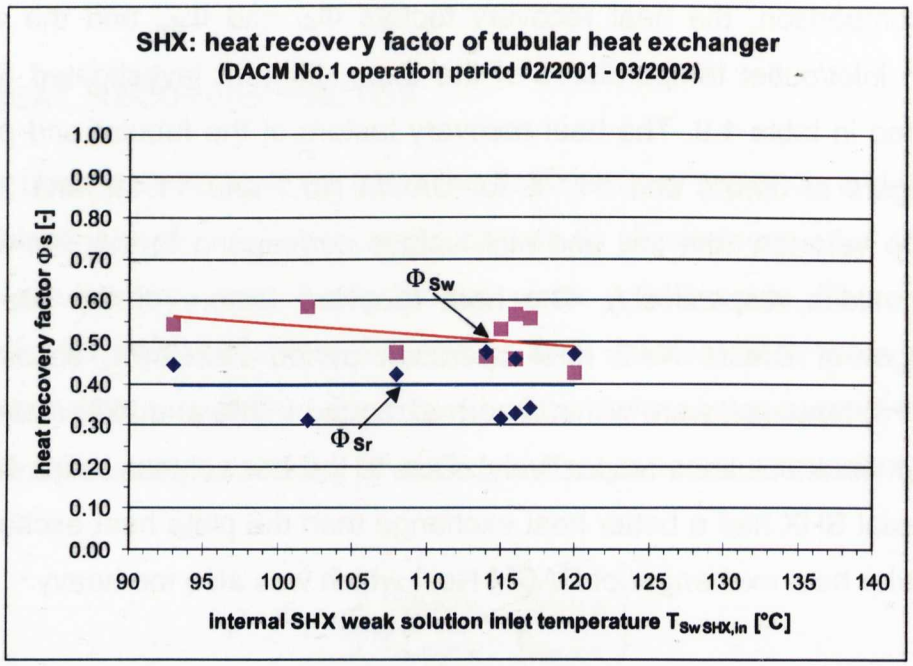

Figure 4.30: Heat recovery factors of the tubular SHX of DACM No.1 (total pressure level of 20×10^5Pa).

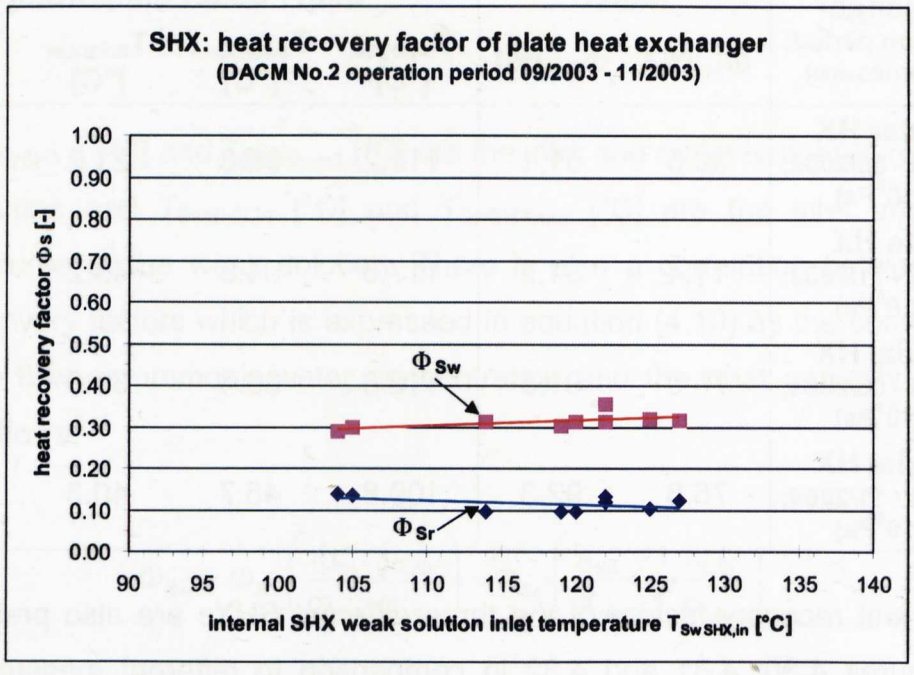

Figure 4.31: Heat recovery factors of the plate SHX of DACM No.2 (total pressure level of 18×10^5Pa).

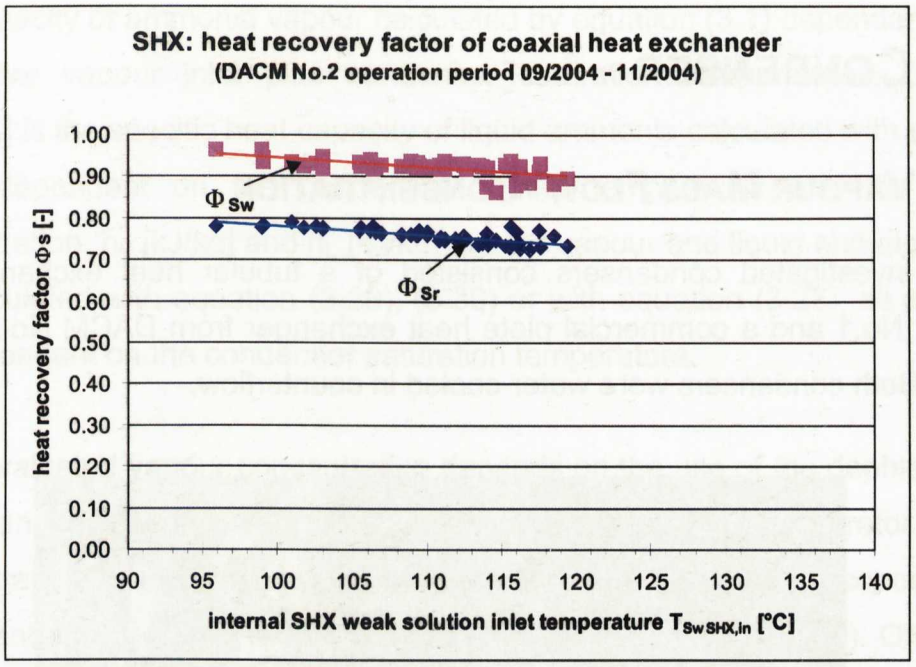

Figure 4.32: Heat recovery factors of the coaxial SHX of DACM No.2 (total pressure level of 12×10^5Pa).

4.6 CONDENSER

4.6.1 VAPOUR MASS FLOW / CONCENTRATION

The investigated condensers consisted of a tubular heat exchanger from DACM No.1 and a commercial plate heat exchanger from DACM No.2 (Figure 4.33). Both condensers were water-cooled in counterflow.

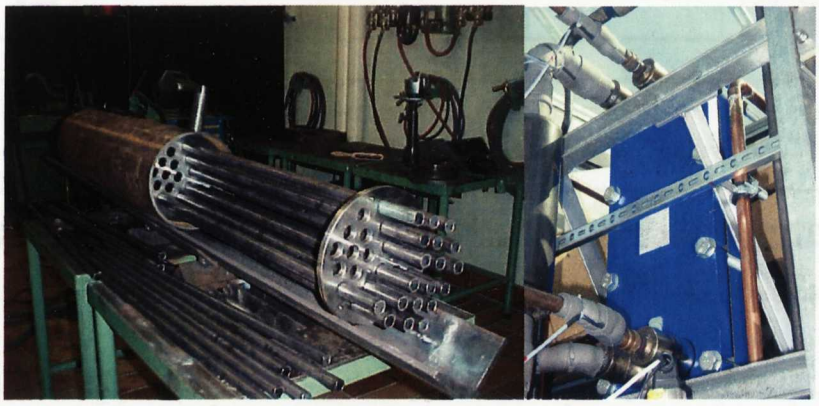

Figure 4.33: Pictures of the tubular HX and plate HX condenser of DACMs No.1 and No.2 (from left to right).

The calculation of the condensed ammonia liquid mass flow m_L [kg/s] is defined by equation (4.20) as the ratio of measured condenser cooling capacity to the capacity of the superheated vapour, the vapour and liquid enthalpies and the capacity of the sub-cooled liquid.

$$\dot{m}_L = \frac{Q_C}{c_{V,NH3} \bullet \left(T_{VC} - T_{C,s}\right) + h_V - h_L + c_{L,NH3/H2O} \bullet \left(T_{C,s} - T_{LC}\right)} \tag{4.20}$$

In this equation, the condenser capacity Q_C [kW] is calculated with equation (4.3), whereas T_{VC} [°C] and T_{LC} [°C] are the measured condenser vapour inlet and condensate outlet temperatures. $T_{C,s}$ [°C] is the condenser saturation temperature calculated with equation (3.20) which is dependant on measured pressure and evaluated vapour concentration. $c_{V,NH3}$ [kJ/kg K] is the specific

heat capacity of ammonia vapour calculated by equation (3.1) dependant on the condenser vapour inlet plus condenser saturation temperatures. $c_{L,NH3/H2O}$ [kJ/kg K] is the specific heat capacity of liquid ammonia calculated with equation (3.11) dependant on the condensate outlet temperature and the vapour concentration. h_V [kJ/kg] and h_L [kJ/kg] are the vapour and liquid enthalpies, and are calculated with equation (3.29), (3.30) or with equation (3.27), all of which, are dependant on the condenser saturation temperature.

The evaluated vapour concentration depends on the use of the dephlegmator. If the ammonia/water vapour is not rectified, then the generator vapour concentration X_{V1} [-] becomes dependant on the weak solution concentration X_{Sw} [-] and the resulting functional relationships are given in (4.21). Otherwise, the rectified vapour concentration X_V [-] is dependant on the rectified liquid ammonia/water concentration $X_{L,deph}$ [-] and the resulting functional relationships are given in (4.22).

$$X_{Sw} = f(T_{SwG}, p);\ X_{V1} = f(X_{Sw}, p);\ \ T_{C,s} = f(X_{V1}, p) \tag{4.21}$$

$$X_{L,deph} = f(T_{VC}, p);\ X_V = f(X_{L,deph}, p);\ \ T_{C,s} = f(X_V, p) \tag{4.22}$$

T_{SwG} [°C] is the generator weak solution outlet temperature, T_{VC} [°C] is the measured condenser vapour inlet temperature or dephlegmator vapour outlet temperature and p [Pa] is the total pressure.

The amount of ammonia liquid mass flow $m_{L,NH3}$ [kg/s] is defined by equation (4.23) as follows:

$$\dot{m}_{L,NH3} = \dot{m}_L \bullet X_V \tag{4.23}$$

where m_L [kg/h] is the total ammonia/water liquid mass flow and X_V [-] is the vapour concentration.

In the starting phase of the DACM, helium that is normally pushed into the evaporator by ammonia vapour coming from the generator is always in the condenser. In **DACM No.1**, helium remained partly in the condenser, so that the maximum heat transfer surface was not available, causing a reduction of the condenser capacity. Due to this reduction, higher generator temperatures and thus a higher condenser pressure were necessary to condense the entering ammonia vapour.

The ammonia liquid mass flows $m_{L,NH3}$ determined from all of the measurements was between 4kg/h and 8kg/h (Figure 4.34). The designed and required ammonia mass flow is approximately 5kg/h to 8kg/h for a 2.5kW evaporator cooling capacity. The evaluated values should have been sufficient, but with the first pilot plant, a saturation of the evaporator by ammonia occurred and therefore the auxiliary gas circulation came partly to a standstill. Consequently, no evaporator cooling capacity could be generated.

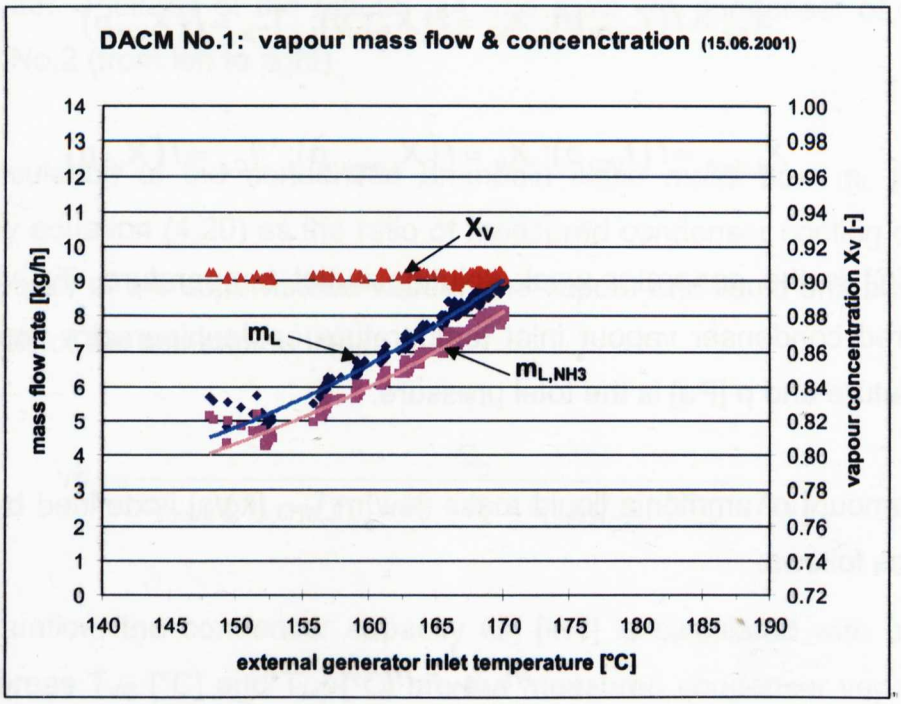

Figure 4.34: Evaluated vapour mass flows and concentration versus external generator inlet temperatures of DACM No.1 with an external generator volume flow of 21l/min.

The investigated condenser of **DACM No.2** worked without problems due to the selected design of a plate heat exchanger. The evaluated ammonia mass flow $m_{L,NH3}$ of the first measurements ranged between 1kg/h and 3kg/h with a 30% initial ammonia mass concentration of the whole ammonia-water solution. After refilling the second pilot plant with a 40% initial ammonia mass concentration, the ammonia mass flow increased to 2kg/h to 4kg/h.

After the modification of the SHX through a coaxial HX, the resulted ammonia liquid mass flow reached higher values of 4kg/h to 6kg/h with an initial ammonia mass concentration of 40% (Figure 4.35). Further measurements with an initial ammonia concentration of 37% led to ammonia condensate mass flows of 2.5kg/h to 8.5kg/h depending on the external generator inlet temperature and the volume flow (Figure 4.36). Therefore, the design values were obtained with the last set-up of the second pilot plant.

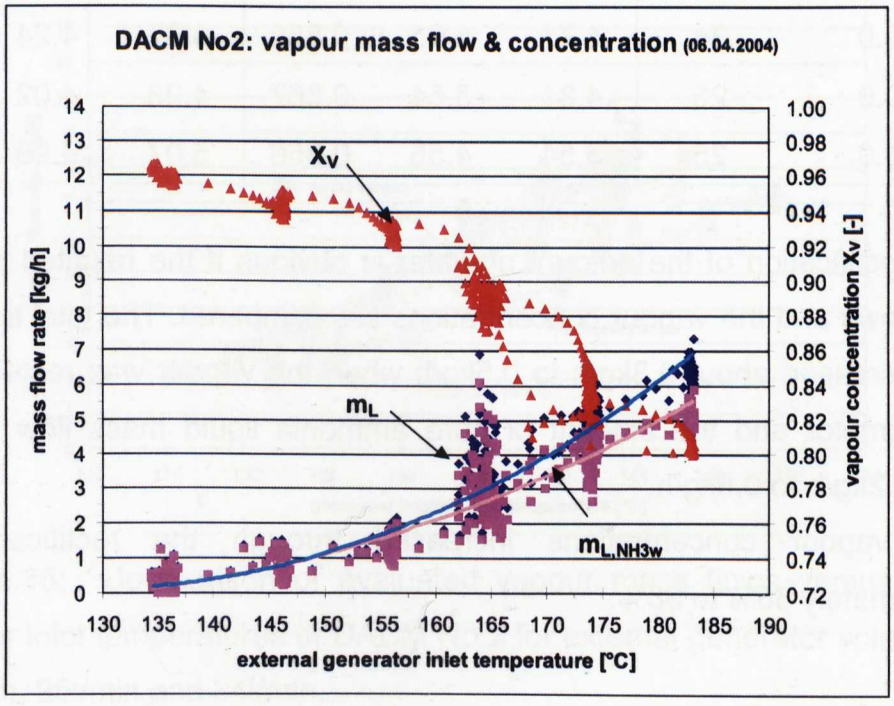

Figure 4.35: Evaluated vapour mass flows and concentration versus external generator inlet temperatures of DACM No.2 with an external generator volume flow of 20l/min.

4.6.2 MASS FLOW WITHOUT / WITH RECTIFICATION

Table 4.10 presents the total vapour/liquid m_L and the ammonia mass flow $m_{L,NH3}$ as well as the ammonia vapour concentration of DACM No.2 for an ammonia initial concentration of 37% with and without rectification of the vapour through the dephlegmator. Without dephlegmator, the condenser vapour inlet temperatures T_{VC} were 70°C to 120°C and with dephlegmator, 55°C to 70°C.

Table 4.10: Evaluated ammonia liquid mass flows and vapour concentrations of DACM No.2 with and without vapour rectification through the dephlegmator.

generator		without dephlegmator			with dephlegmator		
heating inlet temperature $T_{H,in}$ [°C]	ext. volume flow [l/min]	m_L [kg/h]	$m_{L,NH3}$ [kg/h]	X_{V1} [-]	m_L [kg/h]	$m_{L,NH3}$ [kg/h]	X_V [-]
129.0	34	4.71	4.05	0.858	4.37	4.24	0.972
129.0	25	4.34	3.54	0.867	4.05	4.02	0.994
134.0	25	5.54	4.55	0.856	5.07	4.98	0.983

The rectification of the amount of water is obvious if the resulted total liquid mass flows and the vapour concentrations are compared. The total liquid mass flow decreased about 0.3kg/h to 0.5kg/h when the vapour was rectified by the dephlegmator and the amount of pure ammonia liquid mass flow increased about 0.2kg/h to 0.5kg/h.

The vapour concentrations increased through the rectification from approximately 86% to 98%.

4.6.3 VARIED EXTERNAL GENERATOR VOLUME FLOWS

Figure 4.36 shows a comparison of three mass flow curves for different external generator volume flows $V_{H,ext}$. For a generator volume flow of 15l/min and heating inlet temperatures between 122°C and 155°C, total liquid mass flows of 1.9kg/h to 7.2kg/h were obtained. The total liquid mass flow increased when the external generator volume flows were increased. For 25l/min and heating inlet temperatures between 118°C and 148°C, mass flows of 2.2kg/h to 7.9kg/h were obtained. For 34l/min and heating inlet temperatures of 115°C to 145°C, total mass flows of 2.1kg/h up to 8.5 kg/h were obtained.

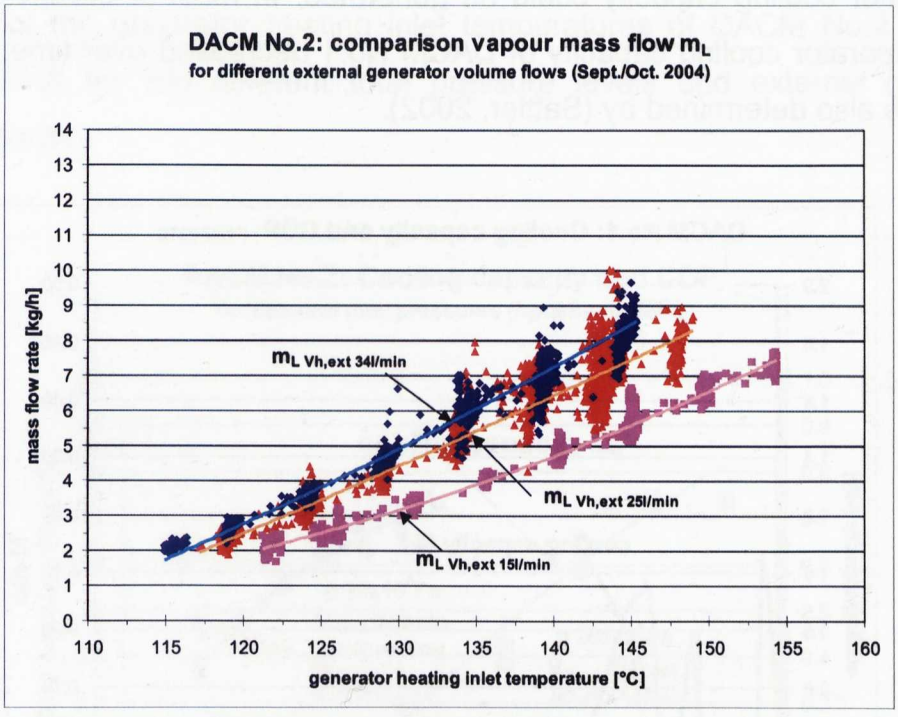

Figure 4.36: Comparison of evaluated vapour mass flows versus external generator inlet temperatures of DACM No.2 for external generator volume flows of 15l/min, 25l/min and 34l/min.

4.7 EVAPORATOR

4.7.1 COOLING CAPACITY AND COP

Most of the operating experiences gained by testing **DACM No.1** showed that instabilities existed in the auxiliary gas circuit which led to high fluctuations of the generated evaporator cooling capacity or COP (Figure 4.37). The low cooling capacity that was achieved, was due to the insufficient constructively available evaporation surface that was used and to the fact that the saturation of the falling film evaporator by ammonia and thereby the auxiliary gas circulation came partly to a standstill (Päßler, 2002). Consequently, no further evaporator cooling capacity could be generated. In most of the investigations the evaporator cooling capacity of DACM No.1 decreased over time, an effect that was also determined by (Sattler, 2002).

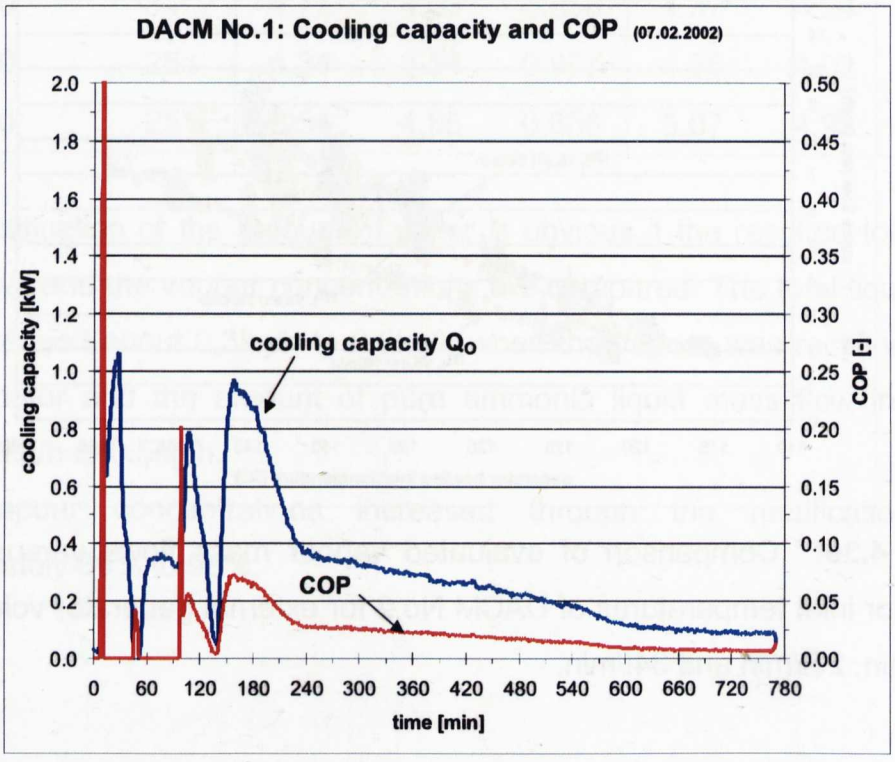

Figure 4.37: Measured decreasing evaporator cooling capacity and COP of DACM No.1.

DACM No.2 reached a maximum average evaporator cooling capacity of 1.5kW but the evaluated ammonia mass flow rates $m_{L,NH3}$ were good enough for higher cooling capacities. The falling film evaporator could not evaporate all of the available liquid ammonia into the helium gas atmosphere, not even with high external evaporator inlet temperatures of around 25°C. Therefore, the falling film evaporator needs to be rebuilt with either more or longer evaporation tubes so that a larger heat transfer surface exists, which would lead to a smaller film thickness and therefore, a longer delay time. For comparison, some calculated results for the delay time and the film thickness of the used falling film evaporator are given in the chapter 3.6.8.

Figure 4.38 shows the measured average cooling capacities and COP as a function of the generator heating inlet temperatures of DACM No.2 with the coaxial SHX for two different total pressure levels and external generator volume flows.

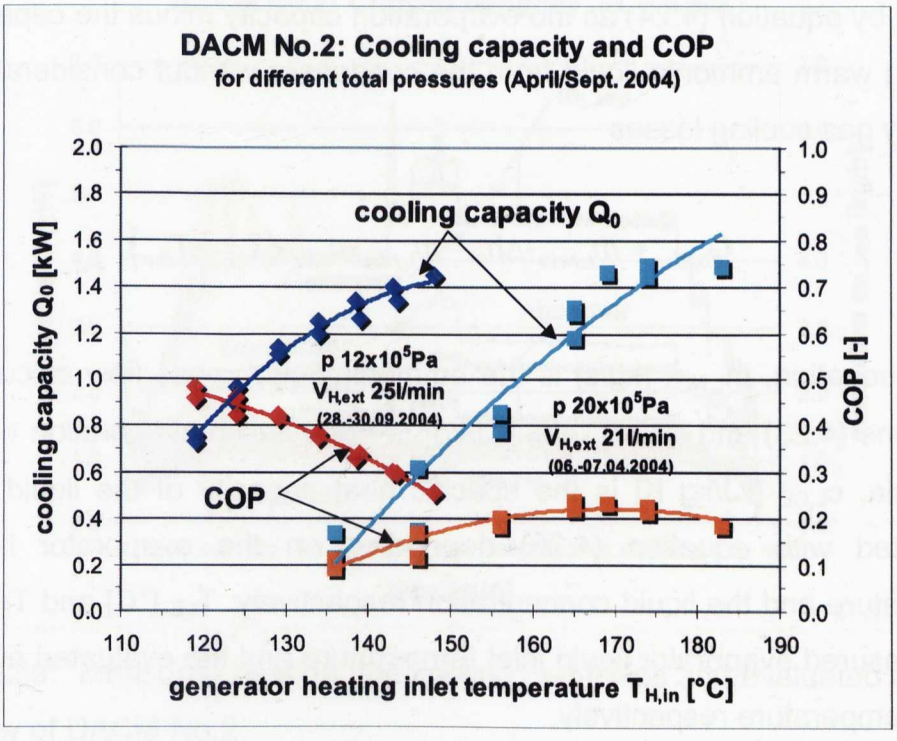

Figure 4.38: Comparison of measured evaporator cooling capacity and COP versus external generator inlet temperatures of DACM No.2 for total pressures of $12x10^5$Pa and $20x10^5$Pa.

The lower total pressure led to lower generator heating capacities for approximately the same obtained evaporator cooling capacities. As a result, the COP range increased from 0.10 to 0.25 to a range of 0.25 up to 0.45 for the lower pressure level. Furthermore, the external generator heating inlet temperature for the operation of DACM No.2 decreased from a range of 135°C to 185°C to values of 115°C to 155°C.

4.7.2 THEORETICAL POSSIBLE COOLING CAPACITY

Another analysis was done for the theoretical possible evaporator cooling capacity of **DACM No.2** using the coaxial SHX, which could be obtained by the available evaluated ammonia condensate mass flow. The resulting values are compared to the measured evaporator cooling capacities.

The measured cooling capacity $Q_{O,meas}$ [kW] is calculated with equation (4.4). The approach for the simplified theoretical cooling capacity $Q_{O,theo}$ [kW] is defined by equation (4.24) as the evaporation capacity minus the capacity of the entering warm ammonia liquid from the condenser without consideration of the auxiliary gas cooling losses

$$Q_{0,theo} = \dot{m}_{L,NH3} \bullet \Delta h_E - \dot{m}_{L,NH3} \bullet c_{L,CE} \bullet \left(T_{LE} - T_{E,e}\right) \qquad (4.24)$$

In this equation, $m_{L,NH3}$ [kg/s] is the ammonia liquid mass flow calculated with equations (4.23) and (4.20), Δh_E [kJ/kg] is the specific evaporation enthalpy of ammonia, $c_{L,CE}$ [kJ/kg K] is the specific heat capacity of the liquid ammonia calculated with equation (4.26) depending on the evaporator liquid inlet temperature and the liquid concentration respectively. T_{LE} [°C] and $T_{E,e}$ [°C] are the measured evaporator liquid inlet temperature and the evaluated evaporation mean temperature respectively.

The specific evaporation enthalpy of ammonia Δh_E [kJ/kg] and the specific heat capacity of liquid ammonia $c_{L,CE}$ [kJ/kg K] are defined by (Hirschberg, 1988) in equation (4.25) and (4.26) as follows:

$$\Delta h_E = 138.35 \cdot \sqrt{132.35 - T_{E,e}} - 2.486 \cdot (132.35 - T_{E,e}) \tag{4.25}$$

$$c_{L,CE} = \begin{pmatrix} 4.1785 + 0.0314 \cdot 10^{-3} \cdot (T_{LE} - 35)^2 \cdot (1 - X_L) \\ + X_L \cdot 10^{-3} \cdot \left(4200 + \left(410 + 6.2 \cdot T_{LE} + 0.044 \cdot T_{LE}^{\,2}\right) \cdot X_L\right) \end{pmatrix} \tag{4.26}$$

where $T_{E,e}$ [°C] is the evaporation mean temperature given by the measured external evaporator outlet temperature $T_{O,out}$ [°C] minus approximately five Kelvin for the lower internal mean evaporator temperature. X_L [-] is the liquid ammonia mass concentration which is equivalent to the vapour concentration.

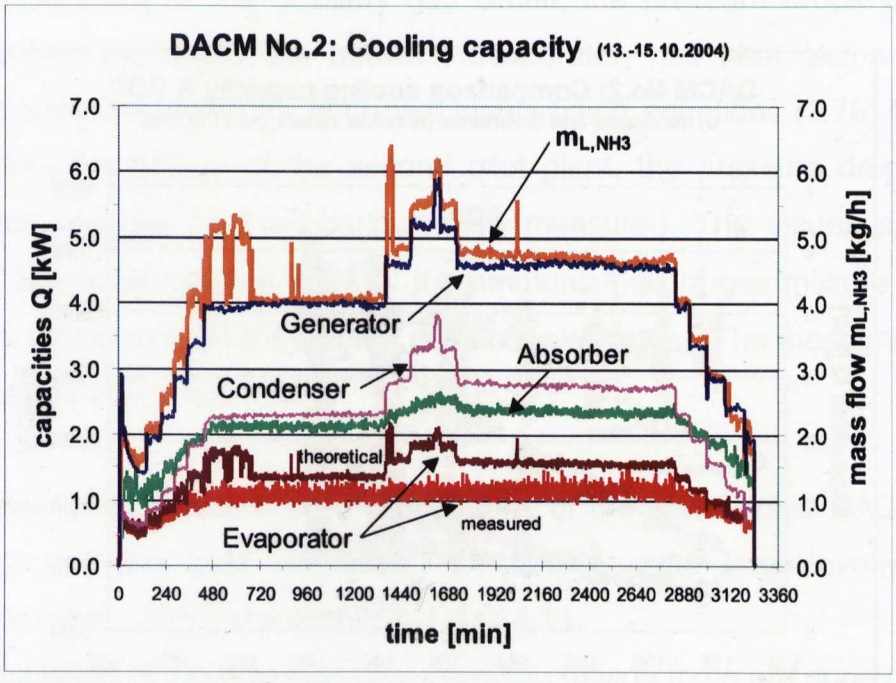

Figure 4.39: Measured heating and cooling capacities and evaluated ammonia mass flow of DACM No.2.

The Figure 4.39 shows that for a long-term measurement, the condenser cooling capacity simultaneously increased with the generator heating capacity

but that the evaporator cooling capacity did not increase and even came to a standstill at 1.5kW. For an available ammonia mass flow larger than approximately 4kg/h, the falling film evaporator was not able to convert the ammonia into the possible cooling capacity.

A comparison of the resulting theoretically possible and the measured cooling capacity of the existing falling film evaporator shows that a cooling capacity of 2.0kW could be reached by the available liquid ammonia. Due to the unused total amount of liquid ammonia, the obtained evaporator cooling capacity was 0.1kW to 0.8kW lower then the theoretically possible one.

Figure 4.40 presents the evaluated measured and theoretical evaporator cooling capacities as well as the measured COP_{meas} [-] and theoretical possible COP_{theo} [-] values versus different generator heating inlet temperatures from 115°C to 145°C. The measured generator heating capacity $Q_{H,meas}$ [kW] is also given in the Figure 4.40 to allow a better interpretation of the evaluated results.

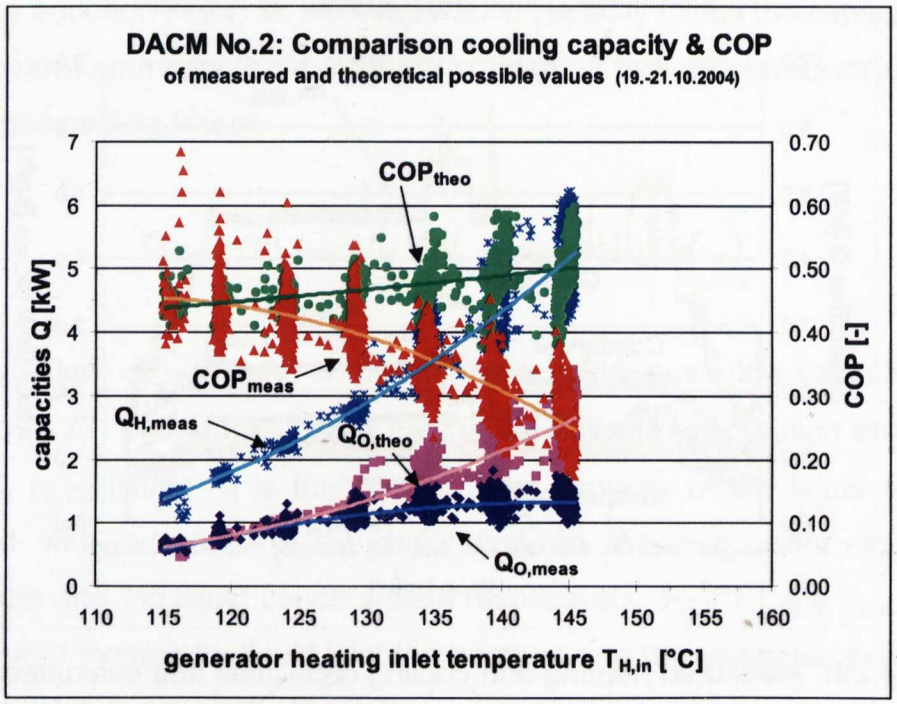

Figure 4.40: Comparison of measured and evaluated theoretical possible evaporator cooling capacity and COP of DACM No.2 versus external generator heating inlet temperatures.

The evaluated theoretical possible evaporator cooling capacity ranges from 0.6kW to 2.7kW as opposed to the measured cooling capacity, which ranges from 0.6kW to 1.4kW. Therefore, with a generator heating inlet temperature of 145°C, the evaporator cooling capacity could be 1.3kW higher than the measured one. The measured cooling capacity stagnate at about 1.5kW.

The corresponding measured COPs decreased from 0.45 to 0.25 because of the increasing measured generator heating capacity which ranged from 1.4kW to 5.4kW depending on the external heating inlet temperature. The theoretical possible COPs again increased from 0.44 to 0.50.

4.8 AUXILIARY GAS CIRCUIT – PRESSURE DROP

In order to study of the auxiliary gas circuit, the pressure drops within the thermosyphon cyclic process between evaporator, gas heat exchanger and absorber were calculated for both pilot plants using equations (3.79) to (3.91). Also, before the set up of the second pilot plant, the pressure drops of the evaporator and gas heat exchanger were measured. The values calculated were for very small volume flows of the ammonia/helium gas mixture ($\leq 4 m^3/h$) at 1.28Pa for the evaporator and the gas heat exchanger. The measured values were between 0.5Pa and 1.4Pa.

The determined pressure drop distributions of the constructed DACMs No.1 and No.2 and the best distribution for DACMs with large overall height (Bäckström et al., 1965) are shown in Table 4.11.

The calculation of the pressure drops and the driving force are done under the assumptions that the total pressure is 18.5×10^5Pa, the evaporator partial pressure is 5×10^5Pa at +5°C as well as 4.8×10^5Pa for the incomplete saturation, the absorber weak solution partial pressure is 2.6×10^5Pa at 50°C and 0.32 weak solution concentration as well as 2.8×10^5Pa because of the incomplete

washout, the evaporator weak gas mixture inlet temperature is 15°C and the weak gas mixture volume flow is approximately 4m³/h.

Table 4.11: Pressure drop distribution of the auxiliary gas circuit components of DACMs No.1 and No.2.

pressure drop distribution	evaporator [%]	gas heat exchanger [%]	absorber [%]
DACM with large overall height (Bäckström *et al.*, 1965)	10	60	30
pilot plant DACM No.1	14	49	37
pilot plant DACM No.2	18	54	28

The total pressure drop in the auxiliary gas circulation of **DACM No.1** was only 0.96Pa and due to the level difference of 1.5m between evaporator and absorber a driving force of 16.85Pa was available.

The pressure drop inside **DACM No.2** is 2.37Pa and the driving force is 5.62Pa at a level difference of 0.5m between evaporator and absorber.

In both cases the driving force is enough to compensate for the pressure drops and to maintain the thermosyphon circulation.

CHAPTER 05

MODELLING AND SIMULATION

5.1 LITERATURE REVIEW

5.1.1 DIFFUSION-ABSORPTION REFRIGERATOR

There exists very little data about completely modelled DAR systems. An early computer model that simulates the Diffusion-Absorption cycle of a refrigerator (DAR) was developed by (Chen, 1995). The model includes the coupling between the horizontal auxiliary gas heat exchanger, the horizontal absorber and the horizontal evaporator and further simple component models for the condenser, rectifier, SHX and generator based on mass and energy balances. For the cycle, the working fluid ammonia/water and the auxiliary gas hydrogen and helium were used. Furthermore, the model was used for the application of hotel air-conditioning with a 1.5kW evaporator cooling capacity and helium as auxiliary gas for fire safety reasons (Kim *et al.*, 1995). A basic design of the gas driven Diffusion-Absorption air conditioner obtains a COP of approximately 0.4.

A further model for the DAR as a simple mathematical model was developed by (Srikhirin *et al.*, 2002) in order to analyse the performance of a refrigerator with the working fluid ammonia/water and helium. For the modelled bubble-pump performance a correlation was presented which was obtained from a simple experiment using air and water. Furthermore, a combined evaporator-absorber effectiveness index was set up which represents the ratio of the evaporated ammonia mass rate to the total amount of ammonia available in the evaporator. The results of the calculation showed that the evaporator and

absorber mass transfer performance have a strong effect on the system performance (COP) which was found to be between 0.09 and 0.15.

Based on the mass, material and energy balances for each component of a DAR system with the three working fluids ammonia, water and hydrogen, a mathematical model was developed to analyse the performance and parameters (Al-Shemmeri *et al.*, 2003). The simulation results showed that the effectiveness of the gas heat exchanger has the largest effect on the COP. An index called the evaporating mass rate of ammonia was also presented, which specifies the evaporating capability of the evaporator.

A thermodynamic model based on mass and energy conservation equations was developed by (Zohar *et al.*, 2005) for an ammonia/water DAR cycle with hydrogen or helium as auxiliary gas. The best performance was obtained for a rich solution concentration ranging between 0.2 and 0.3. The recommended weak solution concentration was 0.1. It was also discovered that as the degree of rectification decreased, the COP decreased as well. The final outcome of the study showed that helium was superior to hydrogen as the COP with helium was up to 40% higher than the cycle working with hydrogen.

5.1.2 DIFFUSION-ABSORPTION HEAT PUMP

A few modified thermodynamic and transport property models were developed for a DAHP by (Wang, 1992) for ammonia/water with both hydrogen and helium as the pressure equalizing gas. Simple thermodynamic models for each component were set up for the DAHP process. A detailed fluid and heat transfer model was additionally set up solely for the auxiliary gas heat exchanger (AGHX). The auxiliary gas charge pressure as well as the effectiveness of the AGHX were found to have a significant influence on the COP.

Further work on the performance modelling of the DAHP with the working fluid ammonia/water and helium was done by (Shi, 1994). The absorber, evaporator and AGHX models were developed individually using the heat and mass transfer theory. The integrated model was coupled with simple models of the remaining components. Parametric studies were carried out in order to predict the performance of the absorber and the evaporator. It was found that the COP increases if the absorber or evaporator tube length increases or if the ambient temperature increases in combination with varied evaporator air temperatures otherwise with an increase of the inlet liquid mass fraction ammonia to the absorber when the mass fraction is less then around 20%. On the other hand, the COP decreases slightly when the height between absorber and the evaporator is increased, but the auxiliary gas mass flow increases. The COP also decreases if the system pressure and the generator heat input increases. The COP remains constant until the liquid ammonia is not totally evaporated inside the evaporator due to the hardware limits and then it decreases. The simulation runs performed in the study resulted in a COP cooling range of 0.12 to 0.19.

All of these presented models use the internal component temperatures for the investigation instead of external temperatures and the respective heat transfer coefficients. Furthermore, the models do not use a bubble pump correlation that includes the solution mass flow dependant on the generator heating temperatures and the external mass flow.

5.2 BASICS OF DACM MODEL

5.2.1 CHARACTERISTIC EQUATION

To simplify the performance calculations of an ACM, characteristic equations have been developed by (Ziegler, 1998a), which are an exact solution of the internal energy balances for only one given design point. These equations are used in a simple linear equation for different boundary conditions. The set up of the data reduction model for the water/lithium bromide ACM is shown in Figure 5.1, where the presented numbers indicate each stage of the process.

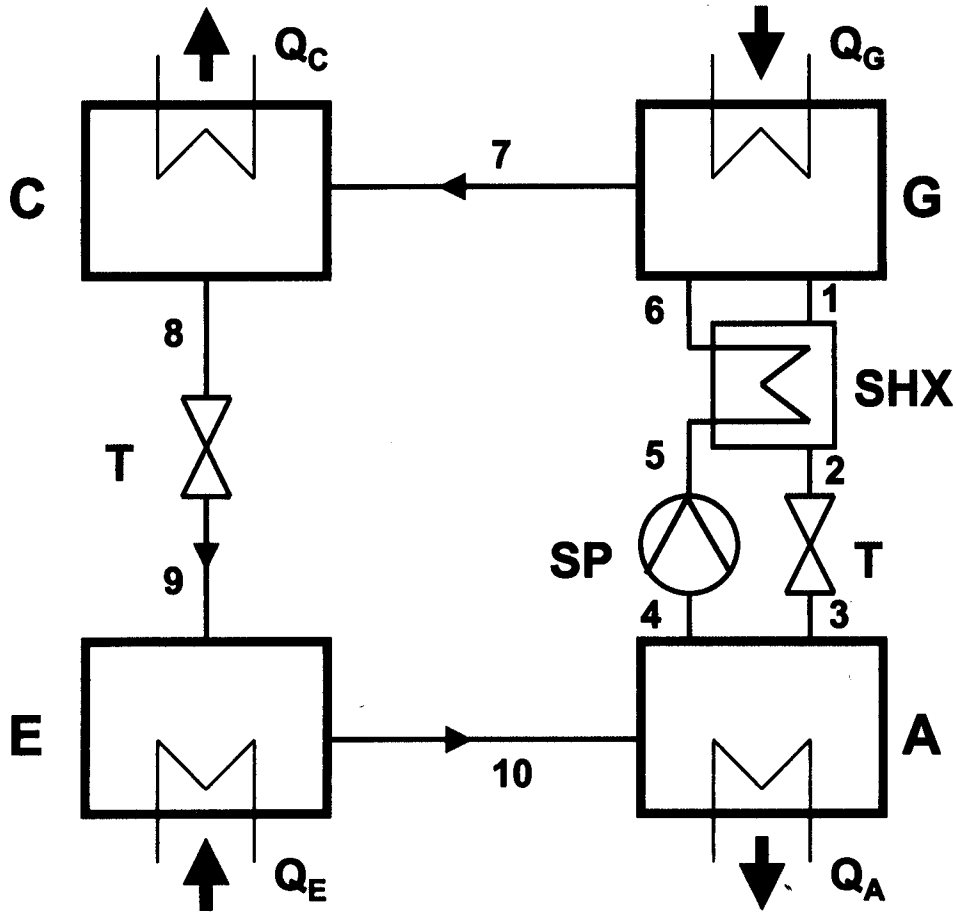

Figure 5.1: Water/lithium bromide ACM data reduction model.

A detailed derivation of the characteristic equation with its coefficients is described in (Schweigler *et al.*, 1999; Hellmann *et al.*, 1999). For larger

deviations from design conditions or for absorption chillers with thermally driven bubble pumps, one single equation does not represent the chiller performance accurately (Albers, 2002; Albers *et al.*, 2003).

The characteristic equation (5.1) for the evaporator cooling capacity Q_E [kW] of the ACM is a simple function of a slope and the characteristic double temperature difference, where the enthalpy and heat transfer coefficients are transformed into s_E and $\Delta\Delta t_{min,E}$.

$$\dot{Q}_E = s_E \bullet \left(\Delta\Delta t - \Delta\Delta t_{min,E}\right) \tag{5.1}$$

The slope s_E [kW/K] contains the enthalpy differences between the inlet and outlet of each component and the heat transfer coefficient UA_X [kW/K] between the external and internal circuits (X = generator G, condenser C, absorber A, evaporator E).

$$s_E = \left(\left(\frac{C_E}{UA_C} + \frac{1}{UA_E}\right) \bullet B + \left(\frac{G_E}{UA_G} + \frac{A_E}{UA_A}\right)\right)^{-1} \tag{5.2}$$

The coefficients C_E [-], G_E [-] and A_E [-] in equation (5.2) stand for the internal specific enthalpy differences of the corresponding heat exchangers in relation to the specific enthalpy difference of the evaporator. These coefficients are derived from simple enthalpy balances published by (Schweigler *et al.*, 1999; Hellmann *et al.*, 1999).

The constant B [-] is the ratio of the slope of the isosteres of the pure refrigerant to the solution which is determined by Dühring's rule for the solution field where the internal temperatures T_X [°C] of the heat exchangers generator, condenser, absorber and evaporator can be combined.

$$B = \frac{(T_G - T_A)}{(T_C - T_E)} \tag{5.3}$$

For single-effect water/lithium bromide ACMs the Dühring factor ranges between 1.1 and 1.2 for normal operation conditions (Albers *et al.*, 2003; Kohlenbach *et al.*, 2004a). For a single-effect ACM or DACM with the working pair ammonia/water, the Dühring factor is determined by the author to be between 1.6 and 2.4, and is dependant on the solution field and the wide possible internal evaporator temperature range of -20°C to +20°C.

The characteristic equation (5.1) is based on a characteristic double temperature difference $\Delta\Delta t$ [K] between the mean external generator and absorber temperatures t_g [°C] and t_a [°C] on the one hand and the external condenser and evaporator temperatures t_c [°C] and t_e [°C] on the other, which is given in equation (5.4) as follows:

$$\Delta\Delta t = t_g - t_a - (t_c - t_e) \cdot B \tag{5.4}$$

where B [-] is the Dühring factor determined by equation (5.3).

The intersection $\Delta\Delta t_{min,E}$ [K] is determined with the efficiency of the SHX and thereby with the dissipated energy which results from the solution circulation between the absorber Q_{Ax} [kW] and the generator Q_{Gx} [kW].

$$\Delta\Delta t_{min,E} = \left(\frac{\dot{Q}_{Ax}}{UA_A} + \frac{\dot{Q}_{Gx}}{UA_G} \right) \tag{5.5}$$

A necessary requirement for the utilisation of the characteristic equation method is the fulfilment of the linear assumptions for the ACM which has to be simulated. This means that all enthalpy coefficients, heat transfer coefficients and unavoidable heat losses are constant and independent of $\Delta\Delta t$. Ziegler (Ziegler, 1998a) have shown that under steady state conditions and constant solution mass flow rates, the assumption of constant parameters can be allowed in most cases. One example of the characteristic equation for a hot-

water driven 10kW H_2O/LiBr Phönix ACM with mechanical solution pump is given by (Kühn *et al.*, 2004) as follows:

$$\dot{Q}_E = 0.41[kW/K] \cdot \Delta\Delta t \tag{5.6}$$

Another one is given for a hot-water driven 35kW H_2O/LiBr Yazaki WFC-10 ACM with a thermally driven solution pump by (Albers *et al.*, 2003).

$$\dot{Q}_E = 1.4[kW/K] \cdot (\Delta\Delta t - 9.1[K]) \tag{5.7}$$

With the characteristic temperature difference $\Delta\Delta t$, is it easy to determine how to compensate for the change of one external temperature by controlling the other external temperatures. The load behaviour of the ACM could be also determined when changing the characteristic temperature difference. For a given cold water temperature, the cooling capacity and the COP mainly depend on the generator heating and the cooling water temperatures for the absorption and condensation processes.

5.2.2 EXPANDED DACM MODEL

Several problems are associated with a steady-state, single characteristic equation that calculates all internal enthalpies only for the design conditions. If a thermally driven bubble pump is used as in a DACM, the rich solution mass flow rate strongly depends on the generator heating temperature and external mass flow of the heating circuit. Also, if the external temperature levels differ significantly from design conditions, the internal temperature levels change and consequently, so do the enthalpies. Therefore, an expanded characteristic equation based on changing internal enthalpies (so-called variable enthalpy) and changing rich solution mass flow rates for each time step was carried out for the DACM.

The expanded characteristic equation is set up for the working pair NH_3/H_2O. Additional components such as the dephlegmator (X = D), the auxiliary gas

circuit or GHX and the bubble pump with the variable mass flow are included to the data reduction model (Figure 5.2). Equations for NH_3/Helium are used to calculate the enthalpies in the auxiliary gas circuit.

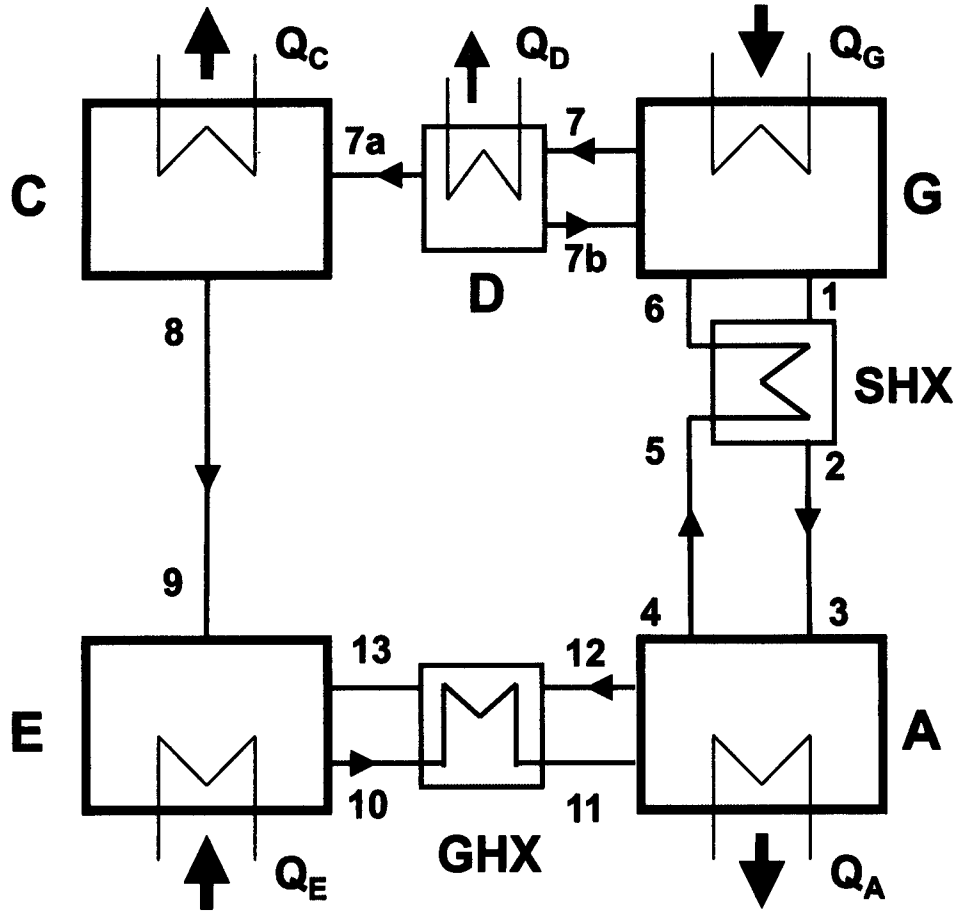

Figure 5.2: Ammonia/water DACM data reduction model.

The expansions lead to additional process conditions such as rectification of the ammonia/water vapour inside the dephlegmator, auxiliary gas cooling losses in the gas circuit and variable mass flow corresponding to external heating temperature based on the characteristics of the bubble pump.

The complete energy and mass balances of the DACM of the internal and external side was set up and solved. New coefficients ($G_{E,deph}$, $D_{E,deph}$, $A_{E,aux}$) were developed for the additional process conditions which are presented in chapter 5.3. The derivation of the new coefficients and the complete expanded characteristic equation for the DACM is given in Appendix B.

According to (Ziegler, 1998b), the arithmetic, instead of the thermodynamic mean temperature can be used for the heat flux calculation with only a small loss in accuracy.

Using the expanded characteristic equation and a dynamic simulation tool, the performance analysis and internal enthalpies can be calculated at each time interval. For this purpose, the simulation environment INSEL (Schumacher, 1991) can be used for the DACM model. As the DACM model is part of a more complex dynamic model that includes varying meteorological conditions, a dynamic system simulation tool such as INSEL needs to be used.

5.2.3 INPUT / OUTPUT DATA

As **input** values for the DACM model, the external inlet temperatures $t_{x,in}$ [°C] as well as external mass flows m_X [kg/s] are required (Figure 5.3). The bubble pump performance is described by the experimentally determined mass flow of the rich ammonia/water solution m_{Sr} [kg/h] (chapter 4.4.4) which varied with increasing generator heating inlet temperatures. Furthermore, the surface wetting factor ε_W [-] for the efficiency of the evaporation process and thereby the distribution of the liquid ammonia into the falling film evaporator is required. For the investigated DACM No.2, the values were fitted by simulation runs depending on the degree of the wetted surface and thereby the generator external mass flow as well as ammonia liquid mass flow.

The required **parameters** for the model are the specific heat capacities $c_{p,x}$ [kJ/kg K] of the heating and cooling fluids and the heat recovery factors Φ_{SHX} [-] and Φ_{GHX} [-] which are determined by the evaluated measurement data of the SHX (chapter 4.5.2) as well as fitted out for the GHX out of the simulation runs. The initial internal mean temperatures T_X [°C] of the main components and the heat transfer coefficients UA_X [kW/K] between external and internal heat transfer are also required.

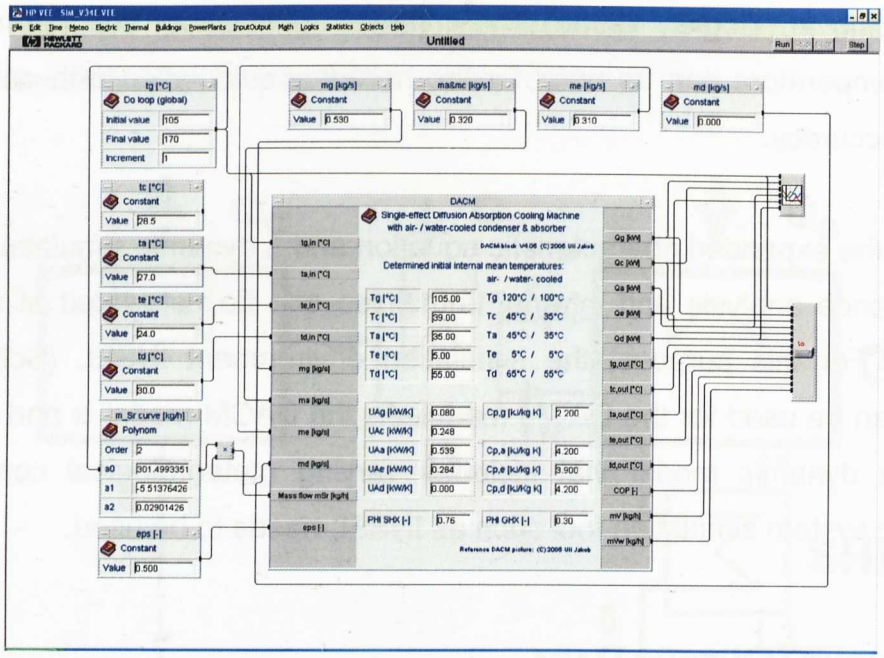

Figure 5.3: Connections of the DACM model presented in the interface HP VEE of the simulation environmental INSEL.

The heat transfer coefficients of the generator UA_G [kW/K], the absorber UA_A [kW/K] and the evaporator UA_E [kW/K] are calculated using the internal heat transfer equations of chapter 3.4.6 and 3.6.8 and the external heat transfer coefficient for tubular heat exchangers with baffles according to (VDI Wärmeatlas, 1988). The results are dependant on the real design and dimensions of the used components. The condenser UA_C [kW/K] and the dephlegmator UA_D [kW/K] heat transfer coefficients are fixed due to evaluated measurement data as constant values of 0.248kWK and 0.021kW/K, which are sufficiently accurate.

The **output** values are the heating and cooling capacities Q_X [kW], the resulting external outlet temperatures $t_{x,out}$ [°C] of the components, the COP of the cooling machine as well as ammonia vapour mass flow m_V [kg/h] and the required weak ammonia/helium gas mixture mass flow m_{Vw} [kg/h].

5.3 MODELLED DACM COMPONENTS

5.3.1 GENERATOR / BUBBLE PUMP

Figure 5.4 shows the generator of the data reduction model with its internal and external inlet and outlet stages for the lifted solution (6 to 1) and the expelled ammonia/water vapour (7) as well as the incoming condensed water vapour (7b).

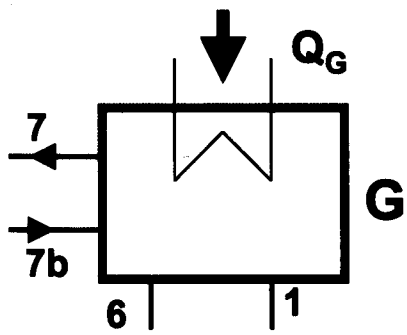

Figure 5.4: Generator of the DACM data reduction model.

For the calculation of the enthalpies, the weak solution X_{Sw} [-] and the non-rectificated vapour X_{V1} [-] are defined as follows:

$$X_{Sw} = f(p_G, T_G) \tag{5.8}$$

$$X_{V1} = f(p_G, X_{Sw}) \tag{5.9}$$

where p_G [Pa] is the generator as well as the simplified total pressure and T_G [°C] is the mean internal generator temperature.

The generator heating capacity Q_G [kW] is calculated by equation (5.10) as follows:

$$\dot{Q}_G = \dot{Q}_E \bullet \left(G_E + G_{E,deph}\right) + \dot{Q}_{Gx} \tag{5.10}$$

where Q_E [kW] is the evaporator cooling capacity, G_E [-] and $G_{E,deph}$ [-] are the specific enthalpy coefficients and Q_{Gx} [kW] is the solution heat loss as defined by:

$$G_E = \frac{(h_7 - h_1)}{q_E} \tag{5.11}$$

$$G_{E,deph} = \frac{(h_7 - h_{7b})}{q_E} \bullet \left(\frac{X_V - X_{V1}}{X_{V1} - X_{L,deph}} \right) \tag{5.12}$$

$$\dot{Q}_{Gx} = \dot{m}_{Sr} \bullet (h_1 - h_6) \tag{5.13}$$

where h_7 and h_1 [kJ/kg] are the outlet and h_{7b} and h_6 [kJ/kg] are the inlet enthalpies, q_E [kJ/kg] is the specific enthalpy difference in the evaporator and X_V [-] as well as $X_{L,deph}$ [-] are the rectificated vapour and condensed water vapour mass concentrations. The mass flow of the rich solution m_{Sr} [kg/s] is given by experimentally determined curves for different external generator inlet temperatures and mass flows (chapter 4.4.2).

The new internal generator temperature T'_G [°C] is determined in equation (5.14) and the external outlet temperature $t_{g,out}$ [°C] can be calculated using equation (5.15) as follows:

$$T_G' = t_g - \frac{\dot{Q}_G}{UA_G} \tag{5.14}$$

$$t_{g,out} = 2 \bullet t_g - t_{g,in} \tag{5.15}$$

where t_g [°C] is the mean external generator temperature defined by equation (5.78), UA_G [kW/K] is the heat transfer coefficient and $t_{g,in}$ [°C] is the generator heating inlet temperature.

5.3.2 DEPHLEGMATOR

The internal and external inlet and outlet stages of the dephlegmator for the rectification of the ammonia/water vapour (7 to 7a) and the condensed water vapour (7b) are shown in Figure 5.5.

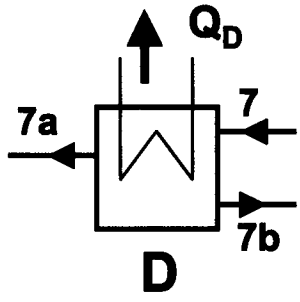

Figure 5.5: Dephlegmator of the DACM data reduction model.

The resulting condensed water vapour $X_{L,deph}$ [-] and the rectified ammonia vapour mass concentration X_V [-] are defined as follows:

$$X_{L,deph} = f(p_D, T_D) \tag{5.16}$$

$$X_V = f(p_D, X_{L,deph}) \tag{5.17}$$

where p_D [Pa] is the dephlegmator as well as the simplified total pressure and T_D [°C] is the mean internal dephlegmator temperature. If no dephlegmator is used for the rectification of the ammonia/water vapour, then X_V is equal to X_{V1}.

The mass flow of the condensed water vapour is defined by equation (5.18) as the rectified vapour mass flow m_V [kg/s] and the mass concentrations:

$$\dot{m}_{L,deph} = \dot{m}_V \bullet \frac{X_V - X_{V1}}{X_{V1} - X_{L,deph}} \tag{5.18}$$

The dephlegmator cooling capacity Q_D [kW] and therefore the specific enthalpy coefficients D_E [-] and $D_{E,deph}$ [-] are calculated using the following equations.

$$\dot{Q}_D = \dot{Q}_E \bullet \left(D_E + D_{E,deph} \right) \tag{5.19}$$

$$D_E = \frac{(h_7 - h_{7a})}{q_E} \tag{5.20}$$

$$D_{E,deph} = \frac{(h_7 - h_{7b})}{q_E} \bullet \left(\frac{X_V - X_{V1}}{X_{V1} - X_{L,deph}} \right) \tag{5.21}$$

Here h_7 [kJ/kg] is the inlet and h_{7a}, h_{7b} [kJ/kg] are the outlet enthalpies. If the dephlegmator is not used, then the coefficient $D_{E,deph}$ is zero and thereby is not considered.

The new internal dephlegmator temperature T'_D [°C] is determined with equation (5.22) and the external outlet temperature $t_{d,out}$ [°C] is calculated with equation (5.23) as follows:

$$T_D' = t_d + \frac{\dot{Q}_D}{UA_D} \tag{5.22}$$

$$t_{d,out} = 2 \bullet t_d - t_{d,in} \tag{5.23}$$

where t_d [°C] is the mean external dephlegmator temperature determined by equation (5.79), UA_D [kW/K] is the heat transfer coefficient and $t_{d,in}$ [°C] is the dephlegmator cooling inlet temperature.

5.3.3 CONDENSER

The condenser inlet and outlet stages of the internal and external circuits are shown in Figure 5.6 as the ammonia vapour inlet (7a) and the condensed liquid ammonia outlet (8).

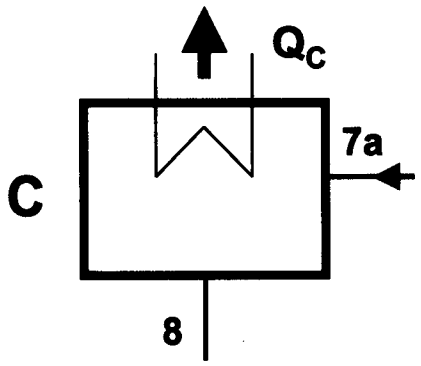

Figure 5.6: Condenser of the DACM data reduction model.

The condenser cooling capacity Q_C [kW] and the specific enthalpy coefficient C_E [-] are calculated using equations (5.24) and (5.25).

$$\dot{Q}_C = \dot{Q}_E \cdot C_E \tag{5.24}$$

$$C_E = \frac{(h_{7a} - h_8)}{q_E} \tag{5.25}$$

where h_{7a} [kJ/kg] is the inlet and h_8 [kJ/kg] is the outlet enthalpy. The new internal condenser temperature T'_C [°C] and the external outlet temperature $t_{c,out}$ [°C] are given as follows:

$$T_C' = t_c + \frac{\dot{Q}_C}{UA_C} \tag{5.26}$$

$$t_{c,out} = 2 \cdot t_c - t_{a,out} \tag{5.27}$$

where t_c [°C] is the mean external condenser temperature determined by equation (5.76), UA_C [kW/K] is the heat transfer coefficient and $t_{c,in}$ [°C] is the condenser cooling inlet temperature. If the absorber and condenser connected in series, then $t_{c,in}$ is $t_{a,out}$.

5.3.4 EVAPORATOR

The internal and external inlet and outlet stages of the evaporator for the incoming liquid ammonia (9) and the rich (10), as well as the weak ammonia/helium gas mixture (13) are shown in Figure 5.7.

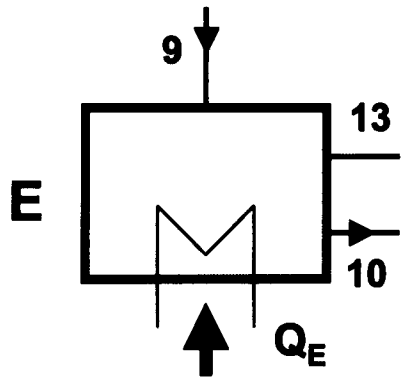

Figure 5.7: Evaporator of the DACM data reduction model.

Based on the basic characteristic equation (5.1), an extended equation for evaporator cooling capacity $Q_{E,aux}$ [kW] with the considerate cooling loss capacity Q_{AUX} [kW] is defined as an extended equation (5.28). $Q_{E,\varepsilon}$ [kW] is an even further application of this equation that takes into account the considerate surface wetting factor ε_W [-] which describes the amount of adjusted falling film surface (chapter 3.6.8).

$$\dot{Q}_{E,aux} = s_E \bullet \left(\Delta\Delta t - \Delta\Delta t_{\min,E}\right) - \dot{Q}_{AUX} \tag{5.28}$$

$$\dot{Q}_{E,\varepsilon} = \varepsilon_W \bullet \dot{Q}_{E,aux} \tag{5.29}$$

The extended slope s_E [kW/K] consist of the normal and additional specific enthalpy coefficients of each component and the heat transfer coefficient $(UA)_X$ [kW/K] between the external and internal circuits.

$$s_E = \left(\left(\frac{C_E}{UA_C} + \frac{1}{UA_E}\right) \bullet B + \left(\frac{G_E + G_{E,deph}}{UA_G} + \frac{A_E + A_{E,aux}}{UA_A}\right)\right)^{-1} \tag{5.30}$$

The characteristic double temperature difference $\Delta\Delta t$ [K] and the intersection $\Delta\Delta t_{min,E}$ [K] are defined in the same way as for the simple characteristic equation by equations (5.4) and (5.5).

For the determination of the cooling loss capacity Q_{AUX} [kW], which is a result of the incoming warm and weak gas mixture, the ammonia liquid mass flow $m_{L,NH3}$ [kg/s] as well as the ammonia vapour mass flow m_V [kg/s] and the auxiliary gas circulation loss (chapter 3.6.4), defined by equation (3.69), are required.

$$\dot{Q}_{AUX} = \dot{m}_{L,NH3} \bullet \left((T_{13} - T_E) \bullet \frac{c_{p,Vw} \bullet \dot{m}_{Vw}}{\dot{m}_{L,NH3}} \right) \tag{5.31}$$

$$\dot{m}_{L,NH3} = \dot{m}_V \bullet X_V \tag{5.32}$$

$$\dot{m}_V = \frac{\dot{Q}_E}{q_E} \tag{5.33}$$

The specific evaporator enthalpy coefficient q_E [kJ/kg] is expanded for the DACM model with the auxiliary gas circuit enthalpy difference H_{AUX} [kJ/kg] (derivation in Appendix B) which is calculated using equation (5.35).

$$q_E = (h_{10} - h_9 + H_{AUX}) \tag{5.34}$$

$$H_{AUX} = (h_{10} - h_{13}) \bullet \left[X_V \bullet \left(\frac{p_{total} - p_{Vr}}{M_{NH3} \bullet (p_{Vr} - p_{Vw})} \right) \bullet \left(M_{He} + (M_{NH3} - M_{He}) \bullet \upsilon_{Vw} \right) \right] \tag{5.35}$$

In this equation, h_9, h_{13} [kJ/kg] are the inlet and h_{10} [kJ/kg] is the outlet enthalpy, p_{total} [Pa], p_{Vr} [Pa] and p_{Vw} [Pa] are the total pressure and the partial pressures of the rich and weak gas mixture. υ_{Vw} [m³/m³] is the volume concentration of the weak gas mixture determined by equation (3.75). Furthermore, M_{He} [kg/kmol] and M_{NH3} [kg/kmol] are the molecular mass of helium and ammonia.

The new internal evaporator temperature T'_E [°C] and the external outlet temperature $t_{e,out}$ [°C] are given as follows:

$$T_E' = t_e - \frac{\dot{Q}_{E,\varepsilon}}{UA_E} \tag{5.36}$$

$$t_{e,out} = 2 \bullet t_e - t_{e,in} \tag{5.37}$$

where t_e [°C] is the mean external evaporator temperature determined by equation (5.75), UA_E [kW/K] is the heat transfer coefficient and $t_{e,in}$ [°C] is the evaporator cooling inlet temperature.

5.3.5 GAS HEAT EXCHANGER

The stages of the internal circuit of the GHX are presented in Figure 5.8, where the cold, rich gas mixture (10) flows from the evaporator to the absorber (11) and the warm, weak gas mixture (12) flows from the absorber back to the evaporator (13).

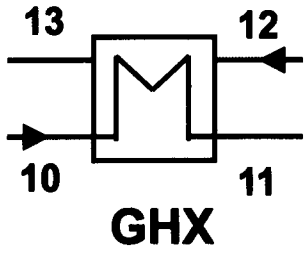

Figure 5.8: Gas heat exchanger (GHX) of the DACM data reduction model.

The GHX has been characterised by a heat transfer effectiveness of 0.25 to 0.30, depending on the ammonia/helium mass flow. The efficiency, which describes the performance of the GHX, is defined by equation (5.38) for the weak Φ_{Vw} [-] or rich Φ_{Vr} [-] gas mixture side.

$$\Phi_{Vw} = \Phi_{Vr} \bullet \left(\frac{\dot{m}_{Vr}}{\dot{m}_{Vw}} \bullet \frac{c_{V,Vr}}{c_{V,Vw}} \right) = \Phi_{vr} \bullet \left(\frac{f_{Vw} - 1}{f_{Vr} - 1} \bullet \frac{c_{V,Vr}}{c_{V,Vw}} \right) \tag{5.38}$$

The internal outlet temperatures T_{11} [°C] and T_{13} [°C] are calculated with the equations (5.39) and (5.40) as follows:

$$T_{11} = T_E + \Phi_{Vr} \cdot (T_A - T_E) \tag{5.39}$$

$$T_{13} = T_A - \Phi_{Vw} \cdot (T_A - T_E) \tag{5.40}$$

5.3.6 ABSORBER

Figure 5.9 shows the internal and external inlet and outlet stages of the absorber for the incoming weak solution (3) as well as the exiting rich solution (4) and the ammonia/helium gas mixture (11 to 12).

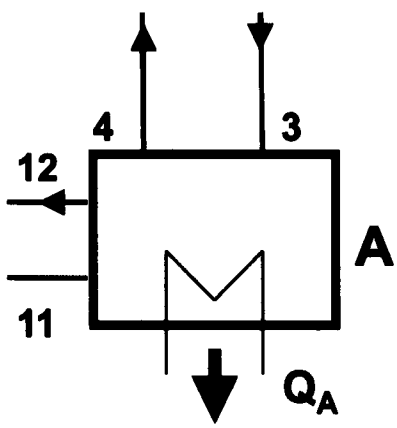

Figure 5.9: Absorber of the DACM data reduction model.

For the calculation of the enthalpies the rich solution X_{Sr} [-] needs to be calculated using the following equation:

$$X_{Sr} = f(p_{A,Sr}, T_A) \tag{5.41}$$

where $p_{A,Sr}$ [Pa] is the absorber partial pressure that is in equilibrium with the rich solution and T_A [°C] is the mean internal absorber temperature.

The absorber cooling capacity Q_A [kW] is calculated with equation (5.42) as follows:

$$\dot{Q}_A = \dot{Q}_E \bullet \left(A_E + A_{E,aux}\right) + \dot{Q}_{Ax} \tag{5.42}$$

where A_E [-] and $A_{E,aux}$ [-] are the specific enthalpy coefficients and Q_{Ax} [kW] is the solution heat loss, which are calculated as follows:

$$A_E = \frac{(h_{11} - h_3)}{q_E} \tag{5.43}$$

$$A_{E,aux} = \frac{(h_{11} - h_{12})}{q_E} \bullet \left[X_V \bullet \left(\frac{p_{total} - p_{Vr}}{M_{NH3} \bullet (p_{Vr} - p_{Vw})} \right) \bullet \left(M_{He} + (M_{NH3} - M_{He}) \bullet \upsilon_{Vw} \right) \right] \tag{5.44}$$

$$\dot{Q}_{Ax} = \dot{m}_{Sr} \bullet (h_3 - h_4) \tag{5.45}$$

where h_3, h_{11} [kJ/kg] are the inlet and h_4, h_{12} [kJ/kg] are the outlet enthalpies.

The new internal absorber temperature T'_A [°C] is determined with equation (5.46) and the external outlet temperature $t_{a,out}$ [°C] can be calculated with equation (5.47) as follows:

$$T_A' = t_a + \frac{\dot{Q}_A}{UA_A} \tag{5.46}$$

$$t_{a,out} = 2 \bullet t_a - t_{a,in} \tag{5.47}$$

where t_a [°C] is the mean external absorber temperature determined by equation (5.77), UA_A [kW/K] is the heat transfer coefficient and $t_{a,in}$ [°C] is the absorber heating inlet temperature.

5.3.7 SOLUTION HEAT EXCHANGER

The stages of the internal circuit of the SHX are presented in Figure 5.10, where the cold, rich solution (5) flows from the absorber to the generator (6) and the incoming hot, weak solution (1) flows from the generator to the absorber (2).

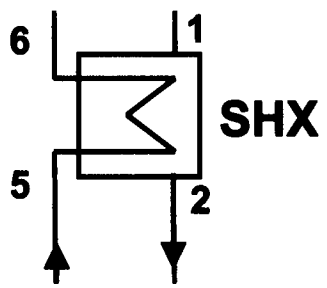

Figure 5.10: Solution heat exchanger (SHX) of the DACM data reduction model.

The SHX has been characterised by a heat transfer effectiveness, assumed to remain the same values evaluated in chapter 4.5.2. The efficiency, which describes the performance of the SHX, is defined by equation (5.48) for the weak Φ_{Sw} [-] or rich Φ_{Sr} [-] solution side.

$$\Phi_{Sw} = \Phi_{Sr} \bullet \left(\frac{\dot{m}_{Sr}}{\dot{m}_{Sw}} \bullet \frac{c_{L,Sr}}{c_{L,Sw}} \right) = \Phi_{Sr} \bullet \left(\frac{X_{Sw} - 1}{X_{Sr} - 1} \bullet \frac{c_{L,Sr}}{c_{L,Sw}} \right) \tag{5.48}$$

The internal outlet temperatures T_6 [°C] and T_2 [°C] are calculated using the following equations:

$$T_6 = T_A + \Phi_{Sr} \bullet (T_G - T_A) \tag{5.49}$$

$$T_2 = T_3 = T_G - \Phi_{Sw} \bullet (T_G - T_A) \tag{5.50}$$

5.3.8 CONVERSION EXTERNAL TEMPERATURES

Instead of using the external mean temperatures t_x [°C], the energy balance equations can also be resolved as a function of the external entrance temperatures $t_{x,in}$ [°C] so that external mass flow rates can be considered in the

model. For the conversion of the external inlet temperatures of the components into mean external temperatures, the capacity equations of the five components evaporator, condenser, absorber, generator and dephlegmator are used as is shown below:

$$\dot{Q}_E = s_E \bullet \left(\Delta\Delta t - \Delta\Delta t_{\min,E}\right) \tag{5.51}$$

$$\dot{Q}_C = s_E \bullet \left(\Delta\Delta t - \Delta\Delta t_{\min,E}\right) \bullet C_E \tag{5.52}$$

$$\dot{Q}_A = s_E \bullet \left(\Delta\Delta t - \Delta\Delta t_{\min,E}\right) \bullet \left(A_E + A_{E,aux}\right) + \dot{Q}_{Ax} \tag{5.53}$$

$$\dot{Q}_G = s_E \bullet \left(\Delta\Delta t - \Delta\Delta t_{\min,E}\right) \bullet \left(G_E + G_{E,deph}\right) + \dot{Q}_{Gx} \tag{5.54}$$

$$\dot{Q}_D = s_E \bullet \left(\Delta\Delta t - \Delta\Delta t_{\min,E}\right) \bullet \left(D_E + D_{E,deph}\right) \tag{5.55}$$

The $\Delta\Delta t$ function of equation (5.4) and the further equations for the arithmetical external temperature difference and the dissipated and supplied capacities at each component with the external mass flows m_x [kg/s] and the specific heat capacities $c_{p,x}$ of the used fluids are stated as follows:

$$t_{x,out} = 2 \bullet t_x - t_{x,in} \tag{5.56}$$

$$\dot{Q}_x = 2 \bullet \dot{m}_x \bullet c_{p,x} \bullet (t_x - t_{x,in}) \tag{5.57}$$

$$\dot{Q}_x = 2 \bullet \dot{m}_x \bullet c_{p,x} \bullet (-t_x + t_{x,in}) \tag{5.58}$$

After equating and rearranging the internal and external capacity equations the following coefficients M_1 to M_{11}, N_1 to N_3 and O_1 to O_2 were substituted to determine the respective mean external temperatures with the following equations.

$$M_1 = \left(B + \frac{2 \bullet \dot{m}_e \bullet c_{p,e}}{s_E}\right) \tag{5.59}$$

$$M_2 = \Delta\Delta t_{\min,E} + \frac{2 \bullet \dot{m}_e \bullet c_{p,e}}{s_E} \bullet t_{e,in} \tag{5.60}$$

$$M_3 = \left(1 - \frac{4 \bullet \dot{m}_c \bullet c_{p,c}}{s_E \bullet C_E}\right) \tag{5.61}$$

$$M_4 = \left(B + \frac{2 \bullet \dot{m}_c \bullet c_{p,c}}{s_E \bullet C_E} \right) \tag{5.62}$$

$$M_5 = \Delta\Delta t_{\min,E} + \frac{2 \bullet \dot{m}_c \bullet c_{p,c}}{s_E \bullet C_E} \bullet t_{a,in} \tag{5.63}$$

$$M_6 = \left(1 + \frac{2 \bullet \dot{m}_a \bullet c_{p,a}}{s_E \bullet \left(A_E + A_{E,aux} \right)} \right) \tag{5.64}$$

$$M_7 = \Delta\Delta t_{\min,E} - \frac{2 \bullet \dot{m}_a \bullet c_{p,a}}{s_E \bullet \left(A_E + A_{E,aux} \right)} \bullet t_{a,in} - \frac{\dot{Q}_{Ax}}{s_E \bullet \left(A_E + A_{E,aux} \right)} \tag{5.65}$$

$$M_8 = \left(1 + \frac{2 \bullet \dot{m}_g \bullet c_{p,g}}{s_E \bullet \left(G_E + G_{E,deph} \right)} \right) \tag{5.66}$$

$$M_9 = \Delta\Delta t_{\min,E} + \frac{2 \bullet \dot{m}_g \bullet c_{p,g}}{s_E \bullet \left(G_E + G_{E,deph} \right)} \bullet t_{g,in} - \frac{\dot{Q}_{Gx}}{s_E \bullet \left(G_E + G_{E,deph} \right)} \tag{5.67}$$

$$M_{10} = \frac{2 \bullet \dot{m}_d \bullet c_{p,d}}{s_E \bullet \left(D_E + D_{E,deph} \right)} \tag{5.68}$$

$$M_{11} = \Delta\Delta t_{\min,E} + \frac{2 \bullet \dot{m}_d \bullet c_{p,d}}{s_E \bullet \left(D_E + D_{E,deph} \right)} \bullet t_{d,in} \tag{5.69}$$

$$N_1 = \frac{M_5}{1 - M_3} - \frac{M_2}{1 - M_3} \tag{5.70}$$

$$N_2 = \frac{(B - M_4)}{1 - M_3} \tag{5.71}$$

$$N_3 = \frac{(M_1 - B)}{1 - M_3} \tag{5.72}$$

$$O_1 = \frac{M_7 - M_2 - \frac{M_5}{1-M_3} + \frac{M_2}{1-M_3} + \frac{M_5 \bullet M_6}{1-M_3} - \frac{M_2 \bullet M_6}{1-M_3}}{\left(\frac{(B-M_4)}{1-M_3} \bullet (M_6 - 1)\right)} \tag{5.73}$$

$$O_2 = \frac{\left(-B + \frac{(M_1 - B) \bullet M_6}{1-M_3} + Z_1 - \frac{(M_1 - B)}{1-M_3}\right)}{\left(\frac{(B-M_4)}{1-M_3} \bullet (M_6 - 1)\right)} \tag{5.74}$$

The solved equations of the external mean temperatures (5.75) to (5.79) with the substituted coefficients M_i, N_i and O_i are used in the following equations:

$$t_e = \frac{M_9 - M_2 \bullet M_8 - N_1 \bullet M_8 + O_1 \bullet N_2 \bullet M_8 - B \bullet M_8 \bullet O_1 + N_1 - O_1 \bullet N_2 + B \bullet O_1}{-O_2 \bullet N_2 \bullet M_8 + N_3 \bullet M_8 + B \bullet M_8 \bullet K_2 - M_1 \bullet M_8 + O_2 \bullet N_2 - N_3 - B \bullet O_2 + B} \tag{5.75}$$

$$t_c = O_1 + t_e \bullet O_2 \tag{5.76}$$

$$t_a = N_1 - t_c \bullet N_2 + t_e \bullet N_3 \tag{5.77}$$

$$t_g = M_2 + t_a + M \bullet t_c - t_e \bullet M_1 \tag{5.78}$$

$$t_d = \frac{t_g - t_a - B \bullet t_c + B \bullet t_e + M_{11}}{M_{10}} \tag{5.79}$$

5.3.9 PERFORMANCE OF TOTAL DACM SYSTEM

The coefficient of performance (COP) of the total DACM system is defined in equation (5.80). The heat input should be exactly the same as the heat output of the system (heat balance should be zero) as is shown in the equation (5.81).

$$COP = \frac{\dot{Q}_{E,\varepsilon}}{\dot{Q}_G} \tag{5.80}$$

$$\dot{Q}_G + \dot{Q}_{E,\varepsilon} / \varepsilon_W = \dot{Q}_D + \dot{Q}_C + \dot{Q}_A \tag{5.81}$$

5.4 MODEL VALIDATION

For the validation of the DACM model, experimental data from DACM No.2 with coaxial SHX were used and compared. The adjusted external mass flows of the heating and cooling circuits are given in table 5.1. The mass flows of the generator were varied from low to high generator external mass flow as is shown below by the presented values. The absorber and condenser are serially connected and therefore the mass flow value is the same for both.

Table 5.1: Adjusted external mass flows of the DACM No.2 with coaxial SHX.

m_x [kg/s]	generator ($V_{H,ext}$)	condenser	absorber	evaporator	dephlegmator (if used)
DACM No.2	0.24 (15l/min) 0.39 (25l/min) 0.53 (34l/min)	0.32	0.32	0.31	0.05

The rich solution mass flow m_{Sr} [kg/h] of the generator / bubble pump performance is determined from various evaluated measurements depending on external generator inlet temperature and external mass flow heating circuit as follows:

$$\dot{m}_{Sr} = \left(2.901426 \cdot 10^{-2} \cdot t_{g,in}{}^{2} - 5.41376426 \cdot t_{g,in} + 301.4993351\right) \cdot \dot{m}_{g} \quad (5.82)$$

The determined initial internal mean temperatures T_X [°C] of the DACM are presented in table 5.2 for the starting point of the simulation runs.

Table 5.2: Initial internal mean temperatures of the DACM No.2 with coaxial SHX.

T_X [°C]	generator	condenser	absorber	evaporator	dephlegmator (if used)
DACM No.2	105.0	39.0	35.0	9.0	55.0

The pressure drop loss along the auxiliary gas circuit tubes were not considered because of the large free tube diameters. Furthermore, the driving pressure difference between evaporator and absorber is set to $1.5x10^5$Pa.

To determine the energy balances, the following assumptions for the parameters Φ_{SHX}, Φ_{GHX} and ε_W were made. The heat recovery factor of the SHX was set to 0.76 as a fit value for the measurement data (chapter 4.5.2). The heat recovery factor of the GHX and the surface wetting factor are determined as fit inputs of empirical values, because they are not yet measurable. Therefore, for the low as well as high generator external mass flow, the Φ_{GHX} is set to 0.25 and 0.30 respectively and for ε_W the values are 0.45 and 0.50 respectively. With a higher ammonia mass flow, the wetting surface inside the falling film tubes increases and thereby the heat recovery factor of the GHX increases.

The simulation runs for the validation were done for the measured conditions of DACM No.2 with coaxial SHX at varied generator heating inlet temperatures ranging from 110°C to 170°C, a constant absorber inlet temperature of 27°C and a constant evaporator inlet temperature of 24°C.

5.4.1 PERFORMANCE AT CONSTANT OR VARIABLE ENTHALPY

The performance of the DACM is first investigated and validated at constant enthalpy based on one given design point or at every time step with changing variable enthalpy. Figure 5.11 and Figure 5.12 show the comparison of the measured and the simulated data for the evaporator cooling capacity and the COP at high as well as low generator external mass flow. The performance of the variable enthalpy describes the experimental data points of the measured performance very well, whereas at constant enthalpy the performance deviated from the measured ones.

The fluctuations of the measured COP at high generator external mass flow are due to the variation of the heating power which is obtained from the measured external mass flow. The figures however, show that the DACM also works at variable heating external mass flows and temperatures.

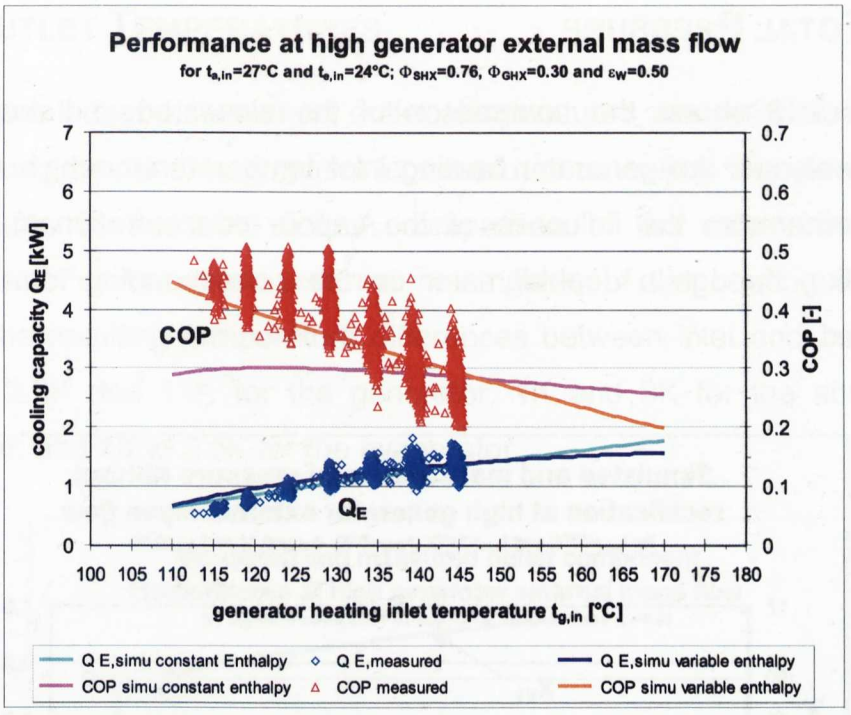

Figure 5.11: Measured and simulated performance of the DACM No.2 with coaxial SHX at high generator external mass flow of 34l/min as well as 0.53kg/s and constant or variable calculated internal enthalpy.

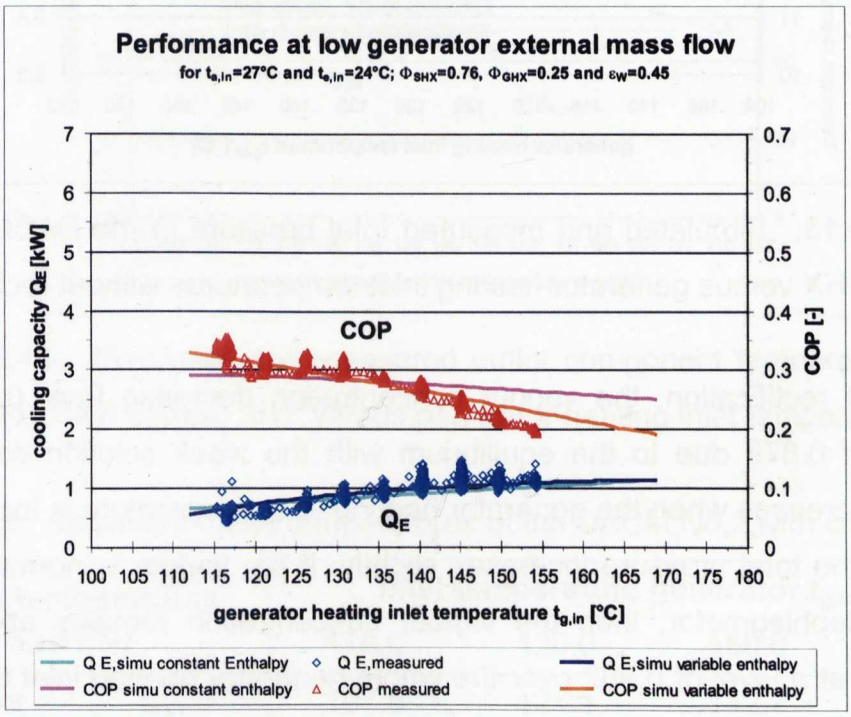

Figure 5.12: Measured and simulated performance of the DACM No.2 with coaxial SHX at low generator external mass flow of 15l/min as well as 0.24kg/s and constant or variable calculated internal enthalpy.

5.4.2 TOTAL PRESSURE

Figure 5.13 shows the comparison of the simulated and measured total pressure versus the generator heating inlet temperatures, which are matched well. Furthermore the influence of the vapour concentration X_{V1} [-] without rectification through a dephlegmator on the corresponding total pressure is presented.

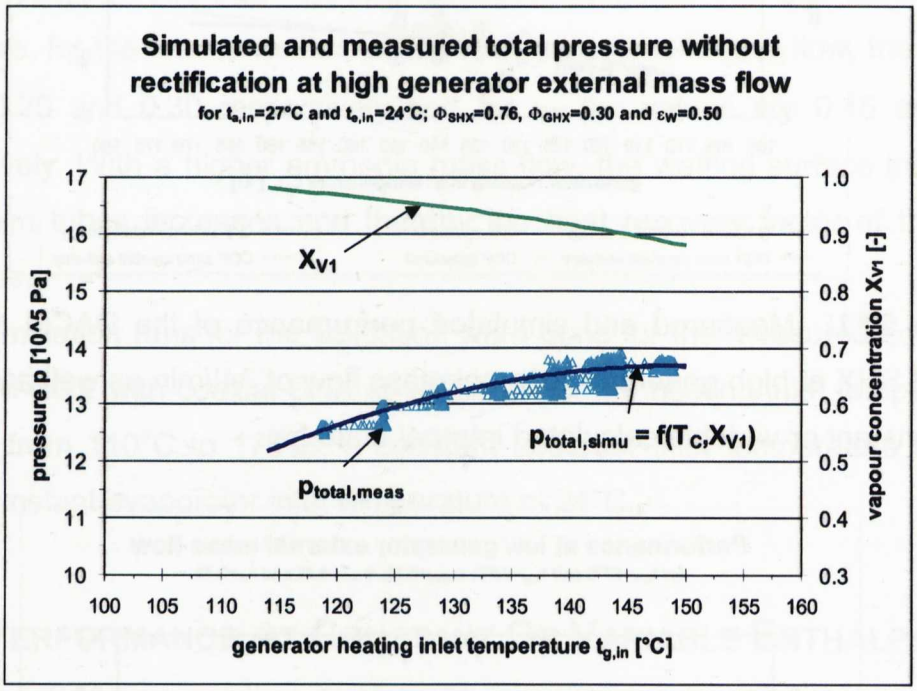

Figure 5.13: Simulated and measured total pressure of the DACM No.2 with coaxial SHX versus generator heating inlet temperatures without rectification.

Without rectification, the vapour concentration decrease from 0.979 to low values of 0.879 due to the equilibrium with the weak solution concentration which decreases when the generator heating inlet temperature is increased and thereby the total pressure increases slightly. If the vapour is normally rectified by the dephlegmator, then the vapour concentration remains approximately constant at a level of 0.982 over the whole generator heating inlet temperature range. Therefore, the total pressure is at a constant pressure level.

5.4.3 OUTLET TEMPERATURES

The simulated and measured outlet temperatures are presented in Figure 5.14 versus generator heating inlet temperatures as well as for selected heating temperatures in the table 5.3. A comparison of the data shows a good accordance. For the given external mass flows of the heating and cooling circuits, the resulting temperature differences between inlet and outlet ranged between 2.5K and 11K for the generator, 1K and 3K for the absorber and condenser, and 1K to 2.5K for the evaporator.

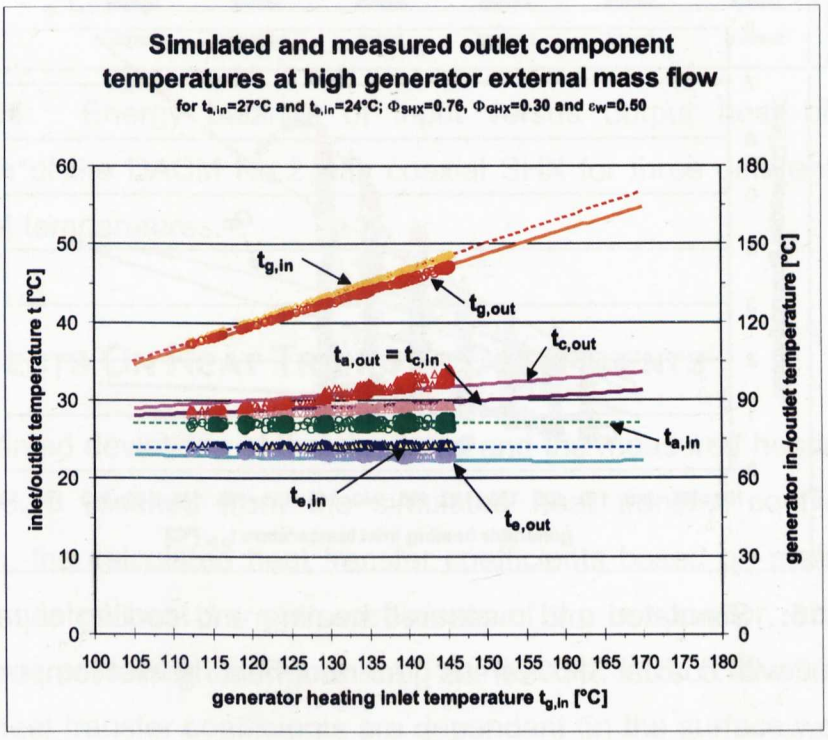

Figure 5.14: Simulated and measured outlet component temperatures of the DACM No.2 with coaxial SHX versus generator heating inlet temperatures.

Table 5.3: Simulated outlet temperatures of the DACM No.2 with coaxial SHX.

outlet temperatures $t_{x,out}$ [°C]		inlet temperature generator $t_{g,in}$ [°C]			
		110.0	130.0	150.0	170.0
generator	$t_{g,in}$	107.5	125.1	142.7	159.1
absorber	$t_{a,in}$ = 27.0	28.0	28.9	29.5	30.2
condenser	$t_{c,in} = t_{a,out}$	28.8	30.6	31.9	33.1
evaporator	$t_{e,in}$ = 24.0	23.1	22.4	21.9	21.7

5.4.4 HEATING AND COOLING CAPACITIES

Figure 5.15 shows the simulated and measured heating as well as cooling capacities. The evaporator and the absorber cooling capacity are matched very well, but below 130°C the simulated generator heating and the condenser cooling capacities slightly deviates from the measured ones.

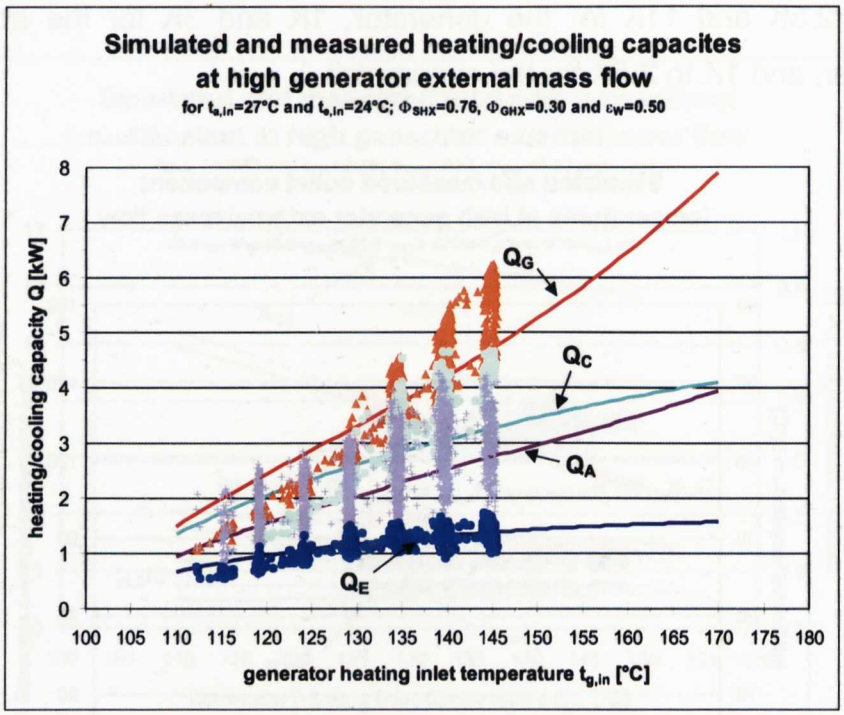

Figure 5.15: Simulated and measured heating and cooling capacities of the DACM No.2 with coaxial SHX versus generator heating inlet temperatures.

For the validation of the simulated heat input and output, the energy balance for three selected generator heating inlet temperatures are presented in Figure 5.16. The heat input of the model should be equal in comparison to the heat output of the DACM system. Using the equation (5.81), the results showed a good accuracy without large deviations.

The model can not be validated for each individual component but for the total DACM system because no detailed internal models are used.

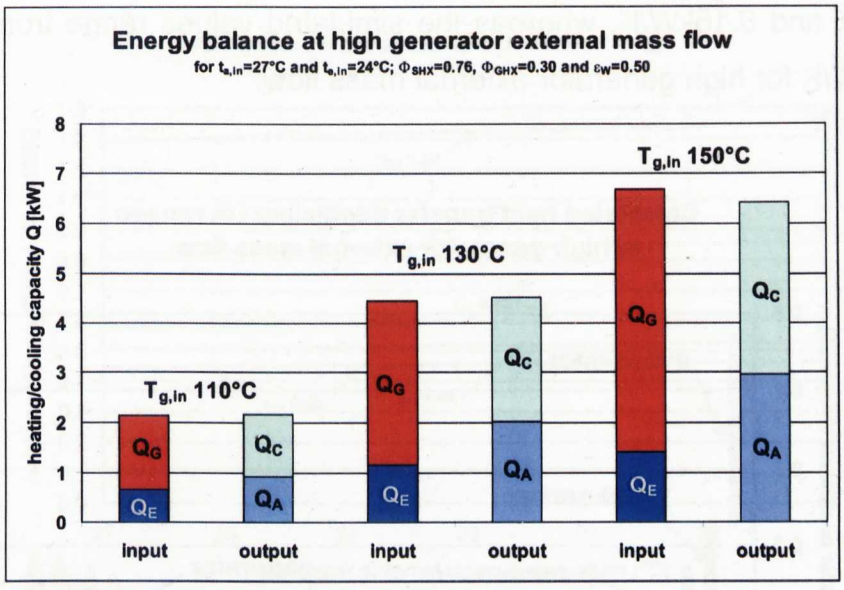

Figure 5.16: Energy balance of input versus output heat of the core components of the DACM No.2 with coaxial SHX for three different generator heating inlet temperatures.

5.4.5 EFFECTS ON HEAT TRANSFER COEFFICIENTS

The presented deviations of the simulated and the measured heating capacity in Figure 5.15 resulted from the simulated heat transfer coefficients. For comparison, the calculated heat transfer coefficients based on measured data and the simulated heat transfer coefficients of the evaporator, absorber and generator are presented in Figure 5.17 as well as 5.18, 5.19 and 5.20. The simulated heat transfer coefficients are dependant on the surface wetting factor as well as the external heating/cooling mass flow.

The simulated heat transfer coefficients UA_E of the evaporator range between 0.22kW/k and 0.54kW/K. The calculated values are in a similar range between 0.23kW/K and 0.48kW/K. The comparison of the heat transfer coefficients of the absorber UA_A shows that the calculated values with a range of 0.05kW/K to 0.24kW/K deviate strongly from the simulated ones between 0.44kW/k and 1.21kW/K. The simulated values are more reliable then the calculated ones, due to the limited validation possibility of the measured data. For the generator the heat transfer coefficients UA_G the calculated values ranges between

0.08kW/K and 0.15kW/K, whereas the simulated values range from 0.10kW/K to 0.13kW/K for high generator external mass flow.

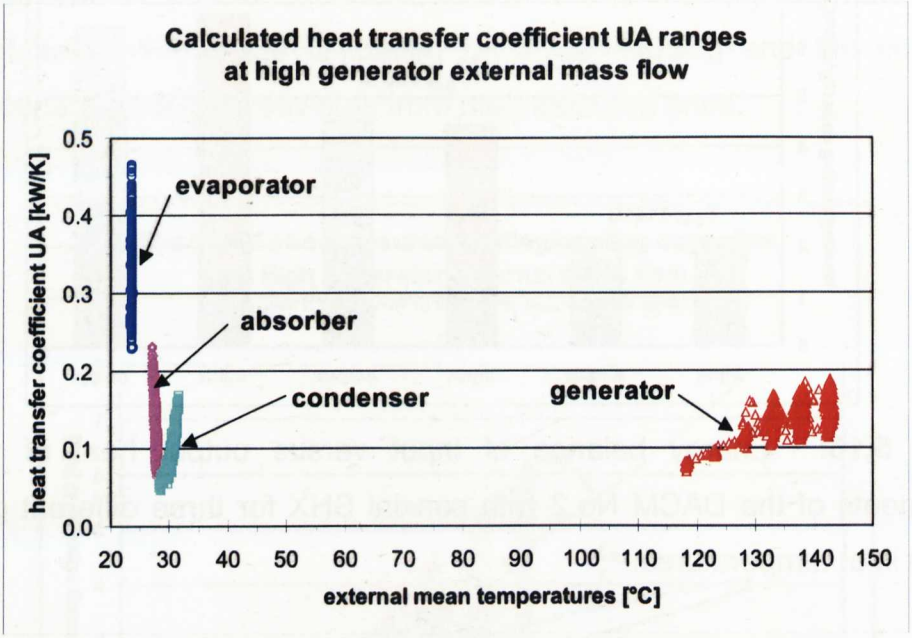

Figure 5.17: Calculated heat transfer coefficients of the core components of the DACM No.2 with coaxial SHX based on measured data versus external mean temperatures.

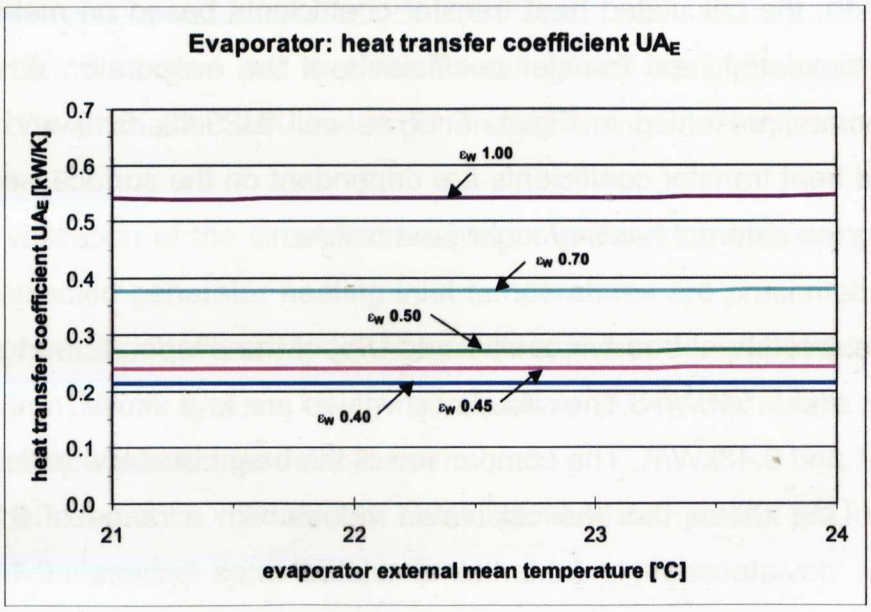

Figure 5.18: Simulated evaporator heat transfer coefficient for different surface wetting factors versus evaporator external mean temperature.

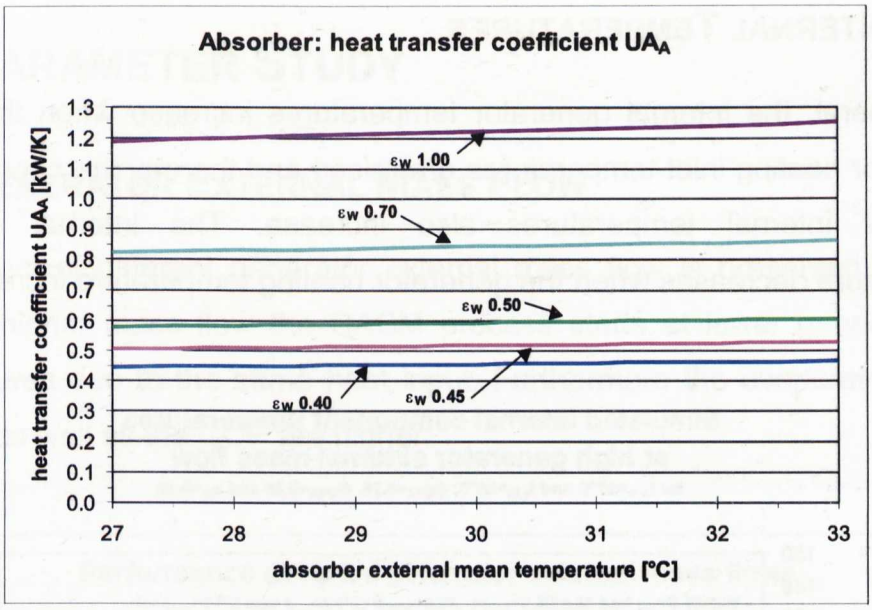

Figure 5.19: Simulated absorber heat transfer coefficient for different surface wetting factors versus absorber external mean temperature.

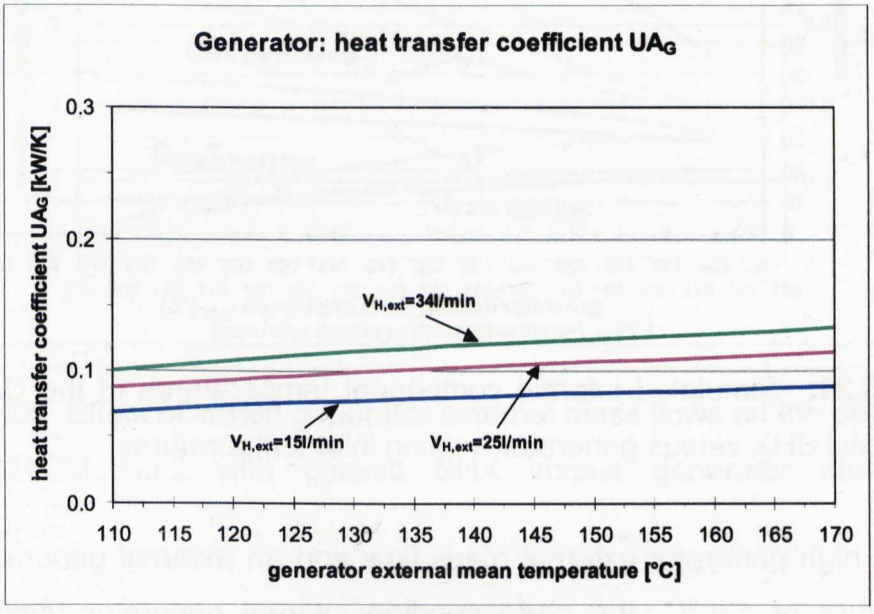

Figure 5.20: Simulated generator heat transfer coefficient for different generator external volume flows versus generator external mean temperature.

The effect of surface wetting factor and external mass flow on the heat transfer coefficient UA is determined by the internal and external heat transfer coefficients h_C (chapter 3.4.6 and 3.6.8).

5.4.6 INTERNAL TEMPERATURES

In general, the internal generator temperatures increase when the external generator heating inlet temperatures are raised and thereby the condenser and absorber internal temperatures also increase. The internal evaporator temperature decreases when the generator heating temperature increases.

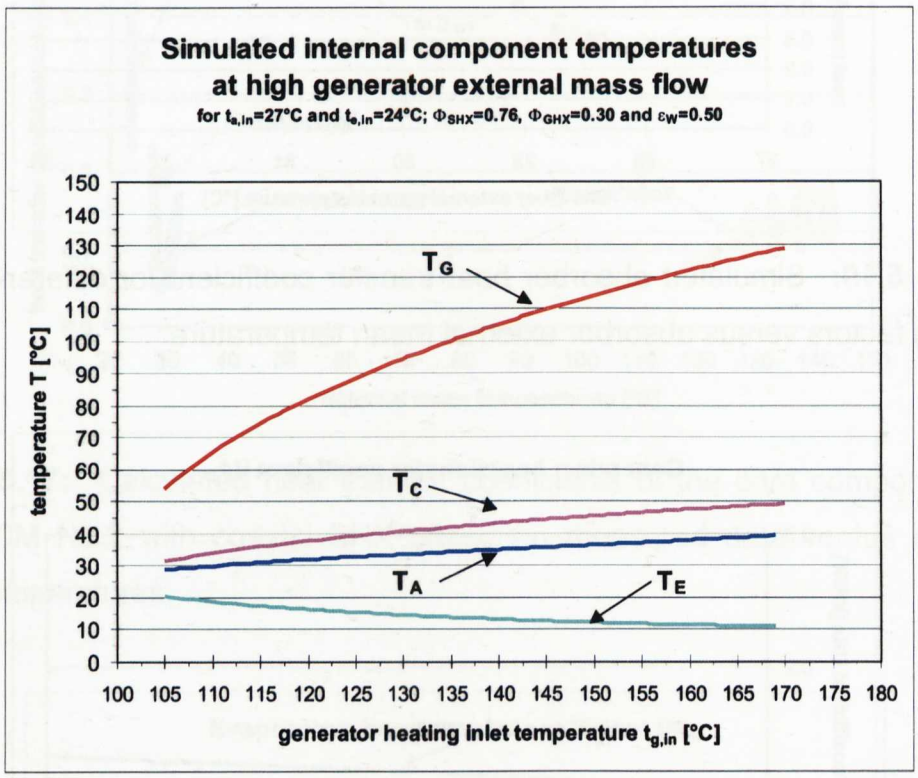

Figure 5.21: Simulated internal component temperatures of the DACM No.2 with coaxial SHX versus generator heating inlet temperatures.

With a high generator external mass flow and an external generator heating temperature of 130°C, the corresponding internal generator temperature is 94.4°C and the internal condenser and absorber temperatures are 40.6°C and 33.4°C respectively. The resulting internal evaporator temperature is 14.5°C. It was not possible to measure the internal temperatures directly as well as to validate them.

5.5 PARAMETER STUDY

5.5.1 GENERATOR EXTERNAL MASS FLOW

The effect of different generator external mass flow is presented in Figure 5.22. At higher mass flow the DACM process starts at lower generator inlet temperatures due to the same heat input. Furthermore the evaporator cooling capacity as well as the COP are higher.

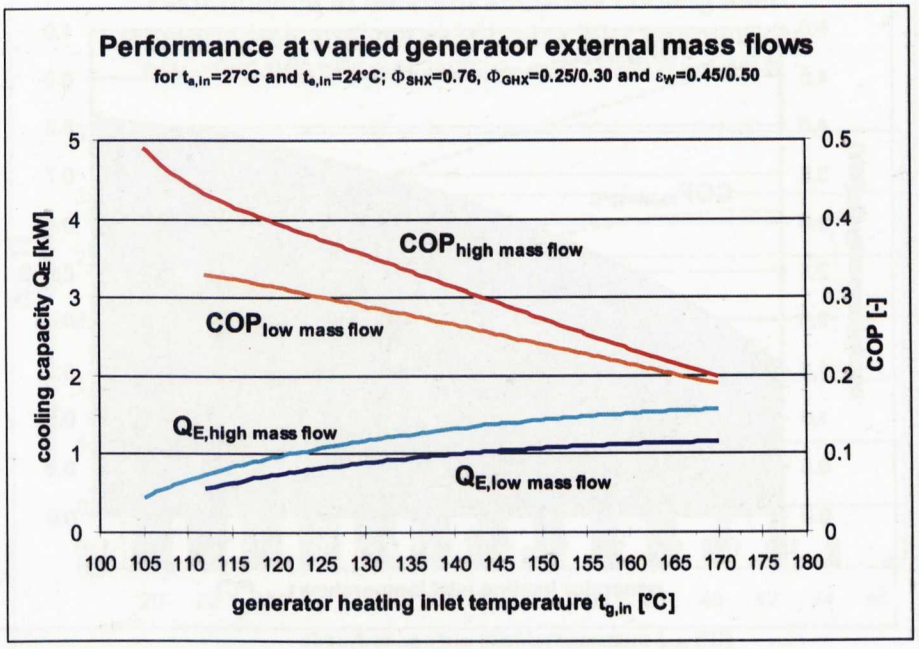

Figure 5.22: Effect of varied generator external mass flows on the performance of the DACM No.2 with coaxial SHX versus generator heating inlet temperatures.

The simulated COP decreases with increasing generator heating inlet temperature as well as heating capacity for low and high mass flow from 0.33 to 0.19 as well as 0.48 to 0.20. For the further parameter investigations the high generator external mass flow is used.

5.5.2 EVAPORATOR TEMPERATURE

The effect of lower evaporator inlet temperature of 12°C as well as a maximum surface wetting factor of 1.00 on the performance of the DACM is presented in Figure 5.23. The COP as well as the evaporator cooling capacity decreases at lower evaporator temperatures.

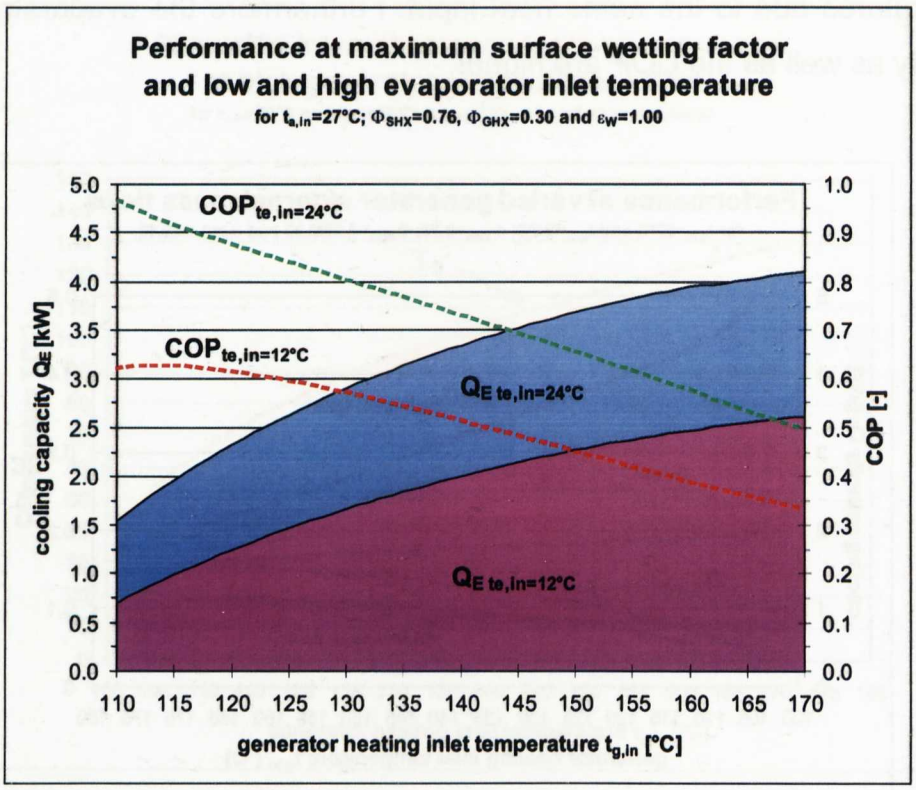

Figure 5.23: Effect on the performance of the DACM No.2 with coaxial SHX at a maximum surface wetting factor of 1.00 and low or high evaporator inlet temperature as well as high generator external mass flow versus generator heating inlet temperatures.

For the current DACM No.2 with coaxial SHX the design cooling capacity of 2.5kW could be reached for low and high evaporator temperatures at a generator heating inlet temperature of 162°C as well as 123°C. The corresponding COPs are 0.38 and 0.85.

5.5.3 COOLING WATER TEMPERATURE

Figure 5.24 shows the influence on the performance at different absorber cooling inlet temperatures and low evaporator inlet temperature of 12°C for three generator heating inlet temperatures of 110°C, 130°C and 150°C. The lower the absorber cooling inlet temperature is, the higher is the resulting evaporator cooling capacity. For an absorber cooling inlet temperature of 28°C the obtainable cooling capacities are 0.7kW, 1.6kW and 2.2kW.

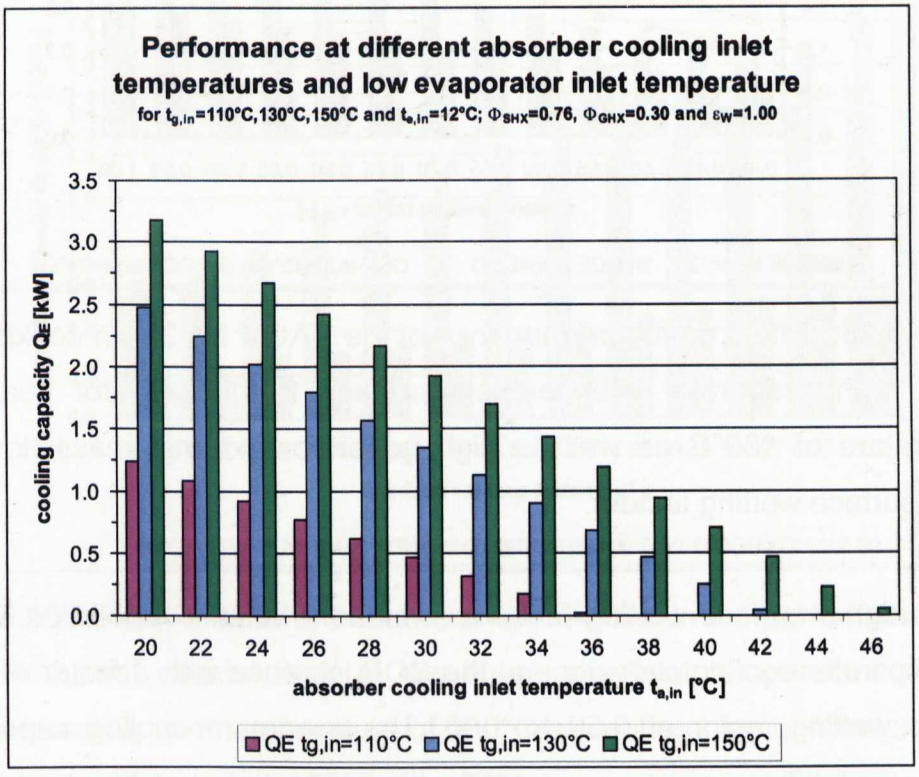

Figure 5.24: Effect of cooling water temperature on the performance of the DACM No.2 with coaxial SHX at low evaporator inlet temperature as well as high generator external mass flow versus absorber cooling inlet temperatures.

5.5.4 SURFACE WETTING FACTOR

The effect of the surface wetting factor on the performance at a constant generator temperature of 130°C and low as well as high evaporator inlet temperature of 12°C and 24°C is shown in Figure 5.25.

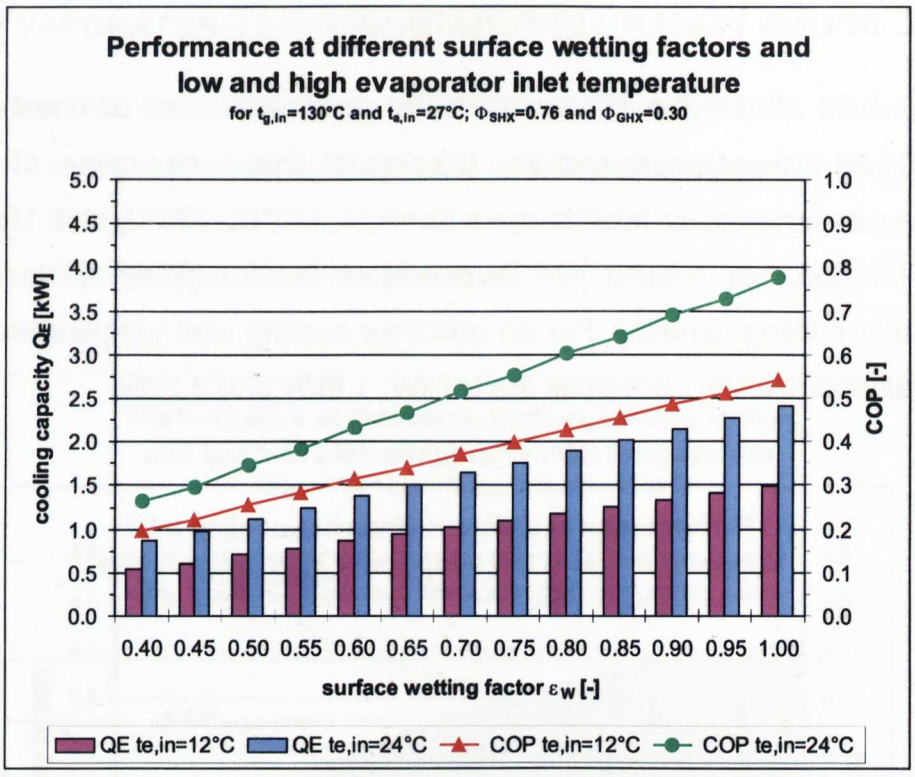

Figure 5.25: Effect on the performance of the DACM No.2 with coaxial SHX at low or high evaporator inlet temperature and fixed generator heating inlet temperature of 130°C as well as high generator external mass flow versus varied surface wetting factors.

With a higher surface wetting factor as well as a better evaporation efficiency, the evaporator cooling capacity and the COP increase with a factor of 2 from a surface wetting factor of 0.50 to 1.00. The maximum cooling capacities for evaporator inlet temperatures of 12°C and 24°C at ε_W = 1.00 are 1.5kW and 2.4kW at COPs of 0.54 and 0.78. To reach a maximum cooling capacity, an impression of surface structure inside the tubes is necessary in order to increase the surface wetting factor to 100% of the disposed total heat transfer surface.

5.5.5 HEAT RECOVERY FACTOR GHX

Figure 5.26 presents the performance at different GHX heat recovery factors for a low evaporator inlet temperature of 12°C and a constant generator temperature of 130°C. The difference between the determined heat recovery

factor of 0.30 and the investigated one of 0.60 of the cooling capacity and COP is about the factor 1.1 to 1.2 higher. To achieve this improvement it is necessary to optimise the heat transfer inside the GHX using constructive steps to reach higher heat recovery factors.

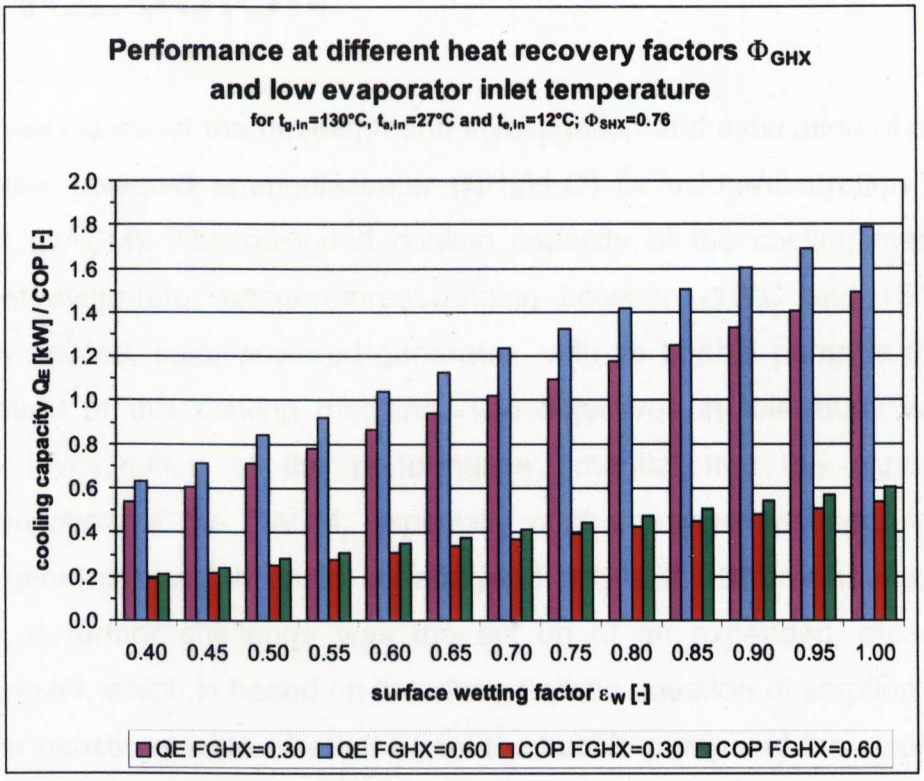

Figure 5.26: Effect of different heat recovery factors on the performance of the DACM No.2 with coaxial SHX at low evaporator inlet temperature and fixed generator heating inlet temperature of 130°C as well as high generator external mass flow versus varied surface wetting factors.

The results of the simulation runs of the DACM showed a strong influence of the surface wetting factor ε_W as well as the heat recovery factor Φ of the GHX of the falling film evaporator on the evaporator cooling capacity. Other important influences on the performance of the DACM are the heat losses Q_{Ax} and Q_{Gx} as well as $\Delta\Delta t_{min,E}$, which are determined by the varied rich solution mass flow m_{Sr} which is dependant on the bubble pump performance. The heat transfer coefficients UA_X and the initial internal component temperatures also have an important influence on the determined performance.

CHAPTER 06

CONCLUSION

This thesis is about the development, investigation and simulation of a single-effect solar powered ammonia/water (NH_3/H_2O) Diffusion-Absorption Cooling Machine (DACM). The designed cooling capacity of the cooling machine is 2.5kW at evaporator temperatures ranging between -10°C and +5°C. The indirectly heated, solar powered generator with its bubble pump is the main new feature of this cooling machine. The objectives in this study were the detailed investigation of the performance potential and the experimental characterisation of the DACM, especially of the newly-developed, indirectly heated generator, which could be analysed only with external measurement devices. A further challenge was the set up of an expanded, steady-state DACM model, which is based on the characteristic equation of sorption chillers. The main questions were whether or not the bubble pump and the auxiliary gas circuit would work and what performance the DACM prototypes could achieve.

A detailed theoretical investigation was done for the performance of the generator as well as for the auxiliary gas circuit. For the optimal operation flow regime for the generator of the DACM, equations for the upper and lower boundary of slug flow are presented. When run under normal operating conditions, slug flow usually occurs when the inner tube diameter ranged between 5mm and 41mm. Furthermore, for a wide operation range of the DACM, the inner heat transfer coefficients for the generator/bubble pump, the falling film evaporator and the falling film absorber are presented.

A further characteristic of the DACM was investigated: the cooling loss, which is caused by the temperature rise in the absorber of the circulated auxiliary gas.

This leads to a strong influence of the heat recovery factor of the gas heat exchanger (GHX).

For this project, two DACM prototypes were built and operated. Data acquisition was conducted under laboratory conditions as well as under simulated field conditions for vacuum-tube collectors. The first pilot plant of the DACM was set up in the Building Physics laboratories at the Stuttgart University of Applied Sciences, Germany in October of 2000. A series of measurements were performed from November of 2000 to March of 2002 on the pilot plant of the first DACM. The results showed that the coefficient of performance values (COP) ranged from 0.1 to 0.2 and that the evaporator cooling capacity of the pilot plant could reach 1.5 kW, but that the operation stability was insufficient.

The second optimised and compacted prototype was built based on the experiences gained from the first, using partly standard components such as nickel soldered plate heat exchangers and a coaxial heat exchanger. For this much more compact prototype, the auxiliary gas circuit was constructively reworked and a further generator was developed. The second prototype was put into operation in July of 2003 and is still running steadily. The achieved COPs were between 0.2 and 0.5 and the continuous evaporator cooling capacity between 1.0kW and 1.6kW at evaporator outlet temperatures for air-conditioning between 22°C and 15°C. Due to insufficient evaporation efficiency a maximum cooling performance of 2.0kW could only be reached if the evaporator temperature was set to a relatively high value of 25°C. The generator heating inlet temperatures of DACM No.1 (147°C-175°C) could be reduced in DACM No.2 to 110°C-155°C.

If the DACM will be powered by vacuum-tube collectors an overall system performance of 0.15 up to 0.25 could be achieved with the latest COP of 0.5 and a collector efficiency including tubing and heat storage of 0.3 to 0.5.

In addition, the performance of the bubble pump as well as that of the evaporator were investigated in detail using experimental data. The lifted ammonia/water mass flows of the bubble pump for the two generators of

DACMs No.1 and No.2 were extracted from experimental data. The developed bubble pumps worked in a wide operation range at varied temperatures as well as external mass flows. For the evaporator, a theoretically possible evaporator cooling capacity was determined based on the evaluated liquid ammonia mass flow of the experimental data. The theoretically possible evaporator cooling capacity of DACM No.2 ranges between 0.6kW and 2.7kW for generator heating inlet temperature of 115°C to 155°C. In comparison, the measured cooling capacities range from 0.6kW to 1.5kW. The falling film evaporator could not evaporate all of the available liquid ammonia into the helium gas atmosphere, not even with high external evaporator inlet temperatures of around 25°C. Therefore, the falling film evaporator needs to be rebuilt with either more or longer evaporation tubes so that a larger heat transfer surface exists, which would lead to a smaller film thickness and therefore, a longer delay time. The corresponding measured COP values decrease from 0.45 to 0.25 because of the increasing measured generator heating capacity which is dependant on the external heating inlet temperature. The theoretically possible COPs again increase from 0.44 to 0.50.

The Diffusion-Absorption Cycle has been modelled starting from the constant characteristic equation of sorption chillers. An expanded, steady-state model was developed based on the exact solution of the internal mass and energy balances of each component as well as the heat transfer between external and internal temperature levels. The internal enthalpies are calculated at each time step. The model was implemented in the simulation environment INSEL and validated by experimental data of the optimised pilot plant, DACM No.2. The results of the simulation runs of the DACM showed that the performance of the DACM with variable enthalpy describes the experimental data points of the measured performance well, whereas with a constant enthalpy model the performance deviated from the measured one.

Furthermore a parameter study was carried out to determine the performance improvement of the DACM at different evaporator inlet as well as cooling water temperatures and surface wetting factors as well as GHX heat recovery factors.

The COP as well as the evaporator cooling capacity decrease at lower evaporator temperatures. For the current DACM No.2 with coaxial solution heat exchanger (SHX), the design cooling capacity of 2.5kW could be reached for 12°C and 24°C evaporator inlet temperatures at a generator heating inlet temperature of 162°C as well as 123°C. The corresponding COPs are 0.38 and 0.85. Furthermore, the lower the absorber cooling inlet temperature, the higher is the resulting evaporator cooling capacity.

A strong influence on the evaporator cooling capacity is given by the surface wetting factor of the falling film evaporator as well as the heat recovery factor of the GHX. With a higher surface wetting factor as well as a better evaporation efficiency, the evaporator cooling capacity and the COP increase by a factor 2 for a surface wetting factor of 0.50 to 1.00. The difference of cooling capacity and COP between the empirically fitted heat recovery factor of 0.30 and a doubled one is about the factor 1.1 to 1.2 higher.

Further development is required for the DACM regarding evaporator cooling capacity and COP as well as decreasing generator heating temperatures, weight and height reduction. The performance could be increased if a surface structuring inside the evaporator falling film tubes could increase the surface wetting factor to 100% of the disposable total heat transfer surface. Another possibility for further improvement is to optimise the heat transfer inside the GHX using constructive steps to reach higher heat recovery factors. Moreover, an increase of generator performance could be reached if more lifting tubes and baffles are used.

For the use of the DACM model with other generator geometry, further measurement data of the bubble pump mass flow are required. Furthermore detailed investigations about the distribution of the ammonia liquid and ammonia/water solution and with that the surface wetting factor in the falling film evaporator and absorber should be carried out to validate the used values for the simulation. Further detailed models for the SHX and the GHX could be developed and implemented into the existing DACM model to replace the empirically-fitted heat recovery factors.

APPENDIX A

COEFFICIENTS FOR THE EQUATIONS OF THERMODYNAMIC PROPERTIES OF AMMONIA/HELIUM GAS MIXTURE

Enthalpy coefficients a_{ij}, b_{ij}, c_{ij} and d_{ij} (table A.1) for the equation (3.42).

Table A.1: Enthalpy coefficients a_{ij}, b_{ij}, c_{ij} and d_{ij} for equation (3.42) of ammonia/helium gas mixtures (Kouremenos *et al.*, 1994).

i \ j		1	2	3	4
1	a	1476.95276	-5.65650225	2.62426466 E-1	-3.83841177 E-3
	b	-212.079758	15.7624807	-2.16320410 E-1	2.00581457 E-3
	c	286.694611	-26.0213814	5.34934223 E-1	-2.86757690 E-3
	d	-352.567474	-1.17947042	1.42833877	-4.22762260 E-2
2	a	5.05881643	2.14781090 E-2	-9.45075124 E-4	1.35851623 E-5
	b	2.86017879 E-2	-6.54046475 E-1	2.38566640 E-2	-3.40542232 E-4
	c	-13.7835731	3.05396199	-1.55906200 E-1	2.45196954 E-3
	d	29.5349674	-3.92910051	1.38182058 E-1	-1.30550574 E-3
3	a	-5.06493356 E-3	6.53379363 E.4	-2.52508962 E-5	3.15325138 E-7
	b	1.68263688 E-1	-2.03084032 E-2	7.85662792 E-4	-9.45719239 E-6
	c	-6.47288560 E-1	7.98220932 E-2	-2.86676338 E-3	3.15920660 E-5
	d	6.53565883 E-1	-8.15208908 E-3	-3.76154800 E-3	1.15498216 E-4
4	c	-1.46762504 E-5	-4.38418239 E-4	3.30343355 E-5	-5.82383961 E-7
	d	-1.00636351 E-2	-1.72583386 E-4	9.15883283 E-5	-2.69018687 E-6

APPENDIX A

Density coefficients e_{ij}, g_{ij}, and q_{ij} (table A.2) for the equation (3.38).

Table A.2: Density coefficients e_{ij}, g_{ij}, and q_{ij} for equation (3.38) of ammonia/helium gas mixtures (Kouremenos *et al.*, 1994).

i \ j		1	2	3
1	e	0.783043504	-3.52830030 E-2	5.24585776 E-4
	g	-5.93995750 E-1	2.65275444 E-2	-3.92446964 E-4
	q	-1.07921604 E-2	2.53040926 E-4	-3.63803338 E-6
2	e	2.84550525 E-3	-1.28720508 E-4	1.91503590 E-6
	g	-1.99616444 E-3	9.02087849 E-5	-1.35969617 E-6
	q	-9.12767136 E-4	6.68256980 E-5	-1.21432697 E-6
3	e	1.10160762 E-7	-1.81692580 E-8	4.61392812 E-10
	g	-2.14225133 E-6	3.39586506 E-7	-8.46036218 E-9
	q	-1.10778664 E-5	6.64228991 E-7	-1.10745945 E-8
4	q	7.08289292 E-7	-5.75426426 E-8	1.13067588 E-9

Thermal conductivity coefficients L_{ij}, M_{ij}, and N_{ij} (table A.3) for the equation (3.39).

Table A.3: Thermal conductivity coefficients L_{ij}, M_{ij}, and N_{ij} for equation (3.39) of ammonia/helium gas mixtures (Kouremenos *et al.*, 1994).

i \ j		1	2	3
1	L	1.39205828 E-1	1.65660545 E-4	-1.57935631 E-6
	M	3.14163335 E-4	9.77224701 E-8	-3.19329674 E-10
	N	1.61763303 E-9	-2.61013877 E-10	6.15206627 E-12
2	L	-1.97049956 E-2	-2.73957357 E-5	2.55797175 E-7
	M	-3.31229057 E-5	-5.79658809 E-9	-1.84836229 E-10
	N	3.20602993 E-8	4.384885683 E-10	-1.08778194 E-11
3	L	-8.41736048 E-2	-1.20077733 E-4	1.17914271 E-6
	M	-1.41068332 E-4	-6.51024194 E-8	8.35924038 E-11
	N	-2.15043112 E-8	8.54476878 E-10	-1.51804679 E-11
4	N	4.41032099 E-8	3.02888436 E-10	-8.93278333 E-12

Viscosity coefficients G_{1j}, and G_{ij} (table A.4) for the equation (3.40).

Table A.4: Viscosity coefficients G_{1j}, and G_{ij} for the equation (3.40) of ammonia/helium gas mixtures (Kouremenos *et al.*, 1994).

i \ j	1	2	3	4
1	125.438244	-5.92668003 E-1	1.70377422 E-3	0.00
2	-3187.94959	32.1592716	-1.02228426 E-1	1.04727586 E-4
3	-3417.10983	46.0480856	-2.05679550 E-1	2.99563317 E-4
4	10066.9955	-120.364932	4.92959221 E-1	-6.73200449 E-4
5	-4220.68275	50.5259062	-2.12384392 E-1	2.98791180 E-4

Saturation mass concentration coefficients t_{ij} (table A.5) for the equation (3.41).

Table A.5: Saturation mass concentration coefficients t_{ij} for equation (3.41) of ammonia/helium gas mixtures (Kouremenos *et al.*, 1994).

i \ j	1	2	3
1	1.02063477	-3.06832790 E-2	3.74321593
2	1.26410694 E-2	2.73928799 E-5	-2.72186275 E-6
3	-2.14083294 E-4	1.36778544 E-5	-1.92138614 E-7
4	-1.54493295 E-6	-8.87888162 E-9	5.82381365 E-10
5	4.82498805 E-8	-3.06660208 E-9	4.73415473 E-11
6	4.64458471 E-10	-2.72208418 E-11	5.41188133 E-13

APPENDIX B

DERIVATION OF EXPANDED CHARACTERISTIC EQUATION OF THE DACM MODEL

Based on the characteristic equation for single-effect water/lithium bromide Absorption Cooling Machines (Ziegler, 1998a), an expanded characteristic equation for a single-effect ammonia/water DACM has been developed by the author. The used indices of the enthalpies are represented in Figure 5.2.

EVAPORATOR

The external, heat transfer and internal energy balance of the evaporator as well as mass and ammonia mass balances are defined as follows:

$$\dot{Q}_E = \dot{m}_e \bullet c_{p,e} \bullet \left(t_{e,in} - t_{e,out}\right) \tag{B.1}$$

$$\dot{Q}_E = UA_E \bullet \left(t_e - T_E\right) \tag{B.2}$$

$$\dot{Q}_E = \dot{m}_{Vr} \bullet h_{10} - \dot{m}_V \bullet h_9 - \dot{m}_{Vw} \bullet h_{13} \tag{B.3}$$

$$\dot{m}_{Vr} = \dot{m}_V + \dot{m}_{Vw} \tag{B.4}$$

$$\dot{m}_{Vr} \bullet f_{Vr} = \dot{m}_V \bullet X_V + \dot{m}_{Vw} \bullet f_{Vw} \tag{B.5}$$

In the first step the mass balance equation (B.4) is to be inserted in the enthalpy balance equation (B.3)

$$\dot{Q}_E = \left(\dot{m}_V + \dot{m}_{Vw}\right) \bullet h_{10} - \dot{m}_V \bullet h_9 - \dot{m}_{Vw} \bullet h_{13} \tag{B.6}$$

Then, enthalpy balance equation (B.6) is rearranged as follows:

$$\dot{Q}_E = \dot{m}_V \bullet (h_{10} - h_9) + \dot{m}_{Vw} \bullet (h_{10} - h_{13}) \tag{B.7}$$

For substituting the mass flow of the weak ammonia/helium gas mixture m_{Vw} [kg/s] by the ammonia vapour mass flow m_V [kg/s], the equations (3.74), (3.75), (3.76) and (5.32) were used and converted into the required quantity. For this, a dimensionless factor Z_{AUX} [-] is defined.

$$\dot{m}_{Vw} = \dot{m}_V \bullet \left[X_V \bullet \left(\frac{p_{total} - p_{Vr}}{M_{NH3} \bullet (p_{Vr} - p_{Vw})} \right) \bullet \left(M_{He} + (M_{NH3} - M_{He}) \bullet \upsilon_{Vw} \right) \right] = \dot{m}_V \bullet Z_{AUX} \tag{B.8}$$

The resulting equation (B.8) is then inserted into the equation (B.7). To simplify the resulting equation, an auxiliary gas circuit enthalpy difference H_{AUX} [kJ/kg] is defined:

$$\dot{Q}_E = \dot{m}_V \bullet (h_{10} - h_9) + \dot{m}_V \bullet (h_{10} - h_{13}) \bullet Z_{AUX} \tag{B.9}$$

$$H_{AUX} = (h_{10} - h_{13}) \bullet Z_{AUX} \tag{B.10}$$

The enthalpy equation (B.9) is therefore rearranged:

$$\dot{Q}_E = \dot{m}_V \bullet \left[(h_{10} - h_9) + H_{AUX} \right] \tag{B.11}$$

Now the extended specific evaporator capacity q_E [kJ/kg] is defined as follows:

$$q_E = (h_{10} - h_9) + H_{AUX} \tag{B.12}$$

and therefore the mass flow of the ammonia vapour m_V [kg/s] results from equations (B.11) and (B.12)

$$\dot{m}_V = \frac{\dot{Q}_E}{q_E} \tag{B.13}$$

APPENDIX B

CONDENSER

The external, heat transfer and internal energy balance of the condenser as well as mass and ammonia mass balances are defined in the following equations:

$$\dot{Q}_C = \dot{m}_c \bullet c_{p,c} \bullet \left(t_{c,out} - t_{c,in}\right) \tag{B.14}$$

$$\dot{Q}_C = UA_C \bullet \left(T_C - t_c\right) \tag{B.15}$$

$$\dot{Q}_C = \dot{m}_V \bullet \left(h_{7a} - h_8\right) \tag{B.16}$$

$$\dot{m}_V = \dot{m}_L \tag{B.17}$$

$$\dot{m}_V \bullet X_V = \dot{m}_L \bullet X_L \tag{B.18}$$

The ammonia vapour mass flow equation (B.13) is insert into the enthalpy balance equation (B.16) and from this the specific condenser enthalpy coefficient C_E [-] is substituted.

$$\dot{Q}_C = \frac{\dot{Q}_E}{q_E} \bullet \left(h_{7a} - h_8\right) = \dot{Q}_E \bullet C_E \tag{B.19}$$

$$C_E = \frac{h_{7a} - h_8}{q_E} \tag{B.20}$$

DEPHLEGMATOR

The external, heat transfer and internal energy balance of the dephlegmator as well as mass and ammonia mass balances are defined by the following equations:

$$\dot{Q}_D = \dot{m}_d \bullet c_{p,d} \bullet \left(t_{d,out} - t_{d,in}\right) \tag{B.21}$$

$$\dot{Q}_D = UA_D \bullet \left(T_D - t_d\right) \tag{B.22}$$

$$\dot{Q}_D = \dot{m}_{V1} \bullet h_7 - \dot{m}_V \bullet h_{7a} - \dot{m}_{L,deph} \bullet h_{7b} \tag{B.23}$$

$$\dot{m}_{V1} = \dot{m}_V + \dot{m}_{L,deph} \tag{B.24}$$

$$\dot{m}_{V1} \bullet X_{V1} = \dot{m}_V \bullet X_V + \dot{m}_{L,deph} \bullet X_{L,deph} \tag{B.25}$$

The mass balance equation (B.24) is inserted into equation (B.23)

$$\dot{Q}_D = \left(\dot{m}_V + \dot{m}_{L,deph}\right) \bullet h_7 - \dot{m}_V \bullet h_{7a} - \dot{m}_{L,deph} \bullet h_{7b} \tag{B.26}$$

and the enthalpy balance equation (B.26) is then rearranged as follows:

$$\dot{Q}_D = \dot{m}_V \bullet \left(h_7 - h_{7a}\right) + \dot{m}_{L,deph} \bullet \left(h_7 - h_{7b}\right) \tag{B.27}$$

For substituting the condensed water vapour mass flow $m_{L,deph}$ [kg/s] with the ammonia vapour mass flow m_V [kg/s], the mass balance equation (B.24) is inserted into the ammonia mass balance equation (B.25) and solved for the required quantity.

$$\dot{m}_{L,deph} = \dot{m}_V \bullet \frac{X_V - X_{V1}}{X_{V1} - X_{L,deph}} \tag{B.28}$$

The ammonia vapour and the condensed water vapour mass flow equations (B.13) and (B.28) are inserted into the enthalpy balance equation (B.27), resulting in the specific dephlegmator enthalpy coefficients D_E [-] and $D_{E,deph}$ [-].

$$\begin{aligned} \dot{Q}_D &= \frac{\dot{Q}_E}{q_E} \bullet \left(h_7 - h_{7a}\right) + \frac{\dot{Q}_E}{q_E} \bullet \left(\frac{X_V - X_{V1}}{X_{V1} - X_{L,deph}}\right) \bullet \left(h_7 - h_{7b}\right) \\ &= \dot{Q}_E \bullet D_E + \dot{Q}_E \bullet D_{E,deph} \end{aligned} \tag{B.29}$$

$$D_E = \frac{h_7 - h_{7a}}{q_E} \tag{B.30}$$

$$D_{E,deph} = \frac{h_7 - h_{7b}}{q_E} \bullet \left(\frac{X_V - X_{V1}}{X_{V1} - X_{L,deph}}\right) \tag{B.31}$$

GENERATOR

The external, heat transfer and internal energy balance of the generator as well as mass and ammonia mass balances are defined in the following equations:

$$\dot{Q}_G = \dot{m}_g \bullet c_{p,g} \bullet \left(t_{g,in} - t_{g,out}\right) \tag{B.32}$$

$$\dot{Q}_G = UA_G \bullet \left(t_g - T_G\right) \tag{B.33}$$

$$\dot{Q}_G = \dot{m}_{V1} \bullet h_7 - \dot{m}_{L,deph} \bullet h_{7b} + \dot{m}_{Sw} \bullet h_1 - \dot{m}_{Sr} \bullet h_6 \tag{B.34}$$

$$\dot{m}_{V1} + \dot{m}_{Sw} = \dot{m}_{L,deph} + \dot{m}_{Sr} \tag{B.35}$$

$$\dot{m}_{V1} \bullet X_{V1} + \dot{m}_{Sw} \bullet X_{Sw} = \dot{m}_{L,deph} \bullet X_{L,deph} + \dot{m}_{Sr} \bullet X_{Sr} \tag{B.36}$$

The mass balance equations (B.24) and (B.35) are inserted into equation (B.34)

$$\dot{Q}_G = \left(\dot{m}_V + \dot{m}_{L,deph}\right) \bullet h_7 - \dot{m}_{L,deph} \bullet h_{7b} + \left(\dot{m}_{L,deph} + \dot{m}_{Sr} - \left(\dot{m}_V + \dot{m}_{L,deph}\right)\right) \bullet h_1 - \dot{m}_{Sr} \bullet h_6 \tag{B.37}$$

The enthalpy balance equation (B.37) is then rearranged as:

$$\dot{Q}_G = \dot{m}_V \bullet \left(h_7 - h_1\right) + \dot{m}_{Sr} \bullet \left(h_1 - h_6\right) + \dot{m}_{L,deph} \bullet \left(h_7 - h_{7b}\right) \tag{B.38}$$

The ammonia vapour mass flow equation (B.13) and the condensed water vapour mass flow equation (B.28) are inserted into the enthalpy balance equation (B.38) and as a result, the specific generator enthalpy coefficients G_E [-] and $G_{E,deph}$ [-] as well as the solution heat loss Q_{Gx} [kW] are obtained.

$$\begin{aligned} \dot{Q}_G &= \frac{\dot{Q}_E}{q_E} \bullet \left(h_7 - h_1\right) + \dot{m}_{Sr} \bullet \left(h_1 - h_6\right) + \frac{\dot{Q}_E}{q_E} \bullet \left(\frac{X_V - X_{V1}}{X_{V1} - X_{L,deph}}\right) \bullet \left(h_7 - h_{7b}\right) \\ &= \dot{Q}_E \bullet G_E + \dot{Q}_{Gx} + \dot{Q}_E \bullet G_{E,deph} \end{aligned} \tag{B.39}$$

$$G_E = \frac{h_7 - h_1}{q_E} \tag{B.40}$$

$$\dot{Q}_{Gx} = \dot{m}_{Sr} \bullet (h_1 - h_6) \tag{B.41}$$

$$G_{E,deph} = \frac{h_7 - h_{7b}}{q_E} \bullet \left(\frac{X_V - X_{V1}}{X_{V1} - X_{L,deph}} \right) \tag{B.42}$$

ABSORBER

The external, heat transfer and internal energy balance of the absorber as well as mass and ammonia mass balances are defined by the following equations:

$$\dot{Q}_A = \dot{m}_a \bullet c_{p,a} \bullet (t_{a,out} - t_{a,in}) \tag{B.43}$$

$$\dot{Q}_A = UA_A \bullet (T_A - t_a) \tag{B.44}$$

$$\dot{Q}_A = \dot{m}_{Sw} \bullet h_3 - \dot{m}_{Sr} \bullet h_4 + \dot{m}_{Vr} \bullet h_{11} - \dot{m}_{Vw} \bullet h_{12} \tag{B.45}$$

$$\dot{m}_{Sw} + \dot{m}_{Vr} = \dot{m}_{Sr} + \dot{m}_{Vw} \tag{B.46}$$

$$\dot{m}_{Sw} \bullet X_{Sw} + \dot{m}_{Vr} \bullet f_{Vr} = \dot{m}_{Sr} \bullet X_{Sr} + \dot{m}_{Vw} \bullet f_{Vw} \tag{B.47}$$

The mass balance equations (B.46) and (B.4) are inserted into equation (B.45)

$$\dot{Q}_A = \left(\dot{m}_{Sr} + \dot{m}_{Vw} - (\dot{m}_V + \dot{m}_{Vw}) \right) \bullet h_3 - \dot{m}_{Sr} \bullet h_4 + (\dot{m}_V + \dot{m}_{Vw}) \bullet h_{11} - \dot{m}_{Vw} \bullet h_{12} \tag{B.48}$$

and the enthalpy balance equation (B.48) is then rearranged as:

$$\dot{Q}_A = \dot{m}_V \bullet (h_{11} - h_3) + \dot{m}_{Sr} \bullet (h_3 - h_4) + \dot{m}_{Vw} \bullet (h_{11} - h_{12}) \tag{B.49}$$

The ammonia vapour and the weak ammonia/helium gas mixture mass flow equations (B.13) and (B.8) are inserted into the enthalpy balance equation

(B.49) and thereby the specific absorber enthalpy coefficients A_E [-] and $A_{E,aux}$ [-] as well as the solution heat loss Q_{Ax} [kW] are obtained.

$$\begin{aligned}\dot{Q}_A &= \frac{\dot{Q}_E}{q_E}\bullet(h_{11}-h_3)+\dot{m}_{Sr}\bullet(h_3-h_4)+\frac{\dot{Q}_E}{q_E}\bullet(h_{11}-h_{12})\bullet Z_{AUX} \\ &= \dot{Q}_E\bullet A_E+\dot{Q}_{Ax}+\dot{Q}_E\bullet A_{E,aux}\end{aligned} \tag{B.50}$$

$$A_E = \frac{h_{11}-h_3}{q_E} \tag{B.51}$$

$$\dot{Q}_{Ax} = \dot{m}_{Sr}\bullet(h_3-h_4) \tag{B.52}$$

$$A_{E,aux} = \frac{h_{11}-h_{12}}{q_E}\bullet Z_{AUX} \tag{B.53}$$

The **capacity equations** could be summarised by the following:

$$\dot{Q}_E = UA_E\bullet(t_e-T_E) \tag{B.54}$$

$$\dot{Q}_C = \dot{Q}_E\bullet C_E = UA_C\bullet(T_C-t_c) \tag{B.55}$$

$$\dot{Q}_G = \dot{Q}_E\bullet G_E+\dot{Q}_{Gx}+\dot{Q}_E\bullet G_{E,deph} = UA_G\bullet(t_g-T_G) \tag{B.56}$$

$$\dot{Q}_A = \dot{Q}_E\bullet A_E+\dot{Q}_{Ax}+\dot{Q}_E\bullet A_{E,aux} = UA_A\bullet(T_A-t_a) \tag{B.57}$$

EXPANDED CHARACTERISTIC EQUATION OF THE DACM

The Dühring rule and with it the constant B [-] accounts for the different slopes of the isosteres in the solution field where the internal temperatures T_X [°C] of the heat exchangers generator, absorber condenser, and evaporator can be combined as follows:

$$(T_G-T_A) = (T_C-T_E)\bullet B \tag{B.58}$$

The resulting capacity equations (B.54), (B.55), (B.57) and (B.56) could be solved for the mean internal temperatures T_X [°C] and put in the Dühring equation (B.58).

$$\left(t_g - \frac{\dot{Q}_E \bullet G_E + \dot{Q}_{Gx} + \dot{Q}_E \bullet G_{E,deph}}{UA_G} - \left(t_a + \frac{\dot{Q}_E \bullet A_E + \dot{Q}_{Ax} + \dot{Q}_E \bullet A_{E,aux}}{UA_A}\right)\right) = \left(t_c + \frac{\dot{Q}_E \bullet C_E}{UA_C} - \left(t_e - \frac{\dot{Q}_E}{UA_E}\right)\right) \bullet B \tag{B.59}$$

The resulting equation (B.59) is then rearranged and solved for the evaporator cooling capacity Q_E [kW].

$$\left(t_g - t_a - \dot{Q}_E\left(\frac{G_E + G_{E,deph}}{UA_G} + \frac{A_E + A_{E,aux}}{UA_A}\right) - \frac{\dot{Q}_{Gx}}{UA_G} - \frac{\dot{Q}_{Ax}}{UA_A}\right) = \left(t_c - t_e + \dot{Q}_E\left(\frac{C_E}{UA_C} + \frac{1}{UA_E}\right)\right) \bullet B \tag{B.60}$$

$$\dot{Q}_E = \left(\left(\frac{C_E}{UA_C} + \frac{1}{UA_E}\right) \bullet B + \left(\frac{G_E + G_{E,deph}}{UA_G} + \frac{A_E + A_{E,aux}}{UA_A}\right)\right)^{-1} \bullet \left(t_g - t_a - (t_c - t_e) \bullet B - \frac{\dot{Q}_{Gx}}{UA_G} - \frac{\dot{Q}_{Ax}}{UA_A}\right) \tag{B.61}$$

Out of the equation (B.61), the characteristic double temperature difference $\Delta\Delta t$ [K] between the mean external generator and absorber temperatures and the external condenser and evaporator temperatures could be formed as follows:

$$\Delta\Delta t = t_g - t_a - (t_c - t_e) \bullet B \tag{B.62}$$

Furthermore, the specific enthalpy and heat transfer coefficients are rearranged into the extended slope s_E [kW/K] and the intersection $\Delta\Delta t_{min,E}$ [K].

$$s_E = \left(\left(\frac{C_E}{UA_C} + \frac{1}{UA_E} \right) \bullet B + \left(\frac{G_E + G_{E,deph}}{UA_G} + \frac{A_E + A_{E,aux}}{UA_A} \right) \right)^{-1} \quad \text{(B.63)}$$

$$\Delta\Delta t_{\min,E} = \left(\frac{\dot{Q}_{Ax}}{UA_A} + \frac{\dot{Q}_{Gx}}{UA_G} \right) \quad \text{(B.64)}$$

The resulting basic characteristic equation for the DACM is therefore:

$$\dot{Q}_E = s_E \bullet \left(\Delta\Delta t - \Delta\Delta t_{\min,E} \right) \quad \text{(B.65)}$$

Based on the basic characteristic equation (B.65), the evaporator cooling capacity $Q_{E,aux}$ [kW] with the considerate cooling loss capacity Q_{AUX} [kW] is defined as an expanded characteristic equation and as $Q_{E,\varepsilon}$ [kW] with the considerate surface wetting factor ε_W [-]. The surface wetting factor describes the amount of falling film surface inside the evaporator tubes (chapter 3.6.8). For the determination of the cooling loss capacity Q_{AUX} [kW] (which results from the incoming warm, weak gas mixture), specifically the auxiliary gas circulation loss $c_{p,Vw}*m_{Vw}/m_{L,NH3}$ [kJ/kg K] (which is defined by equation (3.69)) is required.

$$\dot{Q}_{AUX} = \dot{m}_V \bullet X_V \bullet \left((T_{13} - T_E) \bullet \frac{c_{p,Vw} \bullet \dot{m}_{Vw}}{\dot{m}_{L,NH3}} \right) \quad \text{(B.66)}$$

$$\dot{Q}_{E,aux} = s_E \bullet \left(\Delta\Delta t - \Delta\Delta t_{\min,E} \right) - \dot{Q}_{AUX} \quad \text{(B.67)}$$

$$\dot{Q}_{E,\varepsilon} = \varepsilon_W \bullet \dot{Q}_{E,aux} \quad \text{(B.68)}$$

REFERENCES

AFONSO, A. and COLLARES-PEREIRA, M. and DE OLIVEIRA, J.C. and MENDES, J.F. (2003). *A solar/gas powered absorption prototype to provide small power heating and cooling.* Proceedings of the ISES Solar World Congress 2003. 16.-19. June, International Solar Energy Society (ISES), Göteborg, Sweden. ISBN 91-631-4740-8.

AJIB, S. and SCHULTHEIS, P. (1998). *Untersuchungsergebnisse einer solarthermisch betriebenen Absorptionskälteanlage* (Investigation results of a Solar Thermal Driven Absorption Cooling Unit). TAB Technik am Bau. No. 2, pp. 49-54. ISSN 0341-2032.

AJIB, S. and NILIUS, A. and KARNO, A. (2004). *Erste Untersuchungsergebnisse eines Versuchsstandes einer niedertemperatur-betriebenen Absorptionskältemaschine* (First investigation results at a test stand of a low-temperature driven Absorption Refrigeration Machine). Proceedings of the 14th Symposium Thermische Solarenergie. Ostbayerisches Technologie-Transfer-Institut e.V. (OTTI), Staffelstein, Germany. pp. 488-493. ISBN 3-934681-33-6.

ALBERS, J. (2002). *Betriebserfahrungen mit solar gestützter Absorptionskälte bei den Bundesbauten in Berlin* (Experiences gained in the operation of solar-assisted absorption cooling at the buildings of the German government in Berlin). Proceedings of the 2nd Symposium Solares Kühlen in der Praxis. Fachhochschule Stuttgart - Hochschule für Technik, Germany. Vol. 56, pp. 135-144.

ALBERS, J. (2002). *Simulation des Teillastverhaltens von Absorptions-kälteanlagen für die solare Kälteerzeugung* (Simulation of the part load behaviour of Absorption Chillers for the solar cooling). Proceedings of the 12th Symposium Thermische Solarenergie. 24.-26. April, Ostbayerisches Technologie-Transfer-Institut e.V. (OTTI), Staffelstein, Germany. pp. 246-250, ISBN 3-934681-20-4.

REFERENCES

ALBERS, J. and ZIEGLER, F. (2003). *Analysis of the part load behaviour of sorption chillers with thermally driven solution pump.* Proceedings of the 21st IIR International Congress of Refrigeration. 17th-22nd August, International Institute of Refrigeration (IIR), Washington D.C., USA. ISBN 2-913149-32-4.

ALBRING, P. (2001) *Anlagen und Systeme der solaren Kälteerzeugung* (Plants and systems of the solar cold production). Proceedings of the 1st Symposium Solares Kühlen in der Praxis. Fachhochschule Stuttgart - Hochschule für Technik, Germany. Vol. 53, pp. 105-123.

AL-SHEMMERI, T. and WANG, Y. (2003). *Theoretical investigation and parameter study of a diffusion absorption refrigeration system.* Proceedings of the 21st IIR International Congress of Refrigeration. 17.-22. August, International Institute of Refrigeration (IIR), Washington D.C., USA. ISBN 2-913149-32-4.

AMOUS, M. (1998). *Wärme- und Stoffaustausch bei der Absorption von Ammoniak im Rieselfilm* (Heat and mass transfer by the absorption of ammonia in the falling film) (1st ed.). Aachen: Shaker Verlag, Germany. ISBN 3-8265-4038-7.

BALARAS, C. (2003) *Recent activities on absorption cooling.* Proceedings of the Workshop absorption cooling – research & development. 17.-18. January 2003. Arsenal research, Vienna, Austria.

BÄCKSTRÖM, M. (1954). *The Theory of the Evaporator working with diffusion.* Kylteknisk tidskrift. Vol. 13, No. 2, pp. 22-26. ISSN 0023-5970.

BÄCKSTRÖM, M. (1956). *Einfache Theorie der Gaszirkulation in Sorptions-Kälteapparaten nach v. Platen und Munters* (Simple theory of the gas circulation in Absorption Refrigerating Units of the v. Platen-Munters system). Transactions of the Royal Institute of Technology Stockholm. Uppsala: Almqvist & Wiksells Boktryckeri AB, Sweden. No. 101.

BÄCKSTRÖM, M. and EMBLIK, E. (1965). *Kältetechnik* (Refrigeration Technology) (3rd edit.). pp. 650-653 and pp. 676-706. Karlsruhe: Verlag G. Braun, Germany.

BEHRINGER, H. (1930). Die Flüssigkeitsförderung nach dem Mammutprinzip (The liquid lifting according to the mammoth principle). Unpub. PhD Thesis. Universität Karlsruhe, Germany.

BIESINGER, A. (2002). *Untersuchungen an einem indirekt beheizten Austreiber einer Diffusions-Absorptionskältemaschine (DAKM)* (Investigations on an indirectly heated generator of a Diffusion-Absorption Cooling Machine (DACM)). Unpub. Diploma Degree, Fachhochschule Stuttgart-Hochschule für Technik, Germany.

BLESSING, F. (2001). *Betriebsverhalten von solar betriebenen Diffusions-Absorptionskältemaschinen zur Klimatisierung und Kälteerzeugung* (Operating performance of a solar driven Diffusion-Absorption Cooling Machine for air-conditioning and refrigeration). Unpub. Diploma Degree, Fachhochschule Stuttgart-Hochschule für Technik, Germany.

BOURSEAU, P. and BUGAREL, R. (1986). *Absorption-diffusion machines: comparison of the performance of NH_3-H_2O and NH_3-NaSCN.* Int. J. Refrig.. Vol. 9, No. 4, pp. 206-214. ISSN 0140-7007.

BOURSEAU, P. and MORA, J.C. and BUGAREL, R. (1987). Coupling of *absorption-diffusion refrigeration machine and a solar flat-plate collector.* Int. J. Refrig. Vol. 10, No.4, pp. 209-216. ISSN 0140-7007.

BRAUN, R. and HESS, R. (2002). *Solar Cooling.* Proceedings of the 7th World Renewable Energy Congress. 1.-5. July, World Renewable Energy Network (WREN), Cologne, Germany. ISBN 0-08-044079-7.

BRENDEL, T. and SPINDLER, K. and MUELLER-STEINHAGEN, H. (2004). *Aufbau einer Versuchs- und Demonstrationsanlage zur solaren Kühlung am Institut für Thermodynamik und Wärmetechnik der Universität Stuttgart* (Set up of a test and demonstration rig for solar cooling at the institute of thermodynamic and heat technology of the University of Stuttgart). Proceedings of the 31st Deutsche Klima-Kälte-Tagung, Bremen, Germany. Vol. AA.II.1, pp. 145-158. ISBN 3-932715-36-5.

REFERENCES

BÜCHE, W. (1935). *Der Einfluß der Beheizung auf den Flüssigkeitsumlauf nach dem Thermosyphon-Prinzip am Beispiel der Elektrolux-Kältemaschine* (The influence of heating on the fluid circuit according to the thermosyphon principle as an example of Electrolux refrigerator). Zeitschrift für die gesamte Kälteindustrie, Vol. 42, No. 6, pp. 101-107.

BUDERUS (2003). *Gasbetriebene Wärmepumpe Loganova GWP* (Gas driven heat pump Loganova GWP). Company documents Buderus Heiztechnik GmbH, Wetzlar, Germany. URL: www.heiztechnik.buderus.de.

CAREY, V.P. (1992). *Liquid-vapor phase-change phenomena: An introduction to the thermophysics of vaporization and condensation process in heat transfer equipment* (1st ed.). Washington: Hemisphere Publishing Corporation, USA. ISBN 1-56032-074-5.

CASTRO, J. (2003). *Development of a prototype of an Air-Cooled Water-LiBr Absorption Cooling Machine for solar cooling using numerical simulation tools.* Proceedings of the Workshop absorption cooling – research & development. 17.-18. January 2003. Arsenal research, Vienna, Austria.

CATTANEO, A.G. (1935). *Über die Förderung von Flüssigkeiten mittels der eigenen Dämpfe – Thermosyphon-Prinzip* (About the lifting of liquids by their own vapours – thermosyphon principle). Zeitschrift für die gesamte Kälteindustrie, Vol. 42, No. 1,2 and 3, pp. 2-8, pp. 27-32 and pp. 48-53.

ÇENGEL, Y.A. (1998). *Heat transfer: A practical approach* (1st ed.). Boston: WCB/McGraw-Hill, USA. pp. 451-487 and pp. 623-680. ISBN 0-07-561176-7.

CHEN, J. (1995). *Further Development of the Diffusion-Absorption Refrigerator.* Unpub. PhD Thesis. University of Maryland, USA.

CHEN, J. and KIM, K.J. and HEROLD, K.E. (1996). *Performance enhancement of a diffusion-absorption refrigerator.* Int. J. Refrig. Vol. 19, No. 3; pp. 208-218. ISSN 0140-7007.

CHINNAPPA, J.C.V. (1992). Principles of Absorption Systems Machines. *in* SAYIGH, A.A.M. (Edit.) and MCVEIGH, J.C. *Solar Air Conditioning and Refrigeration* (1st ed.). Oxford: Pergamon Press Ltd., England. pp. 13-65. ISBN 0-08-040750-1.

CHISHOLM, D. (1983). *Two-phase flow in pipelines and heat exchangers*. New York: George Goodwin.

CREATHERM (1987). *Diffusions Absorptions Waermepumpe DAWP* (Diffusion Absorption Heat Pump DAHP). Company documents Creatherm AG, Schlieren, Switzerland.

DELANO, A.D. (1998). *Design Analysis of the Einstein Refrigeration Cycle*. Unpub. PhD Thesis. Georgia Institute of Technology, USA. URL: www.me.gatech.edu/energy/publications.htm.

DER KLIMAMACHER (2003). *Der Welt- und Europamarkt für Raumklimageräte* (The world and European market of air-conditioning units). CCI.Print – Der Klimamacher Wissen+Praxis. Vol. 37, No. 3. ISSN 0009-8914.

DORGAN, C.B. and LEIGHT S.P. and DORGAN, C.E. (1995). *Application Guide for Absorption Cooling/Refrigeration Using Recovered Heat*. ASHRAE ISBN 1-883413-26-5.

DUFF; W.S. and WINSTON, R. and O'GALLAGHER J:J. and BERGQUAM, J. and HENKEL, T. (2003). *Novel ICPC Solar Collector/Double Effect Absorption Chiller Demonstration Project*. Proceedings of the International Solar Energy Conference March 2003. ASME, Hawaii, USA. ISEC2003-44213.

EBER, N. (1967). *A new analysis of rectification in absorption refrigeration*. Proceedings of the 12th IIR International Congress of Refrigeration. International Institute of Refrigeration (IIR), Madrid, Spain. pp. 1339-1351.

EGGER, M. (2000). *Solare Kühlung: Demonstrationsanlage mit Absorptionskältemaschine und Röhrenkollektoren am ZAE Bayern* (Solar cooling: demonstration plant with absorption cooling machine and tube collectors at the ZAE Bayern). Unpub. Diploma Degree, ZAE Bayern, Germany.

EICKER, U. (2002). *Entwicklungstendenzen solarthermischer Kühlverfahren* (Developing tendencies of solar thermal cooling technologies). Proceedings of the 2nd Symposium Solares Kühlen in der Praxis. Fachhochschule Stuttgart - Hochschule für Technik, Germany. Vol. 56, pp. 6-16.

REFERENCES

EICKER, U. (2004). *Perspektiven und Entwicklungstendenzen für Solares Kühlen* (perspectives and development tendencies of solar cooling). Proceedings of the 3rd Symposium Solares Kühlen in der Praxis. Fachhochschule Stuttgart - Hochschule für Technik, Germany. Vol. 65, pp.5-24.

ENTEX (2004a). *Gaswärmepumpe aus der* Schweiz (Gas heat pump from Switzerland). Sonne Wind & Wärme. Vol. 28, No. 10, pp. 34. ISSN 0944-8772.

ENTEX (2004b). Company internet documents Entex Energy Ltd, Eggenwil, Switzerland. URL: www.entex-energy.ch.

GEE; R. and COHEN, G. and GREENWOOD, K. (2003). *Operation and Preliminary Performance of the Duke Solar Power Roof: A roof-integrated Solar Cooling and Heating System.* Proceedings of the International Solar Energy Conference March 2003. ASME, Hawaii, USA. ISEC2003-44035.

GROß, U. (1991). *Kondensation und Verdampfung im geschlossenen Thermosyphon* (Condensation and evaporation in the closed thermosyphon) (1st ed.). Düsseldorf: VDI Verlag, Germany. Fortschritt-Berichte VDI Reihe 19, No. 46. ISBN 3-18-144619-X.

GROSSMAN, G. (2002). *Solar-powered systems for cooling, dehumidification and air-conditioning.* Solar Energy. Vol. 72, No. 1, pp. 53-62. ISSN 0038-092X.

GUINEY, B. and HENKEL, T. (2003). *Solar thermal for cooling, heating and power generation.* Renewable Energy World. Vol. 6, No. 2, pp. 92-98. ISSN 1462-6381.

GUTIÉRREZ, F. (1988). Behaviour of a household *absorption-diffusion refrigerator adapted to autonomous solar operation.* Solar Energy. Vol. 40, No. 1, pp. 17-23. ISSN 0038-092X.

HANSEN, C. (1993a). *Solare Klimatisierung – Beispiel in Benidorm/Spanien* (Solar air-conditioning – example in Benidorm/Spain). Sonnenenergie. Vol. 18, No. 2, pp. 8-9. ISSN 0172-3278.

HANSEN, C. (1993b). *Solare Klimatisierung* (Solar climatisation). Ki Klima-Kälte-Heizung. Vol. 21, No. 9, pp. 356-357. ISSN 0172-1984.

HARTMANN, K. (1992). *Kälteerzeugung in Absorptionsanlagen* (Cold production of absorption plants). Die Kälte- und Klimatechnik. Vol. 45, No. 9. ISSN 0343-2246.

HELLMANN, H.-M. and GROSSMANN, G. (1996). *Improved Property Data Correlations of Absorption Fluid for Computer Simulation of Heat Pump Cycles.* ASHRAE Transactions. AT-96-17-3, pp. 980-997.

HELLMANN, H.-M. and SCHWEIGLER, C. and ZIEGLER, F. (1999). *The characteristic equation of sorption chillers.* Proceedings of the International Sorption Heat Pump Conference (ISHPC 99). 24.-26. March, Munich, Germany. pp. 169-172.

HENNING, H.-M. (2001). *Energetische und wirtschaftliche Aspekte solar unterstützter Klimatisierung* (Energetic and economical aspects of solar assisted air-conditioning). Proceedings of the 1st Symposium Solares Kühlen in der Praxis. Fachhochschule Stuttgart - Hochschule für Technik, Germany. Vol. 53, pp. 22-42.

HENNING, H.-M. (Ed.) (2004). *Solar-Assisted Air-Conditioning in Buildings – A Handbook for Planners* (1st ed.). Wien New York: Springer-Verlag, Austria. pp. 121-124. ISBN 3-211-00647-8.

HEROLD, K.E. and CHEN, J. (1993). *Diffusion-Absorption Heat Pump.* Annual Report for Gas Research Institute, GRI-93/0055. Gas Research Institute, USA.

HEROLD, K.E. (1996). *Diffusion-Absorption Heat Pump.* Final Report for Gas Research Institute,. GRI-96/0271. Gas Research Institute, USA.

HEROLD, K.E. and RADERMACHER, R. and KLEIN, S.A. (1996). *Absorption Chillers and Heat Pumps* (1st edit.). Boca Raton: CRC Press, USA. pp. 235-242. ISBN 0-8493-9427-9.

HIRSCHBERG, H.G. (1988). *Wärmeträger* (Heat Transfer Medium). *in* PLANK, R. *Handbuch der Kältetechnik* (1st ed.). Berlin: Springer-Verlag, Germany. Vol. 6B, pp. 590-623. ISBN 3-540-15477-9.

HÖHNE, J. (1998). *Untersuchungen zum gekoppelten Stoff- und Wärmeübergang bei nichtadiabater Absorption im Film- und Blasenabsorber* (Investigations to the coupled mass and heat transmission by not adiabatic absorption in film and bubble absorber) (1st ed.). Düsseldorf: VDI Verlag, Germany. Fortschritt-Berichte VDI Reihe 3, No. 528. ISBN 3-18-352803-7.

HOLTER, C. and MEIßNER, E. (2003). *Solar cooling system in Pristina/Kosovo.* Proceedings of the ISES Solar World Congress 2003. 16.-19. June, International Solar Energy Society (ISES), Göteborg, Sweden. ISBN 91-631-4740-8.

HÖPER, F. (1999). *Optimierte Anlagenschaltung zur solaren Kühlung mit Absorptionstechnik* (Optimised design for solar cooling with absorption refrigeration units). KI Luft- und Kältetechnik. Vol. 35, No. 8, pp. 397-400. ISSN 0945-0459.

IEA (2002a). Air-Cooled Water-LiBr Absorption Cooling Machine of Low Capacity for Air Conditioning (ACABMA). *in* IEA SHC TASK 25 PROJECT GROUP - SOLAR-ASSISTED AIR-CONDITIONING OF BUILDINGS. *Ongoing research relevant for solar assisted air-conditioning systems - Technical report* (1st ed.). International Energy Agency (IEA) Task 25. pp. 56-59. Appendix 2f.

IEA (2002b). Residential solar air conditioning system (MAGESCLI). *in* IEA SHC TASK 25 PROJECT GROUP - SOLAR-ASSISTED AIR-CONDITIONING OF BUILDINGS. *Ongoing research relevant for solar assisted air-conditioning systems - Technical report* (1st ed.). International Energy Agency (IEA) Task 25. pp. 29-32. Appendix 2a.

INCROPERA, F.P. and DEWITT, D.P. (1996). *Fundamentals of heat and mass transfer* (4th ed.). New York: John Wiley & Sons, USA. pp. 535-570 and pp. 783-817. ISBN 0-471-30460-3.

JAIN, P.C. and GABLE, G.K. (1971). *Equilibrium property data equations for aqua-ammonia mixtures.* ASHRAE Transactions. No. 2180, pp. 149-151.

JAKOB, U. (2000). *Systemtechnische Optimierung einer solarbetrieben Diffusions-Absorptionskälteanlage* (System Optimisation of a Solar Driven Diffusion-Absorption Cooling Unit). Unpub. Diploma Degree, Fachhochschule Stuttgart-Hochschule für Technik, Germany.

JAKOB, U. and SCHNEIDER, D. and EICKER, U. (2001). *Entwicklung einer solar betriebenen Diffusions-Absorptions-Kältemaschine* (Development of a Solar Powered Diffusion-Absorption Cooling Machine). Proceedings of the 11th Symposium Thermische Solarenergie. 9.-11. May, Ostbayerisches Technologie-Transfer-Institut e.V. (OTTI), Staffelstein, Germany. pp. 170-175, ISBN 3 934681-14-X.

JAKOB, U. (2001). *Investigations into Solar Powered Diffusion Absorption Cooling Machines*. Unpub. MPhil to PhD Transfer Report, De Montfort University Leicester, U.K..

JAKOB, U. and EICKER, U. (2002). *Solar Cooling with Diffusion Absorption Principle*. Proceedings of the 7th World Renewable Energy Congress. 1.-5. July, World Renewable Energy Network (WREN), Cologne, Germany. ISBN 0-08-044079-7.

JAKOB, U. (2002). Solar-driven diffusion absorption chiller. *in* IEA SHC TASK 25 PROJECT GROUP - SOLAR-ASSISTED AIR-CONDITIONING OF BUILDINGS. *Ongoing research relevant for solar assisted air-conditioning systems - Technical report* (1st edit.). International Energy Agency (IEA) Task 25. pp. 33-39. Appendix 2b.

JAKOB, U. and EICKER, U. and SCHNEIDER, D. and TAKI, A.H. and COOK, M.J. (2003a). *Entwicklung einer optimierten solar betriebenen Diffusions-Absorptionskältemaschine* (Development of an optimised solar driven Diffusion-Absorption Cooling Machine). Proceedings of the 13th Symposium Thermische Solarenergie. 14.-16. May, Ostbayerisches Technologie-Transfer-Institut e.V. (OTTI), Staffelstein, Germany. pp. 259-264, ISBN 3-934681-26-3.

JAKOB, U. and EICKER, U. and TAKI, A.H. and COOK, M.J. (2003b). *Development of an optimised solar driven Diffusion-Absorption Cooling Machine*. Proceedings of the ISES Solar World Congress 2003. 16.-19. June, International Solar Energy Society (ISES), Göteborg, Sweden. ISBN 91-631-4740-8.

JAKOB, U. and SCHNEIDER, D. and EICKER, U. (2004a). *Entwicklung einer Diffusions-Absorptionskältemaschine kleiner Leistung (2.5 kW)* (Development of a small scale Diffusion-Absorption Cooling Machine (2.5 kW)). Proceedings of the 3rd Symposium Solares Kühlen in der Praxis. Fachhochschule Stuttgart - Hochschule für Technik, Germany. Vol. 65, pp. 125-144.

REFERENCES

JAKOB, U. and EICKER, U. and SCHNEIDER, D. and COOK, M.J. and TAKI, A.H. (2004b). *Neue Ergebnisse einer solar thermisch betriebenen Diffusions-Absorptionskältemaschine kleiner Leistung* (New results of a small scale solar thermal driven Diffusion-Absorption Cooling Machine). Proceedings of the 14th Symposium Thermische Solarenergie. 12.-14. May, Ostbayerisches Technologie-Transfer-Institut e.V. (OTTI), Staffelstein, Germany. pp. 482-487, ISBN 3-934681-33-6.

KAITA, Y. (2001). *Thermodynamic properties of lithium bromide-water solutions at high temperatures*. Int. J. Refrig.. Vol. 24, pp. 374-390. ISSN 0140-7007.

KARBACH, A. and FISCHER, H. and NIEBELING, D. (1997). *Solare Kühlung – Erneuerbare Energien möglichst effizient nutzen* (Solar cooling – use renewable energy possible effectively. HLH. Vol. 48, No. 10, pp. 47-50. ISSN 1436-5103.

KARBACH, A. (1998). Solare Kühlung (Solar cooling). *in* VDI BERICHTE. *Kälteversorgung in der technischen Gebäudeausrüstung* (1st edit.). Düsseldorf: VDI-Verlag, Germany. No. 1432, pp. 85-95. ISBN 3-18-091432-7.

KAUSHIK, S.C. (1983). Solar Absorption Refrigeration and Space Conditioning: Thermal Modelling of Aqua-Ammonia Cycle. *in* SODHA, M.S. (Ed.) and MATHUR, S.S. and MACIK, M.A.S. *Reviews of Renewable Energy Resources* (1st ed.). New Delhi: Wiley Eastern Limited, India. pp. 230-322.

KEIZER, C. (1979). *Absorption refrigeration machine driven by solar heat*. Proceedings of the 15th IIR International Congress of Refrigeration. International Institute of Refrigeration (IIR), Venetian, Italy. pp. 861-868.

KIM, D.S. and INFANTE FERREIRA, C.A. (2003). *Solar Absorption Cooling*. 1st Progress Report. Delft University of Technology, Report K-332. Novem.

KIM, K.J. and CHEN, J. and SHI, Z. and HEROLD, K.E. (1994). *Diffusion-Absorption Heat Pump*. Annual Report for Gas Research Institute, GRI-94/0080. Gas Research Institute, USA.

KIM, K.J. and SHI, Z. and CHEN, J. and HEROLD, K.E. (1995). *Hotel room air conditioner design based on the Diffusion-Absorption cycle*. ASHRAE Technical Data Bulletin. Vol. 11, No. 2, pp. 47-58.

KIMURA, K. (1992). Solar Absorption Cooling. *in* SAYIGH, A.A.M. (Edit.) and MCVEIGH, J.C. *Solar Air Conditioning and Refrigeration* (1st ed.). Oxford: Pergamon Press Ltd., England. pp. 13-65. ISBN 0-08-040750-1.

KOHLENBACH, P. and MEDEL Y MOLERO, S. and SCHWEIGLER, C. and HARM, M. and ALBERS, J. and KUEHN, A. and PETERSEN, S. (2004a). *Weiterentwicklung und Feldtest einer kompakten 10kW H_2O/LiBr Absorptionskälteanlage* (Further development of a compact 10kW H_2O/LiBr Absorption Chiller). Proceedings of the 3rd Symposium Solares Kühlen in der Praxis. Fachhochschule Stuttgart - Hochschule für Technik, Germany. Vol. 65, pp. 145-158.

KOHLENBACH, P. and TAMM, O. and SCHWEIGLER, C. and HARM, M. and ALBERS, J. and KUEHN, A. and PETERSEN, S. (2004b). *Entwicklung eines Systems zur solaren Kühlung im kleinen Leistungsbereich* (Development of a system for solar cooling in the small-scale perfromance range). Proceedings of the 14th Symposium Thermische Solarenergie. Ostbayerisches Technologie-Transfer-Institut e.V. (OTTI), Staffelstein, Germany. pp. 546-551. ISBN 3-934681-33-6. URL Phönix SonnenWärme AG: www.sonnenwaermeag.de.

KOUREMENOS, D.A. and STEGOU-SAGIA, A. (1987). *The evaporation of NH_3 in NH_3/H_2 atmosphere for small absorption refrigeration units. Determination of the inlet mass fraction and mass flow rate of the NH_3/H_2 gas mixture.* Proceedings of the 17th IIR International Congress of Refrigeration. International Institute of Refrigeration (IIR), Vienna, Austria. pp. 1032-1037.

KOUREMENOS, D.A. and STEGOU-SAGIA, A. (1988a). *Measuring the evaporation of NH_3 in triple-fluid gas absorption units.* Int. J. Refrig. Vol. 11, No. 5, pp. 153-158. ISSN 0140-7007.

KOUREMENOS, D.A. and STEGOU-SAGIA, A. (1988b). *Use of helium instead of hydrogen in inert gas absorption refrigeration.* Int. J. Refrig. Vol. 11, No. 9, pp. 336-341. ISSN 0140-7007.

KOUREMENOS, D.A. and STEGOU-SAGIA, A. and ANTONOPOULOS, K.A. (1990). *The irreversible evaporation of ammonia in vertical annular evaporators using helium as inert gas.* Proceedings ASME, Dallas. AES-Vol. 18, pp. 15-24.

REFERENCES

KOUREMENOS, D.A. and STEGOU-SAGIA, A. and ANTONOPOULOS, K.A. (1994). *Three-dimensional evaporation process in aqua-ammonia absorption refrigerators using helium as inert gas.* Int. J. Refrig. Vol. 17, No. 1, pp. 58-67. ISSN 0140-7007.

KOYFMAN, A. and JELINEK, M and LEVY, A. and BORDE, I. (2001). *A study on bubble pump performance for diffusion absorption refrigeration system with organic working fluids.* Proceedings of the 2nd International Heat Powered Cycles Conference. 5.-7. September, Conservatoire national des arts et métiers (Cnam), Paris, France. ISBN 1-902038-01-0.

KOYFMAN, A. (2002). *A Study of Bubble Pump Performance for a Diffusion Absorption Refrigeration System with Organic Working Fluids.* Unpub. M.Sc. Thesis. Ben-Gurion University of the Negev, Israel.

KOYFMAN, A. and JELINEK, M and LEVY, A. and BORDE, I. (2003a). *An experimental investigation of bubble pump performance for diffusion absorption refrigeration system with organic working fluids.* Applied Thermal Engineering. Vol. 23, pp. 1881-1894. ISSN 1359-4311.

KOYFMAN, A. and JELINEK, M and LEVY, A. and BORDE, I. (2003b). *Study of bubble pump performance with organic working fluids.* Proceedings of the 21st IIR International Congress of Refrigeration. 17.-22. August, International Institute of Refrigeration (IIR), Washington D.C., USA. ISBN 2-913149-32-4.

KRÜGER, D. and HENNECKE, K. and SCHWARZBÖZL, P. and LOKURLU, A. and RICHARTS, F. (2002). *Parabolic trough collectors for cooling and heat supply of a hotel in Turkey.* Proceedings of the 7th World Renewable Energy Congress. 1st –5th July, World Renewable Energy Network (WREN), Cologne, Germany. ISBN 0-08-044079-7.

KÜHN, A. and ALBERS, J. and HARM, M. and KOHLENBACH, P. and PETERSEN, S. and SCHWEIGLER, C. and ZIEGLER, F. (2004). *Betriebsverhalten einer 10kW Absorptionskälteanalge für niedrige Antriebstemperaturen* (Operating performance of a 10kW absorption chiller with low driving temperatures). Proceedings of the 31st Deutsche Klima-Kälte-Tagung, Bremen, Germany. Vol. AA.II.1, pp. 169-182. ISBN 3-932715-36-5.

KUNZE, G. (2000). *Efficient Solar Cooling with an improved Ammonia-Absorption System.* Renewable Energy World. Vol. 3, No. 6, pp. 111-112. ISSN 1462-6381.

LAMP, P. and ZIEGLER, F. (1997). *Solar Cooling with closed Sorption Systems.* Proceedings of the Workshop Solar Sorptive Cooling. 16th-17th October, Forschungsverbund Sonnenenergie (FVS), Hardthausen, Germany. pp. 79-92. ISSN 0949-1082.

LANSING, F.L. (1976). *Computer Modeling of a Single-Stage Lithium Bromide/Water Absorption Refrigeration Unit.* The Deep Space Network Progress Report. Jet Propulsion Laboratory (JPL) California Institute of Technology Pasadena, USA. Vol.42-32, April 15, pp. 247-257.

LOEWER, H. (1978). *Solar-Kühlung in der Klimatechnik* (Solar refrigeration for air conditioning installations). Ki Klima-Kälte-Ingenieur. Vol. 6, No. 4, pp. 155-162. ISSN 0340-398X.

LOKURLU, A. and RICHARTS, F. and KRÜGER, D. and PITZ-PAAL, R. (2002). *Wärme- und Kälteversorgung eines Hotels mit Parabolrinnenkollektoren* (Heat and Cooling supply of a Hotel with Parabolic Trough Collectors). Proceedings of the 12th Symposium Thermische Solarenergie. Ostbayerisches Technologie-Transfer-Institut e.V. (OTTI), Staffelstein, Germany. pp. 235-239. ISBN 3-934681-20-4.

LUCAS, P. (1967). *A boiler for absorption units of the inert gas type having a wide range of input power.* Proceedings of the 12th IIR International Congress of Refrigeration. International Institute of Refrigeration (IIR), Madrid, Spain. pp. 1353-1359.

MAIYA, M.P. (1988) *Investigations on Triple Fluid Vapour Absorption Refrigerator.* Unpub. PhD Thesis. Indian Institute of Technology Bombay, India.

MAIYA, M.P. (2003). *Studies on gas circuit of diffusion absorption refrigerator.* Proceedings of the 21st IIR International Congress of Refrigeration. 17.-22. August, International Institute of Refrigeration (IIR), Washington D.C., USA. ISBN 2-913149-32-4.

REFERENCES

MEIßNER, E. and HOLTER, C. and SCHWEYER, K. and THÜRSCHWELLER, S. (2004a). *Projekterfahrungen mit solaren Kältemaschinen: 90kW H_2O-LiBr Absorptionskälteanlage für EAR Tower in Pristina/Kosovo* (Project experiences with solar cooling machines: 90kW H_2O-LiBr absorption cooling machine for the EAR Tower in Pristina/Kosovo). Proceedings of the 3rd Symposium Solares Kühlen in der Praxis. Fachhochschule Stuttgart - Hochschule für Technik, Germany. Vol. 65, pp. 71-80.

MEIßNER, E. and PODESSER, E. and ENZINGER, P. and PEITLER, J. and THÜRSCHWELLER, S. and SCHWEYER, K. (2004b). *Projekterfahrungen mit solaren Kältemaschinen: 17kW NH_3-H_2O Absorptionskälteanlage für Weinkühlung beim Weingut Peitler in der Steiermark/Österreich* (Project experiences with solar cooling machines: 17kW NH_3-H_2O absorption cooling machine for the winery Peitler in the Steiermark/Austria). Proceedings of the 3rd Symposium Solares Kühlen in der Praxis. Fachhochschule Stuttgart - Hochschule für Technik, Germany. Vol. 65, pp. 59-70.

MÖßLE (2000). *Erfahrungen mit der solarunterstützten Klimatisierung* (Experiences with the solar assisted air-conditioning). Proceedings of the Dresdner Colloquium – Solare Klimatiserung. ILK Dresden, Germany.

MUNTERS, C.G. (1932). *Entwicklung des Elektrolux-Kühlapparates* (Development of the Electrolux-refrigerator). Zeitschrift für die gesamte Kälte-Industrie. Vol. 39, No. 11, pp. 197-200 and No. 12, pp. 216-220.

NARAYANKHEDKAR, K.G. and MAIYA, M.P. (1985). *Investigations on triple fluid vapour absorption refrigerator.* Int. J. Refrig. Vol. 8, No. 11, pp. 335-342. ISSN 0140-7007.

NIEBERGALL, W. (1956). *Der Vorgang der Austreibung und Lösungsförderung bei Absorptions-Kältemaschinen mit Thermosyphonpumpe* (The process of expulsion and solution lifting by absorption cooling machines with a thermosyphon pump). Kältetechnik, Vol. 82, No. 8 and 9, pp. 238-243 and pp. 272-275. ISSN 0368-4865.

NIEBERGALL, W. (1959). *Sorptions-Kältemaschinen* (Sorption Cooling Machines). *in* PLANK, R. *Handbuch der Kältetechnik* (1st ed.). Berlin: Springer-Verlag, Germany. Vol. 7, pp. 198-220, pp. 249-271 and pp. 285-313.

NIEBERGALL, W. (1981). *Sorptions-Kältemaschinen* (Sorption Cooling Machines). *in* PLANK, R. *Handbuch der Kältetechnik* (reprint 1st edit.). Berlin: Springer-Verlag, Germany. Vol. 7, pp. 105-114, pp. 249-271, pp. 443-445 and pp. 285-313.

OHN, J. (1995). *Kölner Pilotprojekt: Verwaltungsgebäude solar gekühlt* (Cologne pilot project: administrative building solar cooled). HLH. Vol. 46, No. 12, pp. 58-59, ISSN 1436-5103.

PÄßLER, T. (2002). Untersuchungen an einem vertikalen Rieselfilm-Verdampfer einer solar betriebenen Diffusions-Absorptionskältemaschine (Investigations on a vertical falling film evaporator of solar driven Diffusion-Absorption Cooling Machine). Unpub. Diploma Degree, Fachhochschule Stuttgart-Hochschule für Technik, Germany.

PÁTEK, J. and KLOMFAR, J. (1995). *Simple functions for fast calculations of selected thermodynamic properties of the ammonia-water.* Int. J. Refrig.. Vol. 18, No. 4, pp. 228-234. ISSN 0140-7007.

PFAFF, M. and SARAVANAN, R. and MAIYA, M.P. and SRINIVASAMURTHY, S. (1998). *Studies on Bubble Pump for a Water-Lithium bromide Vapour Absorption Cooler.* Int. J. Refrig. Vol. 21, No. 5, pp. 452-462. ISSN 0140-7007.

PICKERT, F. (1931). *Wirkungsgrad und Berechnungsgrundlagen von Druckluft-Wasserhebern* (Efficiency and calculation fundamentals of compressed air water lifter). Unpub. PhD Thesis. Technische Hochschule Berlin, Germany.

PLANK, R. and KUPRIANOFF, J. (1960). *Die Kleinkältemaschine* (The household refrigeration machine) (2nd ed.). Berlin: Springer-Verlag, Germany. pp. 360-397.

PODESSER, E. (1982). *Kühlung mit Sonnenenergie* (Cooling with sun energy). Ki Klima-Kälte-Heizung. Vol. 10, No. 1, pp. 29-32. ISSN 0172-1984.

PHÖNIX (2004). *Kälte aus Wärme: Solares Kühlen* (Cold made of heat: Solar Cooling). Company internet product information's. Phönix SonnenWärme AG, Germany. URL: www.sonnenwaermeag.de.

QUINETTE, J.-Y. and ALBERS, J. (2002). *Solar Air-Conditioning by Absorption.* Proceedings of the Industry workshop Solare Klimatisierung/Solar Assisted Air Conditioning of Buildings. aircontec – International trade fair for air-conditioning technology at Light+Building. Fachinstitut Gebäude-Klima FGK, Germany. URL: www.sorptionsgestuetzte-klimatisierung.de.

REGLOPLAS (1999). *Datenblatt RO200* (Data sheet RO200). Company product information. aic-regloplas GmbH, Germany.

REISTAD, B. (1968). *Thermal conditions in heat driven refrigerating units for domestic use.* Kylteknisk tidskrift. Vol. 27, No. 3, pp. 43-51. ISSN 0023-5970.

SAFARIK, M. and GRAMLICH, K. and SCHAMMLER, G. (2002). *Solar absorption cooling system with 90°C - latent heat storage.* Proceedings of the 7th World Renewable Energy Congress. 1st –5th July, World Renewable Energy Network (WREN), Cologne, Germany. ISBN 0-08-044079-7.

SAFARIK, M. and GRAMLICH, K. (2003). *Solare Kälteerzeugung mit einer NH_3/H_2O-Absorptionskältemaschine* – Betrieb und Simulation (Solar cold production with a NH_3/H_2O absorpiton chiller – operation and simulation). KI Luft- und Kältetechnik. Vol. 39, No. 10, pp. 463-468. ISSN 0945-0459.

SAFARIK, M. and WEIDNER, G. (2004). *Neue 15kW H_2O-LiBr Absorptionskälteanlage im Feldtest für thermische Anwendungen* (New 15kW H_2O-LiBr Absorption Cooling Machine in filed test for thermal applications). Proceedings of the 3rd Symposium Solares Kühlen in der Praxis. Fachhochschule Stuttgart - Hochschule für Technik, Germany. Vol. 65, pp. 159-171.

SATHE, A. (2001). *Experimental and Theoretical Studies on a Bubble Pump for a Diffusion-Absorption Refrigeration System.* Unpub. Master Thesis. Indian Institute of Technology Madras, India. URL: www.geocities.com/abhijitsathe.

SATTLER, A. (2002). *Instationäres Verhalten und Reproduzierbarkeit des Betriebs einer solar betriebenen Diffusions-Absorptionskältemaschine* (Unsteady behaviour and reproducibility of a solar driven Diffusion-Absorption Cooling Machine). Unpub. Diploma Degree, Fachhochschule Stuttgart-Hochschule für Technik, Germany.

SCHAEFER, L.A. (2000). *Single Pressure Absorption Heat Pump Analysis.* Unpub. PhD Thesis. Georgia Institute of Technology, USA. URL: www.me.gatech.edu/energy/publications.htm.

SCHIBEL, T. (2002). *Solare Klimatisierung Projekte* (Solar air-conditioning projects). Personal email communication with the company Viessmann Werke GmbH & Co, Germany.

SCHIRP, W. (1990). *Gasbeheizte Diffusions-Absorptions-Wärmepumpe (DAWP) für Wohnraumbeheizung, Brauchwassererwärmung und Wohnraumkühlung* (Gas-operated diffusions-absorption heat pumps (DAHP) for domestic heating, hot water supply and room air-conditioning). Ki Klima-Kälte-Heizung. Vol. 18, No. 3, pp. 113-118. ISSN 0172-1984.

SCHUMACHER, J. (1991). *Digitale Simulation regenerativer elektrischer Energieversorgungssysteme* (Digital simulation of regenerative electrical energy supply systems). Unpub. PhD Thesis. Universität Oldenburg, Germany. www.inselDi.com.

SCHWARZ, C. and LOTZ, D. (2001). *Gas-Wärmepumpen -Absorber - Einsatz im Ein- und Zweifamilienwohnhaus* (Gas-heat pumps - Absorber - Use for one- and two-family houses). Proceedings of the Fachtagung Heizen - Kühlen - Klimatisieren mit Gas-Wärmepumpen und -Kälteanlagen. 14. November, ASUE, Fulda, Germany. pp. 35-43. URL: www.asue.de.

SCHWEIGLER, C. and HELLMANN, H.-M. and PREISSNER, M. and DEMMEL, S. and ZIEGLER, F. (1997). *Operation and Performance of a 350kW (100 RT) Single-Effect/Double-Lift Absorption Chiller.* Proceedings of the Workshop Solar Sorptive Cooling. 16th-17th October, Forschungsverbund Sonnenenergie (FVS), Hardthausen, Germany. pp. 93-106. ISSN 0949-1082.

SCHWEIGLER, C. (1999). *Kälte aus Fernwärme – Konzept, Auslegung und Betrieb der Single-Effect/Double-Lift-Absorptionskälteanlage* (Cold from long-distance energy – concept, design and operation of the Single-Effect/Double-Lift absorption cooling plant) (1st ed.). Düsseldorf: VDI-Verlag, Germany. Fortschritt-Berichte VDI Reihe 19, No. 121. ISBN 3-18-312119-0.

REFERENCES

SCHWEIGLER, C. and STORKENMAIER, F. and ZIEGLER, F. (1999). *Die charakteristische Gleichung von Sorptionskälteanlagen* (The characteristic equation of sorption chillers). Proceedings of the 26th Deutsche Klima-Kälte-Tagung, Berlin, Germany.

SCHWEIGLER, C. (2004). *Solare Klimatisierung mit zweistufigen Absorptionskälteanlagen* (Solar Cooling with double-stage Absorption Chillers). Proceedings of the 3rd Symposium Solares Kühlen in der Praxis. Fachhochschule Stuttgart - Hochschule für Technik, Germany. Vol. 65, pp. 211-229.

SELLERIO, U. (1951). *Device to speed the circulation of water solutions in household absorption refrigerators.* Proceedings of the 8th IIR International Congress of Refrigeration. International Institute of Refrigeration (IIR), London, U.K.. pp. 453-459.

SHELTON, S.V. and WHITE STEWART, S. (2002). *Bubble Pump Design for Single Pressure Absorption Refrigeration Cycles.* ASHRAE Transactions. AC-02-13-2. Vol. 108 Pt. 1.

SHI, Z. (1994). *Performance modeling of the Diffusion-Absorption Heat Pump.* Unpub. M.Sc. Thesis. University of Maryland, USA.

SKLAR, S. (2004). *New dawn for distributed energy.* Cogeneration and On-Site Power Production. Vol. 5, No. 4, pp. 115-121. ISSN 1469-0349.

SLIPČEVIĆ, B. (1988). *Wärmeaustauscher* (Heat Exchanger). *in* PLANK, R. *Handbuch der Kältetechnik* (1st ed.). Berlin: Springer-Verlag, Germany. Vol. 6B, pp. 43-45 and pp. 125-126. ISBN 3-540-15477-9.

SMIRNOV, G.F. and BUKRABA, M.A. and FATTUH, T. and NABULSI, B. (1996). *Domestic refrigerators with absorption-diffusion units and heat-transfer panels.* Int. J. Refrig. Vol. 19, No. 8, pp. 517-521. ISSN 0140-7007.

SOLARFROST (2002). *2kW Cooling Machine.* Newsletter November 2002. http://www.solarfrost.com.

SOLITEM (2004). Company internet product and project information's. Solitem GmbH, Germany. URL: www.solitem.de.

SRIKHIRIN, P. and APHORNRATANA, S. and CHUNGPAIBULPATANA, S. (2001). *A review of absorption refrigeration technologies.* Renewable and Sustainable Energy Reviews. Vol. 5, No. 4, pp. 343-372. ISSN 1364-0321.

SRIKHIRIN, P. and APHORNRATANA, S. (2002). *Investigation of a diffusion absorption refrigerator.* Applied Thermal Engineering. Vol. 22, No. 11, pp. 1181-1193. ISSN 1359-4311.

STIERLIN, H. (1964). *Neue Möglichkeiten für den Absorptions-Kühlschrank* (New chances for the absorption refrigerator). Kältetechnik. No. 9, pp. 264-270.

STIERLIN, H. (1971). *Multiple hydrogen circuits in absorption deep freezers.* Proceedings of the 13th IIR International Congress of Refrigeration. International Institute of Refrigeration (IIR), Washington D.C., USA. pp. 525-533.

STIERLIN, H. (1980). *Große Reduktion des Energieverbrauches bei den lautlosen Kühlschränken – Eine neue Generation von Absorptions-Kühlschränken* (A great reduction of energy consumption with the noiseless refrigerators – a new generation of absorption refrigerators). Ki Klima-Kälte-Heizung, Vol. 8, No. 9, pp. 363-368. ISSN 0172-1984.

STIERLIN, H.C. and FERGUSON, J.R. (1990). *Diffusion Absorption Heat Pump (DAHP).* ASHRAE Transactions (AT-90-27-4), Vol. 96, pp. 1499-1505.

STIERLIN, H. and WASSERMANN, U. and DÖRFLER, W. and BÖSEL, J. (1994). *Messungen an Diffusions-Absorptions-Wärmepumpen – DAWP* (Data Recording on Diffusion-Absorption Heat Pumps - DAHP). Unpub. End Report, Bundesamt für Energiewirtschaft (BEW 92-019), Switzerland.

STORKENMAIER, F. and HARM, M. and SCHWEIGLER, C. and ZIEGLER, F. and ALBERS, J. and KOHLENBACH, P. and SENGEWALD, T. (2003). *Small-Capacity Water/LiBr Absorption Chiller for Solar Cooling and Waste-Heat Driven Cooling.* Proceedings of the 21st IIR International Congress of Refrigeration. 17th-22nd August, International Institute of Refrigeration (IIR), Washington D.C., USA. ISBN 2-913149-32-4.

TAITEL, Y. and BARNEA, D. and DUKLER, A.E. (1980). *Modelling flow pattern transitions for steady upward gas-liquid flow in vertical tubes.* AIChE Journal. Vol. 26, No. 3, pp. 345-354.

TEUßER, A. (2004). *Grundlagen für ein Modell für Leistungszahlen thermischer Absorptionskältemaschinen* (Fundamental principles for a model for performances numbers of thermal Absorption Cooling Machines). Unpub. Diploma Degree, Fachhochschule Stuttgart-Hochschule für Technik, Germany.

TYFOROP (1999). *Technische Information TYFOXIT F15-F60* (Technical information TYFOXIT F15-F60). Company product information. Tyforop Chemie GmbH, Germany.

VAZIRI-ELAHI, M. (1944). *Die Diffusionsmaschine nach Maiuri* (The Diffusion machine by Maiuri). Zeitschrift für die gesamte Kälteindustrie, Vol. 51, No. 3/4 pp. 17-24.

VDI-WÄRMEATLAS (1988). *VDI-Wärmeatlas: Berechnungsblätter für den Wärmeübergang* (VDI-heat atlas: calculation sheets for the heat transmission) (5th ed.). Düsseldorf: VDI Verlag, Germany. ISBN 3-18-400760-X.

VICATOS, G. (2000). *Experimental investigation on a three-fluid absorption refrigeration machine*. Proceedings of the Institution of Mechanical Engineers, Part E. Vol. 214, No. 3, pp. 157-172.

WANG, L. (1992). *Simulation of a Diffusion-Absorption Heat Pump Using Helium as Auxiliary Gas*. Unpub. M.Sc. Thesis. University of Maryland, USA.

WANG, L. and HEROLD, K.E. (1992). *Diffusion-Absorption Heat Pump*. Annual Report for Gas Research Institute, GRI-92/0262. Gas Research Institute, USA.

WATTS, F.G. and GULLAND, C.K. (1958). *Triple-fluid vapour-absorption refrigerators.* The J. of Refrig., July and August, pp. 107-115.

WHITE, S.J. (2001). *Bubble Pump Design and Performance*. Unpub. M.Sc. Thesis. Georgia Institute of Technology, USA. URL: www.me.gatech.edu/energy/publications.htm.

WOLKENHAUER, H. and ALBERS, J. (2001). *Systemlösungen und Regelungskonzepte von solarunterstützten Klimatisierungssystemen Teil 1 – Kaltwassersysteme* (System solutions and control strategies of solar assisted air-conditioning systems part 1 – cold water systems). HLH. Vol. 52, No. 12. pp. 41-49. ISSN 1436-5103.

ZIEGLER, F. (1998a). *Sorptionswärmepumpen* (Sorption heat pumps). Forschungsberichte des Deutschen Kälte- und Klimatechnischen Vereins No. 57. DKV, Stuttgart, Germany. ISBN 3-932715-60-8.

ZIEGLER, F. (1998b). *Relationships between temperature differences in heat exchangers of heat transformation devices.* Rev. Gén. de Thermique, Vol. 37, pp. 549-555. ISSN 0035-3159.

ZIEGLER, F. (1998c). Entwicklungstendenzen bei Absorptionskälteanlagen (Development tendency of absorption cooling units). *in* VDI BERICHTE. *Kälteversorgung in der technischen Gebäudeausrüstung* (1st ed.). Düsseldorf: VDI-Verlag, Germany. No. 1432, pp. 23-36. ISBN 3-18-091432-7.

ZIEGLER, F. (1999). *Recent developments and future prospects of sorption heat pump systems.* Int. J. Therm. Sci.. Vol. 38, pp. 191-208. ISSN 1290-0729.

ZOHAR, A. and JELINEK, M. and LEVY, A. and BORDE, I. (2005). *Numerical investigation of a diffusion absorption refrigeration cycle.* Int. J. Refrig., Vol. 28. ISSN 0140-7007.